PAMINA
Performance Assessment Methodologies in Application to Guide the Development of the Safety Case

EVALUATION AND TESTING OF APPROACHES TO TREAT SPATIAL VARIABILITY IN PA DELIVERABLE (D-N°:D2.2.D.1)

Author(s):   **Javier Rodrigo-Ilarri and J. Jaime Gómez-Hernández (UPV)**
Bertrand Iooss (CEA)
Elmar Plischke and Klaus-Jürgen Röhlig (TUC)

Date of issue of this report : **15/04/08**

Start date of project : **01/10/2006**   Duration : **36** Months

Foreword

The work presented in this report was developed within the Integrated Project PAMINA: **P**erformance **A**ssessment **M**ethodologies **IN** **A**pplication to Guide the Development of the Safety Case. This project is part of the Sixth Framework Programme of the European Commission. It brings together 25 organisations from ten European countries and one EC Joint Research Centre in order to improve and harmonise methodologies and tools for demonstrating the safety of deep geological disposal of long-lived radioactive waste for different waste types, repository designs and geological environments. The results will be of interest to national waste management organisations, regulators and lay stakeholders.

The work is organised in four Research and Technology Development Components (RTDCs) and one additional component dealing with knowledge management and dissemination of knowledge:

–   In RTDC 1 the aim is to evaluate the state of the art of methodologies and approaches needed for assessing the safety of deep geological disposal, on the basis of comprehensive review of international practice. This work includes the identification of any deficiencies in methods and tools.

–   In RTDC 2 the aim is to establish a framework and methodology for the treatment of uncertainty during PA and safety case development. Guidance on, and examples of, good practice will be provided on the communication and treatment of different types of uncertainty, spatial variability, the development of probabilistic safety assessment tools, and techniques for sensitivity and uncertainty analysis.

–   In RTDC 3 the aim is to develop methodologies and tools for integrated PA for various geological disposal concepts. This work includes the development of PA scenarios, of the PA approach to gas migration processes, of the PA approach to radionuclide source term modelling, and of safety and performance indicators.

–   In RTDC 4 the aim is to conduct several benchmark exercises on specific processes, in which quantitative comparisons are made between approaches that rely on simplifying assumptions and models, and those that rely on complex models that take into account a more complete process conceptualization in space and time.

The work presented in this report was performed in the scope of RTDC 2.

All PAMINA reports can be downloaded from http://www.ip-pamina.eu.

PAMINA Sixth Framework programme

INDEX

1 – State of the Art on Upscaling techniques

B - Upscaling transport parameters under the non-Fickian Approach

2 – Treatment of spatially dependent input variables in sensitivity analysis of model output methods

3. Global sensitivity analysis of stochastic computer models with generalized additive models

4. Global sensitivity analysis of computer models with functional inputs

3 – Review of spatial variability in Performance Assessments

1. General remarks

2. Compilation of examples

3. Discussion

       3.1. Reliability of models

       3.2. Connection to recent safety cases

       3.3. The role of safety functions

       3.4. Probabilistic safety assessments: Addressing spatial variability in a safety case

4. Bibliography

---

4 – Plan for PA exercises to test techniques for upscaling

Introduction

Available techniques for flow and transport parameters upscaling

Plan to evaluate upscaling on the PA Exercise

References

1. State of the Art on Upscaling Techniques

PART 1

**UPSCALING OF
FLOW PARAMETERS**

PART 1 – UPSCALING OF FLOW PARAMETERS

Hydraulic conductivity upscaling is a process that transforms a grid of hydraulic conductivity defined at the scale of the measurements, into a coarser grid of block conductivity tensors amenable for input to a numerical flow simulator. The need for upscaling stems from the disparity between the scales at which measurements are taken and the scale at which aquifers are discretized for the numerical solution of flow and transport.

The techniques for upscaling range from the simple averaging of the heterogeneous values within the block to sophisticated inversions, after the flow equation at the measurement scale within an area embedding the block being upscaled.

All techniques have their own advantages and limitations. The definition of the geometry of the grid has been intimately linked to the upscaling problem; promising results have been obtained using elastic gridding. The need to perform Monte-Carlo analyses, involving many realizations of hydraulic conductivity, has steered the development of methods that generate directly the block conductivities in accordance with the rules of upscaling, yet conditional to the measurement data.

1.   Introduction

An important issue in the numerical simulation of groundwater flow and mass transport is the problem of scales. Data are collected at a scale different from (usually smaller than) the one used to discretize the aquifer in the numerical model. For instance, field sampled hydraulic conductivities (e.g. from core measurements, slug tests or packer tests) have measurement supports in the order of centimetres to meters, whereas numerical models for groundwater flow require conductivities representative of tens to hundreds of meters.

Since the 1960s different approaches have been used to transform a detailed description of the spatial variability of hydraulic conductivity to a coarser description, as sketched in Fig.1.
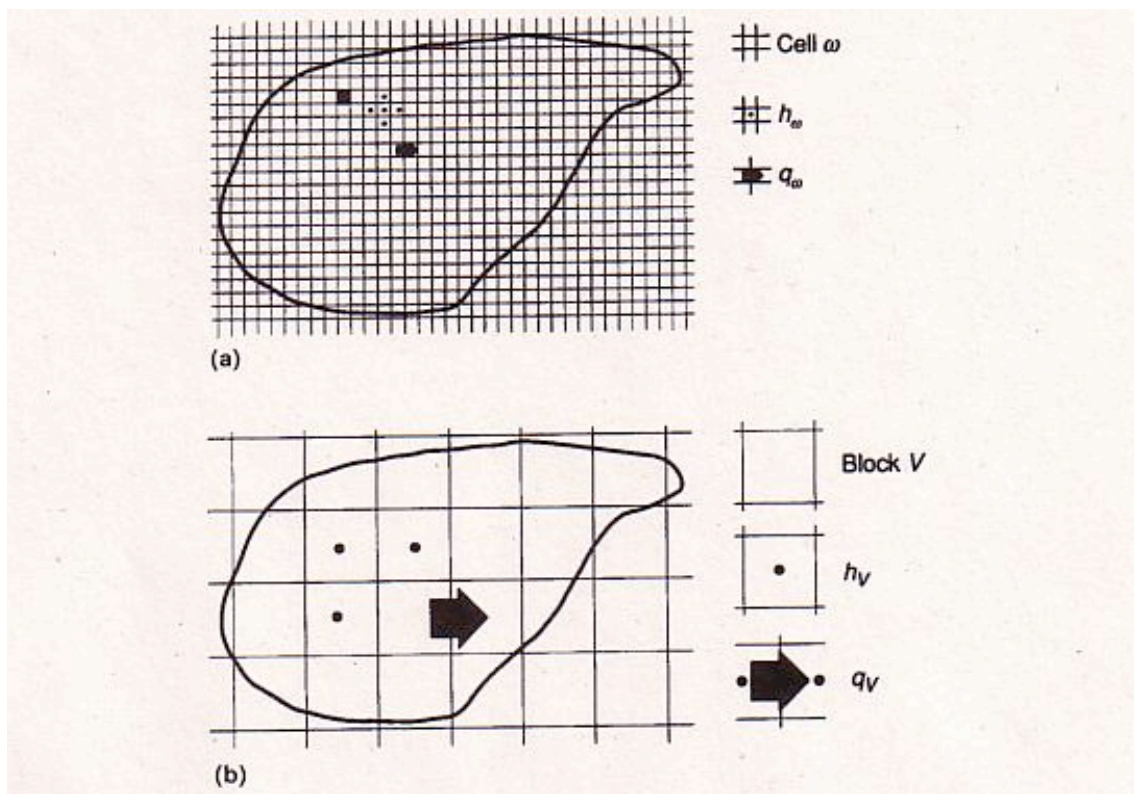

Fig. 1.- The upscaling process. (a) Grid at the measurement scale, with possibly millions of cells. (b) Grid at the numerical scale on which the flow problem will be solved. Computing the conductivity block values in (b) from the corresponding values in (a) is the objective of upscaling.

We will refer to the scale corresponding to the detailed description in Fig. 1(a) as the measurement scale, and to the scale corresponding to the coarser description in Fig. 1(b) as the numerical scale. We will use the terms cell conductivity and block (or equivalent) conductivity to refer to conductivity values at the measurement and numerical scales respectively. We do not discuss the ways in which a grid at the measurement scale can be produced from a few sparse measurements, we will just mention that, in general, such a grid is filled by some (geo) statistical technique (see for instance Deutsch and Journel, 1992). Our starting point is a grid (or several) of conductivity values at the measurement scale that is (are) to be "upscaled" to the numerical scale for input to a numerical groundwater flow simulator.

Some authors use the term "effective conductivity" to refer to block conductivities. We choose not to use it in this sense to avoid confusion with the specific meaning that effective conductivity has in stochastic hydrogeology. The effective conductivity defined in stochastic hydrogeology is a property of the random function model adopted to describe the spatial variability of conductivity: it is not a block property but a point property representing an average process through the ensemble of possible realizations at a point. Only under certain random function models, the effective conductivity is constant in space and coincident with the block conductivity of an infinite block (Matheron, 1967; Dagan, 1979, 1982a,b, 1989). In this respect, effective conductivities can be used as a partial check of upscaling techniques. Although effective conductivities have been the subject of many studies (e..g. Matheron, 1967; Dagan, 1979, 1982a, 1989; Gutjhar et al., 1978, Gelhar and Axness, 1983; Poley, 1988; Ababou and Wood, 1990; Naff 1991; Neuman and Orr, 1993) they are not addressed in this work. The interested reader should refer to the work of Neuman and Orr (1993) which presents the most general results. This document is organized as follows. First, block conductivity is defined, then a review of upscaling methods in a sequence of increasing complexity is given. We include only upscaling methods that deal with single-phase saturated conductivity. Readers interested in conductivity upscaling for unsaturated flow are referred to Yeh et al. (1985), Mantoglou and Gelhar (1987) and Russo (1992). Readers interested in multiphase flow are referred to Haldorsen (1986), Muggeridge (1991) and Fayers and Hewett (1992).

2.   Block conductivity

The usage of the terms equivalent, block, effective or upscaled, applied to conductivity, instead of the simpler usage of the term average, reflects the fact that the conductivity is not an additive property. It is well known for electrical conductance analogy that the equivalent conductivity for a group of cells serially arranged is equal to their harmonic average, whereas if the cells are arranged in parallel the equivalent conductivity is equal to the arithmetic average. Cardwell and Parsons (1945) proved that the equivalent conductivity of a heterogeneous block is bounded above and below by the arithmetic and harmonic averages, respectively.

2.1. Definition

Following Rubin and Gómez-Hernández (1990), block conductivity, $\mathbf{K}_V$ is defined from an extension of Darcy's law as:

$$\frac{1}{V}\int_V \mathbf{q}_w(\mathbf{u})d\mathbf{u} = -\mathbf{K}_V\left(\frac{1}{V}\int_V \nabla h_w(\mathbf{u})d\mathbf{u}\right) \tag{1}$$

where:

    V: represents the block support

    $\mathbf{q}_w$ is the specific discharge vector at cell w within the block

    $\mathbf{u}$ is the position vector that sweeps the inside of the block

    ∇h_w is the gradient of the piezometric head at w.

Vector integration is performed by integration of its components. In words, block conductivity is the tensor that relates the block spatial average of the specific discharge vector to the spatial average of the piezometric head gradient vector.

The cell conductivities $\mathbf{K}_w$ are implicit in Eq. (1) since $\mathbf{q}_{w \text{ and }} \nabla h_w$ are related at the measurement scale through $\mathbf{K}_w$:

$$\mathbf{q}_w = -\mathbf{K}_w \nabla h_w$$

Notice that, by definition, $\mathbf{K}_V$ is, like $\mathbf{K}_w$, a tensor.

In the different approaches to upscaling described next, the definition in Eq. (1) is not always explicitly adopted; in some cases it is implicit to the formulation, in others, alternative definitions are employed. When the latter occurs, the alternative definition is indicated. However, in all cases, the purpose of the upscaling procedure is to obtain a description of conductivity spatial variability at the numerical scale that reproduces some average behaviour of the conductivity field at the measurement scale.

3. Evolution of block conductivity upscaling

We start with the local techniques, that is, those techniques that assume that the block conductivity tensor is intrinsic to the cell conductivities within the block. Then we continue with the non-local techniques, in which block conductivities depend not only on the cell conductivities within the block, but also on the flow boundary conditions necessary to determine $\mathbf{q}_w$ and ∇h_w in Eq. (1). Then, another set of techniques in which the definition of block geometry becomes part of the upscaling problem is presented. Finally, a set of techniques for the direct generation of numerical scale grids from measurement scale data is presented.

3.1. Local techniques

Local techniques consider that block conductivity is intrinsic to the cell conductivities within the block as would be the case if block conductivity is a material property. Local techniques are the natural extension of the one-dimensional results, for which it is known that block conductivity is equal to the harmonic average of the heterogeneous conductivities. In the local techniques the block conductivity is an explicit function of the cell conductivities. The methods described in this subsection rely on the assumption that the cell conductivity tensor $\mathbf{K}_w$ degenerates into a scalar K_w. The simple average approach and the renormalization technique also assume that the resulting block conductivity tensor $\mathbf{K}_V$ is also a scalar K_V. While the first assumption can be justifiable, the second one is more difficult to justify, since the tensorial nature of block conductivities is partly a consequence of the anisotropic spatial correlation of cell conductivities (Lake, 1988), even for the case of scalar cell conductivities.

3.1.1. Simple average

For 1-D flow, block conductivity is equal to the harmonic mean of the cell conductivities within the block. For 2-D flow, there is a very strong result from the theory of effective parameters (Matheron, 1967) that applies for infinite blocks with heterogeneous conductivities having an isotropic spatial correlation and a frequency

distribution which is identical to the frequency distribution of their reciprocals (as is the case if conductivity follows a lognormal distribution). Matheron (1967) proved that, under these conditions, block conductivity is equal to the geometric mean. This result, which, in principle, applies only to infinite blocks has been used extensively in the petroleum and hydrology literature for finite blocks without much justification (e.g. Dagan, 1982b, 1985; Clifton and Neumann, 1982; Hoksema and Kitanidis, 1984, 1985).

Through numerical experiments in 3-D, Warren and Price (1961) concluded that the geometric average is the most appropiate estimator of block conductivities for spatially uncorrelated cell values. Bouwer (1969) used analog simulations to arrive to the same conclusion.

Grindheim (1990) and Durlofsky (1992) investigated the use of simple average methods to compute block conductivities in 2-D for different spatial distribution of the cell conductivities (uncorrelated and correlated, statistically isotropic and anisotropic, and sand-shale binary distributions). Some of the averages investigated include: arithmetic, geometric, harmonic, arithmetic-harmonic and harmonic-arithmetic. By comparing the flow results in the grid at the measurement scale and the flow results in the upscaled grid they concluded that there is no simple average that is valid for all heterogenous formations.

Gómez-hernández and Wen (1994) showed that, in 2-D, the geometric mean gives good estimates of the block conductivity as long as the spatial variability of cell conductivities does not display a strong anisotropy.

3.1.2. Power average

Cardwell and Parsons (1945) proved that block conductivities must lie in between the arithmetic and harmonic averages of the cells within the block. Based on this statement, Journel et al. (1986) proposed the use of a power average to compute equivalent block conductivities:

$$\mathbf{K}_V = \left(\frac{1}{V} \int_V \mathbf{K}_w^p(\mathbf{u}) d\mathbf{u} \right)^{1/p}$$

by varying the exponent p between -1 and 1, the power average varies between the harmonic and the arithmetic averages, with the geometric mean corresponding to p=0. They argue that the exponent p depends on the specific type of cell conductivity spatial heterogeneity and can be obtained by calibration with the results obtained from detailed numerical simulations in a fraction of the blocks being upscaled. The technique was later successfully applied by Deutsch (1989), Gómez-Hernández and Gorelick (1989), Bachu and Cuthiell (1990), Desbarats and dimitrakopoulos (1990) and Desbarats (1992b).

Some of their findings are:

(i) the power p is case-specific and is function of the type of heterogeneity within the block, the block shape and size, and the flow conditions within the block

(ii) for the case of statistically anisotropic cell conductivities, p is direction dependent and can be used to identify the components of a block tensor given that their principal directions are known

(iii) there is no simple way of predicting the value of p without resorting to detailed numerical experiments.

The attractions of this technique are its simplicity, the bounded range of p values, and that it can be used in 2-D and 3-D.

3.1.3. Renormalization

The so-called real-space renormalization technique, primarily developed for the study of critical phenomena in physics, such as percolation (Kirkpatrick, 1973; Wilson, 1979; shah and Ottino, 1986) was applied for the first time to the computation of bock conductivities by King (1989). The technique is based on the calculation of the block conductivity of a very small block (as small as 2 by 2 cells in 2-D) and then successively upscaled using self-repetitive geometry until the final block size is reached. The technique is extremely fast and is not limited by the domain size or variance of the cell conductivities. The speed of the technique relies on an analytical expression of the block conductivity for a 2 by 2 block, which is borrowed from the expression of the electrical conductance of a 2 by 2 resistor network. Initially King

(1989) applied renormalization to 2-D grids of spatially uncorrelated values. Later Shah and Ottino (1986) extended the technique to 3-D and Mohanty and Sharma (1990) to correlated fields. The method provides excellent results (when comparing flow simulations at the measurement and block scales) for statistically isotropic, lognormal conductivity fields. For strongly anisotropic media (such as sand-shale formations) the method did not perform well due to the poor resolution of the successive upscaling around the edges of the shales.

Williams (1989) developed a large cell method based on renormalization for the calculation of block conductivities for strongly anisotropic media with a fraction of impermeable material.

The big advantage of renormalization is its speed. The major drawback is that, implicit to the calculation of electrical conductance for a 2 by 2 resistor network in 2-D, there are boundary conditions applied to the sides of each 2 by 2 block which may be unrealistic. Malick (1995) demonstrated that these possibly unrealistic boundary conditions, when repeatedly applied during the course of renormalization, may cause several error in the final block conductivity estimate. He compared block conductivities obtained using Eq. (1) after the solution of the flow equation at the measurement scale. The error is as large as 70% for a lognormal distribution of conductivities when the coefficient of variation reaches 3 and could be up to 200% for sand-shale distributions with shale density of 50%.

3.1.4. Stream-tube

The stream-tube method (Haldorsen and Lake, 1984; Begg and King, 1985; Haldorsen and Chang, 1986; Begg and Carter, 1987; Begg et al., 1985, 1989) is specially designed to calculate block conductivities in sand-shale formation, that is, for formations in which shale's are dispersed in a homogeneous matrix of sandstone, with a large contrast between the conductivities of sand and shale's, so that horizontal shale's can be regarded as barriers for vertical flow. The thickness of the shale's is assumed to be negligible and they are distributed within the sand in a uniform direction (say, horizontally). In the direction parallel to the shale's, given their negligible width, the block conductivity is equal to the sandstone conductivity. In the direction orthogonal to

the shale's, these act as barriers that increase the tortuosity of the streamlines proportionally to the length and frequency of the shale's.

The block conductivity orthogonal to the shale's is related to the streamline lengths through a tortuosity factor. Begg and King (1985) and Begg et al. (1985, 1989) derived an expression of vertical block conductivity as a function of shale proportion and the statistics of shale length. This functional relation provides a block vertical conductivity without knowledge of the exact geometry of the shales within the block.

The stream-tube method has been widely used in the petroleum industry and demonstrated to give good results. However Desbarats (1987) showed that the method overestimates vertical conductivity when shale density is large, that is, when flow paths become very tortuous.

3.1.5. Flow anisotropy

Of the methods presented before, the power average and the stream-tube approach assumed that block conductivity could be a tensor. In the power average approach, the principal directions of the block conductivity are supposed to be parallel to the block sides, and a different power p is used to determine each principal component. In the stream-tube approach, the principal directions of the block conductivity are supposed to be parallel and orthogonal to the shale orientation. In some cases, it is not possible to be sure which are the principal orientations of the block conductivity tensor, nor to assume that all blocks have the same orientation.

Kasap and Lake (1989) were interested in computing block conductivity tensors when cross-bedding is observed at the measurement scale. This is a case in which the directions of the principal components of block conductivity cannot be known a priori, and can vary from block to block. They developed an analytical technique for computing tensor block conductivities for the case of anisotropic conductivities at the measurement scale. Their method is based on the recurrent use of the block conductivity values obtained for a block-composed of two layers of homogeneous but anisotropic conductivities, under the assumption that flow lines are parallel. Equations were obtained for the tensor elements of the block conductivity and were validated using numerical simulations.

3.2. Non-local techniques

Local techniques derive block conductivities which are explicit functional relations of the cell conductivities within the block. However the dependence of the resulting values on some implicit boundary conditions indicates that the block conductivities are non-local, that is, they are not intrinsic to the block, they also depend on the flow conditions within the block, which, in turn, depend on the boundary conditions.

In the non-local techniques discussed next, block conductivity is not given as an explicit expression of the cell conductivities within the block; instead, Eq. (1) is applied directly after determining the vectors of specific discharge $\mathbf{q}_w$ and piezometric head gradient ∇h_w by solving the groundwater flow equation at the measurement scale. The techniques differ in the extent of the area within which flow is numerically solved at the measurement scale, and on the boundary conditions used for the solution. All of these methods are referred to as Laplacian since they are based on the solution of the Laplace equation.

3.2.1. Simple Laplacian

In the simple Laplacian technique, the block being upscaled is isolated from the rest of the blocks in the aquifer. The principal components of the block conductivity tensor are assumed to be parallel to the block sides, and each principal component is computed by numerically solving a flow problem with prescribed heads in the faces of the block orthogonal to the principal direction and impermeable otherwise. Fig. 2 shows the flow problem that has to be solved to determine the x-component of the block conductivity tensor in a two dimensional block. A similar problem has to be solved for the y-component after rotating the boundary conditions 90º.

Application of Eq. (1) to the solution of these problems yields a very simple expression for the components of the block conductivity as the ratio between the average specific discharge through any cross-section orthogonal to a principal direction, and the overall piezometric gradient between the opposite faces at which prescribed heads are applied (Gómez-Hernández, 1991; Sánchez-Vila, 1995).
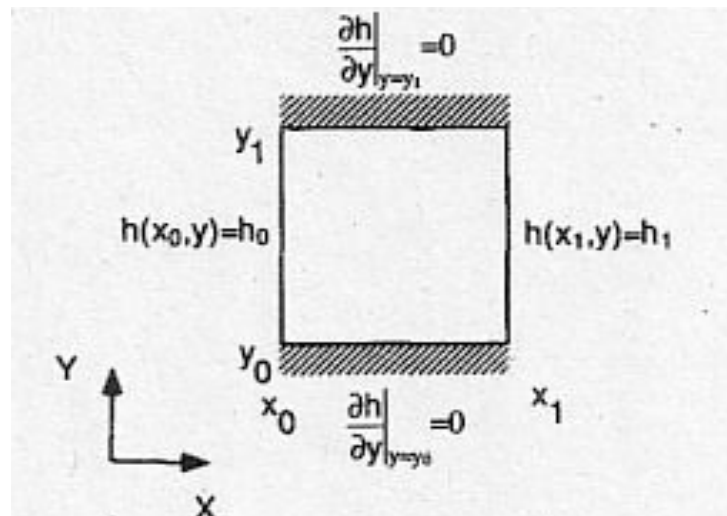
Fig. 2. Boundary conditions used in the simple Laplacian approach. These boundary conditions are used to determine the component $\mathbf{K}_{V,xx}$ of the diagonal block conductivity tensor. The same boundary conditions after rotation of 90º are used to determine the component $\mathbf{K}_{V,yy}$

For the 2-D example in Fig. 2, the expression for the component in the x-direction is

$$K_{V,xx} = -\left(\frac{Q}{y_1 - y_0}\right)\Big/\left(\frac{h_1 - h_0}{x_1 - x_0}\right)$$

where:

Q is the total flow through any cross-section parallel to the y-axis

y_1-y_0 is the block width

h_1-h_0 is the piezometric head drop from face to face

x_1-x_0 is the lock length

Warren and Price (1961) were the first to use this approach. They analyzed random distributions of cell conductivities within the block, and found that the geometric mean was a good approximate of the block conductivities.

The Laplacian techniques suppose a big step towards accuracy in the estimation of block conductivities from the local approaches described previously. However, in this simple Laplacian approach we can criticize the assumption that block conductivity tensors are imposed to have principal components parallel to the block sides, and that the boundary conditions used to solve the flow problems at the measurement scale may be different from the boundary conditions actually existing at the faces of the block in the model.

3.2.2. Simple Laplacian extended

The simple Laplacian method discussed above requires the solution of a small flow problem for each block in the grid. Holden et al. (1989) tries to speed up the method using an iterative approach. If an iterative technique is used for the solution of the flow equation within each block, one could compute, after each iteration, an estimate of the block conductivity tensor components from the h_w and the $\mathbf{q}_w$ values at the current iteration. He key idea is to stop the iterations before the solution to the flow equation converges, under the conjecture that the block conductivity tensor components converge faster than the piezometric head distribution. In their example of 2-D rectangular blocks, they found that with many less iterations than needed for the convergence of piezometric heads, block conductivity tensors converge to a stable solution. Holden and Lia (1992) further extended this technique to calculate full block tensors in 3-D.

3.2.3. Laplacian using flow solution at the measurement scale over the entire aquifer

The boundary conditions used in the simple Laplacian approach are arbitrarily set to help compute directional conductivities in the directions parallel to the block sides. It would be better to use boundary conditions as close as possible to those existing around the block when the flow equation is solved at the measurement scale over the entire aquifer. But, knowledge of the boundary conditions around the block sides requires the solution of the flow equation at the measurement scale over the entire aquifer, defeating the purpose of upscaling, which is to obtain a coarse description of block conductivities to alleviate the cost of solving the flow equation at the measurement scale.

There is one justification for the solution of the flow equation at the measurement scale in order to obtain block conductivities: when block conductivities are to be used as input parameters for multiphase flow modelling. The advent of fast workstations, the computer resources available to petroleum engineers and their interest in accurate predictions of multiphase flow simulations prompted the development, in the petroleum literature, of a series of techniques for the computation of (saturated) block conductivities using the distribution of ∇h_w and $\mathbf{q}_w$ within the block resulting from the solution of the (single-phase) flow equation at the measurement scale over the entire aquifer.

In the quest for accurate block conductivities, it was understood that assuming the principal components of the block conductivity parallel to the block sides was not justified. Therefore, techniques to determine block conductivity tensors with arbitrary orientations of their principal directions had to be developed.

White (1987) and White and Horne (1987) were the first to propose a technique to determine full non-diagonal block conductivity tensors, and the first to suggest that Eq. (1) should be used with values of ∇h_w and $\mathbf{q}_w$ from the solution of the flow equation at the measurement scale over the entire aquifer. In their 2-D exercise, they propose to use the following equation to determine the block conductivity, for each block:

$$\begin{pmatrix} \overline{q}_{w,x} \\ \overline{q}_{w,y} \end{pmatrix} = - \begin{pmatrix} K_{V,xx} & K_{V,xy} \\ K_{V,yx} & K_{V,yy} \end{pmatrix} \cdot \begin{pmatrix} \nabla \overline{h}_{w,x} \\ \nabla \overline{h}_{w,y} \end{pmatrix}$$

where:

      the overbar is used to indicate spatial average within the block

      $q_{w,x}$, $q_{w,y}$, $\nabla h_{w,x}$ and $\nabla h_{w,y}$ are the respective components of vectors $\mathbf{q}_w$ and ∇h_w

      $K_{V,xx}$, $K_{V,xy}$, $K_{V,yx}$ and $K_{V,yy}$ are the tensor components of $\mathbf{K}_V$

The problem with this approach is that the above linear system contains two equations and four unknowns, leaving the definition of the block conductivity undetermined. White and Horne suggested that the problem could be overcome by solving the flow

equation n times at the numerical scale, varying the boundary conditions applied to the entire aquifer. The resulting over-determined set of 2n linear equations is solved by least-squares. The need to use several boundary conditions detaches the computation of the block conductivity tensor from a specific regional flow pattern, thereby producing block tensors that perform well under different flow scenarios.

White and Horne's approach succeeds in obtaining full non-diagonal tensors, and in accounting for aquifer-scale boundary conditions. The major drawback is that it is computationally intensive and that for large aquifers it may be impractical, especially in 3-D.

Pickup et al. (1992) considered that it would be more convenient to try to determine the block conductivity tensor for specific boundary conditions existing at the aquifer scale, instead of producing tensors that are applicable to a wide range of flow conditions. Their argument is that such an approach should yield more accurate block conductivities for the specific flow scenario of interest, with the drawback that the upscaling should be repeated if aquifer conditions change. After solving the flow equation at the measurement scale over the entire aquifer, the boundary conditions at the sides of each block are determined. These boundary conditions are the ones that should be used to solve the flow equation within the block and, by application of Eq. (1), yield the block conductivity tensor. The problem is, as stated before, that solutions of the flow equation corresponding to at least two boundary conditions are necessary to determine uniquely the four components of a 2-D block conductivity tensor. Pickup et al. (1992) proposed solving two flow problems for each block, with boundary conditions derived from the correct boundary conditions by perturbing them enough to produce a different flow pattern within the block but without deviating too much from the correct values. The major drawback of this approach is the high sensitivity of the resulting block conductivities to the magnitude of the perturbation and the difficulty of selecting an appropriate perturbation value.

Another approach based on the solution of the flow equation at the measurement scale with global boundary conditions was developed by Yamada (1995) and will be discussed later in relation to block geometry definition.

3.2.4. Laplacian with skin

To reduce the computer time in White and Horne's method, Gómez-Hernández (1990, 1991) presented another Laplacian approach inspired by that of White and Horne (1987). His method also yields full block conductivity tensors, and attempts to impose realistic boundary conditions on the sides of the block to determine the cell-specific discharges and piezometric head gradients. Instead of solving the flow equation at the measurement scale over the entire aquifer, the flow equation is solved over an area (or volume in 3-D) comprising the block plus a "skin" region. The size of the skin region was arbitrarily set to one-half of the block size in each direction. As in White and Horne (1987), the flow equation must be solved for at least two sets of boundary conditions applied to the outer sides of the skin area in order to determine the block conductivity tensor components. Gómez-Hernández chose to use four sets of boundary conditions as shown in Fig. 3, forcing flow parallel to the block sides and the block diagonals. He showed that this method works well for a variety of heterogeneous formations (isotropic, anisotropic and sand/shale distributions). Holden and Lia (1992) extended this technique to 3-D.
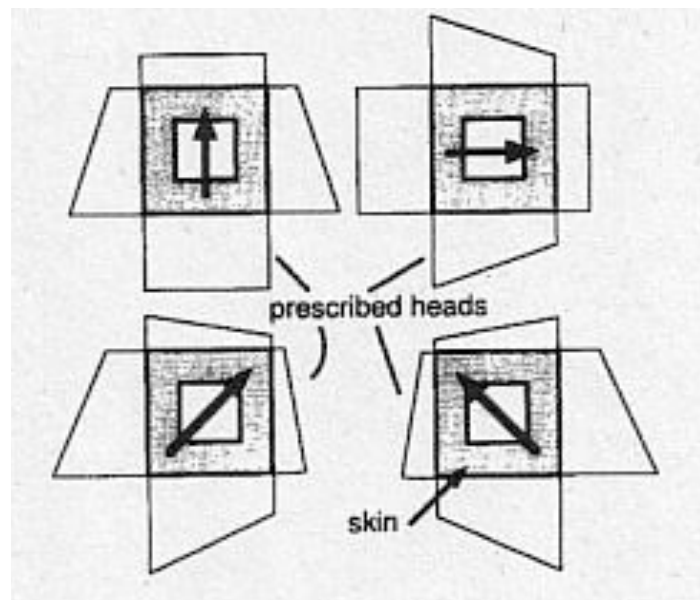
Fig. 3. Boundary conditions used in the Laplacian with skin approach. For each of the four sets of boundary conditions, flow is solved at the measurement scale within an area that contains the block and a "skin" around of half the block size in each direction

3.2.5. Laplacian with periodic boundary conditions

Neither White and Horne (1987) nor gómez-Hernández (1990, 1991) constrain the block conductivity tensor to be positive-definite and symmetric. Conductivity tensors must be positive-definite, otherwise water could move in the direction of increasing piezometric heads. Whether block conductivity tensors must be symmetric is a subject of debate not yet resolved.

Durlofsky and Chung (1990) and Durlofsky (1991) present a Laplacian approach that always yields symmetric and positive definite block conductivity tensors. The novelty of their method is to use the type of boundary conditions that would result from a "periodic" aquifer made up by the repetition in space of the block being upscaled. The method is based on the assumption that the spatial heterogeneity of measurement-scale conductivities occurs at two scales, a large-scale variability that defines the long trends in conductivity variation and a small-scale variability that is periodic in space. The periodicity of the aquifer description implies full correspondence between heads and flows at opposite sides of the block.

The block equation within each block is solved for two orthogonal directions of the overall head gradient. Then, Eq. (1) is established for each solution, resulting in four equations with four unknowns. Durlofsky proves that the solution of these set of equations always yields a symmetric and positive-definite tensor (i.e. $K_{V,xy} = K_{V,yx}$, $K_{V,xx} K_{V,yy} - K_{V,xy} K_{V,yx} \geq 0$). This approach provides exact analytical results for $\mathbf{K}_V$ for truly periodic media. For non-periodic media, the method is theoretically valid if the block size is much larger than the scale of the heterogeneity at the measurement scale.

Comparisons made by Pickup et al. (1992, 1994) showed that Durlofsky's approach is quite accurate and robust even for situations in which periodic boundary conditions do not strictly apply.

3.2.6. Non-parallel flow

The dependence of block conductivities on the boundary conditions applied to the block is evident at this stage. However, all the methods described up to this point use boundary conditions that impose parallel flow through the block. Desbarats (1992a)

studied the problem of determining block conductivities under radial flow. More precisely, he determined a scalar block conductivity to be assigned to a heterogeneous block with a constant-rate well at its centre when prescribed and constant piezometric heads are applied to the block boundaries.

Using an empirical approach he concludes that, in 2-D, a weighted geometric average of the cell conductivities, with weights proportional to the inverse of the squared distance to the well, yields good results for low to moderate variance of log-conductivity. Desbarats (1993) also studied the problem of computing block conductivities for blocks containing two wells in a dipole configuration. For this case, he found that the interwell conductivity approximates to the harmonic mean of the conductivities averaged over circular regions centered at each well.

3.2.7. Analytical approaches

Rubin and Gómez-Hernández (1990) derived, and validated numerically, an analytical expression for 2-D block conductivities for the case of a block embedded in a heterogeneous infinite aquifer with constant specific discharge specified at infinity. Cell conductivities were assumed to be a scalar with an isotropic spatial correlation. It was also assumed that, as a consequence of the latter, block conductivities were also scalar. Under these conditions block conductivity becomes:

$$K_V = K_g\left[1 + \overline{Y'} + \frac{\overline{Y'^2}}{2} + \frac{1}{j_a}\left(\overline{Y'j'_x} - \overline{Y'}\,\overline{j'_x}\right)\right] \qquad (2)$$

where:

K_g is the geometric mean of conductivity over the entire aquifer

The overbar indicates spatial average values over the block V

Y' is the fluctuation of $Y = \ln(K_w)$ with respect to its mean

j_a is the magnitude of the mean piezometric head gradient (which is supposed to be parallel to the x-axis)

j'_x is the fluctuation of the x component of the gradient ∇h_w

This expression, which is only valid for small variances of Y, shows clearly the dependence of the block conductivity on the flow conditions within the block through the terms containing j'$_x$.

Sáez et al. (1989) also provided an analytical expression for block conductivities using the multiple scale method. They considered two observation scales. At the larger scale, the small scale heterogeneity is assumed to be non-detectable, and hydraulic conductivity varies smoothly. At the smaller scale, the heterogeneity of the medium is apparent and hydraulic conductivity varies rapidly and erratically in space. At any given location, the hydraulic conductivity is expressed as the sum of a large scale value plus a perturbation due to the heterogeneity at the smaller scale. Similarly, the hydraulic head is expressed as the sum of the large scale value plus a perturbation. Conductivity for a block much larger than the small scale of theterogeneity is defined as the tensor $\mathbf{K}_V$ for which the large scale component of the hydraulic head satisfies a mass conservation equation:

$$\nabla \cdot \left(\mathbf{K}_V \cdot \nabla h^{(0)} \right) = 0$$

where:

$h^{(0)}$ is the large scale component of the hydraulic head.

Sáez et al. (1989) solved the above equation for the case of a periodic aquifer with unit period being the block for which the equivalent conductivity is sought. They obtained the following expression for block conductivity:

$$\mathbf{K}_V = \mathbf{K}_A + \mathbf{t} \tag{3}$$

that is, block conductivity is the sum of the arithmetic average $\mathbf{K}_A$ and a tortuosity tensor defined by the following spatial average:

$$\mathbf{t} = \frac{1}{V} \int_V \mathbf{K}_w \cdot \nabla \mathbf{g} \, dV$$

where the vector function $\mathbf{g}$ satisfies the boundary-value problem:

$$\nabla \cdot \left(\mathbf{K}_w \nabla \mathbf{g} \right) = -\left(\nabla \cdot \mathbf{K}_w \right) \tag{4}$$

with $\mathbf{g}$ periodic in the unit cell.

The problem with the analytical solution of block conductivity given by Sáez et al. is that it is limited to blocks larger than the scale of the erratic variability of cell conductivities. Furthermore, it requires the permeable medium to be periodic with period equal to the block size.

3.2.8. Method of moments

Kitanidis (1990) used a definition for block conductivity different from that of Eq. (1). His definition is based on the method of moments, first formulated by Aris (1956) and later generalized by Brenner (1980). In the method of moments the definition of block conductivity differs from that in Eq. (1). Instead of trying to find the block conductivity that relates average flow to average gradient, the objective is to find a block value that matches the spatial moments of the hydraulic head in the heterogenous medium as explained below. This definition requires the solution of a transient problem as opposed to the steady-state solution on which Eq. (1) relies. The application of the method of moments is better understood with a example. Consider an infinite 2-D aquifer with constant hydraulic conductivity in which a Dirac pulse in the hydraulic head is introduced at time zero, at the origin. The solution of the transient dissipation of the pulse is given by a Gaussian bell:

$$h(\mathbf{x},t) = (2\pi)^{-3/2} |2\mathbf{D}t|^{-1/2} \exp\left(-\mathbf{x}\mathbf{D}^{-1}\mathbf{x}/4t\right)$$

where:

    t is time

    $\mathbf{D} = \mathbf{K}/S$ is called the diffusivity tensor

    S is the specific storage coefficient

The second moment of the function $h(\mathbf{x},t)$ with respect to the origin is the "moment of inertia" and is given by

$$\Delta(t) = \int \mathbf{x} \cdot \mathbf{x} h(\mathbf{x},t) d\mathbf{x} = 2\mathbf{D}t$$

Note that half the rate of change of the second moment is given by $(1/2)d\Delta(t)/dt = \mathbf{D}$. In the method of moments, the evolution of a Dirac pulse of piezometric head at the origin is solved in the heterogeneous block, and the rate of change of the second moment is identified with the diffusivity tensor of the homogeneous equivalent block conductivity value.

To solve for the evolution of the Dirac pulse some hypotheses are needed. First, the aquifer is assumed to be periodic with a period much larger than the scale of variability of $\mathbf{K}_w$. Second, the moments are defined at two scales (similarly to Sáez et al. (1989); only the moments at the larger scale are of interest. And third, only slowly varying flow is considered. Under these hypotheses the resulting expression for $\mathbf{K}_V$ is very similar to the expression obtained by Sáez et al. (1989). The block conductivity tensor is equal to its arithmetic spatial average plus an integral term equivalent to the tortuosity term in Eq. (3). This integral term is written in terms of a function g that must satisfy a boundary value equivalent to that in Eq. (4).

Dykaar and Kitanidis (1992a,b) discuss a numerical technique for the efficient solution of the boundary value problem (4), called the numerical spectral method. This method has the same drawbacks as the one by Sáez et al. (1989): it is limited to large blocks and requires the assumption that the medium is periodic with period equal to the block size.

3.2.9. Energy dissipation

Indelman and Dagan (1993a,b) and Bϕe (1994) used the concept of energy dissipation to define block conductivity tensors. Energy dissipation is defined as the energy per unit time necessary to force the fluid through the porous medium. A necessary condition on the block conductivity value is that it should produce the same energy dissipation as the heterogeneous block. Bϕe (1994) showed that with this definition, and periodic boundary conditions applied to the sides of the block, the resulting block conductivities coincide with those of Durlofsky (1991). Indelmann and Dagan (1993a,b) were more interested in obtaining the statistical properties of the upscaled blocks, than in the one-to-one relationship between each block and the cell conductivities within. Their approach is mentioned later when discussing the direct generation of block conductivities.

3.3. Block Geometry

All of the methods discussed above investigate upscaling of grids made up of rectangular blocks; none of them has been extended to the case of non-rectangular grids. Much effort has been devoted to computing block conductivities for heterogeneous blocks without paying much attention to the geometry of the blocks. One should not forget that upscaling is not an objective per se: the objective of upscaling is to use the block values for the simulation of (single o multiphase) flow and, possibly, mass transport. Some of the more elaborate Laplacian methods provide, for a fixed block geometry, the best block conductivity estimates one can get. In order to improve these estimates, we should try to optimize the geometrical definition of the blocks.

No matter how good an upscaling method is, it always involves an averaging of the flow problems that filters out some of the details of flow within the block. One can attempt to devise a technique to define the geometry of the blocks so that the averaging implicit in upscaling is minimal in the areas in which the details of flow behaviour are most consequential to the final objective. For instance, if the final objective is to simulate mass transport and early mass arrivals are most consequential, a geometry definition of the blocks trying to delineate fast channels will reduce the impact of the loss of resolution on the prediction of early mass arrivals (e.g. Durlofsky et al., 1994a,b).

Although gridding for flow simulation is an old subject, gridding techniques for flow simulation in conjunction with upscaling are relatively recent. In this section we describe four of these techniques.

3.3.1. Elastic grid

Garcia et al. (1990) introduced the concept of an "elastic grid". They devised an algorithm that starts from an uniform square grid of the aquifer, and then displaces the corners of the blocks with the objective of minimizing the heterogeneity of the cell conductivities within the blocks. Each edge connecting two vertices is assigned an elasticity coefficient that is made a function of the cell conductivity variance of adjoining blocks. The potential energy of each edge is proportional to the square of its

length and its elasticity coefficient. The block vertices are adjusted in an iterative manner until the total potential energy is minimized. This approach results in an irregular grid with blocks that are mildly heterogeneous, and for which simple upscaling techniques should provide good results. A typical grid is shown in Fig. 4.

Farmer et al. (1991) devised a method similar to Garcia et al. in which the optimization is carried out by simulated annealing. Robey (1995) introduced an elastic gridding approach in which the objective to be met by the final grid was related to a global measure of heterogeneity, instead of a local measure as in the approach of Garcia et al.
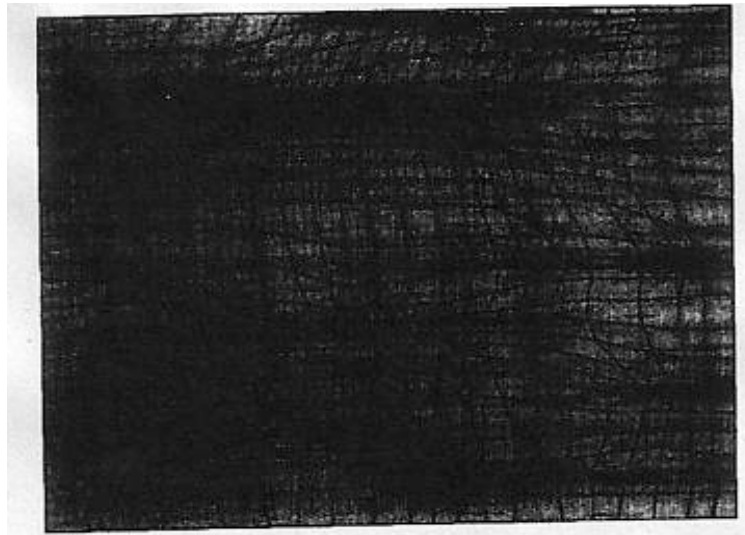
Fig. 4. Elastic grid. A typical elastic grid obtained using the Garcia et al. (1990) method, where the objective is to minimize the cell conductivity heterogeneity within each block. The grid at the measurement scale contains 200 by 150 cells. The grid at the numerical scale contains 30 by 30 blocks. Dark cells indicate high conductivity values

3.3.2. Elastic grid with flow variables

The elastic grid approaches discussed above do not incorporate flow variables for the determination of the block geometries. Tran (1995) and Tran and Journel (1995) realized that minimization of the variance of cell conductivities within the blocks does not ensure that fast flow paths are preserved in the upscaled model. There is a need to define the block geometry as a function of the flow variables. Tran and Journel proposed an extension of White and Horne's (1987) Laplacian method. After solution of

the flow equation at the measurement scale over the entire aquifer, the block geometries are determined by the Garcia et al. (1990) elastic gridding algorithm bit applied to the stream function values. The coefficient of elasticity of any segment joining two vertices is now a function of the variance of the stream values at adjoining blocks. In this way, they ensure that the density of streamlines is approximately constant within each block. Consequently, blocks are small in regions of high flow velocity and large where flow velocity is small. From the point of view of flow and transport at the aquifer scale, Tran and Journel's approach gives better results than those of Garcia et al.

3.3.3. Simplified elastic grid with flow variables

The previous method, although superior to the original method of Garcia et al. (1990), has the same drawbacks as White and Horne's (1987): the flow equation has to be solved at the measurement scale over the entire aquifer, in order to know the streamline function in the cells. Tran's approach is computationally intensive and cannot be used for large aquifers. To solve these problems, Wen (1996) implemented a variation that does not require the solution of the flow equation at the measurement scale. He proposed an iterative approach in which both block conductivities and block geometries are updated at each iteration. His method starts with an elastic grid obtained using the Garcia et al. (1990) method in its original implementation, that is, minimizing the heterogeneity of cell conductivities within the blocks.

Then, an extension of Durlofsky's (1991) Laplacian method for irregular blocks is used to determine block conductivity tensors. The flow equation is solved at the numerical scale (not the measurement scale) using the geometry definition and the block conductivities from the previous iteration. With this solution, velocities are computed in each cell of the aquifer, and the Garcia et al. elastic gridding algorithm is used to redefine the block geometry, with the difference that the potential energy of edges is now proportional to the variance of flow velocity on adjoining blocks, instead of to the variance of cell conductivities. With the new geometry, a new iteration starts: block conductivities are re-computed, and flow is again solved at the numerical scale. The iterative process stops when neither the block geometries nor the block conductivities change substantially from one iteration to the next. This method gives results as good as

Tran's (1995) at a fraction of the cost. Its major drawback is that there is no theoretical proof of convergence of the technique, although for the cases in which it has been tested, convergence was always reached.

3.3.4. Potential-streamfunction space discretization

Yamada (1995) approached the upscaling process with a different perspective. He accepts that the boundary conditions of the simple Laplacian (Fig. 2) may depart frim the actual boundary conditions around the perimeter of the blocks. However, instead of trying to refine the boundary conditions and make them closer to the ones that the blocks actually have when embedded within the aquifer, he searches for the block geometries for which the simple boundary conditions in Fig. 2 apply. These block geometries can easily be defined if the gridding is carried out in the potential stream-function space. After solving the flow equation at the measurement scale, the results are mapped to the potential-streamfunction space. In this space, each block is defined as a rectangle, thus ensuring that in two opposite faces the streamfunction is constant, and in the other two opposite faces the fluid potential is constant. With this definition, the use of now-flow boundary conditions in two sides of the block, and prescribed head conditions in the other two sides, is completely justified. Furthermore, since flow cannot cross streamlines, there is no need to compute any component of the block conductivities in the direction orthogonal to the bounding streamlines (no-flow boundaries). Yamada found that flow simulations performed in the reshaped grid system successfully reproduce the single-phase head distributions and produce reasonable approximations for head and saturation on two-phase problems.

Although this technique is attractive, it has three major drawbacks:

(i)   it has been devised in 2-D and its extension to 3-D is not trivial owing the difficulty of computing streamtubes in 3-D

(ii) the reshaping done in the potential-streamfunction space requires that the streamfunction be single-valued at each location – if point sinks or sources are present, the streamfunction will be multi-valued at the well locations

(iii) it requires the solution of the flow equation at the measurement scale over the entire aquifer

3.4. Direct block conductivity generation

Reconsidering again that the objective of upscaling is the solution of the flow equation at the numerical scale, some authors have concluded that the generation of grids at the measurement scale (Fig. 1(a)), with the sole purpose of upscaling them to produce a block conductivity model, is a waste of resources. The question that these authors have considered is: can block conductivities be generated directly from a few data at the measurement scale, thus avoiding the generation of the measurement scale grid values and the time consuming step of block upscaling, and yet displaying the same characteristics observed in the upscaled models obtained with the other techniques? Fig. 5 sketches this concept. In the top row, the so –called two-step approach (Gómez-Hernández, 1991) is depicted: from a set of measurements, a set of realizations of conductivities is generated at the measurement scale; these realizations are upscaled to the numerical scale, and flow is solved in each of them to arrive at a set of realizations of the spatial distribution of hydraulic conductivity within the aquifer. In the bottom row, the direct simulation approach is depicted: the initial and final points are the same as in the two-step approach, the difference is that the block values are generated directly from the measurements.
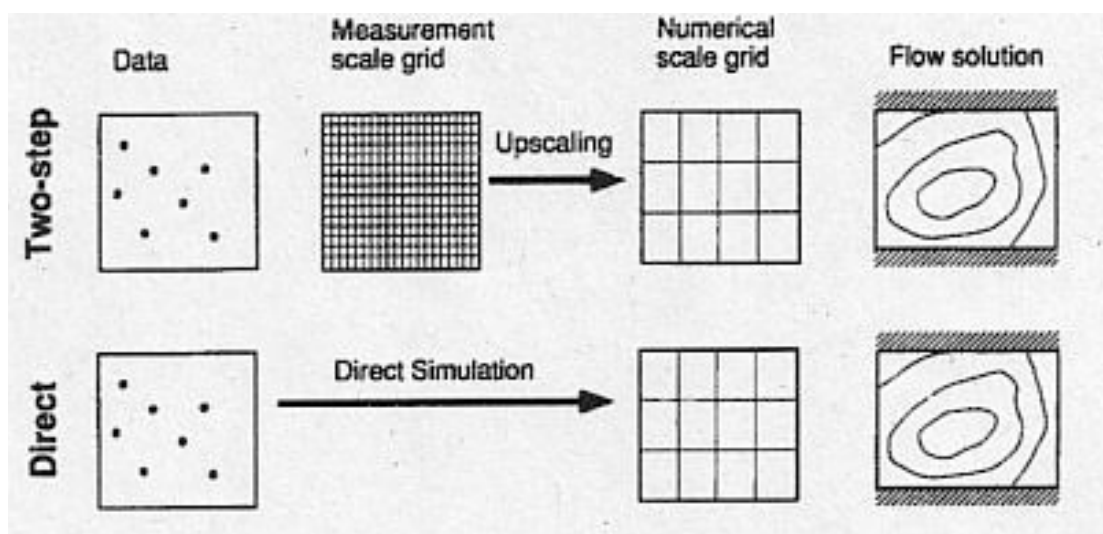
Fig. 5. Two-step versus direct simulation. In the top row, the two-step approach; at the bottom, the direct simulation approach.

3.4.1. Scalar block conductivities

Rubin and Gómez-Hernández (1990) were the first to approach this problem analytically. Taking as a starting point the analytical result of their upscaling technique (Eq. (2)), they computed what should be the expected value and covariance of block conductivities, as well as the cross-covariance between cell and block conductivity values. With these statistics and the hypothesis that the multilognormality assumed for the cell conductivities is preserved after upscaling, they could proceed to the generation of scalar block conductivities conditioned on cell measurements by any standard geostatistical technique. Their method is limited by the assumptions used to derive Eq. (2), namely the isotropic spatial variability of cell conductivities, small variability of log-conductivity, and the assumption that block conductivity is a scalar.

3.4.2. Training images

To overcome the problems of the previous approach, Gómez-Hernández (1990, 1991) proposed the inference of the cell to block covariance's through the use of a training image. The idea is to start by generating a "training grid" at the measurement scale, on which any of the upscaling methods described in the previous sections is used to determine the block conductivity tensors. At this stage, two realizations are available, one with cell conductivities and the other with the corresponding block conductivity tensors; from these two realizations, the cross- and auto-covariances among the cells and the components of the block conductivity tensors can be experimentally inferred. Once the training image has been used to infer these covariances, direct generation of the components of the block conductivity tensor is possible, without the need to resort to upscaling again.

The major disadvantage of this method is that too many auto- and cross- covariances have to be inferred. In 2-D, the number of variables involved, assuming that the block conductivity tensors are symmetric, is four: one for the cell conductivity and three for the block conductivity tensor (the components in the two principal directions and the orientation of the main principal direction). Consequently, the number of covariance's to estimate is nine. In 3-D, in which seven variables would be involved (one for the cells, and six for the tensor), the number of covariance's to infer is 27!

In order to reduce the number of covariances to infer, Tran (1995) proposed to infer the auto- and cross-covariances only for the components of the block conductivity; moreover, he assumed that the principal components of the conductivity tensor are parallel to the block sides, thereby reducing the number of variables to two in 2-D and the number of covariances to three. The conditioning to cell data (for which the cross-covariance cell-block would be required) is resolved through a heuristic approach.

3.4.3. Regularization

Desbarats (1989, 1992b) derived the expected value and variance of block conductivities when these are obtained by power averaging. He used a linear approximation of the log-conductivity obtained by power averaging together with standard regularization techniques (e.g. Journel and Huijbregts, 1978) to compute the expected value ad variance of block values. Desbarats did not pursue the computation of the cell-block covariance, or the block-block covariances, but it would be simple to extend his results to determine these values. Once these covariances are also computed, the direct generation of block conductivities conditional to cell conductivity data is a trivial matter of stochastic co-simulation of multiple variables. The drawbacks of the approach are those stemming from the use of the power-average method to compute block conductivities and from the linearization of the log-conductivity.

3.4.4. Energy dissipation

Using an energy dissipation definition for block conductivity, Indelmann and Dagan (1993a, b) derived the expected value and covariance of the upscaled block values. They stated that imposing the preservation of energy dissipation to compute block conductivities is not enough to enable derivation of a one-to-one relationship between block conductivity and the cell conductivities within. However, they showed that identity between the energies dissipated at the measurement and the numerical scales could be satisfied in a statistical sense. Working under these premises, they proceeded to compute the expected value and covariance of the components of three-dimensional equivalent conductivity symmetrical tensors, arriving, for the most-general three-

dimensional case, at the expressions of six geometrical means and 15 cross-covariances of log-conductivity. These expressions are complex, and the authors indicate the the existence and uniqueness of a solution in the most general case is not proven. However, for the specific cases they analyze, good insight is obtained about the spatial variability of block conductivities. Among their conclusions, they stated that, except for blocks of circular of spherical shape, the block conductivity tensor is always anisotropic. Therefore, in all numerical methods, block conductivities have to be given as a tensor of anisotropic covariance since numerical blocks are never circular or spherical. In their papers, the authors also described the step-by-step procedure for the direct generation of block conductivities. Sánchez-Vila et al. (1995) showed that the method of Rubin and Gómez-Hernández (1990) results in block conductivities which are statistically very similar to those of Indelman and Dagan (1993a, b).

3.4.5. Disadvantages

The direct generation of block conductivities is very appealing since it puts the effort where it is needed, i.e. no time is spent in the generation of grids at the measurement scale and the later upscaling of each block, and block values are generated directly. The main problem of this method is that it can only be applied to blocks of uniform size and cannot benefit from any geometry definition algorithm. The reason is that if different block sizes are considered, conductivity must be considered as a different random variable for each block size. Introducing multiple block sizes would multiply the number of random variables involved and the number of covariances to determine. Only the analytical approaches of Rubin and Gómez-Hernández (1990) and Indelman and Dagan (1993a, b) which provide analytical expressions for block conductivity expressions, could be readily applied to multiple block sizes.

4. Summary

A review of the many existing techniques for conductivity upscaling has been presented. The emphasis of this review has been placed on the methods. An attempt has been made to refer to the seminal papers of each method, and, to the best of our knowledge, all the existing methods for upscaling have been reviewed.

Block conductivities are now understood as not being a material property but dependent on the flow conditions within the block. The observed current line of research in conductivity upscaling focuses on accuracy more than on speed, and on the inclusion of the geometry definition as an integral part of the upscaling process. The idea of direct simulation of block-conductivity, although attractive in concept, needs further testing and refinement.

References – Upscaling of Flow Parameters

Ababou, R. and Wood, E.F., 1990. Comment on "Effective roundwater model parameter values: Influence of spatial variability of hydraulic conductivity, leakage and recharge" by J.J. Gómez-Hernández and S.M. Gorelick, Water Resour. Res. 26(8): 1843-1846.

Aris, R., 1956. On the dispersion of a solute in a fluid flowing through a tube. Proc. R. Soc. London. Ser. A, 235: 67-77.

Bachu, S. and cuthiell, D., 1990. Effects of core-scale heterogeneity on steady state and transient fluid flow in porous media: Numerical analysis. Water Resour. Res., 26(5): 683-874.

Begg, S.H. and King, P.R., 1985. Modelling the effects of shales on reservoir performance: Calculation of effective vertical permeability. Paper SPE 13529.

Begg, S.H., Chang, D.M. and Haldorsen, H.H., 1985. A simple statistical method for calculating the effective vertical permeability of a reservoir containing discontinous shales. Paper SPE 14271.

Begg, S.H. and Carter, R.R., 1987. Assigning effective values to simulator grid-block parameter for heterogeneous reservoir. Paper SPE 16754.

Begg, S.H., Carter, R.R. and Dranfield, P., 1989. Assigning effective values to simulator gridblock parameters for heterogeneous reservoirs. SPE Reservoir Engineering, November: 455-463.

Bøe, Ø., 1994. Analysis of an upscaling method based on conservation of dissipation. Transport in Porous Media, 17(1): 77-86.

Bouwer, H., 1969. Planing and interpreting soil permeability measurements. J. of the Irrigation and Drainage Division of the A.S.C.E., IE(3): 391-402.

Brenner, H., 1980. Dispersion resulting from flow through spatially periodic porous media. Philos. Trans. R. Soc. London, Ser. A, 297 (1498): 81-133.

Cardwell, W.T. and Parsons, R.L., 1945. Averaging permeability of heterogeneous oil sands. Trans. Am. Inst. Min. Metall. Pet. Eng., 160: 34-42.

Clifton, M.P. and Neuman, S.P., 1982. Effect of kriging and inverse modelling on conditional simulation of the Avra Valley aquifer in Southern Arizona. W.R.R., 18(4): 1215-1234

Dagan, G., 1979. Models of groundwater flow in statistically homogeneous porous formations. W.R.R., 15(1); 47-63.

Dagan, G., 1982a. Stochastic modelling of groundwater flow by unconditional and conditional probabilities, 1: Conditional simulation and the direct problem. W.R.R., 18(4): 813-833.

Dagan, G., 1982b. Analysis of flow through heterogeneous random aquifers, 2: Unsteady flow in confined formations. W.R.R., 18: 1571-1585.

Dagan, G., 1985. Stochastic modelling of groundwater flow by unconditional and conditional probabilities, 2: The inverse problem. W.R.R., 21(1): 65-72.

Dagan, G., 1989. Flow and Transport in Porous Formations. Springer-Verlag, New York.

Desbarats, A.J., 1987. Numerical estimation of effective permeability in sand-shale formation. W.R.R., 23(2): 273-286.

Desbarats, A.J., 1989. Support effect and the spatial average of transport properties. Math. Geology, 21(3): 383-389.

Desbarats, A.J., 1992a. Spatial averaging of transmissivity in heterogeneous fields with flow toward a well. W.R.R., 28(3):757-767.

Desbarats, A.J., 1992b. Spatial averaging of hydraulic conductivity in three-dimensional heterogeneous porous media. Math. Geology, 24(3): 249-267.

Desbarats, A.J., 1993. Geostatistical analysis of interwell transmissivity in heterogeneous aquifers. W.R.R., 29(4): 1239-1246.

Desbarats, A.J. and Dimitrakopoulos, R., 1990. Geostatistical modelling of transmissivity for two-dimensional reservoir studies. SPE formation Evaluation, Dic.: 437-443.

Deutsch, C., 1989. Calculating effective absolute permeability in sandstone/shale sequences. SPE Formation Evaluation, September: 343-348.

Deutsch, C. and Journel, A.G., 1992. GSLIB: Geostatistical Software Library and User's Guide. Oxford University Press, New York, 340 pp.

Durlofsky, L.J. and Chung, E.Y., 1990. Effective permeability of heterogeneous reservoir regions. 2nd European Conference on the Mathematics of Oil Recovery, Paris, 1990, pp-57-64.

Durlofsky, L.J., 1991. Numerical calculation of equivalent grid block permeability tensors for heterogeneous porous media. W.R.R., 27(5): 699-708.

Durlofsky, L.J:, 1992. Representation of grid block permeability in coarse scale models of randomly heterogeneous porous media. W.R.R., 28(7): 1791-1800.

Durlofsky, L.J., Jones, R.C. and Milliken, W.J., 1994a. A new method for the scale up of displacement processes in heterogeneous reservoirs. 4th European Conference on the Mathematics of Oil Recovery, Roros, Norway, June, 1994.

Durlofsky, L.J., Milliken, W.J., Dehghani, K. and Jones, R.C., 1994b. Application of a new scale up methodology to the simulation of displacement process in heterogeneous reservoirs. SPE International Petroleum Conference & Exhibition of Mexico, Veracruz, October 1994.

Dykaar, B.B. and Kitanidis, P.K., 1992a. Determination of the effective hydraulic conductivity for heterogeneous porous media using a numerical spectral approach, 1: Method. W.R.R., 28(4): 1155-1166.

Dykaar, B.B. and Kitanidis, P.K., 1992b. Determination of the effective hydraulic conductivity for heterogeneous porous media using a numerical spectral approach, 2: Application. W.R.R., 28(4): 1167-1178.

Farmer, C.L., Heath, D.E. and Moody, R.O., 1991. A global optimization approach to grid generation. 11th SPE Symposium on Reservoir Simulation, Anaheim, CA, February 1991, pp. 341-350.

Fayers, F.J. and Hewett, T.A., 1992. A review of current trends in petroleum reservoir description and assessment of the impacts on oil recovery. Adv. In Water Resources, 15(4): 341-365.

Garcia, M.H., Journel, A.G. and Aziz, K., 1990. An automatic grid generation and adjustment method for modelling reservoir heterogeneities. Report 3, Stanford Center for Reservoir Forecasting, Stanford, CA.

Garcia, M.H., Journel, A.G. and Aziz, K., 1992. Automatic grid generation for modelling reservoir heterogeneities. SPE Reservoir Engineering: 278-284.

Gelhar, L.W. and Axnexx, C.L., 1983. Three-dimensional stochastic analysis of macrodispersion in aquifers. W.R.R., 19(1): 161-180.

Gómez-Hernández, J.J. and Gorelick, S.M., 1989. Effective groundwater model parameter values: Inference of spatial variability of hydraulic conductivity, leakance and recharge. W.R.R., 25(3): 405-419.

Gómez-Hernández, J.J., 1990. Simulation of block permeability conditioned upon data measured at a different scale. In: ModelCARE 90: Calibration and Reliability in Groundwater Modelling. IAHS Publ. no. 195, pp. 407-416.

Gómez-Hernández, J.J., 1991. A stochastic approach to the simulation of block conductivity fields conditioned upon data measured at a smaller scale. Ph. D. thesis, Stanford University, CA.

Gómez-Hernández, J.J. and Wen, X.H., 1994. Probabilistic assessment of travel times in groundwater modelling. J. Stochastic Hydrology and Hydraulics, 8(1): 19-55.

Grindheim, A.O., 1990. An evaluation of homogeneization techniques for estimating effective absolute block permeability by use of a stochastic reservoir description simulator. Master thesis, Norwegian Institute of Technology (NTH).

Gutjahr, A.L., Gelhar, L.W., Bakr, A.A. and MacMillan, J.R., 1978. Stochastic analysis of spatial variability in subsurface flows, 2: Evaluation and application. W.R.R., 14(5): 953-959.

Haldorsen, H.H. and Lake, L.W., 1984. A new approach of shale's management in field scale simulation models. Soc. Of Petrol. Eng. Jour., 24 (August): 447-457.

Haldorsen, H.H., 1986. Simulation parameters assignment and the problem of scale in reservoir engineering. In: Lake, L.W. and Carroll, H.B. (eds.), Reservoir Characterization. Academic Press, pp. 445-485.

Haldorsen, H.H. and Chang, D.M., 1986. Notes on stochastic shale's; from outcrop to simulation model. In: Lake, L.W. and Carroll, H.B. (eds.), reservoir Characterization. Academic Press, pp-445-485.

Hoeksema, R.J. and Kitanidis, P.K., 1984. An application of the geostatistical approach to the inverse problem in two-dimensional groundwater modelling. W.R.R., 20(7): 1003-1020.

Hoekssema, R.J. and Kitanidis, P.K., 1985. Comparison of Gaussian conditional mean and kriging estimation in the geostatistical solution of the inverse problem. W.R.R., 21(6): 825-836.

Holden, L., Hoiberg, J. and Lia, O., 1989. Homogeneization of absolute permeability. Norwegian Computer Centre (NCC) Report.

Holden, L. and Lia, O., 1992. A tensor estimator for the homogeneization of absolute permeability. Transport in Porous Media, 8: 37-46.

Indelman, P. and Dagan, G., 1993a. Upscaling of permeability of anisotropic heterogeneous formations, 1: The general framework. W.R.R., 29(4): 917-923.

Indelman, P. and Dagan, G., 1993b. Upscaling of permeability of anisotropic heterogeneous formations, 2: General structure and small perturbation analysis. W.R.R., 29(4): 925-933.

Journel, A.G., Deutsch, C. and Desbarats, A.J., 1986. Power averaging for block effective permeability. SPE 15128.

Journel, A.G. and Huijbregts, C.J., 1978. Mining Geostatistics. Academic Press, London.

Kasap, E. and Lake, L.W., 1989. An analytical method to calculate the effective permeability tensor of a grid block and its application in an outcrop study. SPE 18434.

King, P.R., 1989. The use of renormalization for calculating effective permeability. Transport in porous Media, 4(1): 37-58.

Kirkpatrick, S., 1973. Percolation and conduction. Rev. Mod. Phys., 45(4): 574-588.

Kitanidis, P.K., 1990. Effective hydraulic conductivity for gradually varying flow. W.R.R., 26(6): 1197-1208.

Lake, L.W., 1988. The origins of anisotropy. J. of Petroleum Tech.: 395-396.

Malick, K.M., 1995. Boundary effects in the successive upscaling of absolute permeability. Master thesis, Stanford University, CA.

Mantoglou, A. and Gelhar, L.W., 1987. Effective hydraulic conductivity of transient unsaturated flow in stratified soils. W.R.R., 23(1): 57-67.

Matheron, G., 1967. Éléments pour une théorie des milieux. Mason et Cie.

Mohanty, S. and Sharma, M.M., 1990. A recursive method for estimating single and multiphase permeabilities. SPE paper 20477 presented at the 65th Annual Technical conference and Exhibition in New Orleans, LA, September 23-26, 1990.

Muggeridge, A.H., 1991. Generation of effective relative permeabilities from detailed simulation of flow in heterogeneous porous media. In: Lake, L.W., carroll, H.B. and Wesson, T.C. (eds.), Reservoir Characteriation II. Academic Press, San Diego, pp. 197-225.

Naff, R.L., 1991. Radial flow in heterogeneous porous media: An analysis of specific discharge. W.R.R., 27(3): 307-316.

Neumann, S.P. and Orr, S., 1993. Prediction of steady flow in nonuniform geologic media by conditional moments: Exact nonlocal formalism, effective conductivities, and weak approximation. W.R.R., 29(2): 341-364.

Pickup, G.E., Jensen, J.L., Ringrose, P.S. and Sorbie, K.S., 1992. A method for calculating permeability tensors using perturbed boundary conditions. In 3rd European Conf. on the Mathematics of Oil Recovery, Delft, The Netherlands, June 1992.

Pickup, G.E., Ringrose, P.S., Jensen, J.L. and Sorbie, K.S., 1994. Permeability tensors for sedimentary structures. Math. Geology, 26(2): 227-250.

Poley, A.D., 1988. Effective permeability and dispersion in locally heterogeneous aquifers. W.R.R., 24(11): 1921-1926.

Robey, T.H., 1995. An adaptive grid technique for minimizing heterogeneity of cells or elements. Math. Geology, 27(6): 706-729.

Rubin, Y. and Gómez-Hernández, J.J., 1990. A stochastic approach to the problem of upscaling of conductivity in disordered media: Theory and unconditional numerical simulations. W.R.R., 26(4): 691-701.

Russo, D., 1992. Upscaling of hydraulic conductivity in partially saturated heterogeneous porous formation. W.R.R., 28(2): 397-409.

Sáez, A., Otero, C.J. and Rusinek, I., 1989. The effective homogeneous behavior of heterogeneous porous media. Transport in Porous Media, 4: 213-238.

Sánchez-Vila, X., 1995. On the geostatistical formulations of the groundwater flow and solute transport equations. Ph. D. thesis, Universitat Politécnica de Catalunya, Barcelona, Spain.

Sánchez-Vila, X., Girardi, J.P. and Carrera, J., 1995. A synthesis of approaches to upscaling of hydraulic conductivity. W.R.R., 31(4): 867-882.

Shah, N. and Ottino, J.M., 1986. Effective transport properties of disordered, multiphase composites: Application of real-space renormalization group theory. Chem. Eng. Sci., 41(2): 283-296.

Tran, T.T., 1995. Stochastic simulation of permeability field and their scale-up for flow modelling. Ph. D. thesis. Stanford University, CA.

Tran, T.T. and Journel, A.G., 1995. Automatic generation of corner-point-geometry flow simulation grids from detailed geostatistical descriptions. Adv. of Water Resour.

Warren, J.E. and Price, H.H., 1961. Flow in heterogenous porous media. Society of Petroleum Engineering Journal, 1: 153-169.

Wen, X.H., 1996. Stochastic simulation of groundwater flow and mass transport in heterogenpus formations: Conditioning and problem of scales. Ph. D. thesis, Universidad Politécnica de Valencia, Spain.

White, C.D., 1987. Representation of heterogeneity for numerical reservoir simulation. Ph. D. thesis, Stanford University, CA.

White, C.D. and Horne, R.N., 1987. Computing absolute transmissivity in the presence of fine-scale heterogeneity. Paper SPE 16011, pp. 209-221.

Williams, J.K., 1989. Simple renormalization schemes for calculating effective properties of heterogeneous reservoirs. In: 1st European Conf. on the Mathematics of Oil recovery, Cambridge, UK, July 1989, pp. 281-298.

Wilson, K.G., 1979. Problems in physics with many scales length. Sci. am. 241 (August): 158-179.

Yamada, T., 1995. A dissipation-based coarse grid system and its application to the scale-up of two phase problems. Ph. D. thesis, Stanford University, CA.

Yeh, T.C., Gelhar, L.W. and Gutjahr, A.L., 1985. Stochastic analysis of unsaturated flow in heterogenous soils, 1: Statistically isotropic media. W.R.R., 21(4): 447-456.

PART 2

**UPSCALING OF
TRANSPORT PARAMETERS**

PART 2 – UPSCALING OF TRANSPORT PARAMETERS

A - Upscaling transport parameters under the Fickian Approach

1. Basic definitions and transport processes

Before starting any developments, it is good practice to provide the reader with a clear view of the context of the study and general definitions of the key terms that will be used. The problem of interest is the movement (or transport) of solutes in natural soils. While the general concept of soil is well established, the definition of soil varies, hinging on the perspective of the discipline employing it as a resource. In this work, soil will be defined as an inert material, made of aggregated solid particles in-between which gas and liquids are present.

A solute is a chemical substance that dissolves in the liquid soil water phase. In this study, only ideal inert solutes that do not undergo decay will be considered. Furthermore, the solute will be assumed to be present in sufficiently low concentration for density effects to be neglected. No chemical process such as hydrolysis, oxydation or interaction with other dissolved species will be considered, nor will biological processes (biodegradation, biotransformation, …). The solute will be assumed to move in a saturated porous medium, i.e. the presence of air as a third phase will not be considered neither.

Basically, three main physical processes control solute transport in the soil : advection, diffusion and mechanical dispersion.

Firstly, advection is mass transport caused by bulk movement of flowing groundwater.

If no other process occurs, then contaminant plumes are simply translated at groundwater velocity. The driving force is the hydraulic gradient and the average transport velocity can be calculated as the Darcy flux divided by the volumetric proportion of mobile fluid in the soil also called effective porosity.

The advective solute mass flux in direction i can be written as

$$q_i^A = v_i C$$

where C [g/m^3] is the solute concentration. This process will play an important role in heterogeneous formations, where velocity fluctuations cannot be neglected.

As spatial concentration gradients exist, diffusion is the net flux of solutes from zones of higher concentration to zones of lower concentration. Diffusion does not depend on any bulk movement of the solution and will occur even if pore water is at rest. The diffusive solute mass flux in direction i [g/m^2/s]) can be described by Fick's first law of diffusion

$$q_i^d = -D^d \frac{\partial C}{\partial x_i}$$

where x_i is the coordinate in direction i and D^d [m^2/s] is an effective diffusion coefficient being related to the molecular diffusion coefficient in liquid phase. At low pore-water velocities, such as in clayey soils, solute transport is dominated by diffusion.

Finally, there is a tendency for solutes to spread out from the flow lines that it would be expected to follow according to the advective hydraulics of the flow system, leading to apparent diffusion coefficients that are higher by several orders of magnitude. This spreading phenomenon is usually called mechanical dispersion and is caused entirely by differential microscopic velocities in the pore space (due, for example, to the non-uniform velocity profile within a pore and to variations in pore diameter and in pore length.

Dispersive solute flux is classically represented using a diffusion-like or Fickian law

$$q_i^D = -\sum_j D_{ij} \frac{\partial C}{\partial x_j}$$

where q_i^D [g/m^2/s] is the dispersive solute mass flux in direction i and D_{ij} [m^2/s] is a second-order tensor called mechanical dispersion.

This Fickian assumption may, most of the time, be questioned. Afterwards some questions about non-Fickian transport are presented.

The solute mass transport equation can be set up by writing the mass balance on a representative elementary volume (R.E.V.) of soil (according to Bear's definition) Combining advective, diffusive and dispersive fluxes leads to

$$\frac{\partial C}{\partial t} = -\sum_i \frac{\partial}{\partial x_i}\left(q_i^A + q_i^d + q_i^D\right)$$

Diffusion and dispersion are usually combined in a single tensor $D_{ij}^H = D^d + D_{ij}$ called hydrodynamical dispersion. Substituting yields

$$\frac{\partial c}{\partial t} = -\sum_i v_i \frac{\partial C}{\partial x_i} + \sum_i \sum_j \frac{\partial}{\partial x_i}\left(D_{ij}^H \frac{\partial C}{\partial x_j}\right)$$

which is usually called the advection-dispersion equation (ADE). In this study, this equation will also be referred to as the classical or Fickian model of solute transport in porous media. In a one-dimensional framework, it reads

$$\frac{\partial C}{\partial t} = -v \frac{\partial C}{\partial x} + D_L \frac{\partial^2 C}{\partial x^2}$$

where $v = v_1$ and $D_L = D_{11}^H$ [m²/s] called longitudinal hydrodynamical dispersion coefficient, is assumed to be constant. The coefficient of mechanical dispersion is found to depend strongly on the advective velocity. The exact relationship between these two parameters can however only be obtained from theoretical considerations for simple or hypothetical pore systems. Except in the case of very simple conceptual models, one can generally find that the coefficient of mechanical dispersion is linearly related to velocity

$$D_{ij} = \sum_k \sum_l \alpha_{ijkl} \frac{v_k v_l}{\|v\|}$$

where α_{ijkl} [m] is a fourth-order tensor called dispersivity assumed to depend only on soil properties and ||v|| is the norm of the velocity vector. In the case of an isotropic homogeneous medium, owing to symmetry properties, the dispersivity tensor can be fully described by two parameters α_L and α_T, respectively called longitudinal and transverse dispersivity, both expressed in length units. In a uniform flow field, if the principal directions of the dispersion tensor are aligned with the principal directions of the velocity flow field, one can write

$$D_L = \alpha_L v + D^d$$
$$D_T = \alpha_T v + D^d$$

where $D_T = D_{22}^H = D_{33}^H$ quantifies mechanical dispersion in a direction transverse to flow.

Extensive experimental validation of this equation has been performed. Reference books usually provide plots of the longitudinal dispersion versus velocity and show that in the laboratory, when diffusion can be neglected, this approximation is valid under typical groundwater flow conditions. Other studies were also conducted at larger scale. Klotz et al. investigated in the laboratory and in the field a more general relation $D_L = \alpha_L v^B + D^d$ and found that parameter B should be close to one. They also showed the dependency of longitudinal dispersivity to soil sedimentological properties.

Although supported by several theoretical models and verified under well-controlled laboratory conditions, the Fickian model of dispersion has shown difficulties in predicting solute transport under certain other conditions. Dispersion is basically an advective process, as it is caused by variations in fluid velocity. However, this process does not only take place at the pore scale, but also occurs at larger scales, ranging from macroscopic to megascopic. At the field scale, commonly encountered geological structures influence contaminant transport drastically, leading to velocity variations over several orders of magnitude. This includes the effects of stratification and the presence of lenses with higher or lower permeablity. At the megascopic scale, differences between geologic formations also cause non-ideality in solute transport. As the flow path increases in length, a solute cloud can encounter greater and greater variations in the aquifer, causing the variability of the velocity field to increase. Because dispersivity is related to the variability of the velocity, neglecting or ignoring the true velocity distribution (i.e. by replacing the heterogeneous medium by an equivalent homogeneous one) must be compensated for by a corresponding higher apparent (or effective) dispersivity, leading to what is commonly called the scale effect of dispersion.

This scale effect first arose from the comparison of laboratory and field values of dispersivity. Whereas typical values of dispersivity from column experiments range between 0.01 and 0.1 m, values of macroscopic dispersivity (or macrodispersivity) are in general three to four orders of magnitude larger. It has also been widely observed that field-scale dispersion coefficients increase with distance and with time.

However, it must be underlined that field dispersivity values reported in the literature are not always reliable. Inverse modelling is the usual tool to determine dispersivity.
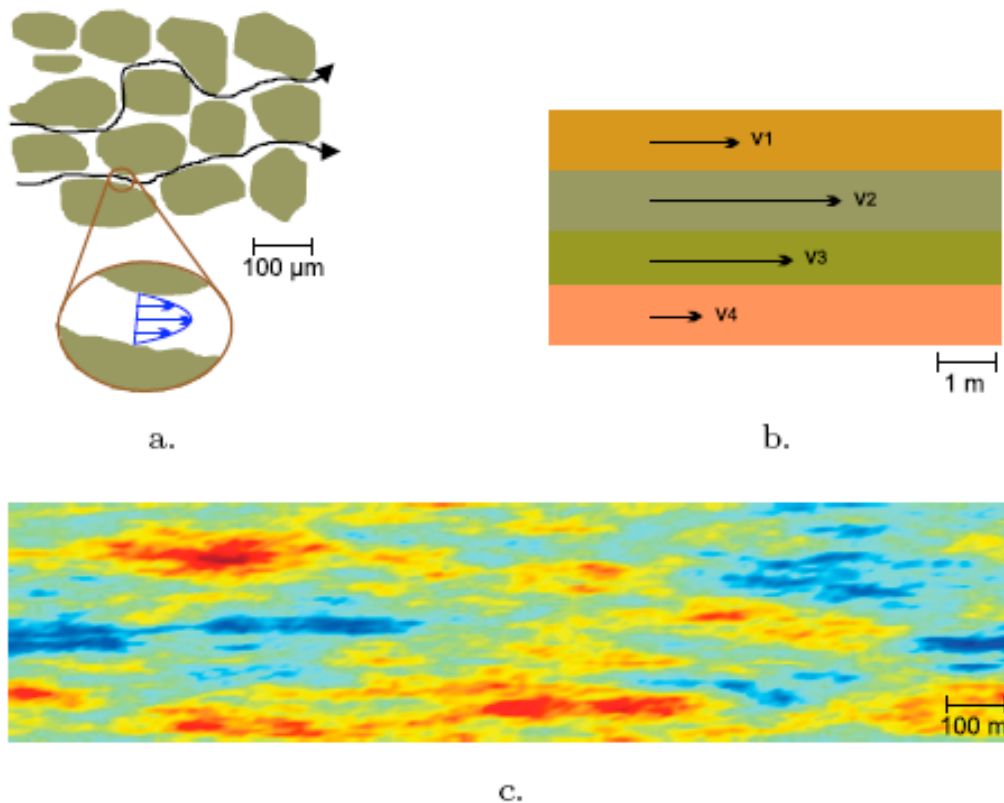
Velocity fluctuations at different scales. a. Pore-to-pore variations. b. Stratification as a cause of variation. c. Randomly heterogeneous two-dimensional anisotropic medium.

The latter is adjusted so that the experimental curve fits a given theoretical solution to the solute transport problem. When interpreting field observations of concentration, numerous factors, such as actual injection conditions, solute density effects or even temporal variations of the advective flow regime or biaised interpretation techniques, are likely to be interpreted as dispersion. For example, Domenico and Robbins (1984) showed that interpreting the two- or three-dimensional spreading of a tracer with a one-dimensional model requires a spatially increasing dispersivity, whereas the use of a dimensionally correct model does not show any dispersion scale-effect.

In studies with insufficient data, the lack of field data is hidden in the dispersion term of the governing transport equation. This was mostly highlighted by Gelhar et al. [1992] who classified results from field studies using a reliability criterion. Despite this criterion, they produced an experimental curve for longitudinal dispersivity versus measurement scale, reprinted on Fig. 1.2, clearly establishing the trend for dispersivity

to increase with distance. Finally, this scale effect was demonstrated using controlled laboratory experiments.
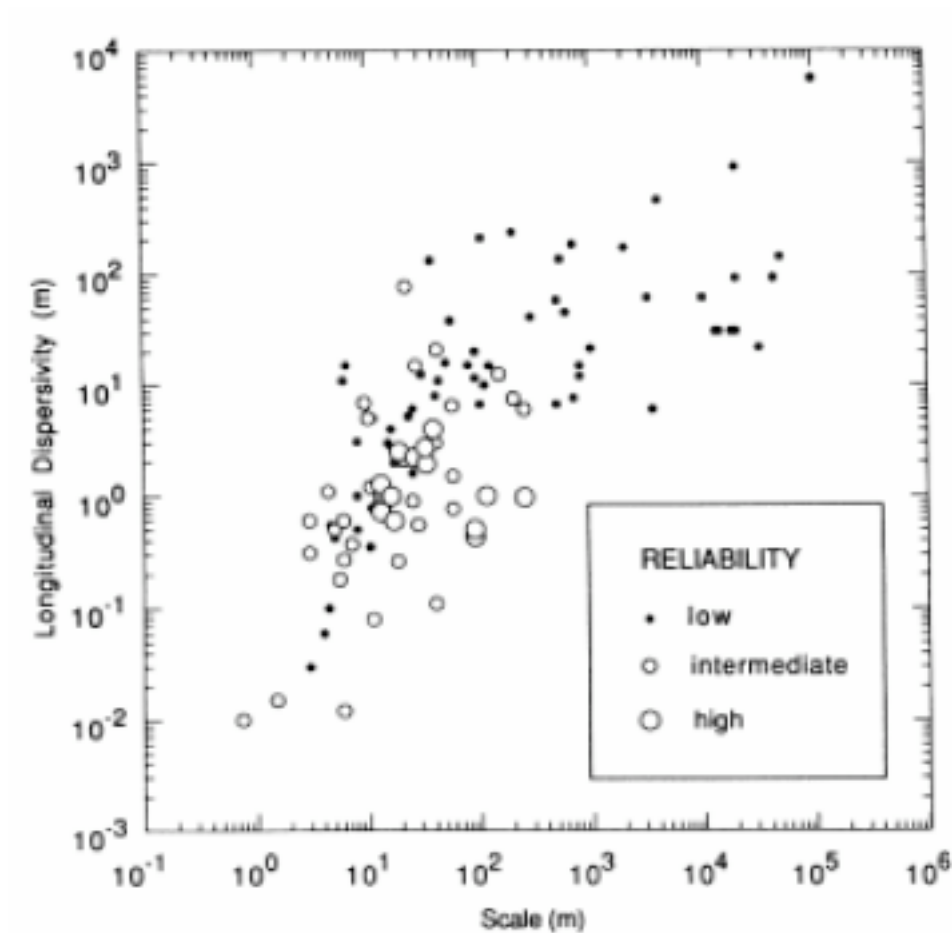
Experimental longitudinal dispersivity values versus measurement scale with data classified by reliability. From Gelhar et al. [1992]

In this chapter, it will be shown how transport parameters and in particular, the longitudinal dispersivity, can be upscaled based on different characterization methods for heterogeneous permeability fields. The major assumption that has to be drawn in this framework is that the classical Fickian transport model remains valid at every scale of interest, provided flow and transport parameters of the medium are properly adapted. Basically, this approach is equivalent to considering a macroscale R.E.V. and deriving equivalent macroscale flow and transport parameters.

Three main approaches for the upscaling of solute transport will be reviewed in this chapter. First, the stochastic theory will be introduced. As the literature in this domain is relatively abundant, we will mainly focus on the general derivation by Gelhar and Axness (1983). Basically, this theory shows how fluctuations in permeability results in an increased spreading of solute plumes.

Then, it will be shown how fractal geometry can give an insight into macrodispersivity. Finally, inclusion models. They allow one to deal with a medium composed of inclusions of given shapes and permeabilities and solve transport considering advection only.

It must be noted that the upscaling of longitudinal dispersivity is always possible in a deterministic framework. Assuming that the heteregeneous permeability field is fully determined, the corresponding transport problem can be solved at a local scale and apparent properties (i.e. effective transport properties of an equivalent homogeneous medium) are obtained by subsequent averaging at a larger scale. In the case of a perfectly stratified aquifer (i.e. where the permeability only depends on the elevation with respect to an arbitrary datum), semi-analytical methods have been developed, based either on moment analysis (Güven et al., 1984) or on modal analysis (Güven et al., 1986).

2. The stochastic approach

Hydraulic properties of subsurface materials, such as hydraulic conductivity, will generally vary in complicated ways in space. It cannot therefore be objectively fully characterized in a deterministic way. However, as subsurface heterogeneity usually results from formation processes (such as e.g. sedimentation), it is not fully random neither, and (geo)statistical methods can be used to identify and characterize its spatial structure. Stochastic analysis enables then the variability in flow and transport to be related to variability and spatial structure associated to hydraulic properties of the heterogeneous medium considered.

In this section several results from stochastic theories applied to solute transport in heterogeneous porous media will be presented. As an introduction, basics of geostatistics and stochastic modelling will be reviewed, and the main assumptions required by the method will be presented. Furthermore, tools to characterize the spatial structure of heterogeneous permeability fields will be presented. Then, the analytical expression of macrodispersivity obtained by Gelhar and Axness will be derived, based on an Eulerian description of the velocity field. Afterwards, a few analytical solutions to be used in the next chapters will be provided.

2.1. Definitions and fundamental assumptions

In a stochastic framework, the hydraulic properties of a heterogeneous medium are treated as random variables. A random variable R can be described in terms of its cumulative probability distribution function (CDF) $F_R(r) = P[R \leq r]$, which denotes the probability that R is less than some specified value r. For a continuous random variable, the probability density function (PDF) can also be used to describe it, and is linked to the CDF using $f_R(r) = dF/dr$. The mean or expected value and the variance of the variable R are

$$\mu_R = E[R] = \int_{-\infty}^{+\infty} r f_R(r) dr$$

$$\sigma_R^2 = E\left[(R - \mu_R)^2\right] = \int_{-\infty}^{+\infty} (r - \mu_R)^2 f_R(r) dr$$

μ_R is a measure of the central tendency of the random variable and σ_R^2 is a measure of the variability associated with the variable. The squareroot of the variance is called standard deviation.

A normal or Gaussian random variable is described by the PDF

$$f_R(r) = \frac{1}{\sqrt{2\pi\sigma_R^2}} \exp\left[\frac{-(r-\mu_R)^2}{2\sigma_R^2}\right]$$

A normal variable is thus entirely characterized by its mean and variance. A log-normal random variable R is such that ln(R) is a normal random variable. In subsurface hydrology, and more particularly in the stochastic approach of transport in heterogeneous formations, hydraulic conductivity is usually assumed to be log-normally distributed. Therefore, one defines Y = ln(K), where the permeability K is expressed in [m/s] and ln is the natural logarithm. This hypothesis has the advantage that negative values are excluded, which is consistent with the physical requirement that permeability is positive.

When we are dealing with more than one variable, it is necessary to consider how the variables are interrelated probabilistically. The joint CDF of two random variables R and S is $F(r,s) = P[R \le r, S \le s]$ and the corresponding joint density probability function is $f(r,s) = \partial^2 F(r,s)/\partial r\partial s$. The degree of linear relationship between R and S is quantified by the covariance

$$\mathrm{cov}(R,S) = E\left[(R-\mu_R)(S-\mu_S)\right] = \int_{-\infty}^{+\infty}\int_{-\infty}^{+\infty}(r-\mu_R)(s-\mu_S)f(r,s)dr\,ds$$

If R and S are independent, then the covariance is zero. However, the inverse statement is not correct : if the covariance is zero, then the random variables are not necessarily independent. They are said to be uncorrelated. Another useful tool to quantify the correlation of two random variables is the variogram

$$\gamma(R,S) = 1/2\,E\left[(R-S)^2\right] = \sigma_R\sigma_S - \mathrm{cov}(R,S)$$

A random function (also called random field or stochastic process) can be viewed as a random variable with an infinite number of components. For instance, hydraulic conductivity of soils can be considered as a spatial multidimensional stochastic process K(x), where x is a vector of spatial coordinates. For a fixed x, the random field is a

random variable, and is completely characterized by its joint PDF to any arbitrary order. A particular record of a stochastic process (e.g. the measured permeability field in a given situation) is referred to as a realization of the stochastic process, whereas the ensemble refers to the collection of all possible realizations of the stochastic process.

In applications related to flow through porous formations, the concept of ensemble is relatively abstract, as one only encounters one single realization of the process. The ensemble then reflects uncertainty in the depiction of the spatial structure of the formation, rather than a set of existing similar formations.

Moreover, this representation relies on a finite-length record composed of discrete values of data measured at some interval. The statistical characterization of the random structure is then based on spatial averages over the single realization available, rather than over ensemble averages. This might not induce a high bias if the ergodic hypothesis prevails and the single realization considered contains the whole information available in each realization of the ensemble.

Because a stochastic process is defined as a random variable at each point (in time or in space), the mean, the variance and the covariance are functions that may vary (in time or in space). In the case of the log-permeability field Y of soils, one could calculate

$$\mu_Y(x) = E[Y(x)] = \int_{-\infty}^{+\infty} y f_Y(y,x)dy$$
$$\sigma_Y^2(x) = E\left[\left(Y(x) - \mu_x^2\right)\right] = \int_{-\infty}^{+\infty} (y - \mu_Y)^2 f_Y(y,x)dy$$

where y are specified values of log-permeability. An important particular class of stochastic processes is that of stationary (or homogeneous) random functions for which both mean and variance are constant (in time or in space). One will thus have $\mu_Y(x) = \mu_Y$ and $\sigma_Y^2(x) = \sigma_Y^2$ For a second-order or weakly stationary random field, the covariance (which is then a function) is moreover only dependent on the separation (in time or in space) of the two random variables considered.

2.2. Covariance function and spectral representation

Assuming two zero-mean weakly stationary random spatial fields f(x) and g(x), their covariance function is noted $C_{fg}(\mathbf{h})$ and only depends on the separation gap $\mathbf{h}$ (where a vector notation was adopted as the covariance can be dependent on the orientation, in

the case of a macroscopically anisotropic random field). f and g could be either permeabilities, heads, velocities, concentrations or any variable of interest. C_{fg} is either called the autocovariance or the crosscovariance, depending on f and g being representative of a same random field or not. The covariance function cannot take any arbitrary parametric shape. It must meet several properties, some of them being difficult to verify. One found therefore convenient to adopt a set of simple covariance models that are known to be valid. One of the most used model is the exponential covariance model, expressed in the one-dimensional case as

$$C_{fg}(h) = \sigma_f \sigma_g \exp\left(-\frac{|h|}{\lambda}\right)$$

where λ is called correlation length or integral scale. Intuitively, λ is a measure of the separation required for two random variables to become uncorrelated. Other one-dimensional covariance models are, among others, the Gaussian and the hole-effect covariance function.

$$C_{fg}(h) = \sigma_f \sigma_g \exp\left(-\left(\frac{h}{\lambda}\right)^2\right)$$

$$C_{fg}(h) = \sigma_f \sigma_g \exp\left(-\frac{|h|}{\lambda}\right)\left(1 - \frac{5}{3}\frac{|h|}{\lambda} + \frac{1}{3}\frac{h^2}{\lambda^2}\right)$$

Next figure illustrates these different models (in the case of autocovariance C_{ff}) and shows one realization of a corresponding stochastic process. Basically, the exponential model can be used to model small-scale sharp variability, whereas the Gaussian model produces softer variations and mild transitions. The hole effect model can be used to represent alternating sequences, such as stratification If a process is stationary, it is virtually always possible to describe it in terms of its frequency content, which is accessible through a Fourier-transform of this process. The Fourier-transform of the covariance function is called the power density spectrum (or spectral density function), is noted S_{fg}, and is evaluated according to

$$S_{fg}(s) = \tilde{f}(s)\tilde{g}^*(s) = \int_{-\infty}^{+\infty} C_{fg}(\mathbf{h})\exp(-2\pi i \mathbf{h} \cdot s)dh$$

where s is the wave number (that has the same number of dimensions as x), $\tilde{f}(s)$ is the Fourier-transform of function f(x) and $\tilde{g}^*(s)$ is the complex conjugate of the Fourier-

transform of function g(x). Inversely, the covariance function can be obtained from the inverse Fourier-transform of the spectral density function

$$C_{fg}(\mathbf{h}) = \int_{-\infty}^{+\infty} S_{fg}(s)\exp(2\pi i\mathbf{h}\cdot s)ds$$
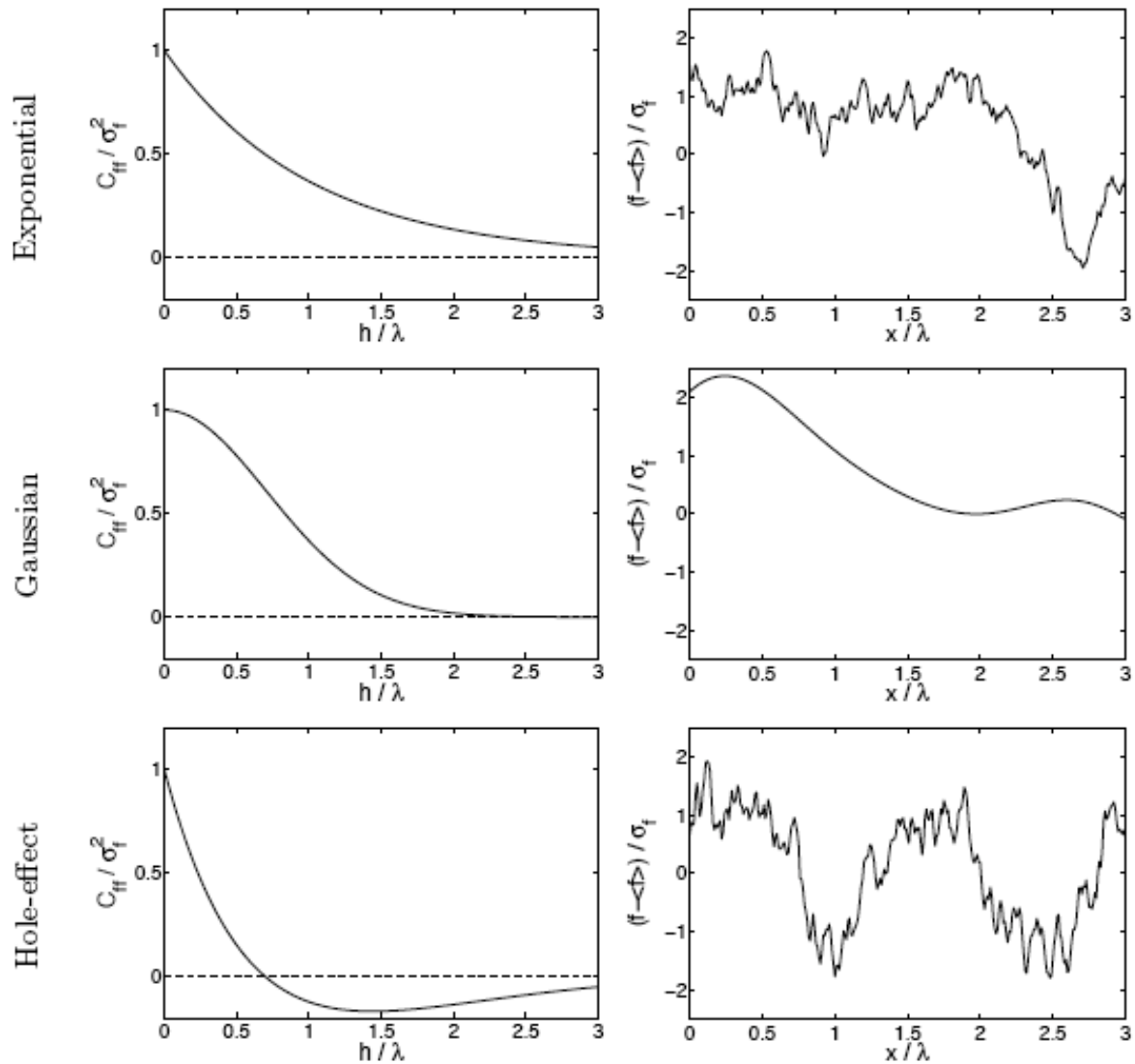
Models of covariance and one realization of a corresponding random field

2.3. Eulerian derivation of macrodispersion

In this section, the general three-dimensional derivation of macrodispersion performed by Gelhar and Axness will be shortly summarized, following the lines of Gelhar and

Cirpka. The starting point is the advection-dispersion equation, expressed with a constant local hydrodynamical dispersion tensor D_{ij}^H and assuming that concentration and migration velocity are stationary random functions.

$$C = \langle C \rangle + C'$$
$$\mathbf{v} = \langle \mathbf{v} \rangle + \mathbf{v}'$$

where bold symbols are vectors. $\langle C \rangle, \langle \mathbf{v} \rangle, C'$ and $\mathbf{v}'$ are respectively mean concentration, mean velocity, concentration fluctuation and velocity fluctuation. Fluctuations are assumed to have a zero mean $\langle C' \rangle = \langle \mathbf{v}' \rangle = 0$. Substituting these expressions, taking expected values and dropping higher-order terms, yield the governing equation for the mean concentration

$$\frac{\partial \langle C \rangle}{\partial t} = -\sum_i \langle v_i \rangle \frac{\partial \langle C \rangle}{\partial x_i} - E\left[\sum_i v_i' \frac{\partial C'}{\partial x_i} \right] + \sum_i \sum_j \frac{\partial}{\partial x_i} D_{ij}^H \frac{\partial \langle C \rangle}{\partial x_j}$$

Considering the classical advection-dispersion equation, a new term arises here. It reflects additional mass transport due to correlation between specific discharge and concentration fluctuations. It produces a large-scale dispersion effect and can be approximated using a Fickian-like law

$$E\left[\sum_i v_i' \frac{\partial C'}{\partial x_i} \right] = \sum_i \frac{\partial}{\partial x_i} \langle v_i' C' \rangle \approx -\sum_i \sum_j \frac{\partial}{\partial x_i} \left(D_{ij}^* \frac{\partial \langle C \rangle}{\partial x_j} \right)$$

D_{ij}^* is the macrodispersion tensor and is assumed to be proportional to the absolute value of migration velocity, as for the local dispersion tensor. It can be evaluated using the governing equation of concentration perturbations. The latter is obtained by

$$\frac{\partial C'}{\partial t} + \sum_i \left(v_i' \frac{\partial \langle C \rangle}{\partial x_i} + \langle v_i \rangle \frac{\partial C'}{\partial x_i} \right) - \sum_i \sum_j \frac{\partial}{\partial x_i} \left(D_{ij}^H \frac{\partial C'}{\partial x_j} \right) = \sum_i \frac{\partial}{\partial x_i} \left(v_i' C' - \langle v_i' C' \rangle \right) \approx 0$$

This approximation is of crucial importance. Basically, it implies that velocity fluctuations are sufficiently small for second-order products to be neglected. For a log-normal permeability field, it can be shown based on a similar stochastic analysis of the flow equation that this condition on velocity perturbation requires a small variance of the Y field, so that it can be linearized. Typically, these developments are assumed to be valid for $\sigma_Y^2 < 1$

In general, these equations must be solved simultaneously. However, a decoupling can be accomplished provided that concentration fluctuations occurs at a much smaller scale than variations associated to the mean concentration. It is then possible to solve it to evaluate the macrodispersive flux and subsequently substitute it in the equation. Assuming that the mean flow occurs in direction i=1 and using the notations introduced simplifies to

$$\frac{\partial C'}{\partial t} = -v_1' \left| \nabla \langle C \rangle \right| - \langle v_1 \rangle \frac{\partial C'}{\partial x_1} + D_L \frac{\partial^2 C'}{\partial x_1^2} + D_T \frac{\partial^2 C'}{\partial x_2^2} + D_T \frac{\partial^2 C'}{\partial x_3^2}$$

where the notation $\left| \nabla \langle C \rangle \right|$ indicates that the gradient of the mean concentration is assumed to be constant in time and in space. This assumption may not be very realistic. But a mean gradient hardly varying over several correlation lengths of the hydraulic conductivity field may be achieved in the large-time limit under ordinary flow conditions, allowing one to apply the theory derived here in field conditions.

Las equation may be transferred into the Fourier-space. Using some basic properties of the Fourier-transform, one obtains

$$\left(\frac{d}{dt} + b \right) \tilde{C}'(s) = -\tilde{v}_1'(s) \left| \nabla \langle C \rangle \right|$$

where ˜ indicates the Fourier-transform and where

$$b = 2\pi i \langle v_1 \rangle s_1 + 4\pi^2 D_L s_1^2 + 4\pi^2 D_T \left(s_2^2 + s_3^2 \right)$$

This is a linear non-homogeneous first-order time differential equation. Since the concentration gradient is taken as a constant and assuming as initial condition a concentration distribution equal to the mean concentration (i.e. a concentration perturbation C' = 0), one obtains

$$\tilde{C}'(s,t) = -\tilde{v}_1'(s) \left| \nabla \langle C \rangle \right| \int_0^t \exp(b(\tau - t)) d\tau = -\frac{\tilde{v}_1'(s) \left| \nabla \langle C \rangle \right|}{b} \left(1 - \exp(-bt) \right)$$

To compute the longitudinal apparent dispersion coefficient it can be used

$$D_L^* = -\frac{1}{\left| \nabla \langle C \rangle \right|} \langle C' v_1' \rangle$$

As $\langle C'v_1' \rangle$ is the integral of the cross-spectral density of concentration and longitudinal velocity fluctuations S_{Cv_1}, last equation can be transformed into

$$\alpha_L^*(t) = \frac{1}{\langle v_1 \rangle} \int_{-\infty}^{+\infty} \frac{1 - \exp(-bt)}{b} \tilde{v}_1'(s) \tilde{v}_1'^*(s) ds = \frac{1}{\langle v_1 \rangle} \int_{-\infty}^{+\infty} \frac{1 - \exp(-bt)}{b} S_{v_1 v_1}(s) ds$$

This equation establishes the link between velocity fluctuations and macrodispersivity. As the velocity spectrum is linked to log-permeability variations, macrodispersivity is basically found to be dependent on the permeability field. Moreover, macrodispersivity is also proved to be time-dependent and vanishes for large time, macrodispersivity converges to a constant asymptotic value.

Similar derivations have been performed by Dagan and by Neuman et al. Dagan used a Lagrangian framework, but had to use an approximate relationship between the Eulerian and the Lagrangian velocity covariance. Neuman et al. used a more abstract mathematical analysis based on semigroup theory. Basically, these derivations all require an assumption of relatively small perturbations, leading to little discrepancy among them and a domain of validity $\sigma_Y^2 < 1$.

2.4. A few analytical solutions

Most of available analytical solutions are based on exponential covariance models and assume that local dispersivities are negligible compared to correlation lengths. The asymptotic value of longitudinal dispersivity in an isotropic medium is given by

$$\alpha_L^*(\infty) = \sigma_Y^2 \frac{\lambda}{\gamma^2}$$

where γ is a flow factor accounting for the dependence of effective permeability on dimensionality. In the two-dimensional case, $\gamma = 1$, whereas in the three-dimensional case, $\gamma = \exp(\sigma_Y^2/6)$. It must be noted that Dagan obtained a similar result using a Lagrangian framework, but with $\gamma = 1$ in the three-dimensional case. Dagan states that taking into account a value $\gamma \neq 1$ is not consistent with first-order approximations adopted, as it introduces a term of order σ_Y^4.

Fig. 2.2 depicts the influence of the variance of the log-permeability field on the asymptotic value of longitudinal apparent dispersivity.
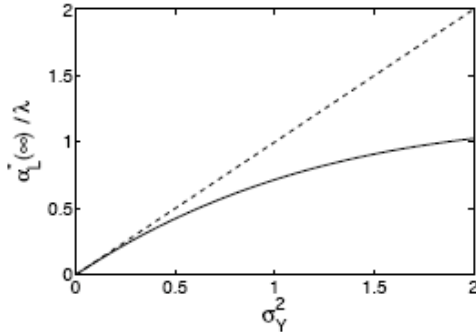
Figure 2.2: Asymptotic longitudinal dispersivity in the isotropic case. 3D (solid line) and 2D (dashed line) case. The solution by Dagan [51] in the 3D case corresponds to the dashed line.
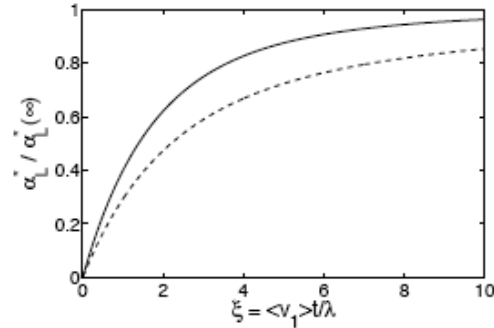
Figure 2.3: Convergence of longitudinal dispersivity in the isotropic case. 3D (solid line) and 2D (dashed line) cases.

The three-dimensional isotropic solution for intermediate times is given by Gelhar, based on an expression derived by Dagan

$$\frac{\alpha_L^*(t)}{\alpha_L^*(\infty)} = 1 - \frac{4}{\xi^2} + \frac{24}{\xi^4} - 8\left(\frac{1}{\xi^2} + \frac{3}{\xi^3} + \frac{3}{\xi^4}\right)\exp(-\xi)$$

where $\xi = \langle v_1 \rangle t / \lambda$. In a two-dimensional isotropic aquifer, it is given by

$$\frac{\alpha_L^*(t)}{\alpha_L^*(\infty)} = 1 - \frac{3}{2\xi} + \frac{3}{\xi^3} - \frac{3}{\xi^2}\left(1 + \frac{1}{\xi}\right)\exp(-\xi)$$

Basically, these results express that the convergence to the asymptotic behavior is only controlled by the ratio of mean travel distance to correlation length.

In the two-dimensional case, as the number of available paths to bypass low permeability zones is lower than in the three-dimensional case, convergence is less rapidly reached (Fig. 2.3).

In the case of a two-dimensional anisotropic situation with flow occuring in a direction at an angle θ with respect to the bedding of the permeability field, asymptotic dispersivity is given by

$$\alpha_L^*(\infty) = \sigma_Y^2 \frac{\lambda_1 \lambda_2}{\gamma^2 \sqrt{\lambda_1^2 \sin^2 \theta + \lambda_2^2 \cos^2 \theta}}$$

where the flow factor is obtained from

$$\gamma = \frac{\exp\left[\sigma_Y^2\left(1/2 - g_{22}\right)\right]}{\sin^2 \theta + B \cos^2 \theta}$$

with $B = \exp\left[\sigma_Y^2(g_{11} - g_{22})\right]$, $g_{11} = \lambda_2/(\lambda_1 + \lambda_2)$ and $g_{22} = \lambda_1/(\lambda_1 + \lambda_2)$.

Fig. 2.4 shows the effect of anisotropy on asymptotic longitudinal dispersivity. For high variance and high anisotropy, flow is mainly directed in the longitudinal direction and little transverse mixing can occur, leading to lower values of longitudinal dispersivity. As anisotropy decreases, transverse mixing increases, leading to higher apparent longitudinal dispersivities. Fig. 2.5 shows that, globally, when flow is not aligned with the main principal direction of the permeability field, apparent dispersivity tends to decrease. No analytical solution for transient apparent dispersivity in two-dimensional anisotropic situation could be found.
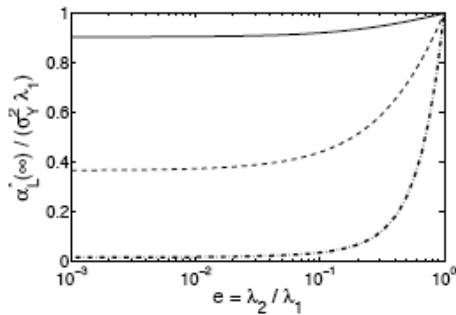
Figure 2.4: Influence of the anistropy on asymptotic longitudinal dispersivity for $\theta = 0$. $\sigma_Y^2 = 0.1$ (solid line), $\sigma_Y^2 = 1$ (dashed line) and $\sigma_Y^2 = 4$ (dot-dashed line).
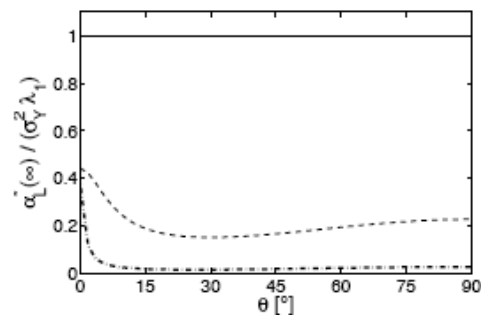
Figure 2.5: Influence of the flow direction on asymptotic longitudinal dispersivity for $\sigma_Y^2 = 1$. $e = 1$ (solid line), $e = 0.1$ (dashed line) and $e = 0.01$ (dot-dashed line).

The perfectly stratified case could be obtained under appropriate conditions $(\lambda_1 \rightarrow \infty, \lambda_2 \rightarrow \infty$ and finite $\lambda_3)$. However, a separate but similar analysis was conducted by Gelhar et al. They assumed a normal permeability distribution (instead of a log-normal one) and obtained

$$\alpha_L^* = \int_{-\infty}^{+\infty} \frac{S_{KK}(s)}{\langle K \rangle^2} \frac{1 - e^{-\alpha_T v t s^2}}{\alpha_T s^2} ds$$

in which $S_{KK}(s)$ is the power density spectrum of the hydraulic conductivity field, characterized by an integral scale λ.

Three different regimes can be identified. At early times, transverse spreading has not caused any mixing yet and solute particles remain on their initial flow line. The concentration distribution behaviour is fully controlled by longitudinal advection and apparent longitudinal dispersivity varies linearly in time

$$\alpha_L^* \to \frac{\sigma_K^2}{\langle K \rangle^2} vt \quad t \to 0$$

After some time, spatial concentration gradients appear due to transverse velocity variations, causing diffusion and dispersion of particles from their initial flow line. Particle velocities then change according to their new flow line, and new concentration gradients appear, causing new transfers of particles between flow lines. For intermediate times, transverse transport processes have ensured mixing over the respective layer thicknesses (or over the integral scale λ), but not over the overall aquifer thickness. In this case, it can be shown that longitudinal dispersivity increases according to the square-root of time. The third regime corresponds to full mixing of the solume plume over the aquifer thickness. This regime was first investigated by Taylor and Aris for laminar flow through a tube, with a deterministic velocity distribution.

They showed that in this regime, commonly referred to as the Taylor dispersion regime, the dispersive flux is Fickian with a constant asymptotic apparent dispersivity. In the stochastic approach of solute transport in perfectly layered soils, this regime only exists provided the covariance function of the permeability field is properly chosen. Using a hole-effect covariance model, Gelhar et al. obtained

$$\alpha_L^*(\infty) = \frac{1}{3} \frac{\sigma_K^2}{\langle K \rangle^2} \frac{\lambda^2}{\alpha_T}$$

Asymptotic apparent longitudinal dispersivity is directly proportional to the variance of the ln(K) field (as $\sigma_K^2 / \langle K \rangle^2 \approx \sigma_Y^2$) but depends on the square of the correlation length. Moreover, its value is inversely proportional to the magnitude of transverse mixing.

3. Fractal models of heterogeneity

The main feature of a fractal object is that its degree of irregularity is independent of the scale. As long as one watches it closer and closer, new small-scale irregularities appear, although it is not possible to detect them from a larger-scale point of view. In normal Euclidian geometry, the length L of a line can be calculated with

$$L = n\varepsilon$$

where n is the number of length units ε. If the size of ε is diminished by 2, then the number of measuring units n increases by 2, keeping the length constant.

Many natural objects do not behave according to this simple relationship. It has been found that, in the case of fractal lines such as coastal lines,

$$F = n\varepsilon^d$$

where F is a measure of the fractal line length (which, contrary to L, is not expressed in [m] but in [m^d]) and d is the dimension in which one has to measure the line length in order to obtain a constant value for F. d is called the fractal dimension. In the case of a line, this parameter may vary from 1 to 2. If d = 1, the measured line is geometrically simple, whereas if d = 2, the line is so irregular that it completely fills a plane. Combining equations leads to

$$L(\varepsilon) = F\varepsilon^{1-d}$$

which describes the dependence of a measured length with the measurement unit ε, according to fractal length F and fractal dimension d.

3.1. Application to solute transport

Fractal geometry was first introduced by Wheatcraft and Tyler to describe solute particle travel paths in heterogeneous media. However, as the Euclidian length of a fractal line increases without bounds as long as the measurement unit decreases, particle travel path cannot be fully fractal. Indeed, water flow does not exactly follow the shape

of the soil grains, otherwise some particules would have an infinite travel time. A cutoff limit ε_c was then introduced for the measurement unit, this limit being comprised between a mean pore size and the size of the R.E.V. for the smallest heterogeneity.

In a single fractal streamtube, if x_F is the actual distance travelled by a particle (in [m]) and if x_S is the longitudinal straight-line distance travelled by this same particle (also expressed in [m]), one has

$$F = x_S^d$$

where the measurement unit is equal to the straight-line path. Substituting this relationship and measuring at the fractal cutoff limit leads to

$$x_F = \varepsilon_c^{1-d} x_S^d$$

which can be viewed as a scaling relationship between measurement scale x_S and real particle travel path x_F . This is illustrated in Fig. 2.6. If measurement scale is divided by 2, if particle travel path is fractal, it is not divided by 2 but by 2^d.
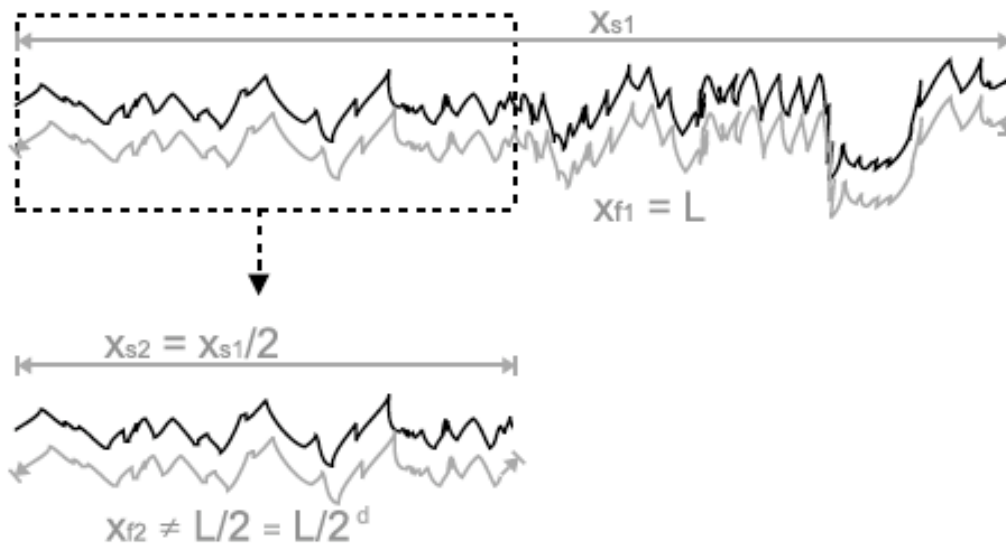
Figure 2.6: Schematic illustration of a fractal particle path.

Provided the Fickian model is valid at some local scale, the spreading of a dissolved particle cloud in space, expressed as the variance of the particle position $\sigma_C^2 = E\left[\left(X - \langle X \rangle\right)^2\right]$, is given by

$$\sigma_C^2 = 2\alpha_L x_F$$

where α_L is the local longitudinal dispersivity. This variance can also be expressed in terms of measured variables

$$\sigma_C^2 = 2\alpha_L^* x_S$$

where α_L^* is the measured (apparent or effective) longitudinal dispersivity. Using this expression we obtain

$$\alpha_L^* = \alpha_L \varepsilon_C^{1-d} x_S^{d-1}$$

which allows the upscaling of longitudinal dispersivity based on a fractal description of the heterogeneous medium. For an homogeneous non-fractalmedium (d = 1), field-scale dispersivity remains equal to local dispersivity. Wheatcraft and Tyler and Zhou and Selim extended this latter equation to transport in a soil composed of a set of fractal streamtubes. However, this approach is rather conceptual, and one could expect a real aquifer to behave somehow differently than a set of disconnected fractal streamtubes. Zhan and Wheatcraft proposed another approach, combining fractal geometry and spectral analysis, that could be more adapted to real field-scale situations.

3.2. Fractal geometry and spectral analysis

Whereas classical stochastic approaches involve ln(K) covariance functions that have a finite correlation length, in order to have a rapid decrease of hydraulic conductivity autocorrelation this assumption is not necessary anymore when using concepts of fractal geometry. Zhan and Wheatcraft proposed to use a power-law covariance model $C_{YY} = |h|^{2H}$ where 0 < H < 1 is called Hurst coefficient and link with the fractal dimension according to H = 1+e_u−d (e_u being the Euclidian dimension). H=1 corresponds thus to a non-fractal medium.

For this type of heterogeneity, Fickian behaviour will never be achieved if the aquifer is not bounded, and longitudinal macrodispersivity will monotonically increase with plume scale to infinity. However, for most geological formations, physical boundaries always exist. A generally encountered situation is that noflow boundaries enclosing the fractal porous medium define the field scale at which contaminants will disperse. Zhan and Wheatcraft then introduced a macroscale cutoff limit L_m, having the same role as the correlation length used in classical stochastic analysis, but being linked to a physical boundary rather than to the structure of the permeability field.

Zhan and Wheatcraft showed that, in the case of a stratified fractal aquifer, asymptotic macrodispersivity can be computed from

$$\alpha_L^*(\infty) = \frac{\sigma_Y^2}{\alpha_T} \frac{2-d}{3-d} \left(\frac{L_m}{2\pi}\right)^2$$

where $1 < d < 2$ and L_m is representative of the aquifer thickness.

Relative macrodispersivity can be computed according to

$$\frac{\alpha_L^*}{\alpha_L^*(\infty)} = 1 - \exp\left[-\frac{\xi}{(2\pi)^2}\right] + \frac{1}{2-d}\frac{\xi}{(2\pi)^2}\exp\left[-\frac{\xi}{(2\pi)^2}\right] - \frac{1}{2-d}\left[\frac{\xi}{(2\pi)^2}\right]^{3-d}\Gamma\left(d-1,\frac{\xi}{(2\pi)^2}\right)$$

where $\gamma = 1$ and $\gamma = 1 + \sigma_Y^2/6$ in two and three-dimensional cases respectively.

Fig. 2.7 shows the dependency of asymptotic dispersivity on Hurst coefficient for two- and three-dimensional problems. These results are qualitatively consistent with results from stochastic theories, as an increase in the correlation of the medium (i.e. an increase of the Hurst coefficient or an increase of the correlation length) results in a higher asymptotic longitudinal apparent dispersivity and that an increase in the Euclidian dimension of the problem results in a decrease of the dispersivity. It should be noted that a totally fractal medium (H = 0) yields a macroscopic dispersivity equal to zero, which is again consistent with stochastic theories ($\alpha_L^* = 0$ for $\lambda = 0$) but contradictory with results of streamtubes models developed in the previous section.

Fig. 2.8 shows the transient development of apparent longitudinal dispersivity in the case of a perfectly stratified aquifer.

In the anisotropic case, Zhan and Wheacraft also developed two and three-dimensional analytical solutions for asymptotic apparent dispersivity.
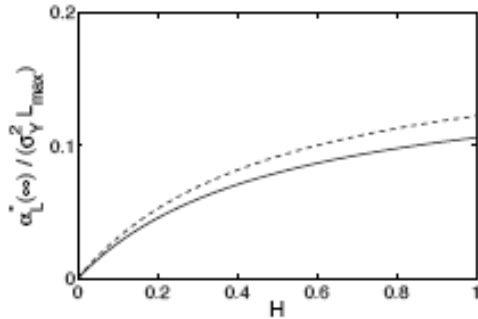
Figure 2.7: Influence of Hurst coefficient on asymptotic dispersivity for two-dimensional (solid line) and three-dimensional (dashed line) medium. $\sigma_Y^2 = 1$.
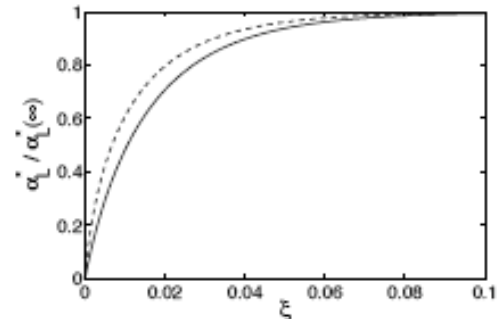
Figure 2.8: Influence of fractal dimension on the transient behavior of apparent longitudinal dispersivity in a perfectly stratified aquifer. $d \to 1$ (solid line) and $d \to 2$ (dashed line).
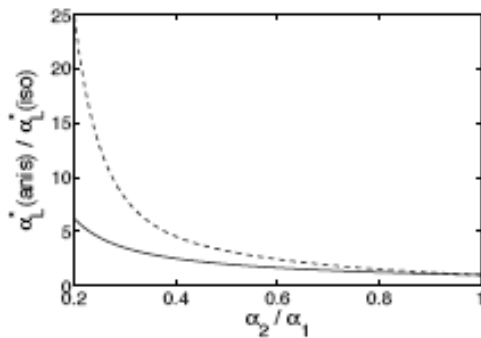
Figure 2.9: Influence of the anisotropy ratio on apparent longitudinal dispersivity in a two-dimensional aquifer for flow parallel to the bedding. $H \to 0$ (solid line) and $H \to 1$ (dashed line).
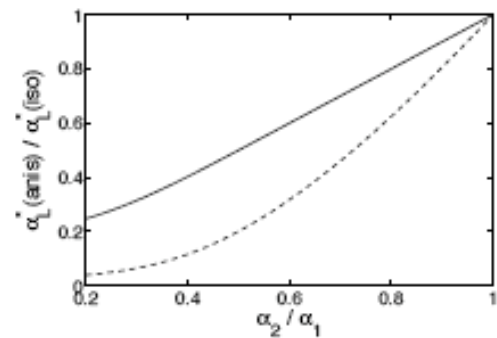
Figure 2.10: Influence of the anisotropy ratio on apparent longitudinal dispersivity in a two-dimensional aquifer for flow perpendicular to the bedding. $H \to 0$ (solid line) and $H \to 1$ (dashed line).

4. Inclusion models

Transport in aquifers made of inclusions of highly contrasted permeabilities has only been very recently investigated. Desbarats performed pioneering numerical simulations using a binary medium with inclusions of low permeability and showed that permeability contrast and inclusion volumetric proportion were the main controlling parameters for transport. Rubin proposed a first-order stochastic approach and derived analytical results in the case of bimodal isotropic media. Like other results from stochastic theories, Rubin's results are only valid for low permeability contrasts. Eames and Bush and later Dagan and Lessoff and Lessoff and Dagan studied transport properties of two- and three-dimensional bimodal fields composed of inclusions of fixed size and of constant permeability, disposed at random in an homogeneous matrix. Their developments were conducted under the assumption of low volumetric proportion of inclusions (i.e. in the dilute system limit) so that advective transport could be solved by isolating one inclusion and the dispersive effect of a collection of lenses was determined subsequently in a simple additive manner. Dagan et al. and Fiori et al. further refined the analysis by considering distributions of ellipses of different size and of different permeabilities, and by computing the transient development of apparent dispersivity.

They released the dilute system approximation by considering instead the selfconsistent approach, in which the flow and transport problems are solved for a single inclusion embedded in a equivalent homogeneous medium replacing the neighbouring inclusions. However, they limited their analysis to isotropic media and compared the results with numerical simulations. Dagan and Fiori and Fiori and Dagan studied transport properties of media with composite inclusions, that allowed them to derive results without relying neither on the dilute system nor on the self-consistent approach. However, they also conducted their analysis in the isotropic case. Fiori et al. and Jankovic et al. performed extensive numerical simulations on bimodal isotropic medium for different volumetric proportions of inclusions (ranging from 5 to 40%) and for different permeability ratios (ranging from 0.01 to 10). They found that the self-consistent approach could be reasonably adopted in each of their tested case.

In this section, it is thus proposed to further study the model suggested by Dagan et al. developped under the self-consistent approximation, and to extend it to anisotropic formations using the results proposed by Dagan and Lessoff and Lessoff and Dagan.

4.1. Conceptual model

Dagan et al. have suggested to model heterogeneous formations as multiphasic ones, made up of M types of block geometry and of N different types of material. Blocks are assumed not to overlap (Fig. 2.11 a.). A point of the medium lies in the block i, j of shape i (i = 1 . . .M) and of material j (j = 1 . . .N) with a known probability p_{ij} . p_{ij} thus denotes the volumetric proportion of blocks of size i and of material j in the medium. Centroid positions of blocks x_{ij} are however not known and are treated as random variables.
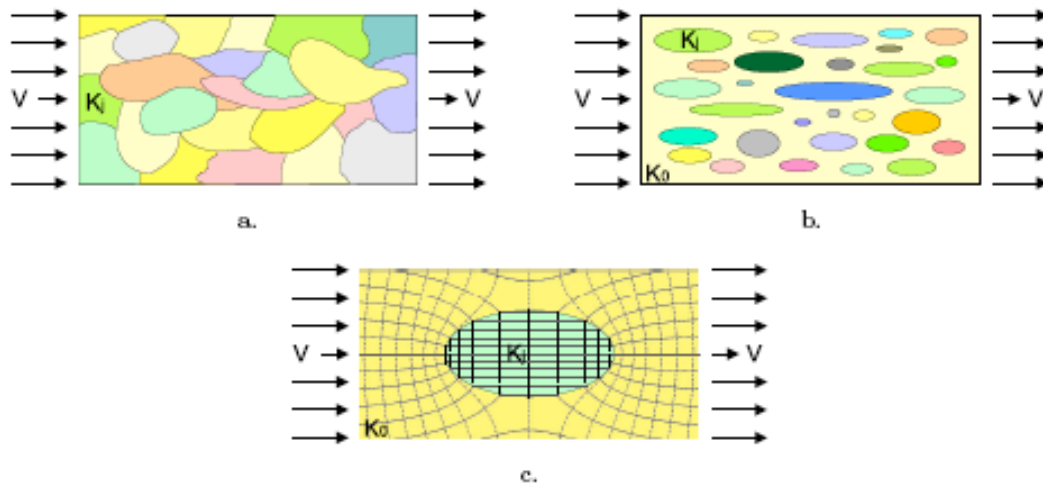
Figure 2.11: Conceptual model and the self-consistent approximation. a. Statistically homogeneous but anisotropic heterogeneous permeability field. b. Model of inclusions of regular shape disposed at random in a matrix. c. Single inclusion embedded in a matrix. *Adapted from Dagan et al. [55].*

If K_j is the permeability of material j, the overall conductivity field is given by

$$K(x) = \sum_i \sum_j K_k I\left(x - \bar{x}_{ij}\right)$$

where the indicator function $I\left(x - \bar{x}_{ij}\right)$ is equal to 1 for x belonging to the inclusion (i, j) and is equal to zero otherwise. It is emphasized that permeabilities of two neighbouring blocks remain uncorrelated. Mean and variance of the log-permeability field can be computed from

$$\ln\left(K_g\right) = \sum_i \sum_j p_{ij} m_j$$

$$\sigma_Y^2 = \frac{1}{2} \sum_i \sum_j \sum_{k \neq j} \left(m_j - m_k\right)^2 p_{ij} p_{ik}$$

where $m_j = \ln(K_j)$. The variance of such media can be very high, well above the classical limit $\sigma_Y^2 < 1$ established for the validity of first-order stochastic theories.

To further simplify the model, Dagan et al. propose to represent blocks as inclusions of regular size, such as ellipses or spheroids, and to assume that they are submerged in a matrix of arbitrary conductivity K_0 to be determined below (Fig. 2.11 b.). Dagan et al. state that, despites these limitations and provided the distribution of sizes and permeabilities is properly chosen, this type of permeability field can properly mimic any given permeability distribution and any two-point anisotropic covariance function.

In a given heterogeneous formation of this geometry, the solution of the flow field can be represented as a distribution of singularities of source type, each source corresponding to a given block. The self-consistent approach proceeds by isolating one inclusion of shape i and permeability K_j and by suppressing the remaining ones in the matrix of permeability K_0 (Fig. 2.11 c.). The flow and transport problems are then solved assuming there is no interaction between each block. As K_0 could be any reference permeability somehow linked to the effective permeability K_e of the medium, the self-consistent approach assumes $K_0 = K_e$ and K_0 reflects the presence of neighbourings blocks that have been suppressed. The derivation of K_e for two- and three-dimensional isotropicmedia is given by Dagan and extended to three-dimensional anisotropic media.

4.2. Advective transport by the Lagrangian approach

Under ergodic condition, the spatial moments of a solute plume can be computed from the statistical moments of the trajectory of a single particle. One will then consider a solute particle injected at time t = 0 and at position x_0.

The trajectory of this particle is x = X(t, x_0) and is given by

$$\mathbf{X}(t, x_0) = x_0 + \mathbf{V}t + \sum_i \sum_j \mathbf{X}'_{ij}$$

where $\mathbf{V}$ is the far field velocity and $\mathbf{X}'_{ij}$ is the trajectory fluctuation caused by block (i,j). Trajectory second moments are given by

$$X_{ms}(t) = \sum_i \sum_j E\left[X'_{ij,m}(x_0 - \bar{x}_{ij}) X'_{ij,s}(x_0 - \bar{x}_{ij}) \right]$$

where m and s refer to the components of the vectors of the trajectory fluctuations.

Details of the computation method are given by Lessoff and Dagan and by Fiori et al.
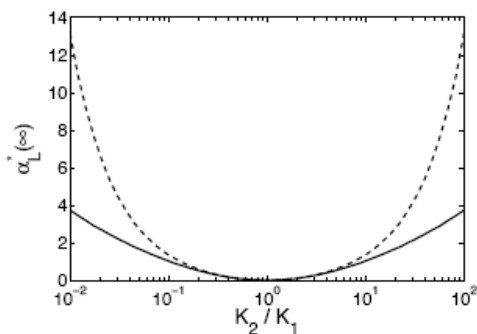
Figure 2.12: Influence of permeability contrast on apparent longitudinal dispersivity. Proportions of inclusions are $p_1 = p_2 = 0.5$. $e = 1$ (solid line) and $e = 1/4$ (dashed line).
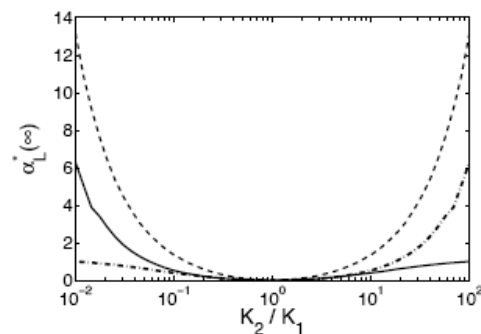
Figure 2.13: Influence of permeability contrast on apparent longitudinal dispersivity. Anisotropy ratio is $e = 1/4$ and proportions of inclusions are $p_2 = 0.1$ (solid line), $p_2 = 0.5$ (dashed line) and $p_2 = 0.9$ (dot-dashed line).

Figs. 2.12 to 2.15 show the behaviour of the asymptotic dispersivity for a two-facies permeability field (facies 1 and 2) of varying permeability contrast, anisotropy ratio and volumetric proportion. Each point on these figures requires computation of effective permeability and computation of asymptotic dispersivity. It appears that for equal volumetric proportion of facies, curves are symmetric. For higher anisotropy ratio,

apparent longitudinal dispersivity incresases, which is in accordance with results obtained by Lessof and Dagan under the dilute assumption. When the medium is mainly composed of a low-permeability facies, apparent dispersivity increases when permeability decreases. However, as discussed qualitatively by Dagan and Lessoff and Dagan et al., the behaviour for low permeability inclusions is altered by transverse dispersivity and molecular diffusion, which provide a cutoff in asymptotic longitudinal macrodispersivity.

When the medium is predominantly composed of high permeability inclusions, apparent dispersivity converges to a constant value for increasing permeability. Apparent dispersivity is maximum for a volumetric proportion of inclusions close to 50 %.

5. Conclusion

In this chapter, three methods for the upscaling of longitudinal dispersivity in heterogeneous media were detailed. These methods allow one to compute apparent (or effective) values of longitudinal dispersivity to be used in the ADE for an equivalent homogeneous medium.

The stochastic method is relatively popular but is bound to a strong limitation of low permeability variability. The other limitation of this method is that it is based on a statistical characterization of the permeability field. This characterization ideally requires vast amounts of data, that are generally not available in field-scale problems.

The fractal method that has been presented does not require an assumption low variability. However, it basically requires similar characterization methods as the stochastic approach, as the transport problem is parametrized using a covariance function for the permeability field and a large scale cutoff distance. Finally, the self-consistent approach allowed one to derive apparent dispersivity values in the case of highly heterogeneous media. The main limitation of this approach is that diffusive and local-scale dispersive transport are not considered, which might induce a serious bias when considering media with relatively low permeabilities.

The basic approach for modelling large-scale solute transport consists then to use the upscaled dispersion coefficients in the classical advection-dispersion equation and solve it at the scale of interest. However, as the time needed to reach the asymptotic large-scale Fickian behavior turns out to be extremely long, the assumption of a constant macrodispersion coefficient can still be questionable in most of the case. The remaining solution consists in solving the ADE with time- or space-dependent dispersion coefficients, either numerically or analytically.

Upscaling transport parameters under the non-Fickian Approach

1. Introduction

The question of how to quantify contaminant transport in porous soils and rock has been the focus of research over several decades in hydrology, as well as in the closely related disciplines of soils science and petroleum engineering. Landmark tracer breakthrough experiments, dating mostly from the 1950s and 1960s, formed the basis for theoretical developments and analyses that considered almost exclusively the classical advection-dispersion equation (ADE). The ADE, and variants thereof, have continued to be used to this day as the principal means for considering and quantifying tracer transport in porous media.

However, just how suitable is the ADE framework for describing tracer transport in porous media? Even early pioneering experiments reported the occurrence of systematic errors in fitting breakthrough curves (BTCs) using the classical ADE. In a series of careful and well-documented column experiments, Scheidegger (1959) observed that deviations in fits of the ADE to the BTCs could not be explained simply by the usual variability (error) in experimental measurements. Scheidegger (1959, p.103) stated: "The deviations are systematic which appears to point toward an additional, hitherto unknown effect." Aronofsky and Heller (1957) also analyzed published tracer experiments and reported that systematic deviations arise between measurements and predictions using the ADE. Indeed, over the last 4 decades several other studies have pointed out some specific and serious inadequacies in the applicability of the classical ADE, even with small-scale laboratory experiments on homogeneous samples. Silliman and Simpson (1987) demonstrated convincingly in laboratory experiments the scale dependency of the dispersivity coefficient; this is in a stark contrast to the fundamental assumption that the dispersivity is a constant derived from the microgeometry of the porous medium. Such scale-dependent behaviour is typical of "non-Fickian" or "anomalous" transport. These issues are by no means limited to laboratory-scale experiments. Deviations from the classical ADE behaviour are even more significant in natural systems.

While the ADE can treat "homogeneous" porous media under some conditions, such homogeneity rarely, if ever, exists. The heterogeneity of natural geological formations at a wide range of scales necessitates consideration of more sophisticated transport theories. Why is the conceptual picture underlying the classical ADE formulation limited? What is missing from this picture describing the transport behaviour of a contaminant in a natural porous medium? The answers to these questions lie in the basic recognition that in all geological formations, heterogeneities are present at all scales, from the submillimeter pore scale to the basin scale itself. We emphasize that the term "heterogeneities" can refer o variations in the distribution of the geometrical properties (e.g., porosity and hydraulic conductivity), as well as to variations in the biogeochemical properties of the medium, all of which can affect tracer transport.

Three points of conceptual understanding can be drawn immediately from this fact:

(1) The high degree of variability in these heterogeneities rules out, a priori, the possibility of obtaining complete knowledge of the pore space in which fluids and contaminants are transported

(2) The paths travelled by a contaminant in an aquifer are strongly influenced by the heterogeneities of the geological formation, as well as by the initial and boundary conditions (BCs), which determine the underlying flow field.

(3) Tracer migration is sensitive o heterogeneities at all scales, so that we should not be surprised that small-scale heterogeneities can significantly affect large-scale behaviour.

The key consequence of these points is a critical consideration of the idea of "homogeneity" of the medium for the purposes of modelling transport and/or defining "effective" transport parameters. It has been shown that even carefully packed, laboratory-scale flow cells and columns containing porous media contain "heterogeneities". Studies using magnetic resonance imaging to visualize flow conditions within "homogeneous" geological materials in laboratory-scale, column experiments report the existence of preferential flow paths, wich strongly influence both water flow and tracer transport (e.g., Hoffman et al., 1996; Oswald et al., 1997). These

paths occur because of the presence of macrostructures (caused, e.g., from bridging effects) as well as by microstructures that reflect grain-size heterogeneities.

At the field scale the issue of "homogeneization" of course arises. Do the above mentioned laboratory-scale heterogeneities simply average out and become insignificant at large scales? If so, how large is "large"? As already noted above, heterogeneities are present at all scales. Thus, for example, the existence of preferential flow paths has been reported even in apparently "structureless" soils at the field scale (e.g., Ghodrati and Jury, 1992).

The nature of contaminant transport in geological materials is thus linked inextricably to the extent and scale dependence of heterogeneities. The transport that is anomalous, or non-Fickian, occurs when the contaminant encounters, at each scale, a sufficiently broad spectrum of velocities and stagnant areas resulting from the heterogeneities. In addition to the strong influence of preferential flow paths and slow flow or diffusion-dominated regions, tracers can, in many cases be affected by biogeochemical heterogeneities; these heterogeneities enable a wide range of reaction processes that (temporarily or permanently) delay the advance of a tracer. Non-Fickian behaviour is fundamentally different from fickian transport, which is the usual assumption invoked, explicitly or implicitly, for application of the classical ADE and many of its variants. These other treatments, and many stochastic approaches, focus on definition of an effective "macrodispersion" parameter at any given scale of interest. This issue is discussed in detail below.

The concept of anomalous transport was first introduced by Montroll and Scher (1973) and Scher and Montroll (1975) and has subsequently been shown to have ubiquitous applicability to transport and diffusion in disordered systems. The original application of the concept and its quantitative predictions (Scher and Montroll, 1975) was in the field of electronic transport in amorphous semiconductors (Tiedje, 1984) and in polymeric media (Bos and Burland, 1987) where it was well confirmed by an extensive number of experimental studies. Subsequent use of these ideas expanded into many
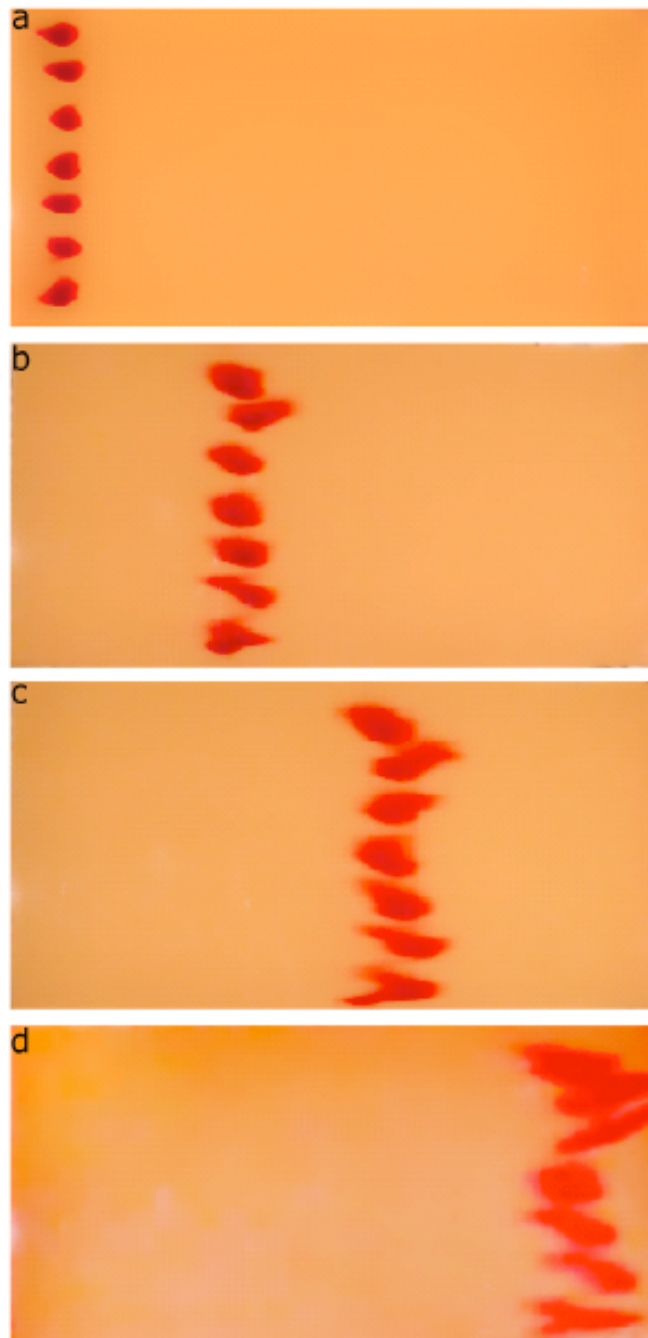
Fig. 1.- Photographs of a homogeneous, saturated sand pack with seven dye tracer point injections being transported, under constant flow of 53 mL/min, from left to right. Times at (a) t=20, (b) t=105, (c) t=172 and (d) t=255 min after injection.

Internal areas, e.g., the anomalous diffusion of defects as a basis for the universal stretched exponential relaxation behaviour in a diverse number of materials (Shlesinger, 1988). The present application to contaminant transport in geological formations is a uniquely rich example, as the full chemical plume and BTCs can be measured directly; this application has represented a new level of confirmation and further development of the theory.

Here and throughout, we use the term "anomalous" and "non-Fickian" interchangeably to denote any transport which differs from that described by the classical ADE. The ADE describes Fickian behaviour in the sense that mechanical dispersion is assumed to be quantifiable by a macroscopic form of Fick's law, and the resulting temporal and spatial concentration distributions of an initial pulse are equivalent to a normal, otherwise known as a Gaussian, distribution.

To illustrate just how frequently non-Fickian transport occurs, consider tracer migration through an "homogeneous", fully saturated sand pack. As indicated above, preferential paths for fluid flow and tracer transport are present even in these conditions, as shown, for example in Figure 1.

dimensions of the flow cell are 86 cm (length), 45 cm (height) and 10 cm (width). Reprinted from Levy and Berkowitz (2003)

Contrary to Fickian transport the individual dye plumes are not symmetrical ellipses, nor are the different plumes identical to each other. Moreover, measurements of tracer BTCs in such "homogeneous", meter-length flow cells have been shown to display "anomalous" early time arrivals (i.e., later than Fickian) and late time tails [Levy and Berkowitz, 2003]. Detailed analysis (see section 3.4.2) shows that the motion and spreading of these chemical plumes are characterized by distinct temporal scaling; that is, the time dependence of the spatial moments does not correspond to a normal (or Gaussian) distribution. In sections 2–5 we discuss the Continuous Time Random Walk (CTRW) approach to these transport phenomena, and in sections 6 and 7 we contrast it with other approaches that have been fully discussed in the literature.

2. Continuous Time Random Walk Framework

Two well-studied, generic geological media that possess heterogeneities on a very wide range of spatialscales are porous sedimentary rock and ''random'' fracture networks (RFN) in low-permeability rock. At the field scale a reasonable definition of the macroscopic characteristics (e.g., individual facies) of these geological formations can be feasible, thus enabling, at a sufficiently coarse resolution, modeling of flow and transport conditioned on these features.

However, in practice, there is always some scale, λ, below which ($y < \lambda$) heterogeneities are unresolved. The omnipresent question is, Can one justify the use of average local properties (e.g., mean velocity and dispersion) at the scale λ, or does the range of unresolved heterogeneities $y < \lambda$ have a key influence on overall transport behaviour? The answer is very often a practical one, not an intrinsic one, depending on the width of the distribution of material properties for $y < \lambda$.

To account for the effect of a sufficiently broad (statistical) distribution of material properties (e.g., of permeabilities) on the overall transport, one must consider a probabilistic approach that will generate a probability density function (pdf) describing key features of the transport.

This pdf, denoted $\psi(\mathbf{s},t)$, is discussed thoroughly starting in section 2.3. The effects of multiscale heterogeneities on contaminant transport patterns are significant, and consideration only of the mean transport behaviour, e.g., the spatial moments of the concentration distribution, is not sufficient.

An essential input to the calculation of the field-scale transport is the plume motion and/or BTC across the λ scale. The CTRW is a probabilistic approach for calculating the latter based on a pdf of transition times (see section 2.1) generated by the range of heterogeneities. The nature of the transport, non-Fickian or Fickian, is determined by the functional shape of the pdf.

2.1. Conceptual Picture. Tracer Transitions

Contaminant motion in geological formations can be treated by considering particles (which represent, e.g., dissolved solutes) undergoing various types of transitions. These transitions encompass both the displacement due to structure and heterogeneity as well as the time taken to make the particle movement between, e.g., pores or fracture intersections. We conceptualize transport as a series of such particle transitions with a focus on retaining the full distribution of the transition times.

The variability in the hydraulic and geochemical properties of the geological domain cause a variety of particle transitions at velocity changes within the flow field, between flowing and stagnant zones, between mobile and immobile states, between macropores and micropores, between fractures and adjacent host rock, and by changes in advective paths at fracture and macropore intersections. This picture of motion by transitions will be referred to as "CTRW theory", whereas the mathematical formalism used to implement the motion will be called the "CTRW framework."

Each transition can be quantified as $w(\mathbf{s},\mathbf{s}')$, the rate of particle transfer to position $\mathbf{s}$ from $\mathbf{s}'$, and can be considered on any spatial scale, e.g., on a pore scale between pore positions through an interpore throat (i.e., a ''tube''). A multiple rate approach considers the range of these rates $\{w\}$. At this point one can see the basic problem in working with average rates in some representative region or volume, traditionally referred to as a "representative elementary volume" (REV). A particle "encounter" with a sparsely distributed, very small rate w_0 can have a large impact on the overall transport, but w_0 can be entirely absent in a REV average of $\{w\}$; other problems with the REV have been pointed out previously in the literature.

Thus the details of the distribution of $\{w\}$, or as we will show the ensemble average of the $\{w\}$ over all the configurations of a specific system, are key to the nature of the transport. The variation in spatial displacements in the distribution of $w(\mathbf{s},\mathbf{s}')$ is small in the type of transport typically encountered in geological formations. For example, the "tube" lengths in the pore-scale model above have a narrow distribution. However, the variation in rates (i.e., values of $w(\mathbf{s},\mathbf{s}')$), which is governed by the velocity spectrum of the flow field, is very large for highly disordered media; for example, the fluid flow

distribution in the "tubes" governs the transit time between pore sites (see section 3.8).

Hence the temporal distribution of the pdf (i.e., the range of $\left[w(\mathbf{s},\mathbf{s}') \right]^{-1}$) discussed at the beginning of section 2 dominates the nature of the transport. The emphasis on temporal aspects of particle transport, induced by the spatial heterogeneity, is a key feature of the CTRW approach. We consider the significance of this emphasis further when we contrast CTRW to the usual ADE framework in section 6.1.

For now, we picture tracer transport as a series of discrete (in space) transitions. These can be defined naturally, for example, as transitions through a fracture network between fracture intersections. If we carefully retain the temporal distribution of these transitions, this picture can be expanded easily to a continuous-in-space formulation.

2.2. Basic Formulation of Transport

Our point of departure is a general framework that can encompass all of the processes enumerated above as special cases and reduce to the ADE for a "perfectly homogeneous" medium. Defining this overarching framework is a transport equation incorporating the full range of $\{w\}$ for any given realization of the domain,

$$\frac{\partial C(\mathbf{s},t)}{\partial t} = -\sum_{\mathbf{s}'} w(\mathbf{s}',\mathbf{s})C(\mathbf{s},t) + \sum_{\mathbf{s}'} w(\mathbf{s}',\mathbf{s})C(\mathbf{s}',t) \tag{1}$$

where $C(\mathbf{s}, t)$ is the normalized particle concentration or probability at point $\mathbf{s}$ and time t in a specific realization of the domain and the dimension of $\sum_{\mathbf{s}} w$ is reciprocal time.

Equation (1) expresses a conservation of mass at each site $\mathbf{s}$ and describes the rate of concentration change at $\mathbf{s}$ as a function of the distribution of probabilities of moving from $\mathbf{s}$ to $\mathbf{s}'$ and from $\mathbf{s}'$ to $\mathbf{s}$. This equation is known as the "master equation" (ME) [Oppenheim et al., 1977; Shlesinger, 1996]. It has been utilized widely in the physics and chemistry literature, e.g., electron hopping in random systems [e.g., Klafter and Silbey, 1980a]. In most of the applications considered here, the transition rates describe the effects of the velocity field on the particle motion. It is important to point out that the transport equation (1) does not separate the effects of the varying velocity field into an advective and dispersive part of the motion.

Specification of $w(\mathbf{s},\mathbf{s}')$ involves detailed knowledge of the system, i.e., characterization of the heterogeneities on all length scales that influence the calculation of the flow field. Below the λ scale we must resort to a statistical description of this subdomain and hence to a distribution of $\{w\}$. To realize this probabilistic approach, we consider the ensemble average of (1), which can be shown [Klafter and Silbey, 1980b] to be of the form

$$\frac{\partial c(\mathbf{s},t)}{\partial t} = -\sum_{\mathbf{s}'} \int_0^t \phi(\mathbf{s}'-\mathbf{s},t-t')c(\mathbf{s},t')dt' + \sum_{\mathbf{s}'} \int_0^t \phi(\mathbf{s}-\mathbf{s}',t-t')c(\mathbf{s}',t')dt' \qquad (2)$$

where c($\mathbf{s}$, t) is the mean, ensemble-averaged, normalized concentration and $\phi(\mathbf{s},t)$ is defined in (7).

The form of (2) is a "generalized master equation" (GME) which in contrast to (1) is nonlocal in time, that is, (2) contains an integral over time requiring knowledge of the past state of the concentration.

The ensemble average of a set of local (in time) kinetic equations (e.g., equation (1)) for a disordered system leads to a nonlocal transport equation, because all of the $\{w\}$ are made available to each site and the role of $w(\mathbf{s}',\mathbf{s})$ is replaced by a function of time which depends on a distribution of transit times between sites. Hence the ensemble average of any set of equations describing the dynamics of a physical model of a disordered system will lead to a nonlocal equation. (For a simple example see section 7.1 (especially (90) and (91)).)

The various nonlocal transport equations often have similar form, but there is no intrinsic relation between them as each depends on the physical model that generated them (see section 6.2). In fact, the use of nonlocal equations for a broad class of transport problems has a long history [e.g., Zwanzig, 1960; Mori, 1965, and references therein].

Applications more specifically related to the present ones include those of Kenkre et al. [1973], Montroll and Scher [1973], Scher and Lax [1973a], Shlesinger [1974], Scher and Montroll [1975], and Klafter and Silbey [1980a].

The transition rates in (2) are time-dependent but stationary, depending only on the difference **s-s**'. Hence, depending on available knowledge of the system, λ can range from meters to tens and hundreds of meters. As in (1), note that in (2) there is no separation between an advective and dispersive part of the motion.

2.3. CTRW Transport Equations

Using the Laplace transform, it can be shown [Kenkre et al., 1973; Shlesinger, 1974] that the GME (2) is completely equivalent to a CTRW (see Appendix A)

$$R(\mathbf{s},t) = \sum_{\mathbf{s}'} \int_{\mathbf{0}}^{\mathbf{t}} \psi(\mathbf{s} - \mathbf{s}', t - t') R(\mathbf{s}', t') dt' \tag{3}$$

where R(**s**, t) is the probability per time for a walker to just arrive at site s at time t and $\psi(\mathbf{s},t)$ is the probability per time for a displacement **s** with a difference of arrival times of t.

The initial condition for R(**s**, t) is $\delta_{\mathbf{s},0}\,\delta(t - 0^+)$, which can be appended to (3). The $\psi(\mathbf{s},t)$ is the basic pdf discussed at the beginning of section 2; $\psi(\mathbf{s},t)$ determines the nature of the transport, as will be considered in applications below.

A random walk with continuous time was introduced by Montroll and Weiss [1965] using a distribution $\psi(t)$ (see (5)) for the step time. The generalization of the formalism, i.e., the appearance of equation (3) with the joint distribution $\psi(\mathbf{s},t)$ and labeled "CTRW", and the physical application to transport, was first given by Scher and Lax [1973a]. Equation (3) describes a semi-Markovian process, Markovian in space but not in time, which accounts for memory in particle transitions. The CTRW reduces to a Markovian random walk for a single rate.

The correspondence between (2) and (3) is

$$c(\mathbf{s},t) = \int_{\mathbf{0}}^{\mathbf{t}} \psi(t - t') R(\mathbf{s}, t') dt' \tag{4}$$

where

$$\psi(t) = 1 - \int_0^t \psi(t')dt' \tag{5}$$

is the probability for a walker to remain on a site,

$$\psi(t) \equiv \sum_{\mathbf{s}} \psi(\mathbf{s},t) \tag{6}$$

$$\tilde{\phi}(\mathbf{s},u) = \frac{u\tilde{\psi}(\mathbf{s},u)}{1-\tilde{\psi}(u)} \tag{7}$$

where the Laplace transform (L) of a function f(t) is denoted by $\tilde{f}(u)$.

Equations (3)–(5) are in the form of a convolution in space and time and can therefore be solved using Fourier (F) and Laplace transforms [Scher and Lax, 1973a]. The general solution, for periodic BCs in a lattice of size N (with site positions $\mathbf{s} = \sum_{j=1}^{3} s_j a_j, s_j = 1,2,3,...,N$ and a_j=lattice constant), is

$$C(\mathbf{k},u) = \frac{1-\overline{\psi}(u)}{u}\frac{1}{1-\Lambda(\mathbf{k},u)} \tag{8}$$

Where $C(\mathbf{k},u)$ and $\Lambda(\mathbf{k},u)$ are the Fourier transforms of $\tilde{c}(\mathbf{s},u)$ and $\tilde{\psi}(\mathbf{s},u)$ respectively, where for each component of $\mathbf{k}$ the range of k values is $k_i = 2\pi l_i/N$, and l_i is an integer, $-(N-1)/2 \leq l_i \leq (N-1)/2$, for odd N.

An input of $\psi(\mathbf{s},t)$ in Λ in (8) leads to the determination of c($\mathbf{s}$, t), which represents the tracer plume concentration after a F and L inversion. Because N is considered to be very large, the solution (8) is regarded as being in the infinite domain, vanishing at infinity.

Solutions for a bounded domain and for more general boundary conditions can also be developed. Note also that as N is very large, the lattice constant can be arbitrarily small and, for example, $\psi(\mathbf{s},t)$ can have a range of many lattice sites. The lattice thus acts as a "scaffold" to determine the solution (8) and does not confine the spatial distribution of the plume.

In addition to the determination of the concentration plume (8), another key function in CTRW is the first passage time distribution F(**s**, t), the probability density for a walker starting at the origin to reach s for the first time.

The solution in (8) is for periodic BCs; experiments and observations often call for an absorbing BC or exit plane. The main measurement for these experiments is the BTC, which is equivalent to the F(**s**, t) evaluated on a plane (e.g., s_1=L).

The implicit relation for F(**s**,t) is

$$R(\mathbf{s},t) = \delta_{\mathbf{s},0}\delta\left(t - 0^+\right) + \int_0^t F(\mathbf{s},t')R(0,t-t')dt' \tag{9}$$

Which states that the walker arrives at **s** for the first time at time t' and in the remaining time t-t', the walker can visit and leave **s** an arbitrary number of times but ends at **s**.

Equation (9) contains a convolution in time, and so in Laplace space the relation becomes an algebraic one that is solved easily:

$$\tilde{R}(\mathbf{s},u) = \delta_{\mathbf{s},0} + \tilde{F}(\mathbf{s},u)\tilde{R}(0,u) \tag{10}$$

thus:

$$\tilde{F}(\mathbf{s},u) = \frac{\tilde{R}(\mathbf{s},u) - \delta_{\mathbf{s},0}}{\tilde{R}(0,u)} \tag{11}$$

To obtain a BTC, we first consider that the walk starts from a plane, e.g. s_1=0, and evaluate F(**s**,t) at a fixed distance s_1=L by summing over the other s_i directions (i>1),

$$f_B(t) \equiv \sum_{s_2,s_3} F\left(s_1 = L, s_2, s_3, t\right) \tag{12}$$

2.4. Numerical Inversion of Laplace Transforms

The analytical solutions developed in section 2.3, are of limited use in their Laplace space form. We therefore need to invert these solutions to the time domain. The inversion for the L involves finding the solution g(t) of an integral equation of the first kind [Krylov and Skoblya, 1977]:

$$\int_0^\infty g(t)e^{-ut}dt = G(u) \qquad (13)$$

where G(u) is a given function of the complex parameter u.

In a few important cases we can develop G(u) in an asymptotic form, for small u behavior, and solve for g(t) for large t by analytic means. In general, we must resort to numerical means. We use the de Hoog et al. [1982] Laplace inversion algorithm, which makes use of complex-valued Laplace parameters.

The algorithm works as follows: Suppose that one is interested in the solution for a range of times spanning from t_{min} to t_{max}. This range of times is then discretized in a time vector of arbitrary length N. It was observed that simultaneous inversion for times covering several orders of magnitudes gives inaccurate results for the small times.

Therefore the algorithm splits the time vector for which we want to obtain the concentrations into sections of the same order of magnitude (usually a logarithmic cycle), and the individual sections are inverted at a given time. So if the time vector spans n orders of magnitude, the inversion process will run n times. It is often a good idea to discretize the time vector in such a way that its values are equally spaced on a logarithmic scale.

The solution of the complex-valued partial differential equation (pde) must be known for a series of u values determined by the expression

$$u_{k,j} = \frac{1}{2T_k}\left(-\log_{10}\varepsilon + j2\pi\sqrt{-1}\right) \qquad (14)$$

where T_k is the maximum time for the kth piece of time vector (k=1,...,n), and j=1,...,m. The ε parameter is typically of the order of 10^{-9}, and m is the number of terms in the Fourier series expansion (obtained from the inversion integral using the trapezoidal rule), typically in the range of 20 to 40. Note that, for each of the n pieces, the complex-valued $u_{k,j}$ in the above formula have an invariant real part and a variable imaginary part where the Fourier series expansion is calculated (with the use of an accelerated convergence method of the algorithm [de Hoog et al., 1982]). Practically, the user provides the full range of times and the numerical inversion subroutine will call

the pde solver $n \times m$ times, one for each of the $u_{k,j}$ values determined by the above procedure. The output is a series of concentration values at the discretized times in the time vector.

On the basis of the solutions discussed herein and the work of Dentz et al. [2004] and Cortis et al. [2004b], a CTRW ''toolbox'' has been developed [Cortis and Berkowitz, 2005] that provides a collection of easy-to-use MATLAB scripts and functions to calculate the full temporal and spatial behavior of a migrating tracer. The CTRW toolbox is freely available at http://www.weizmann.ac.il/ESER/People/Brian/CTRW.

2.5. Critique of the CTRW Approach

The applicability of the CTRW approach to a range of experiments was shown in section 3, and the numerical simulations of transport in nonstationary domains demonstrate further applicability of CTRW to field situations.

These features indicate that the interactions between the transporting particle and the medium can be mapped effectively onto an appropriate choice of $\psi(s, t)$. Furthermore, a few characteristics of the $\psi(s, t)$ are very often sufficient to capture completely the particle dynamics. This description begs the immediate question of how one obtains $\psi(s, t)$. A considerable effort may be required, but one can proceed in a hierarchy of levels of approximation. Here we suggest five possible approaches:

(1) Fit the measurements with a simple form of $\psi(s, t)$, e.g., (45), and use β as a fitting parameter.

(2) Develop a ''library'' of $\psi(s, t)$ for different types of geological formations and flow conditions.

(3) Obtain the velocity histogram for a RFN [Scher et al., 2002a], a porous medium [Bijeljic and Blunt, 2006], or permeability field [Di Donato et al., 2003] and model $\psi(s, t)$.

(4) Perform a numerical simulation on part of a complex system, e.g., an array of intersecting fracture platelets, and determine $\psi(s, t)$ in terms of variables such as platelet size and aperture and then use a pdf of these variables to develop $\psi(s, t)$ for the entire system.

(5) Determine the w(s, s') and calculate the ensemble average. Also, in the case of a multiple trapping scenario, constraints on ψ(s, t) can be obtained by using its specific connection to mass transfer.

Explicit and analytical linking or conditioning of ψ(s, t) to known physical information, such as the heterogeneity of the hydraulic conductivity field, is certainly a key area to develop. A step in this direction is given by Dentz and Berkowitz [2005], who demonstrate a ψ(s, t) that is based explicitly on the underlying heterogeneity distribution, for the case of transport under spatially random adsorption. On the other hand, it should be recognized that there naturally are limitations to full determination of ψ(s, t), or for that matter any such effective transport description, from purely theoretical considerations.

However, to reiterate, on a practical level such full determination of ψ(s, t) is not crucial. The remarkable feature documented in this paper is that a very few parameters capturing the important features of ψ(s, t) are sufficient to account quantitatively for a host of observations. Even the well-known determination of the macrodispersion coefficient given by Gelhar and Axness [1983], as used in the ADE, is predicated on the assumption of Fickian transport but also on ignoring completely the dependence of this parameter on the cutoff (transition) time between non-Fickian and Fickian transport.

Moreover, a priori prediction of this transition is not trivial, being dependent on, e.g., the velocity distribution, the particle residence time, the heterogeneity scale of the hydraulic conductivity, and the boundary conditions. Thus full specification of a transport equation and parameter values must ultimately rest on site-specific measurements. As noted in the preceding paragraph, several approaches can be taken to obtain this information. In particular, because the underlying permeability distribution of a domain gives rise to the velocity distribution, which thus includes naturally all correlations affecting transport, the velocity distribution can be used to define the actual particle distributions. Treatment of many sorption and other multiple trapping pictures is straightforward and shown by, e.g., Margolin et al. [2003]. Further extension of the CTRW formulation, i.e., specification of either a ψ(s, t) and/or modifications to account explicitly for biogeochemical reactions such as precipitation/dissolution or other, often nonlinear (feedback), reactions is another area for future research.

Another important area for further development focuses on methods of solving the transport equation. While the mathematics are somewhat more extended than those involved with the familiar ADE, CTRW solutions are accessible, and the pde formulation enables adaptation of many existing solution techniques. This review has focused on the methodology of Laplace transforms, but one can work directly in the time domain, if desired.

Because CTRW results from an ensemble average, the concentration distribution in CTRWis also an ensembleaveraged quantity, which we usually assume to be sufficient for a system size large compared to the scale of heterogeneity. The variation in the concentration, at a specific location, among different realizations of the underlying random fields is thus not quantified explicitly; that is, the average concentration is an ensemble average. In other words, if the system size L is much greater than the scale of heterogeneity l, then the rearrangement of the heterogeneity disorder from one realization to the next will result in a small change in a given neighborhood. Hence the variation from the ensemble-averaged $C(s, t)$ is expected to be small. Furthermore, the dynamics of $c(s, t)$ are governed by $\psi(s, t)$, which is a pdf based on the flow field (and thus heterogeneity distribution) of the entire system; this feature enhances the sampling of each locale to the heterogeneity distribution of the whole system. In contrast, if L l, then the variations in realization-to-realization configurations can lead to large heterogeneity differences in a given locale and therefore large variations in concentration. For systems with L l it is best to use the hybrid approach; the ensemble average is then used for the small-scale residual heterogeneities. Thus the issue of variations is closely tied to the comparison between L and l. On a physical basis the ensemble average is best utilized when $L > l$.

On a formal basis, ''predictive uncertainty'' in the CTRW can be considered on two levels. The first level involves the GME (2), which is an equation for the ensemble-averaged $C(s, t)$. In principle, an equation for the variance of this function can also be developed from the master equation itself. The second level is a practical one: How sensitive are the results to variations in the parameters that one inputs into $\psi(s, t)$? In any application with a model $\psi(s, t)$ one can easily use Monte Carlo simulations to compute the effects of these variations on final predictions and hence assess the ''predictive uncertainty.'' It remains to examine these issues in detail.

3. Advection-Dispersion Equation and Upscaling

In section 1 we discussed the intensive efforts to model transport in porous media over the last decades. Many of these efforts are basically tied to the ADE. Afterwards we have discussed in detail the ramifications of the ADE approach and related modeling frameworks. We then contrast them to the CTRW framework with a particular emphasis on the different methods of averaging of the disorder-induced fluctuations of transport quantities.

The ADE is used extensively in all the natural sciences; for example, in semiconductor physics it describes the flow of electrons due to an applied voltage and allows for diffusive motion driven by spatial variations of the electron density. In liquid transport the ADE is used, e.g., to calculate Taylor dispersion (molecular diffusion of particles in a flowing fluid in a pipe). The ADE is

$$\frac{\partial c(\mathbf{s},t)}{\partial t} = -\mathbf{v} \cdot \nabla c(s,t) + \mathbf{D} : \nabla\nabla c(\mathbf{s},t)$$

which is the same as the equation for constant fluid velocity v and dispersion D. Hence one derivation of the ADE applied to porous media can be based on the kinetics described by the master equation (1) with a Taylor expansion of C(s, t), and w(s, s') [Berkowitz et al., 2002].

The classical derivation of the ADE for porous media [e.g., Bear, 1972] is based on the assumption of the existence of a representative elementary volume (REV), i.e., on the assumption that at some scale x >> y the variations of the porous medium at the x scale can be considered homogeneous. The other required assumptions are that

(1) the porous medium is fully saturated;

(2) Darcy's law applies;

(3) transport of a tracer can be split a priori into an advective part and a mechanical dispersion part;

(4) mechanical dispersion obeys Fick's law, where the coefficient D is assumed to be composed of a molecular diffusion part, Dm, and a velocity-dependent part, which in one-dimensional form is written $D = Dm + v\alpha$, with α the so-called dispersivity usually assumed to be a characteristic length of the pores inside the REV

(5) the transport velocity equals the fluid velocity; and

(6) the spatial variation of the fluid velocity inside the REV can be neglected.

The historical motivation for the REV stems from the need to use a continuous mechanistic approach for porous media, i.e., media which are inherently discontinuous at the scale of the pores. For some quantities this is a very useful notion, as in defining geometrical properties like porosity, specific surface, and permeability as an average over the REV. These quantities can in some sense be considered ''local quantities.'' Averaging over the REV to define other quantities such as dispersivity is more limited and is a point of departure from the CTRW approach.

It must be recognized that use of the ADE, at a variety of different scales, is a key aspect of the vast majority of transport theories. The dispersivity a then takes on the role of a ''scaling'' parameter in the sense that varying its magnitude is the basis for fitting ADE solutions to BTC measurements ranging over several orders of magnitude. A major drawback of the approach is that, in contrast to the fundamental assumption that a is an intrinsic porous medium constant, ''force fitting'' the ADE to measurements over scales from the small laboratory column to the large field scale demonstrates an ad hoc ''space dependence'' or ''time dependence'' of a [e.g., Lallemand-Barres and Peaudecerf, 1978; Gelhar et al., 1992].

A number of approaches have been made to connect the different scales with D or a as a fitting parameter. All of these approaches start from the assumption that the ADE equation holds at some microscopic scale and then assume further that some kind of

macrodispersion parameter can be found starting from the information contained at a microscopic scale. In many approaches it is also assumed that the ADE form holds at each scale with upscaled coefficients. The two main approaches, which to some degree overlap, we denote for brevity as ''averaging'' and ''stochastic'' methods.

3.1. Volume Averaging

3.1.1. Methods

The aim of averaging is to start with the ADE at the microscopic scale and move to a larger scale to obtain an ADE with modified coefficients. The challenge is to account for the deviation from the mean, due to the microscopio fluctuations, of the velocity and dispersion. We will highlight a few of these different approaches.

In ''volume averaging,'' moving up from one scale to another in a porous medium necessitates the use of some kind of average operator on the microscopic fields at the scale Ly to obtain fields which are significant at the macroscopic scale Lx. This average operator acts on some volume of the porous medium and assigns a macroscopic value to it. Therefore, unlike the microscopic fields, the macroscopic fields are smeared over space.

The question then arises: What is the ''correct'' size of the averaging volume? The usual answer is to define a REV as the smallest volume of integration for which there are no fluctuations in the averages of one or more of the characteristic features of the porous medium; for example, Bear [1972] defines the REV in terms of porosity. The size of the REV, Lx, must be intermediate between a characteristic microscopic length and a characteristic macroscopic length scale of the sample, LR, i.e., Ly << Lx << LR.

Sometimes these length scales depend not only on the microstructure of the porous medium but also on the physical process under study. It is also possible that porous media with clear separations of the geometric scales do not have a REV for a particular physical process. We argue that this is the case for the dispersion problem in porous media.

Moreover, Berkowitz and Bachmat [1987] showed that a REV-like dispersion tensor is necessarily scale (REV size) dependent when deviations of the macroscopic velocity are taken into account. A general definition of the volume average operator, indicated by angle brackets, can be made in terms of convolution products of spatial distribution functions [Cushman, 1984; Quintard and Whitaker, 1994]. An important result relating the gradient of some quantity φ at the microscales and macroscales is represented by a theorem that states that the average of the gradient of φ, $\langle \nabla\varphi \rangle$, at the microscopic scale y equals the gradient at the macroscopic scale x of the averaged physical quantity $\langle \nabla\varphi \rangle$ plus a fluid-solid surface average contribution.

A modified accounting for the role of deviations from average values, which arise from the same upscaling framework, is to use the ''volume averaging with closure'' method. Here the term ''closure'' refers to a particular integrodifferential problem, which determines definition of the deviations of the quantities of interest from their mean value using a pde. This method thus attempts to assign coefficients that prescribe the functional dependence of deviations from average quantities on the basis of a physically meaningful microscopic process. A detailed account of the approach is given by Whitaker [1999].

The basic requirements of this method are

(1) separation of the microscopic and macroscopic length scales (see discussion below);

(2) periodicity on the boundaries of the REV;

(3) a phenomenological (postulated) relationship between the deviations of the quantities of interest from the average value and the gradient of the average quantity itself;

(4) a coefficient of proportionality in requirement 3 that usually satisfies an integrodifferential problem that is similar to, or can be mapped onto, the original microscopic equations; and

(5) a starting microscale equation that is invariably an ADE.

A typical definition of the macrodispersion coefficient (for constant porosity n and dropping the bold notation for vectors) is given by

$$\frac{\partial \langle c \rangle}{\partial t} + \langle v \rangle \frac{\partial \langle c \rangle}{\partial s} - \frac{\partial}{\partial s}\left(D \frac{\partial \langle c \rangle}{\partial s} \right) = 0$$

$$D = D_m + D_m \frac{1}{V_f} \int_{A_{fs}} (b_f - b_s) n_{fs} dA - \langle (v - \langle v \rangle)b \rangle,$$

$$(c - \langle c \rangle) = b \frac{\partial \langle c \rangle}{\partial s},$$

where the vector b is given by the problem

$$v \frac{\partial b}{\partial t} - \frac{\partial}{\partial s}\left(D_m \frac{\partial b}{\partial s} \right) = -(v - \langle v \rangle)$$

$$\frac{\partial b}{\partial s} = -I \quad \text{on} \quad A_{fs}$$

$$b = 0, \quad \text{for} \quad t = 0,$$

where, I is the identity tensor, Afs denotes the fluid-solid surface, Vf is the fluid volume, nfs is the normal vector to the fluid-solid surface, and the subscripts f and s denote fluid and solid phases, respectively. Thus the uncertainty in the fluctuations from the mean is mapped onto the quantity b, which, in turn, solves a microscopic ADE problem. The requirement of periodicity at the scale of the REV is key to this method. Bhattacharya and Gupta [1990] proved that to derive the ADE (in a central limit theorem framework, for instance), the requirement of periodicity (or quasiperiodicity) on the fluid velocity v is needed.

''Homogenization theory'' [see, e.g., Rubinstein and Mauri, 1983; Bourgeat et al., 1988] and the ''renormalization group'' are upscaling techniques that have been used in the context of volume averaging. These approaches require an underlying REV at some scale for which a significant average concentration can be defined locally. Locality is enforced by the specification of periodic BCs on the relevant quantities over the local cell (REV).

In these theories an important parameter for the upscaling of the equations is $\epsilon = L_y/L_x$, where L_x is the length scale of the macroscopic variations and L_y is the length scale corresponding to the local variations.

The homogenization method establishes a hierarchy of equations based on an expansion of the original transport problem in ϵ. A closure hypothesis is needed to truncate the hierarchy; the usual one chosen is a Fickian one [see, e.g., Bourgeat et al., 1988]. Rigorous derivation of a stochastic homogenization method that does not require periodic BCs is given by Auriault and Adler [1995] and Lunati et al. [2002].

''Renormalization group'' techniques have been used in the context of subsurface hydrology to determine macrodispersion coefficients for solute transport in random flow fields [e.g., Koch and Shaqfeh, 1992; Zhang, 1995; Jaekel and Vereecken, 1997]. Starting from an ADE with random advection, the macrodispersion coefficients are expanded into a perturbation series in the fluctuations of the random flow field. The renormalization group represents in this context a tool to systematically sum up certain contributions of the perturbation series (and in its simplest application a so-called one-loop renormalization is used).

The resulting macrodispersion coefficients are beyond second-order perturbation theory in the random field fluctuations, similar to the results obtained from the application of ''Corrsin's conjecture'' [e.g., Dagan, 1994b; Zhang, 1995]. The latter, however, has been shown to be inconsistent in two dimensions [Dagan, 1994b; Dentz et al., 2003; Attinger et al., 2004].

3.1.2. Length-Scale and Timescale Separation. A Critical Discussion of the ADE and Averaging

At the start of this section we noted basic assumptions required for applicability of the ADE. The assumptions that a porous medium can be considered homogeneous at the relevant scale of measurement and that transport mechanisms can be separated a priori into components of advection and hydrodynamic dispersion are highly restrictive. However, as discussed in section 1, illustrated in the ''homogeneous'' medium shown in Figure 1, the key underlying assumption that small fluctuations can be neglected is clearly inadequate. Thus ADE-type descriptions of tracer transport and use of, e.g., REV approaches are rarely fully correct even on local scales of several centimeters.

At best, ADE-type descriptions usually capture only the average properties of tracer migration. Only when the transport length is orders of magnitude larger than the heterogeneity scale does homogenization occur, with the result that Fickian transport is indeed present in the system. For real domains with a finite hierarchy of heterogeneity scales, but also finite (and usually limited) domain lengths, i.e., for the vast majority of field-scale transport problems of interest, a REV-like homogenization limit does not exist. To make matters more complex, determination of the ''cutoff'' at which Fickian transport descriptions are correct is far from rigorous.

Let us consider these issues further, recognizing that an efficient and meaningful upscaling to large spatial and temporal scales is required of any practical transport theory. As shown by Levy and Berkowitz [2003], analysis of solute transport in ''macroscopically homogeneous'' media indicates that flow and transport do not ''homogenize'' on the same temporal and spatial scales. The fundamental importance of time and length scales relative to the scales of heterogeneity and domain size were also examined in the context of the two column experiments in section 3.5. The transition from non-Fickian to Fickian behavior as the column length increased showed that the difference in residence time was the determining factor. In other words, the validity of Darcy's law on certain spatial scales does not automatically imply that transport of a passive solute can be described by the standard Fickian theory.

A consequence of this fact is that the effects of transport processes cannot simply be separated into ''independent'' mechanisms. Because the timescale changes as the overall flow rate changes, the transport parameters (e.g., β or equivalent parameters for other forms of $\psi(t)$ in the CTRW framework) are not ''intrinsic'' and constant. This result is in stark contrast to the specification of precisely these assumptions for, e.g., the dispersivity a in the ADE. This behavior accounts also for the intertwining of the two dispersion mechanisms in the CTRW-based FPME formulation in contrast to the usual ADE or stochastic approaches, which attribute the spreading of the BTC only to the second spatial moment of the tracer distribution. The memory function is indicative of a nonlocal-in-time dispersion, whereas the $D\psi$ parameter, required to fit the entire BTC, provides a measure of the local-in-space dispersion.

Traditional transport theories have focused on spatial heterogeneity. A key feature of the CTRW approach, on the other hand, is the emphasis on temporal aspects of particle transport, induced by spatial heterogeneity. Shifting the focus to work within the CTRW framework therefore represents a change in paradigm.

As discussed in section 6.1.1, some of the averaging techniques require that the porous medium be periodic (i.e., the hypothesis of periodicity is a crucial one in the argument of Brenner [1980], together with the hypothesis of ergodicity). While assuming periodicity is a convenient idealization for small-scale fluid flow applications [see, e.g., Dorfman and Brenner, 2002, and references therein], specification of natural geological structures as periodic is not an appropriate starting point for modeling contaminant migration. Another consequence of the periodicity requirement should also be recognized: Brenner [1980] showed that for periodic porous media the ''fluid velocity'' v is necessarily identical to the ''transport velocity'' $v\psi$ and traced the difference between the two velocities only to some particle-size dependent exclusion effect. While this is certainly an important factor, for instance, in colloidal transport (where dispersion generally plays a minor role), other mechanisms are present as well.

CTRW theory, on the other hand, is not limited by the assumption of periodicity (nor of ergodicity). Periodicity is, in fact, strictly forbidden at a local scale, because the structure of the master equation (1) requires, in general, an accounting of all jumps in the domain. Relaxing these assumptions in a CTRW framework leads to the correct physical picture that the fluid velocity v is, in general, different from the tracer transport velocity vψ. In the CTRW picture the relative weights of each jump, and therefore the possibility for a tracer to explore different positions in space, are governed by the transition times w-1.

3.2. Stochastic Approach

Rather than give a comprehensive review, in this section we highlight two important aspects of the stochastic approach to subsurface hydrology that are of relevance in the present context:

> (1) non-Fickian transport and

> (2) effective transport descriptions and their relation to CTRW. We emphasize that the term ''stochastic approach'' is a general one and can, in principle, include a wide variety of formulations (including CTRW) and solution methods. However, we shall use the term as it has been identified in recent years, namely, with the particular framework outlined below.

The stochastic approach has been considered extensively in subsurface hydrology and applied to a wide variety of transport situations ranging from passive and reactive solute transport to the study of seawater intrusion in spatially heterogeneous environments. For thorough overviews of stochastic modeling in hydrology we refer the interested reader to the textbooks by, e.g., Dagan [1989], Gelhar [1993], Dagan and Neuman [1997], Zhang [2002], and Rubin [2003]. Critical reckoning of the current position of stochastic modeling in subsurface hydrology can be found in a series of papers [Christakos, 2004; Dagan, 2004; Freeze, 2004; Ginn, 2004; Molz, 2004; Neuman, 2004; Rubin, 2004; Sudicky, 2004; Winter, 2004; Zhang and Zhang, 2004].

In a stochastic approach, spatially and temporally fluctuating system parameters such as hydraulic conductivity, porosity, and chemical properties of the medium, for example, are modeled as random fields characterized by specific, experimentally accessible statistical properties. The effective transport behavior of a solute can then be obtained by ensemble averaging of the observables of interest over all realizations of the respective random fields.

3.2.1. Transport Coefficients and Non-Fickian Behaviour

The influence of medium heterogeneities on largescale transport can be quantified in terms of effective transport coefficients such as the effective center of mass velocity and effective dispersion coefficients, which are derived from the first and second moments of the normalized concentration c(s, t), respectively.

In the stochastic approach, large-scale transport coefficients are defined as averages over all possible realizations of the respective random fields. We focus here on ''ensemble dispersion'' coefficients $D_{ij}^{ens}(t)$ [e.g., Kraichnan, 1959; Roberts, 1961; Gelhar and Axness, 1983; Neuman et al., 1987; Dagan, 1984, 1988], which are derived from the ensemble-averaged concentration distribution, c(s, t):

$$D_{ij}^{ens}(t) = \frac{1}{2}\frac{d}{dt}\left[\int s_i s_j c(\mathbf{s},t)d^ds - \int s_i c(\mathbf{s},t)d^ds \int s_j c(\mathbf{s},t)d^ds\right]$$

Note that the $D_{ij}^{ens}(t)$ characterize the spreading of the average solute distribution and not necessarily solote spreading in a typical heterogeneity realization, as opposed to ''effective'' dispersion coefficients [e.g., Batchelor, 1949; Kitanidis, 1988; Dagan, 1990, 1991; Rajaram and Gelhar, 1993; Zhang and Zhang, 1996; Attinger et al., 1999; Dentz et al., 2000]. The $D_{ij}^{ens}(t)$ is independent of time if, e.g., the concentration distribution is Gaussian. We focus on $D_{ij}^{ens}(t)$ because it is related to the dispersive flux in an effective upscaled transport equation for the average solute concentration.

A principal result of the stochastic approach is that of Gelhar and Axness [1983], who expressed the heterogeneity- induced solute spreading by means of a longitudinal macrodispersion coefficient $D_L{}^{mac}(t)$ related to the variance σ_{ff}^2 and correlation length l of the log-hydraulic conductivity field f(s) and the mean, ensemble-averaged, groundwater flow velocity [[v]],

$$D_L^{mac}(t) \equiv \lim_{t \to \infty} D_{l1}^{ens}(t) \propto \sigma_{ff}^2 l[[v]].$$

Frequently, large-scale transport is modeled by advectivedispersive transport with local-scale dispersion substituted by the (constant) macrodispersion coefficients. The assumptions underlying this approach are that

    (1) large-scale transport obeys the same dynamic equation as transport on a local scale and

    (2) (constant) local-scale transport coefficients can simply be substituted by their (constant) largescale counterparts given as suitably defined ensemble averages.

However, the $D_{ij}^{ens}(t)$ are, in general, functions of time or transport distance, as discussed, e.g., in section 6.1 [e.g., Koch and Brady, 1987, 1988; Dagan, 1988; Neuman and Zhang, 1990; Koch and Shaqfeh, 1992], i.e.,

$$D_{ij}^{ens} = D_{ij}^{ens}(t)$$

which implies that large-scale solute dispersion is, in general, non-Fickian.

Here we review briefly aspects of non-Fickian dispersion as a consequence of the correlation structure of the loghydraulic conductivity. We note for comparison, the CTRW theory also relates the statistical properties of the hydraulic conductivity, through determination of the statistical distribution of 1/v, directly to the $\psi(t)$ and the memory function M(t). A related treatment based on analysis of transport in streamlines is given by Di Donato et al. [2003].

3.2.2. Discussion

Most stochastic approaches to subsurface transport model local-scale transport by a spatially and temporally local transport equation that is characterized by spatially and temporally varying transport parameters. Thus nonlocal effects caused by small-scale heterogeneities are not taken into account in the ''traditional'' stochastic approaches.

While not a prerequisite, a local-scale ADE-like equation is almost invariably chosen as the starting point for development of an upscaled transport equation. As discussed in section 6, the application of (74) to describe local-scale transport in a saturated aquifer assumes that transport is Fickian in an homogeneous region. However, in real aquifers the ''homogeneous'' regions are restricted in size. As pointed out by, e.g., Levy and Berkowitz [2003] and Cortis et al. [2004a], tracer transport even over small domain sizes is not necessarily Fickian, and flow and transport do not ''homogenize'' on the same temporal and spatial scales. The effect of non-Fickian transport characteristics at the local scale remains to be explored within the framework of the stochastic approach.

A closely related problem arises: In terms of defining a local-scale equation one must ask, How local is ''local''? The heterogeneity of the conductivity field is often used to fix the heterogeneity of the velocity field (through Darcy's law), neither of which is well defined at the pore scale. As such the assumed local transport equation can be considered applicable only at some scale larger than that of the pores. In the same sense the relevant stochastic field is thus not the conductivity field but rather the velocity field.

Discussion of a number of issues related to the very existence and definition of ''macrodispersion'' is in order. First, expressions for the macrodispersion, are valid only in a large time, Fickian regime for transport. This limit is rarely, if ever, reached in practice. Second, the cutoff at which macrodispersion is reached is not well defined because of memory effects. Thus the classical ''macrodispersion'' parameter is not necessarily an ''absolute'' quantity. Another interesting perspective that questions whether macrodispersion coefficients exist is given by Lowe and Frenkel [1996].

Furthermore, conceptual questions that remain to be fully addressed refer to the issue of self-averaging [e.g., Bouchaud and Georges, 1990; Clincy and Kinzelbach, 2001; Eberhard, 2004], i.e., determining the length and timescales over which the ensemble average ''observables'' are representative (and not artifacts of the statistical ensemble) of the corresponding observables in a single realization; that is, their sample to sample fluctuations become small. Examples for when this self-averaging property does not apply are transport in a stratified medium [Clincy and Kinzelbach, 2001; Eberhard, 2004] and transport in a randomly fluctuating transient velocity field in an homogeneous medium [Dentz and Carrera, 2003]. Neuman [1993] and [Guadagnini and Neuman, 2001] developed moment equations for the ensemble moments of the solute concentration to study the uncertainty of the average solute concentration due to the sample-to-sample fluctuations of the solute concentration from realization to realization of the underlying random fields.

Practical application of the stochastic approach to quantify the full evolution of a migrating contaminant plume remains a key issue. The overwhelming emphasis of such studies has focused on spatial moment characterizations of tracer plume migration and/or determination of the macrodispersion parameter.

It is unfortunate, and somewhat perplexing, that with the intense efforts of the last decades on stochastic analyses, consideration of full, measured BTCs and efforts to fit them has rarely been attempted. Clearly, for real applications we must consider the full spatial and temporal evolution of a migrating tracer plume. A criticism to this effect was voiced by Gelhar [1997, p. 174], who stated that the emphasis of the ''stochastic approach'' over the previous decade had been on ''… theoretical refinements of practically insignificant, but conveniently solvable, problems ….''

To conclude, both the CTRW approach and the effective transport description resulting from a stochastic transport model describe effective solute transport in terms of nonlocal transport equations. The basic difference between the CTRW approach and the others discussed in this section lies in the basic starting point to quantify transport and in the method to account for the impact of fluctuations present in disordered systems.

In each chosen locale the CTRW model incorporates a full pdf of the range of transition rates composing the transport. A good illustration of this difference is given by Bijeljic and Blunt [2006]. The excellent comparison they obtained for the experimentally measured macrodispersion as a function of Pe required quantification of the b, derived from the full pdf of the interpore transit times. This key information is suppressed by the averaging over a locale to obtain coefficients for the ADE. The correct determination of macrodispersion requires full knowledge of the entire time dependence of the spatial moments of the plume (i.e., a solution of a nonlocal-in-time equation) together with the cutoff time.

4. Alternative Effective Transport Formulations

Recent attention has been focused on two alternative formulations to treat solute transport, based on the multirate mass transfer (MRMT) approach [Pfister and Scher, 1978; Roth and Jury, 1993; Harvey and Gorelick, 1995; Haggerty and Gorelick, 1995; Haggerty et al., 2000; Carrera et al., 1998] and on the use of fractional differential equations (FDE) [Benson et al., 2000; Metzler and Klafter, 2000; Baeumer et al., 2001; Schumer et al., 2003].

We note, parenthetically, that two other oft quoted formulations to quantify solute transport are based on transfer functions [Jury, 1982; Jury et al., 1986] and stochastic convective [Dagan and Bresler, 1979; Sposito et al., 1986] concepts.

The transfer function approach is a general descriptive method to characterize solute flux in heterogeneous media; a medium is treated as a black box, and heterogeneity-induced effective transport mechanisms are not specified. Transport of a solute is thus characterized by a transfer function (Green's function), which represents the solute arrival time distribution at a control plane in response to an instantaneous pulse at an input plane.

The stochastic convective model is essentially a specific implementation of the transfer function approach, which assumes that solute transport takes place in independent stream tubes with constant flow velocity. There is no mass exchange between stream tubes by local dispersion. The influence of a broad range of flow velocities on solute arrival is then taken into account by averaging the solution of the one-dimensional ADE [Dagan and Bresler, 1979; Sposito et al., 1986].

Determination of the number and properties of the stream tubes is ill-defined and nonunique, and the method provides only a purely empirical fit to existing measurements. Another drawback with these approaches is that parameters fit for a specific BTC are not generally relevant for BTC fits or predictions at other times or distances.

4.1. Multirate Mass Transfer

The MRMT approach distinguishes mobile and immobile solute fractions. MRMT thus models the effect of medium heterogeneities on effective solute transport by a distribution of typical mass transfer (exchange) times between mobile and immobile solute phases. The discussion of MRMT includes naturally multiporosity and mobile-immobile models, matrix diffusion, multiple trapping, and transport under linear first-order reactions. MRMT has been applied to quantify transport of linearly sorbing solutes [Sardin et al., 1991; Roth and Jury, 1993], and transport in media characterized by regions of fast and very slow solute transport. In the latter context one encounters multiporosity and, as a special case, double porosity models [Feehley et al., 2000] and mobile-immobile [Nkedi-Kizza et al., 1984] and matrix diffusion models [e.g., Glueckauf, 1955; Neretnieks, 1980; Rao et al., 1980; Cunningham et al., 1997; Carrera et al., 1998]. These are all summarized under the name MRMT models [Pfister and Scher, 1978; Haggerty and Gorelick, 1995; Haggerty et al., 2000] because they describe linear mass transfer from mobile to immobile solute phases.

In MRMT the total solute concentration c($\mathbf{s}$, t) is decomposed into a mobile (subscript m) and an immobile (subscript im) fraction:

$$c(\mathbf{s},t) = c_m(\mathbf{s},t) + c_{im}(\mathbf{s},t)$$

The temporal change in the total concentration is balanced by the divergence of advective and dispersive flux in the mobile phase, which yields together with the equation presented the transport equation [Roth and Jury, 1993; Haggerty and Gorelick, 1995]

$$\frac{\partial c(\mathbf{s},t)}{\partial t} = -v \cdot \nabla c_m(\mathbf{s},t) + \nabla \cdot D \nabla c_m(\mathbf{s},t)$$

This equation is closed by a linear relation between the mobile and immobile concentrations, [Pfister and Scher, 1978] or [Carrera et al., 1998; Haggerty et al., 2000; Dentz and Berkowitz, 2003].

To better understand this relation between $c_m(\mathbf{s}, t)$ and $c_{im}(\mathbf{s}, t)$, we first start with a multiple trapping process, which is a specific case of MRMT that involves first-order transitions into and out of immobilizing sites (traps).

This was the first example of MRMT shown to be a subset of CTRW [Schmidlin, 1977; Noolandi, 1977; Pfister and Scher, 1978]. It can therefore be shown that MRMT is a special case of CTRW

4.1.1. Diffusive Mass Transfer

For diffusive mass transfer the trapping rate $\omega(t_r) = \theta/t_r$, where θ denotes the volume ratio between the mobile and immobile regions. In this case, $P(t_r)$ denotes the distribution density of typical diffusion times in the immobile regions. For diffusion into spherical immobile regions the transfer function is given by [Haggerty and Gorelick, 1995; Dentz and Berkowitz, 2003]

$$R(t/t_r) = t_r L^{-1} \left\{ \frac{3}{\sqrt{ut_r}} \left[\coth\left(\sqrt{ut_r}\right) - \frac{1}{\sqrt{ut_r}} \right] \right\}$$

while for diffusion into layered immobile regions one finds

$$R(t/t_r) = t_r L^{-1} \left[\frac{1}{\sqrt{ut_r}} \tanh\left(\sqrt{ut_r}\right) \right]$$

4.1.2. "First Order" Mass Transfer

For ''first-order'' mass transfer between mobile and immobile regions (e.g., the trapping case above [Pfister and Scher, 1978; Haggerty et al., 2000]) and for linear kinetic adsorption [Roth and Jury, 1993] the transfer function is given by

$$R(t/t_r) = \exp(-t/t_r)$$

The functional form of $\omega(t_r)$ depends on the particular trapping mechanism. For purely advective trapping, $\omega(t_r) = \omega_0$ is constant; for "diffusive" trapping, i.e., if diffusive

mass transfer is to be mimicked by a first-order mechanism, then $\omega(t_r) = \theta/t_r$ [Dentz and Berkowitz, 2003].

4.1.3. Synthesis

The main point is that CTRW encompasses MRMT as a special case. The relation between MRMT and decoupled CTRW on the basis of this expression has been studied in detail by Pfister and Scher [1978] and Dentz and Berkowitz [2003].

The representation of different functions in a MRMT form, although formally possible, is not a physically meaningful MRMT process.

4.2. Fractional Derivative Equations

FDE formulations to quantify transport have received attention in recent years [e.g., Benson et al., 2000; Metzler and Klafter, 2000; Baeumer et al., 2001; Schumer et al., 2003; Zhang et al., 2005]. A detailed treatise is given by Metzler and Klafter [2000]. It should be recognized that the term "fractional" can refer to fractional order differentiation in time or space or both. Moreover, a number of definitions for fractional operators exist [Metzler and Klafter, 2000]. In principle, one can derive both temporal and spatial FDEs from a limiting form of the CTRW solution (8) by expanding $\Lambda(\mathbf{k},u)$ in (8) for small values of u and $\mathbf{k}$, rearranging the equation, and using appropriately defined operators. FDEs have also been demonstrated to be special cases of other transport formulations [e.g., Cushman and Ginn, 2000]. Here we demonstrate that the "usual" temporal fractional derivative equation for transport is a specialized, asymptotic limit of the CTRW formulation. We also discuss other limitations of using the temporal and spatial FDEs for transport modeling in porous media systems. It is interesting to note that while the (temporal) FDE is usually written phenomenologically, as a "generalized analog" to the ADE, its underlying physical and mathematical picture is elucidated when seen as a limited subset of the CTRW formulation.

The temporal FDE can be written as [Metzler and Klafter, 2000]

$$\frac{\partial c(\mathbf{s},t)}{\partial t} = -\frac{\partial^{1-\beta}}{\partial t^{1-\beta}} \left\{ \mathbf{v}'(\mathbf{s}) \cdot \nabla c(\mathbf{s},t) - \nabla \cdot \left[\mathbf{D}'(\mathbf{s}) \cdot \nabla c(\mathbf{s},t) \right] \right\}$$

with the definition of the operator

$$\frac{\partial^{-\gamma}}{\partial t^{-\gamma}}c(\mathbf{s},t) \equiv \frac{1}{\Gamma(\gamma)}\int_0^t \frac{c(\mathbf{s},t')}{(t-t')^{1-\gamma}}dt'$$

The primes on $\mathbf{v}'$ and $\mathbf{D}'$ indicate that these quantities do not have the same dimensions as usual; that is, $\mathbf{v}'$ has dimensions $[L]/[t^\beta]$. Another advantage of the CTRW transport equations, is that we can define a dimensionless time $\tau \equiv t/\bar{t}$, where $\bar{t}$ is a time unit determined by the physical model for $\psi(t)$. The comparison between FDE and CTRW must include this difference in time units. The operator shown before was constructed to possess the important relation of its L,

$$L\left[\partial^{-\gamma}c(\mathbf{s},t)/\partial t^{-\gamma};u\right] = u^{-\gamma}\tilde{c}(\mathbf{s},u)$$

One apparent attraction of the FDE to some proponents is its pde form which is similar to the familiar ADE. More significantly, the pde form of the CTRW transport equation contains the FDE as a particular case, and its evaluation for a range of BCs is straightforward.

In contrast to the temporal FDE a spatial FDE assumes a transition time distribution $\psi(t)$ with a finite first moment and a transition length distribution p(**s**) with a diverging second moment. This latter condition is unphysical, implying that some particles must execute long jumps instantaneously. This case can be shown to be a Markovian process (rather than a temporally based semi-Markovian one) called a Lévy flight. It is important to recognize that a Lévy flight refers to a random movement in space, where the length of the transitions is considered over discrete steps, but time is not involved. Lévy walks, on the other hand, attach a time "penalty" by assigning a velocity to each transition in space. In the simplest case this velocity is constant; relaxation of this condition leads back to the more general CTRW formulation [Klafter et al., 1987; Shlesinger et al., 1993]. Lévy walks cannot be described in terms of simple fractional transport equations [Metzler, 2000].

Application of a spatial FDE to tracer migration in geological formations demands a domain that contains "streaks" of high and low hydraulic conductivity, arranged so as to lead to particle transitions of high and low velocity. In other words, the physical picture of a Lévy flight requires a wide distribution of streak lengths to obtain a non-Fickian distribution of particle transitions. Recall though that non- Fickian patterns arise even without the clear presence of such a conductivity distribution. Moreover, even within a long streak, particle scatter will reduce or eliminate the number of long excursions.

The spatial FDE thus uses the power law form $p(\mathbf{s}) \approx |s|^{-1-\varsigma}, 0 < \varsigma < 2$, for the transition length, which is the characteristic function of a centered and symmetric Lévy distribution.

For $\varsigma \geq 2$ one recovers the usual Gaussian behavior. With an asymptotic (small $\mathbf{k}$) form for p($\mathbf{s}$) one can obtain [Metzler et al., 1998] a spatial FDE

$$\frac{\partial}{\partial t}c(\mathbf{s},t) + \cdot \nabla c(\mathbf{s},t) = D^{\varsigma}\nabla^{\varsigma}c(\mathbf{s},t)$$

where here D is a generalized diffusion parameter.

In terms of the CTRW framework a power law p($\mathbf{s}$) can be considered in a decoupled form of $\psi(\mathbf{s},t)$ or, alternatively, directly in a coupled $\psi(\mathbf{s},t)$. With regard to the former a power law p($\mathbf{s}$) is not generally required.

We conclude this section by pointing out also that the FDE approach, both temporal and spatial, does not recognize the transport velocity to be fundamentally different from the fluid velocity. Thus the FDE places the mechanism for non- Fickian behavior entirely on the value of the exponent controlling the (spatial or temporal) power law distribution.

We stress once again that in contrast the CTRW formulation is more comprehensive: The memory function accounts for the nonlocal-in-time dispersion, whereas $\mathbf{D}_{\psi}$ provides a measure of the local-in-space dispersion.

5. Conclusions

Quantification of contaminant transport in geological formations has been a long-standing problem. The difficulty in capturing the complexities of tracer plume migration patterns suggests that local, small-scale heterogeneities cannot be neglected; we have shown that these unresolvable heterogeneities contribute significantly to the occurrence of non-Fickian transport. Indeed, BTCs of passive tracers in even macroscopically "homogeneous" granular materials exhibit non-Fickian features: Early and late arrival times are observed to differ systematically from theoretical predictions based on solution of the ADE for uniform porous media. Even in these small-scale, "homogeneous" domains, subtle and residual pore-scale disorder effects can account for these observations.

We have reviewed a recent, different approach to this problem based on a CTRW framework. The theory developed within this framework is structured by a conceptual picture of transport as a sequence of particle transfer rates. The starting point to arrive at the CTRW is the master equation, which describes the kinetics of the probability of site occupancy, incorporating these rates, for a single realization of an heterogeneous medium. The ensembleaveraged ME is the GME, which we show is equivalent to the CTRW, and serves as the transport equation. A particularly convenient approximation of this equation is the pde "similar" in form, in Laplace space, to the well-known ADE.

On this basis we can state that the CTRW framework represents a powerful and effective means to quantify transport in a wide range of porous and fractured media. It enables calculation of both BTCs and the full temporal and spatial evolution of contaminant plumes, covering both the premacrodispersion and macrodispersion regime time ranges. Further, as the calculation does not resort to using perturbation theory, the results are valid for strongly heterogeneous formations (e.g., log hydraulic conductivity variance >10). The CTRW theory can be extended naturally to treat transport in nonstationary domains with specific conditioning information.

[1] Anderman, E. R., and Hill, M. C. Modflow-2000, the U.S. Geological Survey modular ground-water model. Documentation of the advective-transport observation (ADV2) package, version 2. Tech. Rep. 01-54, U.S. Geological Survey, 2001.

[2] Anderman, E. R., and Hill, M. C. Modflow-2000, the U.S. Geological Survey modular ground-water model. Documentation of effective porosity parameters in the advective-transport observation (ADV2) package. Tech. rep., U. S. Geological Survey, 2003.

[3] Anderson, M. P. Using models to simulate the movement of contaminants through groundwater flow systems. Critical Reviews in Environmental Control, 2 (1979), 97–156.

[4] Aral, M. M., and Liao, B. Analytical solutions for two-dimensional transport equation with time-dependent dispersion coefficients. Journal of Hydrologic Engineering 1, 1 (1996), 20–32.

[5] Aris, R. On the dispersion of a solute in a fluid flowing through a tube. Proc. Royal Soc. London A235 (1956), 67–77.

[6] Baeumer, B., Benson, D. A., and Meerschaert, M. M. Advection and dispersion in time and in space. Physica A 350 (2005), 245–262.

[7] Baeumer, B., Benson, D. A., Meerschaert, M. M., and Wheatcraft, S. W. Subordinated advection-dispersion equation for contaminant transport. Water Resources Research 37, 6 (2001), 1543–1550.

[8] Bahr, J. M., and Rubin, J. Direct comparison of kinetic and local equilibrium formulations for solute transport affected by surface reactions. Water Resources Research 23, 3 (1987), 438–452.

[9] Bajracharya, K., and Barry, D. A. Nonequilibrium solute transport parameters and their physical significance : numerical and experimental results. Journal of Contaminant Hydrology 24 (1997), 185–204.

[10] Barth, G. R., Hill, M. C., Illangasekare, T. H., and Rajaram, H. Predictive modeling of flow and transport in a two-dimensional intermediatescale, heterogeneous medium. Water Resources Research 37, 10 (2001), 2503– 2512.

[11] Barth, G. R., Illangasekare, T. H., Hill, M. C., and Rajaram, H. A new tracer-density criterion for heterogeneous porous media. Water Resources Research 37, 1 (2001), 21–31.

[12] Baveye, P., Jacobson, A., Allaire, S., Tandarich, J., and Bryant, R. Whither goes soil science in the us and canada? Survey results and analysis. Soil Science in press (2006).

[13] Bear, J. Dynamics of fluids in porous media. American Elsevier Publishing Company, 1972.

[14] Bellin, A., Salandin, P., and Rinaldo, A. Simulation of dispersion in heterogeneous porous formations : statistics, first-order theories, convergence of computations. Water Resources Research 28, 9 (1992), 2211–2227.

[15] Benson, D. A., , Meerschaert, M. M., Baeumer, B., and Scheffler, H.-P. Aquifer operator scaling and the effect on solute mixing and dispersion. Water Resources Research 42 (2006), doi:10.1029/2004WR003755.

[16] Benson, D. A. The fractional advection-dispersion equation : development and application. PhD thesis, University of Nevada, Belgium, May 1998.

[17] Benson, D. A., Tadjeran, C., Meerschaert, M. M., Farnham, I., and Pohll, G. Radial fractional-order dispersion trough fractured rocks. Water Resources Research 40 (2004), doi:10.1029/2004WR003314.

[18] Benson, D. A.,Wheatcraft, S.W., and Meerschaert, M. M. Application of a fractional advection-dispersion equation. Water Resources Research 36, 6 (2000), 1403–1412.

[19] Benson, D. A., Wheatcraft, S. W., and Meerschaert, M. M. The fractional-order governing equation of Lévy motion. Water Resources Research36, 6 (2000), 1413–1423.

[20] Berentsen, C. Upscaling of flow in porous media from a tracer perspective. PhD thesis, T. U. Delft, The Netherlands, 2003.

[21] Berentsen, C. W. J., Verlaan, M. L., and van Kruijsdijk, C. P. J. W. Upscaling and reversibility of Taylor dispersion in heterogeneous porous media. Physical Review E 71 (2005), doi:10.1103/PhysRevE.71.046308.

[22] Berkowitz, B., Klafter, J., Metzler, R., and Scher, H. Physical pictures of transport in heterogeneous media : advection-dispersion, random walk and fractional derivatives formulations. Water Resources Research 38, 10 (2002).

[23] Berkowitz, B., Kosakowski, G., Margolin, G., and Scher, H. Application of continuous time random walk theory to tracer test measurements in fractured and heterogeneous porous media. Groundwater 39, 4 (2001), 593–604.

[24] Berkowitz, B., and Scher, H. On characterization of anomalous dispersion in porous and fractured media. Water Resources Research 31, 6 (1995), 1461–1466.

[25] Berkowitz, B., and Scher, H. The role of probabilistic approaches to transport theory in heterogeneous media. Tranport in Porous Media 42 (2001),241–263.

[26] Berkowitz, B., Scher, H., and Silliman, S. E. Anomalous transport in laboratory-scale, heterogeneous porous media. Water Resources Research 36, 1(2000), 149–158.

[27] Berkowitz, B., Scher, H., and Silliman, S. E. Correction to : Anomalous transport in laboratory-scale, heterogeneous porous media. Water Resources Research 36, 5 (2000), 1371.

[28] Bogaert, P. Introduction a la geostatistique. Université catholique de Louvain, Louvain-la-Neuve, Belgium, 2003.

[29] Bridge, J. S., and Leeder, M. R. A simulation model for alluvial stratigraphy.Sedimentology 26 (1979), 617–644.

[30] Bromly, M., and Hinz, C. Non-fickian transport in homogeneous unsaturated repacked sand. Water Resources Research 40 (2004),doi:10.1029/2003WR002579.

[31] Brusseau, M. L. Application of a multiprocess nonequilibrium sorption model to solute transport in a stratified porous medium. Water Resources Research27, 4 (1991), 589–595.

[32] Brusseau, M. L., Gerstl, Z., Augustijn, D., and Rao, P. S. C. Simulating solute transport in an aggregated soil with the dual-porosity model: measured and optimized parameter values. Journal of Hydrology 163 (1994), 187–193.

[33] Brusseau, M. L., Hu, Q., and Srivastava, R. Using flow interruption to identify factors causing non ideal contaminant transport. Journal of Contaminant Hydrology 24 (1997), 205–219.

[34] Caccia, D. C., Percival, D., Cannon, M. J., Raymond, G., and Bassingthwaighte,J. B. Analyzing exact fractal time series: evaluating dispersional analysis and rescaled range methods. Physica A 246 (1997), 609–632.

[35] Camacho, J. Purely global model for Taylor dispersion. Physical Review E48, 1 (1993), 310–321.

[36] Camacho, J. Thermodynamic functions for Taylor dispersion. Physical Review E 48, 3 (1993), 1844–1849.

[37] Camacho, J. Thermodynamics of Taylor dispersion : Constitutive equations. Physical Review E 47, 2 (1993), 1049–1053.

[38] Carle, S. F. T-Progs : Transition probability geostatistical software version 2.1. University of Carlifornia, Davis, 1999.

[39] Carle, S. F., and Fogg, G. E. Transition probability-based indicator geostatistics. Mathematical Geology 28, 4 (1996), 453–476.

[40] Carle, S. F., and Fogg, G. E. Modeling spatial variability with one and multidimensional continuous-lag Markov chains. Mathematical Geology 29, 7 (1997), 891–918.

[41] Chao, H.-C., Rajaram, H., and Illangasekare, T. Intermediate scale experiments and numerical simulations of transport under radial flow in twodimensional heterogeneous porous medium. Water Resources Research 36, 10 (2000), 2869–2878.

[42] Christakos, G., Bogaert, P., and Serre, M. Temporal GIS: Advanced Functions for Field-Based Applications. Springer-Verlag, New York, 2002.

[43] Cirpka, O. A. Spectral methods for flow and transport in heterogeneous formations. In 20th Course on Groundwater Management : Stochastic tools for groundwater modelling (ETH-Z̈urich, March 10-14 2003).

[44] Coats, K. H., and Smith, B. D. Dead-end pore volume and dispersion in porous media. Society of Petroleum Engineering Journal 4 (1964), 73–84.

[45] Cortis, A., and Berkowitz, B. Computing anomalous contaminant transport in porous media : The CTRW Matlab toolbox. Groundwater 43, 6 (2005), 947–950.

[46] Cortis, A., Gallo, C., Scher, H., and Berkowitz, B. Numerical simulation of non-Fickian transport in geological formations with multiple-scale heterogeneities. Water Resources Research 40 (2004), doi:10.1029/2003WR002750.

[47] Curtis, G. P., Davis, J. A., and Naftz, D. L. Simulation of reactive transport of uranium(VI) in groundwater with variable chemical conditions. Water Resources Research 42 (2006), doi:10.1029/2005WR003979.

[48] Cushman, J. H., and Ginn, T. R. Fractional advection-dispersion equation : a classical mass-balance with convolution-Fickian flux. Water Resources Research 36, 12 (2000).

[49] Cvetkovic, V., and Haggerty, R. Transport with multiplerate exchange in disordered media. Physical Review E 65 (2002), doi:10.1103/PhysRevE.65.051308.

[50] Dagan, G. Models of groundwater flow in statistically homogeneous porous formations. Water Resources Research 15, 1 (1979), 47–63.

[51] Dagan, G. Solute transport in heterogeneous formations. Journal of Fluid Mechanics 145 (1984), 151–177.

[52] Dagan, G. Time-dependent macrodispersion for solute transport in anisotropic heterogeneous aquifer. Water Resources Research 24, 9 (1988), 1491–1500.

[53] Dagan, G. Flow and Transport in porous formations. Springer, New-York, 1989.

[54] Dagan, G., and Fiori, A. Time-dependent transport in heterogeneous formations of bimodal structure. 1. The model. Water Resources Research 39, 5 (2003), doi:10.1029/2002WR001396.

[55] Dagan, G., Fiori, A., and Jankovic, I. Flow and transport in highly heterogeneous formations. 1. Conceptual framework and validity of first-order approximations. Water Resources Research 39, 9 (2003), doi:10.1029/2002WR001717.

[56] Dagan, G., and Lessoff, S. C. Solute transport in heterogeneous formations of bimodal conductivity distribution. 1. Theory. Water Resources Research 37, 3 (2001), 465–472.

[57] Dai, Z., Ritzi, R. W., and Dominic, D. F. Improving permeability semivariograms with transition probability models of hierarchical sedimentary architecture derived from outcrop analog studies. Water Resources Research 41 (2005), doi:10.1029/2004WR003515.

[58] Dai, Z., Ritzi, R. W., Huand, C., Rubin, Y. N., and Dominic, D. F. Transport in heterogeneous sediments with multimodal conductivity and hierarchical organization across scales. Journal of Hydrology 294 (2004), 68–86.

[59] Danquigny, C., Ackerer, P., and Carlier, J.-P. Laboratory tracer tests on 3d heterogeneous porous media. Journal of Hydrology 294 (2004), 196–212.

[60] de Marsily, G., Delay, F., Teles, V., and Schafmeister, M. T. Some current methods to represent the heterogeneity of natural media in hydrogeology. Hydrogeology Journal, 6 (1998), 115–130.

[61] Dentz, M., and Berkowitz, B. Transport behavior of a passive solute in continuous time random walks and multirate mass transfer. Water Resources Research 39, 5 (2003), doi:10.1029/2001WR001163.

[62] Desbarats, A. J. Macrodispersion in sand-shale sequences. Water Resources Research 26, 1 (1990), 153–163.

[63] Deutsch, C. V., and Journel, A. G. GSLIB : Geostatistical software library and user's guide, 2nd ed. Applied Geostatistics Series. Oxford University Press, New-York, 1998.

[64] Deutsch, C. V., and Wang, L. Hierarchical object-based stochastic modeling of fluvial reservoirs. Mathematical Geology 28, 7 (1996), 857–880.

[65] Domenico, P. A., and Robbins, G. A. A dispersion scale effect in model calibration and field tracer experiments. Journal of Hydrology, 70 (1984), 123– 132.

[66] Domenico, P. A., and Schwartz, F. W. Physical and Chemical hydrogeology. J. Wiley and sons, 1998.

[67] Eames, I., and Bush, J. W. M. Longitudinal dispersion by bodies fixed in a potential flow. Proc. Royal Soc. London 455 (1999), 3665–3686.

[68] Elfeki, A. M. M., Uffink, G. J. M., and Barends, F. B. J. Groundwater contaminant transport: impact of heterogeneous characterization. Balkema, Rotterdam, 1997.

[69] Feehley, C. E., Zheng, C., and Molz, F. J. A dual-domain mass transfer approach for modeling solute transport in heterogeneous aquifers : application to the Macrodispersion Experiment (MADE) site. Water Resources Research 36, 9 (2000), 2501–2515.

[70] Fernandez-Garcia, D., Illangasekare, T. H., and Rajaram, H. Conservative and sorptive forced-gradient and uniform flow tracer tests in a threedimensional laboratory test aquifer. Water Resources Research 40 (2004), doi:10.1029/2004WR003112.

[71] Fernandez-Garcia, D., Sanchez-Vila, X., and Illangasekare, T. H. Convergent-flow tracer tests in heterogeneous media : combined experimentalnumerical analysis for determination of equivalent transport parameters. Journal of Contaminant Hydrology 57 (2002), 129–145.

[72] Fetter, C. W. Contaminant Hydrology, 2nd ed. Prentice Hall, Englewood Cliffs, New-Jersey, 1999.

[73] Fiori, A., and Dagan, G. Time-dependent transport in heterogeneous formations of bimodal structure. 2. Results. Water Resources Research 39, 5 (2003), doi:10.1029/2002WR001398.

[74] Fiori, A., Jankovic, I., and Dagan, G. Flow and transport in highly heterogeneous formations. 2. Semianalytical results for isotropic media. Water Resources Research 39, 9 (2003), doi:10.1029/2002WR001719.

[75] Fiori, A., Jankovic, I., and Dagan, G. Flow and transport through twodimensional isotropic media of binary conductivity distribution. Part 1 : Numerical methodology and semi-analytical solutions. Stochastic Environmental Research and Risk Assessment 17 (2003), 370–383.

[76] Freeze, R. A., and Cherry, J. A. Groundwater. Prentice Hall, 1979.

[77] Fried, J. J. Groundwater Pollution. Elsevier, 1975.

[78] Frippiat, C. C., and Holeyman, A. E. Upscaling of solute transport in mildly heterogeneous media: comparison of Fickian and non-Fickian approaches. In Calibration and Reliability in Groundwater Modelling: From Uncertainty to Decision

Making, vol. 304. International Association of Hydrological Science, 2006, pp. 167–173.

[79] Gelhar, L. W. Stochastic subsurface hydrology. Prentice Hall, Englewood Cliffs, New-Jersey, 1993.

[80] Gelhar, L. W., and Axness, C. L. Three-dimensional stochastic analysis of macrodispersion in aquifers. Water Resources Research 19, 1 (1983), 161–180.

[81] Gelhar, L. W., Gutjahr, A. L., and Naff, R. L. Stochastic analysis of macrodispersion in a stratified aquifer. Water Resources Research 15, 6 (1979), 1387–1397.

[82] Gelhar, L. W., Welty, C., and Rehfeldt, K. R. A critical review of data on field-scale dispersion in aquifers. Water Resources Research 28, 7 (1992), 1955–1974.

[83] Gerke, H. H., and van Genuchten, M. T. A dual-porosity model for simulating the preferential movement of water and solutes in structured porous media. Water Resources Research 29, 2 (1993), 305–319.

[84] Gomez-Hernandez, J. J., andWen, X.-H. To be or not to be multi-Gaussian? A reflection on stochastic hydrogeology. Advances in Water Resources 21, 1 (1998), 47–61.

[85] Greenkorn, R. A. Flow phenomena in porous media. Marcel Dekker, 1983.

[86] Griffioen, J. Suitability of the first-order mass transfer concept for describing cyclic diffusive mass transfer in stagnant zones. Journal of Contaminant Hydrology 34 (1998), 155–165.

[87] Griffioen, J. W., Barry, D. A., and Parlange, J.-Y. Interpretation of two-region model parameter. Water Resources Research 34, 3 (1998), 373–384.

[88] Guswa, A. J., and Freyberg, D. L. Slow advection and diffusion through low permeability inclusions. Journal of Contaminant Hydrology 46 (2000), 205–232.

[89] Güven, O., and Molz, F. J. Deterministic and stochastic analyses of dispersion in an unbounded stratified porous medium. Water Resources Research 22, 11 (1986), 1565–1574.

[90] Güven, O., Molz, F. J., and Melville, J. G. An analysis of dispersion in a stratified aquifer. Water Resources Research 20, 10 (1984), 1337–1354.

[91] Haggerty, R., and Gorelick, S. M. Multiple-rate mas transfer for modeling diffusion and surface reactions in media with pore-scale heterogeneity. Water Resources Research 31, 10 (1995), 2383–2400.

[92] Haggerty, R., McKenna, S., and Meigs, L. C. On the late-time behavior of tracer test breakthrough curves. Water Resources Research 36, 12 (2000), 3467–3479.

[93] Haggerty, R., and Reeves, P. C. Stammt-l 1.0, formulation and user's guide. Tech. Rep. 520308, Sandia National Laboratories, 2002.

[94] Hantush, M. M., and Marino, M. A. Interlayer diffusive transfer and transport of contaminants in stratified formations. I. Theory. Journal of Hydrologic Engineering 3, 4 (1998), 232–240.

[95] Hantush, M. M., and Marino, M. A. Interlayer diffusive transfer and transport of contaminants in stratified formations. II. Analytical solutions. Journal of Hydrologic Engineering 3, 4 (1998), 241–246.

[96] Harbaugh, A. W., Banta, E. R., Hill, M. C., and McDonald, M. G. Modflow-2000, the U.S. Geological Survey modular ground-water model. User guide to modularization concepts and the ground-water flow process. Tech. Rep. 00-92, USGS, 2000.

[97] Harvey, C., and Gorelick, S. M. Rate-limited mass transfer or macrodispersion: which dominates plume evolution at the Macrodispersion Experiment (MADE) site ? Water Resources Research 36, 3 (2000), 637–650.

[98] Hassanizadeh, S. M. On the transient non-Fickian dispersion theory. Transport in Porous Media 23 (1996), 107–124.

[99] Hill, M. C., Banta, E. R., Harbaugh, A. W., and Anderman, E. R. Modflow-2000, the U.S. Geological Survey modular ground-water model. User guide to the observation, sensitivity and parameter-estimation processes and three post-processing programs. Tech. Rep. 00-184, USGS, 2000.

[100] Hsu, K.-C. The influence of the log-conductivity autocovariance structure on macrodispersion coefficients. Journal of Contaminant Hydrology 65 (2003), 65– 77.

[101] Huang, K., van Genuchten, M. T., and Zhang, R. Exact solutions for one-dimensional transport with asymptotic scale-dependent dispersion. Appl. Math. Modelling 20 (1996), 298–308.

[102] Hunt, B. Contaminant sources solutions with scale-dependent dispersivities. Journal of Hydrologic Engineering 3, 4 (1998), 268–275.

[103] Hunt, B. Scale-dependent dispersion from a pit. Journal of Hydrologic Engineering 7, 2 (2002), doi:10.1061/(ASCE)1084–0699(2002)7:2(168).

[104] Illangasekare, T. H., Ramsey, J. L., Jensen, K. H., and Butts, M. B. Experimental study of movement and distribution of dense organic contaminants in heterogeneous aquifers. Journal of Contaminant Hydrology 20 (1995), 1–25.

[105] Jankovic, I., Fiori, A., and Dagan, G. Flow and transport in highly heterogeneous formations. 3. Numerical simulations and comparison with theoretical results. Water Resources Research 39, 9 (2003), doi:10.1029/2002WR001721.

[106] Jankovic, I., Fiori, A., and Dagan, G. Flow and transport through twodimensional isotropic media of binary conductivity distribution. Part 2 : Numerical simulations and comparison with theoretical results. Stochastic Environmental Research and Risk Assessment 17 (2003), 384–393.

[107] Jarvis, N. J., Jansson, P.-E., Dk, P. E., and Messing, I. Modelling water and solute transport in macroporous soil. I. Model description and sensitivity analysis. Journal of Soil Science 42 (1991), 59–70.

[108] Javaux, M., and Vanclooster, M. Scale- and rate-dependent solute transport within an unsaturated sandy monolith. Soil Science Society of America Journal 67, 5 (2003), 1334–1343.

[109] Jose, S. C., Rahman, A., and Cirpka, O. A. Large-scale sandbox experiment on longitudinal effective dispersion in heterogeneous porous media. Water Resources Research 40 (2004), doi:10.1029/2004WR003363.

[110] Journel, A. G., and Isaaks, E. H. Conditional indicator simulation : Application to a Saskatchewan uranium deposit. Mathematical Geology 16, 7 (1984), 685–718.

[111] Klotz, D., Seiler, K.-P., Moser, H., and Neumaier, F. Dispersivity and velocity relationship from laboratory and field experiments. Journal of Hydrology 45 (1980), 169–184.

[112] Koltermann, C. E., and Gorelick, S. M. Paleoclimatic signature in terrestrial flood deposit. Science 256 (1992), 1775–1782.

[113] Koltermann, C. E., and Gorelick, S. M. Heterogeneity in sedimentary deposits : a review of structure-imitating, process-imitating and descriptive approaches. Water Resources Research 32, 9 (1996), 2617–2658.

[114] Kreft, A., and Zuber, A. On the physical meaning of the dispersion equation and its solutions for different initial and boundary conditions. Chemical Engineering Science 33 (1978), 1471–1480.

[115] Labolle, E. M. RWHet : random walk particle model for simulating transport in heterogeneous permeable media version 2.0. University of California, Davis, 2000.

[116] Lallemand-Barrès, A., and Peaudecerf, P. Recherche des relations entre la valeur de la dispersivité macroscopique d'un milieu aquifère, ses autres caractéristiques et les conditions de mesure. Etude bibliographique. Bulletin du BRGM 2e s´erie - section III, 4 (1992), 277–284.

[117] Lambot, S., Slob, E. C., van den Bosch, I., Stockbroeckx, B., Scheers, B., and Vanclooster, M. Estimating soil electric properties from monostatic ground-penetrating radar signal inversion in the frequency domain. Water Resources Research 40 (2004), doi:10.1029/2003WR002095.

[118] Landman, A.-J. unpublished. PhD thesis, TU Delft, The Netherlands, 2004.

[119] Leij, F. J., and Dane, J. H. Solute transport in a two-layer medium investigated with time moments. Soil Science Society of America Journal 55 (1991), 1529–1535.

[120] Lessoff, S. C., and Dagan, G. Solute transport in heterogeneous formations of bimodal conductivity distribution. 2. Applications. Water Resources Research 37, 3 (2001), 473–480.

[121] Levy, M., and Berkowitz, B. Measurement and analysis of non-Fickian dispersion in heterogeneous porous media. Journal of Contaminant Hydrology 64 (2003), 203–226.

[122] Lin, A. Y.-C., Debroux, J.-F., Cunningham, J. A., and Reinhard, M. Comparison of Rhodamine WT and bromide in the determination of hydraulic characteristics of constructed wetlands. Ecological Engineering 20 (2003), 75– 88.

[123] Liu, G., Zheng, C., and Gorelick, S. M. Limits of applicability of the advection-dispersion model in aquifers containing connected high-conductivity channels. Water Resources Research 40 (2004), doi:10.1029/2003WR002735.

[124] Logan, J. D. Solute transport in porous media with scale-dependent dispersion and periodic boundary conditions. Journal of Hydrology, 184 (1996), 261–276.

[125] Lu, S., Molz, F. J., and Fix, G. J. Possible problems of scale dependency in applications of the three-dimensional fractional advection-dispersion equation to natural porous media. Water Resources Research 38, 9 (2002).

[126] Lu, S., Molz, F. J., Fogg, G. E., and Castle, J. W. Combining stochastic facies and fractal models for representing natural heterogeneity. Hydrogeology Journal, 10 (2002), 475–482.

[127] Margolin, G., and Berkowitz, B. Application of continuous time random walk to transport in porous media. Journal of Physical Chemistry B 104 (2000), 3942–3947.

[128] Margolin, G., and Berkowitz, B. Correction to : Application of continuous time random walk to transport in porous media. Journal of Physical Chemistry B 104 (2000), 3942.

[129] Margolin, G., and Berkowitz, B. Spatial behavior of anomalous transport. Physical Review E 65 (2002).

[130] Margolin, G., and Berkowitz, B. Continuous time random walk revisited: first passage time and spatial distributions. Physica A 334 (2004), 46–66.

[131] Marle, C., Simandoux, P., Pacsirszky, J., and Gaulier, C. Etude du d´eplacement de fluides miscibles en milieu poreux stratifié. Rue de l'Institut Francais du Pétrole 22, 2 (1967), 272–294.

[132] Matheron, G., and De Marsily, G. Is transport in porous media always diffusive ? A counterexample. Water Resources Research 16, 5 (1980), 901–917.

[133] Meerschaert, M. M., Benson, D. A., and Baeumer, B. Multidimensional advection and fractional dispersion. Physical Review E 59, 5 (1999), 5026–5028.

[134] Meerschaert, M. M., Benson, D. A., and Baeumer, B. Operator Lévy motion and multiscaling anomalous diffusion. Physical Review E 63 (2001), 1112–1117.

[135] Meerschaert, M. M., Benson, D. A., Scheffler, H.-P., and Baeumer, B. Stochastic solution of space-time fractional diffusion equations. Physical Review E 65, 4 (2002), 102–105.

[136] Mercado, A. The spreading pattern of injected water in a permeability stratified aquifer. In Artifical recharge and management of aquifers (1967), IAHSAIHS, Ed., vol. 72, pp. 23–36.

[137] Metzler, R., and Klafter, J. The random walk's guide to anomalous diffusion: a fractional dynamics approach. Physics Reports 339 (2000), 1–77.

[138] Molz, F. J., G¨uven, O., and Melville, J. G. An examination of scaledependent dispersion coefficient. Groundwater 21, 6 (1983), 715–725.

[139] Montroll, E. W., and Weiss, G. H. Random walks on lattices. II. Journal of Mathematical Physics 6, 2 (1965), 167–181.

[140] Murphy, E. M., Ginn, T. R., Chilakapati, A., Resch, T., Phillips, J., Wietsma, T., and Spadoni, C. M. The influence of physical heterogeneity on microbial degradation and distribution in porous media. Water Resources Research 33 (1997), 1087–1104.

[141] Neuman, S. P., Winter, C. L., and Newman, C. M. Stochastic theory of field-scale Fickian dispersion in anistropic porous media. Water Resources Research 23, 3 (1987), 453–466.

[142] Nkedi-Kizza, P., Biggar, J. W., Selim, H. M., van Genuchten, M. T., Wierenga, P. J., Davidson, J. M., and Nielsen, D. R. On the equivalence of two conceptual models for describing ion exchange during transport through an aggregated oxisol. Water Resources Research 20, 8 (1984), 1123–1130.

[143] Pang, L., and Hunt, B. Solutions and verification of a scale-dependent dispersion model. Journal of Contaminant Hydrology, 53 (2001), 21–39.

[144] Parker, J. C., and Valocchi, A. J. Constraints on the validity of equilibrium and first-order kinetic models in structured soils. Water Resources Research 22, 3 (1986), 399–407.

[145] Peters, G. P., and Smith, D. W. Spatially and temporally varying dispersivity. In GeoEng 2000 Conference Proceedings (2000).

[146] Pickens, J. F., and Grisak, G. E. Modeling of scale-dependent dispersion in hydrogeologic systems. Water Resources Research 17, 6 (1981), 1701–1711.

[147] Pickens, J. F., and Grisak, G. E. Scale-dependent dispersion in a stratified granular aquifer. Water Resources Research 17, 4 (1981), 1191–1211.

[148] Ptak, T., and Schmid, G. Dual-tracer transport experiments in a physically and chemically heterogeneous porous aquifer : effective transport parameters and spatial variability. Journal of Hydrology 183 (1996), 117–138.

[149] Rao, P. S. C., Rolston, D. E., Jessup, R. E., and Davidson, J. M. Solute transport in aggregated porous media : theoretical and experimental evaluation. Soil Science Society of America Journal 44 (1980), 1139–1146.

[150] Rentier, C. Méthode stochastique de d´elimination des zones de protection autour des captages d'eau. PhD thesis, Université de Liège, Belgium, November 2002.

[151] Rovey, C. W., and Niemann, W. L. Do conservative solutes migrate at average pore-water velocity ? Groundwater 43, 1 (2005), 52–62.

[152] Rubin, Y. Flow and transport in bimodal heterogeneous formations. Water Resources Research 31, 10 (1995), 2461–2468.

[153] Rubin, Y., and Dagan, G. Stochastic analysis of the effects of boundaries on spatial variability in groundwater flows: 2. Impervious boundary. Water Resources Research 25, 4 (1989), 707–712.

[154] Sabatini, D. A. Sorption and intraparticule diffusion of fluorescent dyes with consolidated aquifer media. Groundwater 38, 5 (2000), 651–656.

[155] Sabatini, D. A., and Al Austin, T. Characteristics of Rhodamine WT and Fluorescein as adsorbing ground-water tracers. Groundwater 29, 3 (1991), 341– 349.

[156] Sakaki, T., and Komatsu, M. Physical properties of silica sands for laboratory experiments. Colorado School of Mines, ESE division, internal report, April 2005.

[157] Salandin, P., and Fiorotto, V. Solute transport in highly heterogeneous aquifers. Water Resources Research 34, 5 (1998), 949–961.

[158] Salandin, P., Rinaldo, A., and Dagan, G. A note on transport in stratified formations by flow tilded with respect to the bedding. Water Resources Research 27, 11 (1991), 3009–3017.

[159] Saupe, D., and Peitgen, H. The Science of Fractal Images. Springer-Verlag, 1988, p. 312 p.

[160] Sauty, J. Mise au point et utilisation d'abaques pour l'interprétation des expériences de tra¸cages dans les nappes d'eau souterraine. Bulletin du BRGM 2e série - section III, 4 (1978), 285–291.

[161] Sauty, J. An analysis of hydrodispersive transfer in aquifers. Water Resources Research 16, 1 (1980), 145–158.

[162] Scheidegger, A. E. Typical solutions of the differential equations of statistical theories of flow through porous media. Transactions, American Geophysical Union 39, 5 (1958), 929–932.

[163] Scheidegger, A. E. The physics of flow through porous media. Mac Millan Company, 1960.

[164] Scher, H., and Lax, M. Stochastic transport in a disordered solids. II Impurity conduction. Physical Review B 7 (1973), 4502–4519.

[165] Schäfer, W., and Kinzelbach, W. K. H. Transport of reactive species in heterogeneous porous media. Journal of Hydrology 183 (1996), 151–168.

[166] Schincariol, R. A., and Schwartz, F. An experimental investigation of variable density flow and mixing in homogeneous and heterogeneous media. Water Resources Research 26, 10 (1990), 2317–2329.

[167] Schumer, R., Benso, D. A., Meerschaert, M. M., and Baeumer, B. Fractal mobile/immobile solute transport. Water Resources Research 39, 10 (2003), doi:10.1029/2003WR002141.

[168] Schumer, R., Benson, D. A., Meerschaert, M. M., and Baeumer, B. Multiscaling fractional advection-dispersion equations and their solutions. Water Resources Research 39, 1 (2003).

[169] Schumer, R., Benson, D. A., Meerschaert, M. M., and Wheatcraft, S. W. Eulerian derivation of the fractional advection-dispersion equation. Journal of Contaminant Hydrology, 48 (2001), 69–88.

[170] Silliamn, S. E., and Zheng, L. Comparison of observations from a laboratory model with stochastic theory: Initial analysis of hydraulic and tracer experiments. Tranport in Porous Media 42, 1/2 (2001), 85–107.

[171] Silliman, S. E. Laboratory study of chemical transport to wells within heterogeneous porous media. Water Resources Research 37, 7 (2001), 1883–1892.

[172] Silliman, S. E., and Caswell, S. Observations of measured hydraulic conductivity in two artificial, confined aquifers with boundaries. Water Resources Research 34, 9 (1998), 2203–2213.

[173] Silliman, S. E., Konikow, L., and Voss, C. Laboratory investigation of longitudinal dispersion in anisotropic porous media. Water Resources Research 23, 11 (1987), 2145–2151.

[174] Silliman, S. E., and Simpson, E. S. Laboratory evidence of the scale effect in dispersion of solutes in porous media. Water Resources Research 23, 8 (1987), 1667–1673.

[175] Sposito, G., and Weeks, S. W. Tracer advection by steady groundwater flow in a stratified aquifer. Water Resources Research 34, 5 (1998), 1051–1059.

[176] Strack, O. D. L. A mathematical model for dispersion with a moving front in groundwater. Water Resources Research 28, 11 (1992), 2973–2980.

[177] Sudicky, E. A., Gillham, R. W., and Frind, E. O. Experimental investigation of solute transport in stratified porous media. 1. The non-reactive case. Water Resources Research 21 (1985), 1035–1041.

[178] Sutton, D. J., Kabala, Z. J., Francisco, A., and Vasudevan, D. Limitations and potential of commercially available Rhodamine WT as a groundwater tracer. Water Resources Research 37, 6 (2001), 1641–1656.

[179] Taylor, G. I. Dispersion of soluble matter in solvent flowing slowly through a tube. Proc. Royal Soc. London A219 (1953), 186–203.

[180] Taylor, G. I. Conditions under which dispersion of a solute in a stream of solvent can be used to measure molecular diffusion. Proc. Royal Soc. London A225 (1954), 473–477.

[181] Teles, V., Delay, F., and de Marsily, G. Comparison of genesis and geostatistical methods for characterizing the heterogeneity of alluvial media : groundwater flow and transport simulations. Journal of Hydrology 294 (2004), 103–121.

[182] Tompson, A. F. B. On a new functional form for the dispersive flux in porous media. Water Resources Research 24, 11 (1988), 1939–1947. [183] Tompson, A. F. B., and Gray, W. G. A 2nd-order approach for the modeling of dispersive transport in porous media. 1. Theoretical development. Water Resources Research 22, 5 (1986), 591–599.

[184] Trefry, M. G., Ruan, F. P., and McLaughlin, D. Numerical simulations of preasymptotic transport in heterogeneous porous media : departures from the Gaussian limit. Water Resources Research 39, 3 (2003), doi:10.1029/2001WR001101.

[185] Ursino, N., Gimmi, T., and Flühler, H. Combined effects of heterogeneity, anisotropy, and saturation on steady state flow and transport: a laboratory sand tank experiment. Water Resources Research 2 (37), 201–208.

[186] Valocchi, A. J. Validity of the local equilibrium assumption for modeling sorbing solute transport through homogeneous soils. Water Resources Research 21, 6 (1985), 808–820.

[187] van Genuchten, M. T., Tang, D. H., and Guennelon, R. Some exact solutions for solute transport through soils containing large cylindrical macropores. Water Resources Research 20, 3 (1984), 335–346.

[188] van Genuchten, M. T., and Wagenet, R. J. Two-site/two-region models for pesticide transport and degradation : theoretical development and analytical solutions. Soil Science Society of America Journal 53, 5 (1989), 1303–1310.

[189] van Genuchten, M. T., and Wierenga, P. J. Mass transfer studies in sorbing porous media. I. Analytical solutions. Soil Science Society of America Journal 40, 4 (1976), 473–480.

[190] van Genuchten, M. T., and Wierenga, P. J. Mass transfer studies in sorbing porous media. II. Experimental evaluation with tritium (3H2O)., volume = 41, year = 1977. Soil Science Society of America Journal (1977), 272–278.

[191] van Genuchten, M. T., Wierenga, P. J., and O'Connor, G. A. Mass transfer studies in sorbing porous media. III. Experimental evaluation with 2,4,5T.,. Soil Science Society of America Journal 41 (1977), 278–285.

[192] Vanclooster, M., Javaux, M., and Vanderborght, J. Solute transport in soils. Encyclopedia of Hydrological Sciences. John Wiley and sons, 2005.

[193] Wang, P. P., Zheng, C., and Gorelick, S. M. A general approach to advective-dispersive transport with multirate mass transfer. Advances in Water Resources 28 (2005), 33–42.

[194] Weissmann, G. S., Carle, S. F., and Fogg, G. E. Three-dimensional hydrofacies modeling based on soil surveys and transition probability geostatistics. Water Resources Research 35, 6 (1999), 1761–1770.

[195] Weissmann, G. S., and Fogg, G. E. Multi-scale alluvial fan heterogeneity modeled with transition probability geostatistics in a sequence stratigraphic framework. Journal of Hydrology 226 (1999), 48–65.

[196] Welty, C., and Elsner, M. Construction of random fields in the laboratory for observations of fluid flow and mass transport. Journal of Hydrology 202 (1997), 192–211.

[197] Wheatcraft, S. W., and Tyler, S. W. An explanation of scale-dependent dispersivity using concepts of fractal geometry. Water Resources Research 24, 4 (1988), 566–578.

[198] Wood, B. D., Dawson, C. N., Szecsody, J. E., and Streile, G. P. Modeling contaminant transport and biodegradation in a layered porous media system. Water Resources Research 30, 6 (1994), 1833–1845.

[199] Yates, S. R. An analytical solution for one-dimensional transport in heterogeneous porous media. Water Resources Research 26, 10 (1990), 2331–2338.

[200] Yu, C., Warrick, A. W., and Conklin, M. H. A moment method for analysing breakthrough curves of step inputs. Water Resources Research 35, 11 (1999), 3567–3572.

References – Upscaling of transport Parameters under the Non Fickian approach

Abramowitz, M., and I. Stegun (1970), Handbook of Mathematical Functions, Dover, Mineola, N. Y.

Adams, E. E., and L.W. Gelhar (1992), Field study of dispersion in a heterogeneous aquifer: 2. Spatial moment analysis, Water Resour. Res., 28(12), 3293–3308.

Aronofsky, J. S., and J. P. Heller (1957), A diffusion model to explain mixing of flowing miscible fluids in porous media, Trans. Am. Inst. Min. Metall. Pet. Eng., 210, 345–349.

Attinger, S., M. Dentz, H. Kinzelbach, and W. Kinzelbach (1999), Temporal behavior of a solute cloud in a chemically heterogeneous porous medium, J. Fluid Mech., 386, 77–104.

Attinger, S., M. Dentz, and W. Kinzelbach (2004), Exact transverse macro dispersion coefficients for transport in heterogeneous porous media, Stochastic Environ. Res. Risk Assess., 18(1), 9–15.

Auriault, J. L., and P. M. Adler (1995), Taylor dispersion in porous media—Analysis by multiple scale expansions, Adv. Water Resour., 18, 217–226.

Baeumer, B., D. A. Benson, M. M. Meerschaert, and S. W. Wheatcraft (2001), Subordinated advection-dispersion equation for contaminant transport, Water Resour. Res., 37(6), 1543–1550.

Batchelor, G. K. (1949), Diffusion in a field of homogeneous turbulence. I. Eulerian analysis, Austral. J. Sci. Res., 2, 437–450.

Bear, J. (1972), Dynamics of Fluids in Porous Media, Elsevier, New York.

Benson, D. A., S. W. Wheatcraft, and M. M. Meerschaert (2000), The fractional-order governing equation of Lévy motion, Water Resour. Res., 36(6), 1413–1423.

Berkowitz, B., and Y. Bachmat (1987), A scale-dependent equation for solute transport in porous media, Transp. Porous Media, 3, 199–205.

Berkowitz, B., and H. Scher (1997), Anomalous transport in random fracture networks, Phys. Rev. Lett., 79(20), 4038–4041.

Berkowitz, B., and H. Scher (1998), Theory of anomalous chemical transport in fracture networks, Phys. Rev. E, 57(5), 5858–5869.

Berkowitz, B., H. Scher, and S. E. Silliman (2000), Anomalous transport in laboratory-scale, heterogeneous porous media, Water Resour. Res., 36(1), 149–158.

Berkowitz, B., J. Klafter, R. Metzler, and H. Scher (2002), Physical pictures of transport in heterogeneous media: Advection-dispersion, random walk and fractional derivative formulations, Water Resour. Res., 38(10), 1191, doi:10.1029/2001WR001030.

Bhattacharya, R., and V. K. Gupta (1990), Dynamics of Fluids in Hierarchical Porous Media, chap. IV, pp. 61–95, Elsevier, New York.

Bijeljic, B., and M. J. Blunt (2006), Pore-scale modeling and continuous time random walk analysis of dispersion in porous media, Water Resour. Res., 42, W01202, doi:10.1029/2005WR004578.

Bijeljic, B., A. H. Muggeridge, and M. J. Blunt (2004), Pore-scale modeling of longitudinal dispersion, Water Resour. Res., 40, W11501, doi:10.1029/2004WR003567.

Bos, F. C., and D. M. Burland (1987), Hole transport in polyvinylcarbazole—The vital importance of excitation-light intensity, Phys. Rev. Lett., 58(2), 152–155.

Bouchaud, J. P., and A. Georges (1990), Anomalous diffusion in disordered media: Statistical mechanisms, models and physical applications, Phys. Rep., 195(4–5), 127–293.

Bourgeat, A., M. Quintard, and S. Whitaker (1988), Éléments de comparaison entre la méthode d'homogénéisation et la méthode de prise de moyenne avec fermeture, C. R. Acad. Sci., Ser. II, 306, 463–466.

Brenner, H. (1980), Dispersion resulting from flow through spatially periodic porous media, Proc. R. Soc. London, Ser. A, 297(1430), 81–133.

Bromly, M., and C. Hinz (2004), Non-Fickian transport in homogeneous unsaturated repacked sand, Water Resour. Res., 40, W07402, doi:10.1029/2003WR002579.

Carrera, J., X. Sánchez-Vila, I. Benet, A. Medina, G. Galarza, and J. Guimerà (1998), On matrix diffusion: Formulations, solution methods, and qualitative effects, Hydrogeol. J., 6, 178–190.

Christakos, G. (2004), A sociological approach to the state of stochastic hydrogeology, Stochastic Environ. Res. Risk Assess., 18(4), 274–277.

Clincy, M., and H. Kinzelbach (2001), Stratified disordered media: Exact solutions for transport parameters and their self-averaging properties, J. Phys. A Math. Gen., 34, 7141–7152.

Cortis, A., and B. Berkowitz (2004), Anomalous transport in ''classical'' soil and sand columns, Soil Sci. Soc. Am. J., 68, 1539–1548.

Cortis, A., and B. Berkowitz (2005), Computing 'anomalous' contaminant transport in porous media: The CTRW MATLAB toolbox, Ground Water, 43(6), 947–950.

Cortis, A., Y. Chen, H. Scher, and B. Berkowitz (2004a), Quantitative characterization of pore-scale disorder effects on transport in ''homogeneous'' granular media, Phys. Rev. E, 70(10), 041108, doi:10.1103/PhysRevE.70.041108.

Cortis, A., C. Gallo, H. Scher, and B. Berkowitz (2004b), Numerical simulation of non-Fickian transport in geological formations with multiple-scale heterogeneities, Water Resour. Res., 40, W04209, doi:10.1029/2003WR002750.

Cunningham, J. A., C. J. Werth, M. Reinhard, and P. V. Roberts (1997), Effects of grain-scale mass transfer on the transport of volatile organics through sediments: 1. Model development, Water Resour. Res., 33(12), 2713–2726.

Cushman, J. (1984), On unifying the concepts of scale, instrumentation, and stochastics in the development of multiphase transport theory, Water Resour. Res., 20(11), 1668–1676.

Cushman, J. (1991), On diffusion in fractal media, Water Resour. Res., 27(4), 643–644.

Cushman, J., and T. Ginn (1993), Non-local dispersion in media with continuously evolving scales, Transp. Porous Media, 13, 123–138.

Cushman, J. H., and T. R. Ginn (2000), Fractional advective dispersion equations: A classical mass balance with convolution-Fickian flux, Water Resour. Res., 36, 3763–3766.

Cushman, J. H., and M. Moroni (2001), Statistical mechanics with three-dimensional particle tracking velocimetry experiments in the study of anomalous dispersion. I. Theory, Phys. Fluids, 13, 75–80.

Cushman, J. H., X. Hu, and T. R. Ginn (1994), Nonequilibrium statistical mechanics of preasymptotic dispersion, J. Stat. Phys., 75(5/6), 859–878.

Cushman, J. H., B. X. Hu, and F.-W. Deng (1995), Nonlocal reactive transport with physical and chemical heterogeneity: Localization errors, Water Resour. Res., 31(9), 2219–2237.

Cushman, J. H., L. S. Bennethum, and B. X. Hu (2002), A primer on up-scaling tools for porous media, Adv. Water Resour., 25, 1043–1067.

Dagan, G. (1984), Solute transport in heterogenous porous formations, J. Fluid Mech., 145, 151–177.

Dagan, G. (1987), Theory of solute transport by groundwater, Annu. Rev. Fluid Mech., 19, 183–215.

Dagan, G. (1988), Time-dependent macrodispersion for solute transport in anisotropic heterogeneous aquifers, Water Resour. Res., 24(9), 1491–1500.

Dagan, G. (1989), Flow and Transport in Porous Formations, Springer, New York.

Dagan, G. (1990), Transport in heterogeneous porous formations: Spatial moments, ergodicity, and effective dispersion, Water Resour. Res., 26(10), 1287–1290.

Dagan, G. (1991), Dispersion of a passive scalar in non-ergodic transport, J. Fluid Mech., 233, 197–210.

Dagan, G. (1994a), The significance of heterogeneity of evolving scales to transport in porous formations, Water Resour. Res., 30(12), 3327–3336.

Dagan, G. (1994b), An exact nonlinear correction to transverse macrodispersivity for transport in heterogenous formations, Water Resour. Res., 30(10), 2699–2705.

Dagan, G. (2004), On application of stochastic modeling of groundwater flow and transport, Stochastic Environ. Res. Risk Assess., 18(4), 266–267.

Dagan, G., and E. Bresler (1979), Solute dispersion in unsaturated soil at field scale, I, Theory, Soil Sci. Soc. Am. J., 43, 461–466.

Dagan, G., and S. P. Neuman (Eds.) (1997), Subsurface Flow and Transport: A Stochastic Approach, Cambridge Univ. Press, New York.

de Hoog, F. R., J. H. Knight, and A. N. Stokes (1982), An improved method for numerical inversion of Laplace transforms, SIAM J. Sci. Stat. Comput., 3, 357–366.

Deng, F.-W., J. H. Cushman, and J. W. Delleur (1993), A fast Fourier transform stochastic analysis of the contaminant transport problem, Water Resour. Res., 29(9), 3241–3247.

Dentz, M., and B. Berkowitz (2003), Transport behavior of a passive solute in continuous time random walks and multirate mass transfer, Water Resour. Res., 39(5), 1111, doi:10.1029/2001WR001163.

Dentz, M., and B. Berkowitz (2005), Exact effective transport dynamics in a one-dimensional random environment, Phys. Rev. E, 72(3), 031110, doi:10.1103/PhysRevE.72.031110.

Dentz, M., and J. Carrera (2003), Effective dispersion in temporally fluctuating flow through a heterogeneous medium, Phys. Rev. E, 68(3), 036310, doi:10.1103/PhysRevE.68.036310.

Dentz, M., H. Kinzelbach, S. Attinger, and W. Kinzelbach (2000), Temporal behavior of a solute cloud in a heterogeneous porous medium: 1. Point-like injection, Water Resour. Res., 36(12), 3591–3604.

Dentz, M., H. Kinzelbach, S. Attinger, and W. Kinzelbach (2003), Numerical studies of the transport behavior of a passive solute in a two-dimensional incompressible random flow field, Phys. Rev. E, 67(4), 046306, doi:10.1103/PhysRevE.67.046306.

Dentz, M., A. Cortis, H. Scher, and B. Berkowitz (2004), Time behavior of solute transport in heterogeneous media: Transition from anomalous to normal transport, Adv. Water Resour., 27, 155–173, doi:10.1016/j.advwatres.2003.11.002.

Di Donato, G., E.-O. Obi, and M. J. Blunt (2003), Anomalous transport in heterogeneous media demonstrated by streamlinebased simulation, Geophys. Res. Lett., 30(12), 1608, doi:10.1029/2003GL017196.

Di Federico, V., and Y.-K. Zhang (1999), Solute transport in heterogeneous porous media with long-range correlations, Water Resour. Res., 35(10), 3185–3191.

Domenico, P. A., and Robbins, G. A. A dispersion scale effect in model calibration and field tracer experiments. Journal of Hydrology, 70 (1984), 123–132.

Dorfman, K. D., and H. Brenner (2002), Generalized Taylor-Aris dispersion in discrete spatially periodic networks: Microfluidic applications, Phys. Rev. E, 65(2), 021103, doi:10.1103/Phys-RevE.65.021103.

Eberhard, J. (2004), Approximations for transport parameters and self-averaging properties for point-like injections in heterogeneous media, J. Phys. A Math. Gen., 37, 2549–2571.

Eggleston, J., and S. Rojstaczer (1998), Identification of large-scale hydraulic conductivity trends and the influence of trends on contaminant transport, Water Resour. Res., 34(9), 2155–2168.

Einstein, A. (1905), Über die von der molekulartheoretischen Theorie der Wärme geforderte Bewegung von in ruhenden Flüssigkeiten suspendierten Teilchen, Ann. Phys. Leipzig, 17, 549–560.

Feehley, C. E., C. Zheng, and F. J. Molz (2000), A dual-domain mass transfer approach for modeling solute transport in heterogeneous aquifers: Application to the macrodispersion experiment (MADE) site, Water Resour. Res., 36(9), 2501–2515.

Freeze, R. A. (2004), The role of stochastic hydrogeological modelling in real-world engineering applications, Stochastic Environ. Res. Risk Assess., 18(4), 286–289.

Gelhar, L. W. (1993), Stochastic Subsurface Hydrology, Prentice-Hall, Upper Saddle River, N. J.

Gelhar, L. W. (1997), Perspectives on field-scale application of stochastic subsurface hydrology, in Subsurface Flow and Transport: A Stochastic Approach, edited by G. Dagan and S. P. Neuman, pp. 157–176, Cambridge Univ. Press, New York.

Gelhar, L. W., and C. L. Axness (1983), Three-dimensional stochastic analysis of macrodispersion in aquifers, Water Resour. Res., 19(1), 161–180.

Gelhar, L. W., C. Welty, and K. R. Rehfeldt (1992), A critical review of data on field-scale dispersion in aquifers, Water Resour. Res., 28(7), 1955–1974.

Ghodrati, M., and W. A. Jury (1992), A field study of the effects of water application method and surface preparation method on preferential flow of pesticides in unsaturated soil, J. Contam. Hydrol., 11, 101–125.

Ginn, T. R. (2004), On the application of stochastic approaches in hydrogeology, Stochastic Environ. Res. Risk Assess., 18(4), 282–284.

Glueckauf, E. (1955), Theory of chromatography, part 10—Formulae for diffusion into spheres and their application to chromatography, Trans. Faraday Soc., 51, 1540–1551.

Guadagnini, A., and S. Neuman (2001), Recursive conditional moment equations for advective transport in randomly heterogeneous velocity fields, Transp. Porous Media, 42, 37–67.

Güven, O., Molz, F. J., and Melville, J. G. An analysis of dispersion in a stratified aquifer. Water Resources Research 20, 10 (1984), 1337–1354.

Güven, O., and Molz, F. J. Deterministic and stochastic analyses of dispersion in an unbounded stratified porous medium. Water Resources Research 22, 11 (1986), 1565–1574.

Haggerty, R., and S. M. Gorelick (1995), Multiple-rate mass transfer for modeling diffusion and surface reactions in media with pore-scale heterogeneity, Water Resour. Res., 31(10), 2383–2400.

Haggerty, R., S. A. McKenna, and L. C. Meigs (2000), On the late time behavior of tracer test breakthrough curves, Water Resour. Res., 36(12), 3467–3479.

Harvey, C. F., and S. M. Gorelick (1995), Temporal moment-generating equations: Modeling transport and mass transfer in heterogeneous aquifers, Water Resour. Res., 31(8), 1895–1911.

Hatano, Y., and N. Hatano (1998), Dispersive transport of ions in column experiments:An explanation of long-tailed profiles, Water Resour. Res., 34(5), 1027–1033.

Hoffman, F., D. Ronen, and Z. Pearl (1996), Evaluation of flow characteristics of a sand column using magnetic resonance imaging, J. Contam. Hydrol., 22, 95–107.

Hornung, G., B. Berkowitz, and N. Barkai (2005), Morphogen gradient formation in a complex environment: An anomalous diffusion model, Phys. Rev. E, 72(4), 041916, doi:10.1103/PhysRevE.72.041916.

Hu, B. X., F.-W. Deng, and J. H. Cushman (1995), Nonlocal reactive transport with physical and chemical heterogeneity: Linear nonequilibrium sorption with random kd, Water Resour. Res., 31(9), 2239–2252.

Jaekel, U., and H. Vereecken (1997), Renormalization group analysis of macrodispersion in a directed random flow, Water Resour. Res., 33(10), 2287–2299.

Jiménez-Hornero, F. J., J. V. Giráldez, A. Laguna, and Y. Pachepsky (2005), Continuous time random walks for analyzing the transport of a passive tracer in a single fissure, Water Resour. Res., 41, W04009, doi:10.1029/2004WR003852.

Jury, W. A. (1982), Simulation of solute transport using a transfer function model, Water Resour. Res., 18(2), 363–368.

Jury, W. A., G. Sposito, and R. E. White (1986), A transfer function model of solute movement through soil: 1. Fundamental concepts, Water Resour. Res., 22(2), 243–247.

Kenkre, V. M., E. W. Montroll, and M. F. Shlesinger (1973), Generalized master equations for continuous-time random walks, J. Stat. Phys., 9(1), 45–50.

Kirchner, J. W., X. Feng, and C. Neal (2000), Fractal stream chemistry and its implications for contaminant transport in catchments, Nature, 403, 524–527.

Kitanidis, P. K. (1988), Prediction by the method of moments of transport in heterogeneous formations, J. Hydrol., 102, 453–473.

Klafter, J., and R. Silbey (1980a), On electronic energy transfer in disordered systems, J. Phys. Chem., 72(2), 843–848.

Klafter, J., and R. Silbey (1980b), Derivation of continuous-time random walk equations, Phys. Rev. Lett., 44(2), 55–58.

Klafter, J., A. Blumen, and M. F. Shlesinger (1987), Stochastic pathway to anomalous diffusion, Phys. Rev. A, 35(7), 3081–3085.

Klotz, D., Seiler, K.-P., Moser, H., and Neumaier, F. Dispersivity and velocity relationship from laboratory and field experiments. Journal of Hydrol- ogy 45 (1980), 169–184.

Koch, D. L., and J. F. Brady (1987), A non-local description of advection-diffusion with application to dispersion in porous media, J. Fluid Mech., 180, 387–403.

Koch, D. L., and J. F. Brady (1988), Anomalous diffusion in heterogeneous porous media, Phys. Fluids A, 31, 965–1031.

Koch, D. L., and E. S. G. Shaqfeh (1992), Averaged equation and diagrammatic approximations to the average concentration of a tracer dispersed by a Gaussian random velocity field, Phys. Fluids A, 4, 887–894.

Kosakowski, G. (2004), Anomalous transport of colloids and solutes in a shear zone, J. Contam. Hydrol., 72, 23– 46, doi:10.1016/j.jconhyd.2003.10.005.

Kosakowski, G., B. Berkowitz, and H. Scher (2001), Analysis of field observations of tracer transport in a fractured till, J. Contam. Hydrol., 47, 29–51.

Kraichnan, R. H. (1959), The structure of isotropic turbulence at very high Reynolds numbers, J. Fluid Mech., 5, 497–543.

Kreft, A., and A. Zuber (1978), On the physical meaning of the dispersion equation and its solutions for different initial and boundary conditions, Chem. Eng. Sci., 33, 1471–1480.

Krylov, V. I., and N. S. Skoblya (1977), A Handbook of Methods of Approximate Fourier Transformation and Inversion of the Laplace Transform, MIR, Moscow.

Labolle, E. M., and G. E. Fogg (2001), Role of molecular diffusion in contaminant migration and recovery in an alluvial aquifer system, Transp. Porous Media, 42, 155–179.

Lallemand-Barres, P., and P. Peaudecerf (1978), Recherche des relations entre la valeur de la dispersivité macroscopique d'un aquifère, ses autres caractéristiques et les conditions de mesure, Bull. Bur. Rech. Geol. Min. Fr., Sect. 3, 4, 277–284.

Levy, M., and B. Berkowitz (2003), Measurement and analysis of non-Fickian dispersion in heterogeneous porous media, J. Contam. Hydrol., 64, 203–226.

Lowe, C. P., and D. Frenkel (1996), Do hydrodynamic dispersion coefficients exist?, Phys. Rev. Lett., 77(22), 4552–4555.

Lu, S. L., F. J. Molz, G. E. Fogg, and J. W. Castle (2002), Combining stochastic facies and fractal models for representing natural heterogeneity, Hydrogeol. J., 10, 475–482.

Lunati, I., S. Attinger, and W. Kinzelbach (2002), Macrodispersivity for transport in arbitrary nonuniform flow fields: Asymptotic and preasymptotic results, Water Resour. Res., 38(10), 1187, doi:10.1029/2001WR001203.

Margolin, G., and B. Berkowitz (2002), Spatial behavior of anomalous transport, Phys. Rev. E, 65(3), 031101, doi:10.1103/PhysRevE.65.031101.

Margolin, G., M. Dentz, and B. Berkowitz (2003), Continuous time random walk and multirate mass transfer modeling of sorption, Chem. Phys., 295, 71–80.

Matheron, M., and G. de Marsily (1980), Is transport in porous media always diffusive?, Water Resour. Res., 16, 901–917.

Metzler, R. (2000), Generalized Chapman-Kolmogorov equation: A unifying approach to the description of anomalous transport in external fields, Phys. Rev. E, 62(5), 6233–6245.

Metzler, R., and J. Klafter (2000), The random walk's guide to anomalous diffusion: A fractional dynamics approach, Phys. Rep., 339(1), 1–77.

Metzler, R., and J. Klafter (2004), The restaurant at the end of the random walk: Recent developments in fractional dynamics of anomalous transport processes, J. Phys. A, 37, R161–R208.

Metzler, R., J. Klafter, and I. M. Sokolov (1998), Anomalous transport in external fields: Continuous time random walks and fractional diffusion equations extended, Phys. Rev. E, 58(2), 1621–1633.

Molz, F. (2004), A rational role for stochastic concepts in subsurface hydrology: A personal perspective, Stochastic Environ. Res. Risk Assess., 18(4), 278–279.

Montroll, E. W., and H. Scher (1973), Random walks on lattices. IV. Continuous time random walks and influence of absorbing boundaries, J. Stat. Phys., 9(2), 101–135.

Montroll, E. W., and G. H. Weiss (1965), Random walks on lattices. II, J. Math. Phys., 6(2), 167–181.

Mori, H. (1965), Transport collective motion and Brownian motion, Prog. Theor. Phys., 33(3), 423–455.

Naff, R. L. (1990), On the nature of the dispersive flux in saturated heterogenous porous media, Water Resour. Res., 26(5), 1013–1026.

National Research Council (1996), Rock Fractures and Fluid Flow: Contemporary Understanding and Applications, Natl. Acad. Press, Washington D. C.

Neretnieks, I. (1980), Diffusion in the rock matrix: An important factor in radionuclide transport?, J. Geophys. Res., 85(B8), 4379–4397.

Neuman, S., and Y. Zhang (1990), A quasi-linear theory of non-Fickian and Fickian subsurface dispersion: 1. Theoretical analysis with application to isotropic media, Water Resour. Res., 26(5), 887–902.

Neuman, S. P. (1993), Eulerian-Lagrangian theory of transport in space-time nonstationary velocity fields: Exact nonlocal formalism by conditional moments and weak approximation, Water Resour. Res., 29(3), 633–645.

Neuman, S. P. (2004), Stochastic groundwater models in practice, Stochastic Environ. Res. Risk Assess., 18(4), 268–270.

Neuman, S. P., C. L.Winter, and C. M. Newman (1987), Stochastic theory of field-scale Fickian dispersion in anisotropic porous media, Water Resour. Res., 23(3), 453–466.

Nielsen, D. R., and J. W. Biggar (1962), Miscible displacement in soils: III. Theoretical considerations, Soil Sci. Soc. Am. Proc., 26, 216–221.

Nkedi-Kizza, P., J. W. Biggar, H. M. Selim, M. T. van Genuchten, P. J. Wierenga, J. M. Davidson, and D. R. Nielsen (1984), On the equivalence of two conceptual models for describing ion exchange during transport through an aggregated oxisol, Water Resour. Res., 20(8), 1123–1130.

Noolandi, J. (1977), Multiple-trapping model of anomalous transittime dispersion in a-Se, Phys. Rev. B, 16, 4466–4473.

O'Brien, G. S., C. J. Bean, and F. McDermott (2003a), Numerical investigations of passive and reactive flow through generic single fractures with heterogeneous permeability, Earth Planet. Sci. Lett., 213(3–4), 271–284.

O'Brien, G. S., C. J. Bean, and F. McDermott (2003b), A numerical study of passive transport through fault zones, Earth Planet. Sci. Lett., 214(3–4), 633–643.

Oppenheim, I., K. E. Shuler, and G. H. Weiss (1977), Stochastic Processes in Chemical Phsyics: The Master Equation, MIT Press, Cambridge, Mass.

Oswald, S., W. Kinzelbach, A. Greiner, and G. Brix (1997), Observation of flow and transport processes in artificial porous media via magnetic resonance imaging in three dimensions, Geoderma, 80, 417–429.

Pfister, G., and H. Scher (1978), Non-Gaussian transient transport in disordered solids, Adv. Phys., 27, 747–798.

Quintard, M., and S. Whitaker (1994), Transport in ordered and disordered porous media I: The cellular average and the use of weighting functions, Transp. Porous Media, 14, 163–177.

Rajaram, H., and L. W. Gelhar (1993), Plume-scale dependent dispersion in heterogeneous aquifers: 2. Eulerian analysis and three-dimensional aquifers, Water Resour. Res., 29(9), 3261–3276.

Rajaram, H., and L. W. Gelhar (1995), Plume-scale dependent dispersion in aquifers with a wide range of scales of heterogeneity, Water Resour. Res., 31(10), 2469–2482.

Rao, P. S. C., R. E. Jessup, D. E. Rolston, J. M. Davidson, and D. P. Kilcrease (1980), Experimental and mathematical description of nonadsorbed solute transfer by diffusion in spherical aggregates, Soil Sci. Soc. Am. J., 44(4), 684–688.

Roberts, P. H. (1961), Analytical theory of turbulent diffusion, J. Fluid Mech., 11, 257–283.

Roth, K., and W. A. Jury (1993), Linear transport models for adsorbing solutes, Water Resour. Res., 29(4), 1195–1203.

Rubin, Y. (2003), Applied Stochastic Hydrogeology, Oxford Univ. Press, New York.

Rubin, Y. (2004), Stochastic hydrogeology: Challenges and misconceptions, Stochastic Environ. Res. Risk Assess., 18(4), 280–281.

Rubinstein, J., and R. Mauri (1983), Dispersion and convection in periodic porous media, SIAM J. Appl. Math., 46(6), 1018–1023.

Sardin, M., D. Schweich, F. J. Leij, and M. T. van Genuchten (1991), Modeling the nonequilibrium transport of linearly interacting solutes in porous media: A review, Water Resour. Res., 27(9), 2287–2307.

Scheidegger, A. E. (1959), An evaluation of the accuracy of the diffusivity equation for describing miscible displacement in porous media, Proc. Theory Fluid Flow Porous Media Conf., 2nd, 101–116.

Scher, H., and M. Lax (1973a), Stochastic transport in a disordered solid. I. Theory, Phys. Rev. B, 7, 4491–4502.

Scher, H., and M. Lax (1973b), Stochastic transport in a disordered solid. II. Impurity conduction, Phys. Rev. B, 7, 4502–4519.

Scher, H., and E. W. Montroll (1975), Anomalous transit time dispersion in amorphous solids, Phys. Rev. B, 12, 2455–2477.

Scher, H., G. Margolin, and B. Berkowitz (2002a), Towards a unified framework for anomalous transport in heterogeneous media, Chem. Phys., 284, 349–359.

Scher, H., G. Margolin, R. Metzler, J. Klafter, and B. Berkowitz (2002b), The dynamical foundation of fractal stream chemistry: The origin of extremely long retention times, Geophys. Res. Lett., 29(5), 1061, doi:10.1029/2001GL014123.

Schmidlin, F. W. (1977), Theory of trap-controlled transient photoconduction, Phys. Rev. B, 6, 2362–2385.

Schumer, R., D. A. Benson, and M. M. Meerschaert (2003), Fractal mobile/immobile solute transport, Water Resour. Res., 39(10), 1296, doi:10.1029/2003WR002141.

Shlesinger, M. F. (1974), Asymptotic solutions of continuous-time

random walks, J. Stat. Phys., 10(5), 421–434.

Shlesinger, M. F. (1988), Fractal time in condensed matter, Annu Rev. Phys. Chem., 39, 269–290.

Shlesinger, M. F. (1996), Random Processes, Encyclopedia of Applied Physics, vol. 16, John Wiley, Hoboken, N. J.

Shlesinger, M. F., G. M. Zaslavsky, and J. Klafter (1993), Strange kinetics, Nature, 363, 31–37.

Shvidler, M. J. (1993), Correlation model of transport in random fields, Water Resour. Res., 29, 3189–3199.

Sidle, C., B. Nilson, M. Hansen, and J. Fredericia (1998), Spatially varying hydraulic and solute transport characteristics of a fractured till determined by field tracer tests, Funen, Denmark, Water Resour. Res., 34(10), 2515–2527.

Silliman, S. E., and E. S. Simpson (1987), Laboratory evidence of the scale effect in dispersion of solutes in porous media, Water Resour. Res., 23(8), 1667–1673.

Sposito, G., R. E. White, P. R. Darrah, and W. A. Jury (1986), A transfer function model of solute transport through soil: 3. The convection dispersion equation, Water Resour. Res., 22(2), 255–262.

Stark, C. P., and M. Stieglitz (2000), The sting in a fractal tail, Nature, 403, 493–495.

Sudicky, E. (2004), On certain stochastic hydrology issues, Stochastic Environ. Res. Risk Assess., 18(4), 285.

Tiedje, T. (1984), Information about band-tail states from time-offlight experiments, in Semiconductors and Semimetals, Part C, vol. 21, pp. 207–238, Elsevier, New York.

Villermaux, J. (1974), Deformation of chromatographic peaks under the influence of mass transfer phenomena, J. Chromatogr. Sci., 12, 822–831.

Villermaux, J. (1987), Chemical engineering approach to dynamic modelling of linear chromatography, J. Chromatogr., 406, 11–26.

Weisbrod, N., M. R. Niemet, and J. Selker (2003), Light transmission technique for the evaluation of colloidal transport and dynamics in porous media, Environ. Sci. Technol., 37(16), 3694–3700.

Weissmann, G. S., S. F. Carle, and G. E. Fogg (1999), Threedimensional hydrofacies modeling based on soil surveys and transition probability geostatistics, Water Resour. Res., 35(6), 1761–1770.

Whitaker, S. (1999), The Method of Volume Averaging, Springer, New York.

Winter, C. L. (2004), Stochastic hydrology: Practical alternatives exist, Stochastic Environ. Res. Risk Assess., 18(4), 271–273.

Zhang, D. (2002), Stochastic Methods for Flow in Porous Media: Coping With Uncertainties, Elsevier, New York.

Zhang, D., and S. Neuman (1995), Eulerian-Lagrangian analysis of transport conditioned on hydraulic data: 1. Analytical-numerical approach, Water Resour. Res., 31(1), 39–52.

Zhang, Q. (1995), Transient behavior of mixing induced by a random velocity field, Water Resour. Res., 31, 2955–2963.

Zhang, X., J. W. Crawford, L. K. Deeks, M. I. Stutter, A. G. Bengough, and I. M. Young (2005), A mass balance based numerical method for the fractional advection-dispersion equation: Theory and application, Water Resour. Res., 41, W07029, doi:10.1029/2004WR003818.

Zhang, Y., and D. Zhang (1996), Nonergodic solute transport in three-dimensional heterogeneous isotropic aquifers, Water Resour. Res., 32, 2955–2963.

Zhang, Y.-K., and D. Zhang (2004), Forum: The state of stochastic hydrology, Stochastic Environ. Res. Risk Assess., 18(4), 265.

Zwanzig, R. (1960), Ensemble method in the theory of irreversibility, J. Chem. Phys., 33(5), 1338–1341.

B. Berkowitz and H. Scher, Department of Environmental Sciences and Energy Research, Weizmann Institute of Science, Rehovot 76100, Israel. (brian.berkowitz@weizmann.ac.il; harvey.scher@weizmann.ac.il)

A. Cortis, Earth Sciences Division 90-1116, Lawrence Berkeley National Laboratory, 1 Cyclotron Road, Berkeley, CA 94720, USA. (acortis@lbl.gov)

M. Dentz, Department of Geotechnical Engineering and Geosciences, Technical University of Catalonia (UPC), Barcelona E-08034, Spain. (marco.dentz@upc.es)

2. Treatment of spatially dependent input variables in sensitivity analysis of model output methods

TITLE: TREATMENT OF SPATIALLY DEPENDENT INPUT VARIABLES IN SENSITIVITY ANALYSIS OF MODEL OUTPUT METHODS

AUTHOR(S) : Bertrand IOOSS

ABSTRACT:

This report constitutes deliverable CEA/DEN/DER for the component RTDC 2 of European project PAMINA (Performance Assessment Methodologies in Application to Guide the Development of the Safety Case) 6th PCRD. This task concerns the treatment of the spatial variability of the geological media in the uncertainty and sensitivity analyses of computer codes used for the safety analyses of the deep waste storage facilities. In this report, one restricts to methodological aspects. We describe various techniques to perform global sensitivity analyses of numerical models with spatially variable input parameters. We are specially interested by the models which depend on geostatistical simulations, such as a heterogeneous field of permeability modelled by a random field. This problem is also seen within a more general mathematical framework : analysis of numerical models with functional inputs (random fields, stochastic processes, random sets, …).

KEY WORDS: IMPACT CALCULATION, ENVIRONMENT, HYDROGEOLOGY, UNCERTAINTY, SENSITIVITY, GEOSTATISTICAL SIMULATION

1. INTRODUCTION

This report consists in deliverable CEA/DEN/DER for the component RTDC 2 of European project PAMINA (Performance Assessment Methodologies IN Application to guide the development of the safety case) 6th PCRD. This task concerns the treatment of the spatial variability of the geological media in the uncertainty and sensitivity analyses of computer codes used for the safety analyses of the deep waste storage facilities. In this report, one restricts to methodological aspects.

The chapter 2 describes various techniques to perform global sensitivity analyses of numerical models with spatially variable input parameters. We are specially interested by the models which depend on geostatistical simulations, such as a heterogeneous field of permeability modelled by a random field. The application (called MARTHE) concerns the modelling of the radionuclide migration of a radioactive waste disposal site.

Chapters 3 and 4 deal with a more general mathematical framework : the uncertainty and sensitivity analyses of numerical models with functional inputs (as for example random fields, stochastic processes and random sets). We explain a new methodology, based on metamodel (i.e. response surface) construction, to deal with CPU time expensive computer code, containing functional inputs. In chapter 3, we apply it on the MARTHE application (a spatial random field input), while in chapter 4, we apply it on another computer model which contains a temporal stochastic process in its input variables.

2. SENSITIVITY ANALYSIS OF A HYDROGEOLOGICAL MODEL DEPENDENT ON GEOSTATISTICAL SIMULATIONS OF THE PERMEABILITY FIELD

2.1 ABSTRACT

This research focused on developing a transport model for ^{90}Sr in a saturated porous medium for an interim radwaste storage site in Moscow (Russia). A previous global sensitivity analysis of the model led to the conclusion that the calculated concentrations for the piezometers were mainly influenced by a) the distribution coefficient of ^{90}Sr in the different layers of the domain and b) the intensity of infiltration in the pipe leakage zones, and not by the hydrodynamic parameters (dispersivity, porosity, etc.)

The effect of the shape of the coarse sandy layer is investigated in this new study. A technique based on geostatistical simulation is being developed to simulate the shape of this layer. Standard techniques can no longer be used to deal with the sensitivity analysis of such a model, i.e. with random input fields. Different qualitative and quantitative analytical methods are proposed. These methods make it possible to quantify the effect of poorly understanding the shape of the coarse sand layer. The sensitivity analysis also makes it possible to detect other influential parameters for this new modelling technique. The precision on these influential parameters or on the shape of the layer can therefore be improved, thereby considerably decreasing the uncertainty on model prediction.

2.2 INTRODUCTION

This study follows on from the internship by E. Volkova carried out within the collaborative agreement between the Kurchatov Institute (Moscow, Russia) and the French Atomic Energy Commission (France). This aim of this internship was to develop a transport model for water-saturated porous media using the MARTHE software (BRGM[1]) for an interim radwaste storage site (STDR) in Moscow (Russia). The main objective was to model the transport of strontium-90, a mobile radioactive element found in soils – in the upper aquifer of the site. To begin with, modelling was performed during a pre-established measurement period (2002 – 2004) in order to compare the model results with the in-field measurements. For predictive purposes, modelling was then continued up to 2010 to determine the degree of potential contamination in the aquifer. In order to identify the code input parameters considered to have the most effect on the calculation result, statistical methods for uncertainty and sensitivity analyses were used (Law & Kelton [10], Helton *et al.* [6], Devictor & Bolado [4], Iooss [7]). Considering the complexity of the numerical model and the long CPU time, an intermediary phase was required to build the metamodels for a limited number of code simulations (Volkova *et al.* [14]). Additional research was also carried out to improve the metamodel building phase (Marrel *et al.* [11]).

This first study made it possible to reach the conclusion that the concentration in the piezometers, as modelled by MARTHE, was more influenced by the distribution coefficient of ^{90}Sr in the different layers of the domain and by the intensity of infiltration in the pipe leakage zones, than by the other model parameters. Therefore, the improved precision of these parameters would make it possible to considerably decrease uncertainty on the model prediction. Owing to this result, one of the lines of research suggested by this work consists in quantifying the influence of the shapes of certain less-permeable zones of the model. During the first study, these shapes (resulting from interpolation methods based on in-field data) were assumed to be unchanging. In the second study, we suggested varying them using geostatistical simulations.

---

[1] French public organisation specialised in geosciences

Research therefore aimed to study the effect of geostatistical simulations on variations in the output concentrations calculated by the MARTHE model. Input geostatistical simulations of numerical models were only briefly discussed in the sensitivity analyses, whether this be on a theoretical, methodological or practical level. The different solutions discussed in the literature are examined in Iooss & Ribatet [8] (see chapter 4) who came to the conclusion that these solutions cannot be applied when the model is non-linear, requires long CPU times, and has many uncertain input parameters and output variables. Furthermore, the solution recommended by Iooss et al. [9] (see chapter 3) based on a double metamodel has proven to be difficult to apply to this application. This is due to the input dimensions, the inconsistency in concentration values (some are very low while others are extremely high), and most probably the very strong influence of geostatistical simulations in relation to other scalar input parameters. Other approaches have to be considered, as the functional decomposition of the random field (Busby et al. [0]).

It was possible to foresee simpler methods in the second study owing to feedback from the first study. The only difference between the two models lies in the replacement of four random input parameters (permeability in different zones) by the simulation of the random field. The same sets of simulation runs were performed on the other random input parameters. This particularly made it possible to calculate this sensitivity of the model to the random field through comparisons with the results of the first model (without the random field).

This chapter will describe the new transport scenario based on the MARTHE code, using geostatistical simulations of the shape of zones. The fourth section will discuss the application of different techniques used to qualitatively and quantitatively analyse the effect of geostatistical simulations on model output variables. The fifth section discusses the use of metamodels and the associated results. A concise summary of all these results is given by way of conclusion.

2.3 SCENARIO WITH GEOSTATISTICAL SIMULATIONS

The construction of the first model for the STDR site (Volkova et al. [14]) required using the available data. The modelled hydrogeological aquifer was sub-divided into three layers representing the different geological media: two layers of fine-grained sand and an intermediary layer of coarse-grained sand. The thickness of each layer is variable and was calculated by interpolation of the lithologic data taking into account all the drill holes in the area. The data also revealed that the coarse sand layer was not found everywhere in the domain: there are drill holes that do not contain this layer. The shape of these zones void of coarse sand was interpolated using specialised software and the drill hole data. Figure 2.1 shows the limit according to a horizontal plane between the intermediary layer of coarse sand and the upper layer, making it possible to visualise the absence of this layer in certain places (blue zones).

The numerical model – based on MARTHE – consists in propagating a source term over a period from August 2002 to December 2010. The numerical diagram in question requires a CPU time of about 15 minutes for one simulation. A total of 300 different simulations were performed by randomly varying 20 scalar input parameters using a Monte-Carlo technique. The total CPU time added up to three full days. All these calculations were analysed in the first study (Volkova et al. [14]).

Our next objective was to vary the shape of the zones in which there was no coarse sand. A method of geostatistical simulations was established in order to do this. This method is based on a simulation method for categorical variables (called "indicator principle component approach") resulting from the "ipcsim" program of the GSLib software (Deutsch & Journel [3]). A spatial two-category variable was used to simulate the shape of the zones void of coarse sand. The first category corresponds to the presence of the layer of coarse sand, whereas the second indicates the zones void of coarse sand. A Gaussian-type variogram was chosen with a correlation length adapted to the heterogeneities that require simulating. The variogram was built on the basis of the coarse sand layer thickness observed in the 66 drill holes on the site. Furthermore, the simulations

were conditioned: for all simulated fields, the absence or presence of coarse sand corresponded to all the available observations. Two different simulations are given in Figure 2.2.
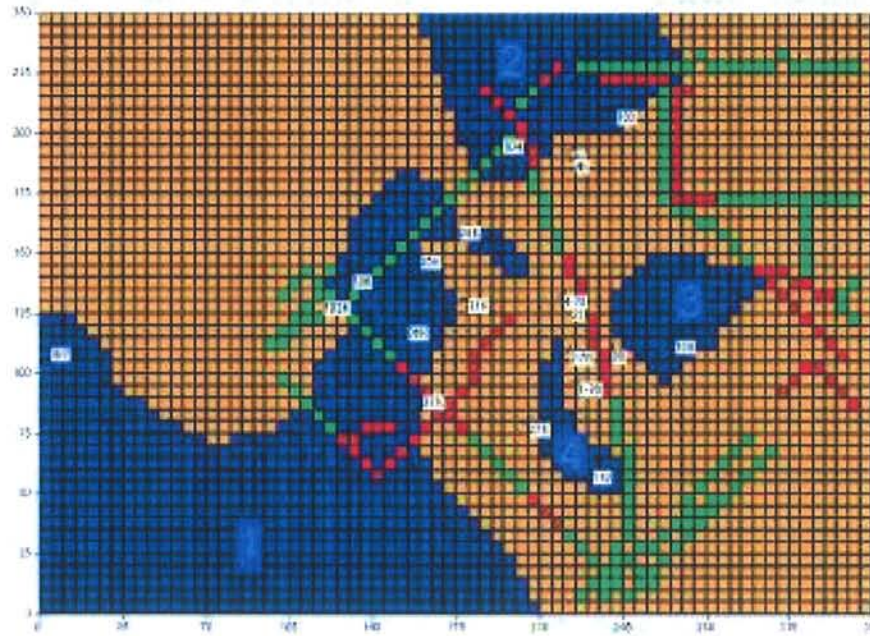
Figure 2.1: Materialisation of the model taking into account different zones in the second layer. Blue zones (numbered 1 to 4) – no coarse sand; Orange zones – presence of coarse sand; Green zones – moderate infiltration near the pipes; Red zones – high infiltration near the pipes; the other number correspond to the 20 piezometers.
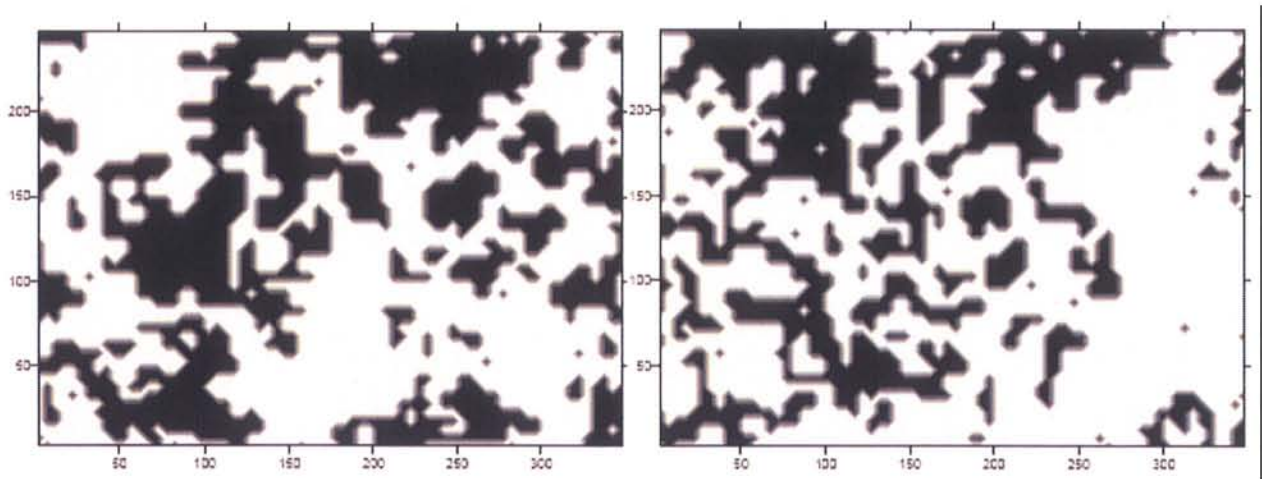
Figure 2.2: Examples of fields indicating the absence of the second layer (black zones).

For each calculation, a generated field was used in the matrix of permeability values for the second layer of the model. When a mesh corresponds to the first category (presence of coarse sand), the permeability of this grid cell is considered equal to the parameter per2 (characteristic value for coarse sand). When a mesh corresponds to the second category (no coarse sand), the permeability for this mesh is considered equal to the permeability of the first layer (upper layer) of the model (parameter per1). The same procedure was used to generate volume distribution coefficients (by using the parameters kd1 and kd2), as well as longitudinal (parameters d1 and d2) and transverse (parameters dt1 and dt2) dispersivity values for the second layer of the model.

The initial study involved 20 scalar input parameters. Seeing that the variable shapes were taken into account for the second layer, the parameterisation of the model must be reviewed. In the first study, 5 parameters were associated with the permeability of the model's second layer: perz1, perz2, perz3, perz4 – for the four blue zones (Figure 2.1) and per2 for the orange zone of the second layer. The value of per2 for zones with coarse sand was applied for the second layer (white zones in Figure 2.2), whereas per1 was applied for zones void of coarse sand (black zones in Figure 2.2). Four input parameters were therefore deleted. These are permeabilities for the different blue zones in Figure 2.1.

Table 2.1 provides a summary of all the scalar parameters considered uncertain in this new model:
- nominal values of parameters,
- distribution types,
- parameters of their distribution (minimum and maximum limits for the uniform distribution and the coefficients of the Weibull law). The parameters of the uniform distribution have been obtained by bibliographical analyses while the parameters of the Weibull distribution have been obtained from a probability distribution fitting procedure on experimental data.

	Parameters	Notation	Model value	Distribution type	Interval or distribution parameters
1	Permeability of layer 1	per1	8	Uniform	1 - 15
2	Permeability of layer 2	per2	15	Uniform	5 - 20
3	Permeability of layer 3	per3	8	Uniform	1 - 15
8	Longitudinal dispersivity of layer 3	d1	0.8	Uniform	0.05 - 2
9	Longitudinal dispersivity of layer 3	d2	0.8	Uniform	0.05 - 2
10	Longitudinal dispersivity of layer 3	d3	0.8	Uniform	0.05 - 2
11	Transverse dispersivity of layer 1	dt1	0.08	Uniform	$0.01*d1 - 0.1*d1$
12	Transverse dispersivity of layer 2	dt2	0.08	Uniform	$0.01*d2 - 0.1*d2$
13	Transverse dispersivity of layer 3	dt3	0.08	Uniform	$0.01*d3 - 0.1*d3$
14	Volumetric distribution coefficient c. 1	kd1	5.1	Weibull	1.1597, 19.9875
15	Volumetric distribution coefficient c. 2	kd2	0.34	Weibull	0.891597, 24.4455
16	Volumetric distribution coefficient c. 3	kd3	5.1	Weibull	1.27363, 22.4986
17	Porosity (all layers)	por	0.3	Uniform	0.3 – 0.37
18	Infiltration type 1	i1	0.0001	Uniform	0 – 0.0001
19	Infiltration type 2	i2	0.004	Uniform	i1 – 0.01
20	Infiltration type 3	i3	0.02	Uniform	i2 - 0,1

Table 2.1: Input parameters for the sensitivity analysis with nominal values, distribution type and distribution coefficients.

There are now 16 random scalar input parameters in addition to the spatial parameter for the shape of the second layer, taken into account by the geostatistical simulations. As in the first study, the output variables under investigation correspond to the calculated concentrations in 2010 for the different piezometers on the site, which results in a total of 20 output variables.

Owing to an increased heterogeneity in the medium where the radionuclide spreads, MARTHE calculations based on geostatistical simulations are much more CPU time-consuming than the previous calculations. The numerical scheme results in a CPU time of about 40 minutes for one simulation. For each simulation, the 16 scalar input parameters were varied randomly (Latin hypercube sampling (LHS) plan). In total, 300 simulations of the MARTHE model were performed, resulting in 8 full days of calculations.

In fact, the simulation sets for the 16 scalar input parameters are the same as those used in the previous study (excepting the four input parameters in excess). It will therefore be possible to calculate the correlation coefficients between the outputs of the two numerical models in order to measure the degree of similarity between the two models, and thereby determine the impact of the

geostatistical simulations. However, as the two output variables relative to the two models in the same piezometer are not statistically independent, it will not be possible to perform standard statistical tests to compare their distribution.

2.4 EFFECT OF GEOSTATISTICAL SIMULATIONS

2.4.1 Comparison of distributions

To analyse the effect of geostatistical simulations on the output of the MARTHE model, a preliminary approach consisted in studying the change in the distributions of the model output variables between calculations without geostatistical simulation and calculations with geostatistical simulation. On the basis of 300 simulations performed for each model, the histograms for each output were represented by superposing that of the geostatistical-free model on that of the geostatistical model.

Figure 2.3 shows the superposition of the histograms for concentrations from two different piezometers. Visually speaking, such a representation provides a lot of information. It can be seen in these two examples that the addition of the geostatistical simulation variable has little impact on the concentration distributions.
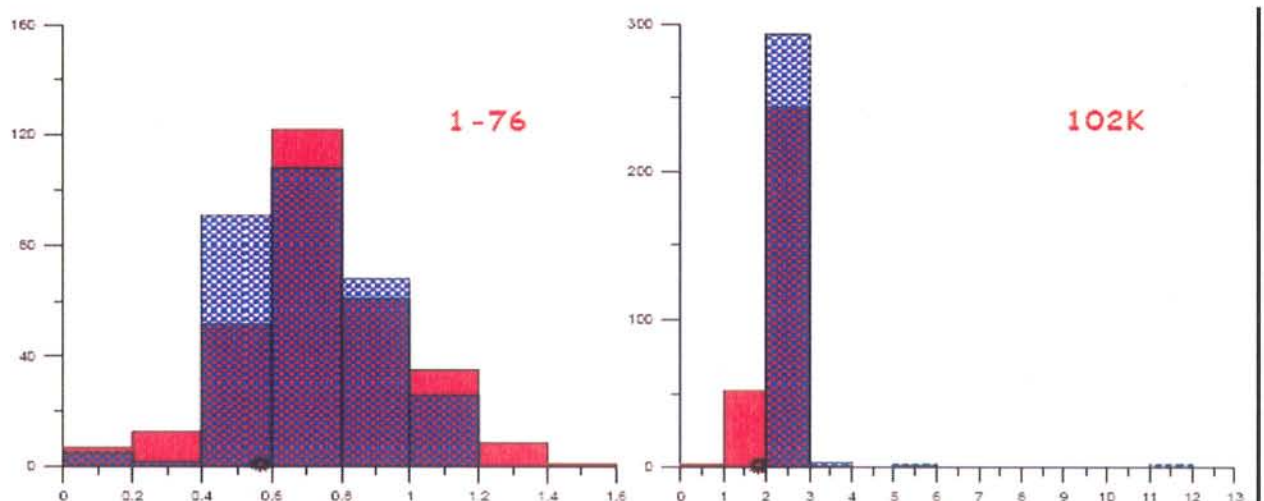
Figure 2.3: Output histograms without geostatistical simulation (red) and with geostatistical simulation (blue) for two MARTHE outputs (concentrations for piezometers p1-76 and p102K).

However, comparison is difficult considering that the histograms have been divided up into different classes of values, which prevents us from observing any subtlety in the distribution of the values. To resolve this problem, density smoothing techniques were used via a non-parametric method based on smoothing kernels (Gaussian in this case). We chose to use the "density" function of the R statistics software (R Development Core Team [12], Venables & Ripley [13]). Figure 2.4 represents the smoothed densities of the calculated concentrations over the 20 piezometers. Each figure makes it possible to visualise the impact of adding the geostatistical simulation variable (red curves in relations to the blue curves).
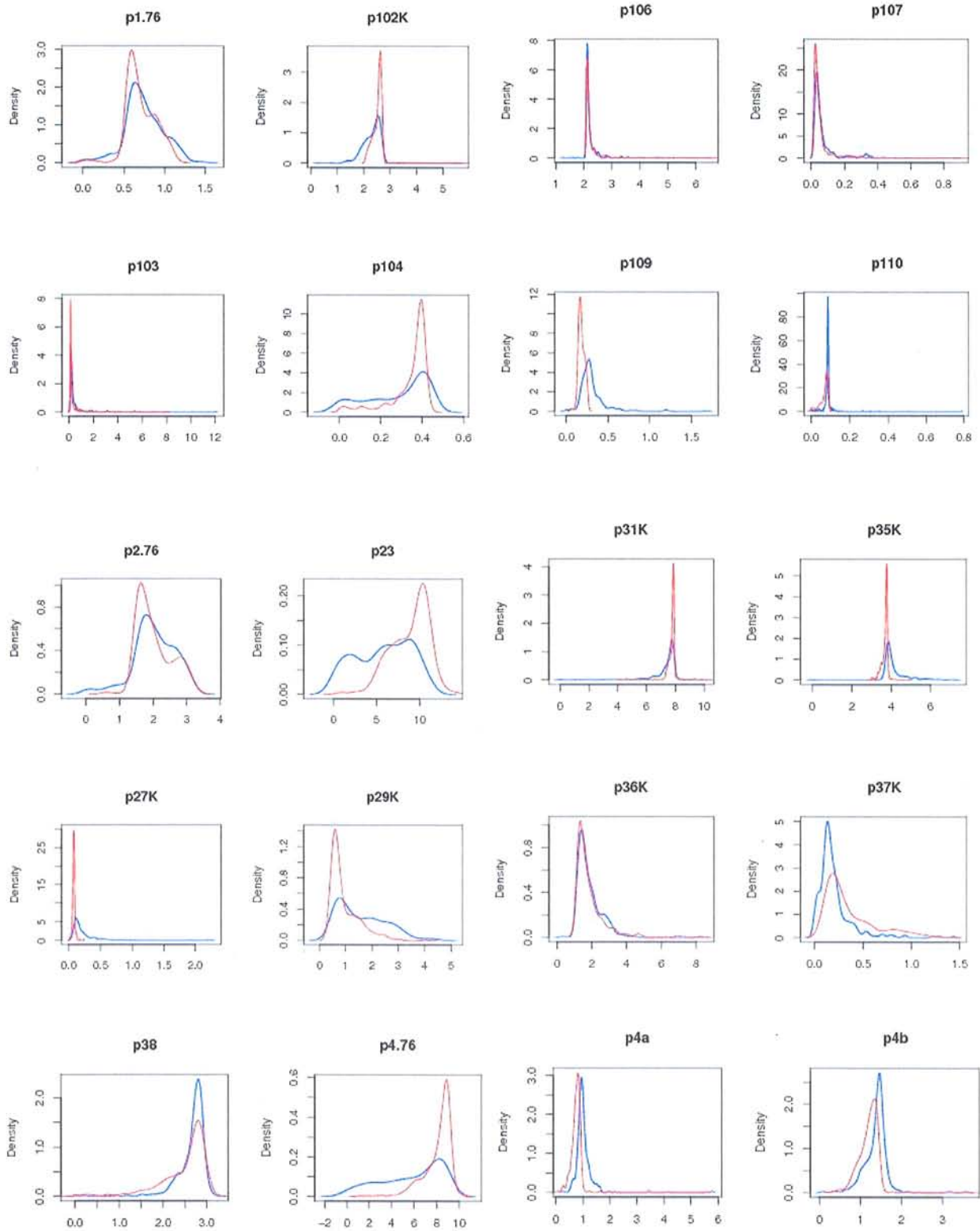
Figure 2.4: MARTHE output densities both without geostatistical simulation (blue curves) and with geostatistical simulation (red curves).

In view of these figures, the MARTHE outputs can be qualitatively classified into three categories:

- outputs where the distributions between calculations without geostatistical simulations and calculations with geostatistical calculations are similar (p103, p106, p107, p36K), which means that the shape of the second layer has little impact on MARTHE;

- outputs where the distributions between calculations without geostatistical simulations and calculations with geostatistical calculations are slightly different (p1-76, p102K, p110, p2-76, p27K, p31K, p38, p4a, p4b);

- outputs where the distributions between calculations without geostatistical simulations and calculations with geostatistical calculations are different (p104, p109, p23, p29K, p35K, p37K, p4-76), which means that the shape of the second layer has a great impact on MARTHE.

There is apparently no link between this classification and the spatial location of the piezometers on the site (see Figure 2.1). As in the previous study, this confirms the complexity and the non-linearity of the simulated numerical models.

Generally speaking, it was observed that the distribution of values did not tend to spread, as we could have expected when integrating geostatistical simulations into the model. The distribution even tends to retract (see piezometers p102K, p104, p109, p27K, p29K, p31K, p35K, p4-76), which does not at all prejudice the effect of the geostatistical simulations. This first purely-visual analysis requires confirmation (or negation) by quantitative analysis.

2.4.2 Correlations

2.4.2.1 Correlation coefficients

The standard correlation coefficient (Pearson) measures the degree of linear correlation between two quantitative numerical variables. Spearman's correlation coefficient measures the degree of monotonic correlation between two quantitative variables. It is therefore worth calculating these coefficients between the outputs of two numerical models: a model with 20 scalar input parameters without geostatistical simulation and another model with 16 scalar input parameters with geostatistical simulation. For each of the 300 calculations for the two models, 16 input parameters are similar. The Pearson and Spearman correlation coefficients therefore measure the linear or monotonic effect of replacing four input parameters (permeabilities in zones without coarse sand) by a geostatistical simulation of the shape of these zones. They are very sensitive to several extreme values of a sample, which means they must be considered qualitatively and with caution.

Table 2.2 shows the two correlation coefficients between each output of the two models. In the following analysis, the highest coefficient (absolute value) between that of Pearson and that of Spearman was used for each output.

Piezometer	p1-76	p102K	p103	p104	p106	p107	p109	p110	p2-76	p23
Pearson	35.16	-1.16	69.48	58.41	18.97	63.64	24.14	-13.01	11.20	63.4£
Spearman	43.68	76.52	8 76.52	58.57	40.71	46.04	25.81	21.45	28.52	67.9£
Piezometer	p27K	p29K	p31K	p35K	p36K	p37K	p38	p4-76	p4a	p4b
Pearson	12.70	70.89	31.80	-13.00	60.63	34.44	58.5€	68.66	46.90	47.4:
Spearman	12.89	79.33	52.34	-20.45	58.93	36.88	-20.4	73.63	4.09	45.0∠

Table 2.2: Correlation coefficients (expressed as a percentage) between the outputs of the model without geostatistical simulation and the outputs of the model with geostatistical simulation.

In view of Table 2.2, the MARTHE outputs can be classified into three categories:

- outputs where the correlation coefficients are particularly high (> 66%): p102K, p103, p23, p29K, p4-76, which means that the shape of the second layer has little impact on MARTHE;

- outputs where the correlation coefficients are close to 50% (between 33% and 66%): p1-76, p104, p106, p107, p31K, p36K, p37K, p38, p4a, p4b;
- outputs where the correlation coefficients are low (<33%): p109, p110, p2-76, p27K, p35K, which means that the shape of the second layer has a high impact on MARTHE.

Upon preliminary analysis, the results of this interpretation seem to differ from the results mentioned in paragraph 2.4.1.

Based on these results, it was nevertheless remarked that the piezometers revealing a high impact of the shape of the second layer were located in the lower left zone of the model (see Figure 2.1), i.e. out of the way in relation to the spread of contamination over time. This seems to correspond to piezometers with low concentrations (because contamination diffusion is poor in this direction), which probably means that the data cannot be considered robust enough in relation to a change in the model (like the same of layer).

2.4.2.2 Correlation ratios

When measuring the correlation between a quantitative variable Y and a qualitative variable X (which has a certain number of categories), the following correlation ratio is applied:

$$\eta_{Y|X}^2 = \frac{Var[E(Y|X)]}{Var(Y)}$$

which corresponds to the variance of the quantitative variable Y for each category of X. For our application, we can therefore assume that Y is the output variable (^{90}Sr concentration), and that X corresponds to an input parameter with two categories: with and without geostatistical simulation. The ratio of the empirical correlation can be calculated according to the following equation:

$$e^2(Y) = \frac{n_1 n_2}{n^2} \frac{(\overline{Y_1} - \overline{Y_2})^2}{\sigma^2(Y)}$$

where n is the total size of the data sample (X, Y), n_1 and $\overline{Y_1}$ are the frequency and the mean of Y_1 corresponding to the first category of X (no simulations), n_2 and $\overline{Y_2}$ are the frequency and mean of corresponding to the second category of Y (with simulations), and $\sigma(Y)$ is the variance of Y. In this case, n = 600 and $n_1 = n_2 = 300$.

When e^2 is equivalent to zero, there is generally independence between X and Y: the input parameter X does not affect the variation in the output of model Y. This means that the presence (or absence) of geostatistical simulations does not affect the concentrations obtained. When e^2 is close to 1 (or to 100%), it means that there is strong dependence between the categories of the input parameter X and the response Y.

The correlation ratios are given in Table 2.3. In this table, certain results seem incorrect as they are greater than 100%. In fact, the hypotheses associated with the calculation of these correlation ratios are not met because the data is not inter-independent. They are highly correlated for certain outputs between two categories (as seen in the previous paragraph).

Piezometer	p1-76	p102K	p103	p104	p106	p107	p109	p110	p2-76	p23
e^2	0.65	49.37	0.02	1.90	**4.98**	0.18	8.81	0.29	0.05	5351
Piezometer	p27K	p29K	p31K	p35K	p36K	p37K	p38	p4-76	p4a	p4b
e^2	10.93	240.7	168.8	**1.6₄1**	**1.64**	13.30	12.69	2899	26.40	9.77

Table 2.3: Correlation ratios between the output of two numerical models and the "presence/ absence" category of the geostatistical simulation (as a percentage).

In view of this table, it is possible to classify MARTHE outputs into three categories:
- outputs where the correlation ratios are less than 10%: p1-76, p103, p104, p107, p109, p110, p2-76, p36K, p4b, which means that the shape of the second layer has little effect on the MARTHE model;
- outputs where the correlation ratios are greater than 10% and less than 100%: p102K, p27K, p37K, p38, p4a;
- outputs where the correlation ratios are abnormal because they are higher than 100%: p23, p29K, p31K, p35K, p4-76, which means that the shape of the second layer has a high impact on the MARTHE model.

As a first approach, these results seem rather different from the results in paragraph 2.4.2.1, and more similar to those in paragraph 2.4.1. However, the confidence level given to these results is relative seeing that the basic hypothesis of inter-independence of data was not met.

2.4.2.3 Comparison of sensitivity analyses

The next step was to perform sensitivity analyses in relation to the scalar input parameters for the two MARTHE models: the model without geostatistical simulation and the model with geostatistical simulation. Owing to the high non-linearity and even the non-monotony of the outputs of the two MARTHE numerical models, we decided to use sensitivity indices based on the statistical tests that only require the independence of the initial sample, and no hypothesis on the complexity of the model. This was the case here, as the sets of input parameters were established randomly (according to the LHS plan).

Helton *et al.* [6] provide a detailed list of indices based on statistical tests (parametric or non-parametric). The idea is to partition the variation range of an input (and possibly the output) into several parts, before testing to see if the distribution is different between the parts. It is therefore necessary to use tests that enable the comparison of several (especially more than two) samples: F-ANOVA, χ^2, Kruskal-Wallis, etc. The results are given in terms of the p-value, and are therefore not expressed quantitatively as is the case for the standard regression coefficients which take into account contribution to the output variance. However, the hypothesis of linearity or of monotony is no longer required to validate the indices. The only hypothesis given concerns the independence of observations. For the LHS plans, where observations are not independent, it seems that this hypothesis is not restrictive and that the tests are both robust and fully applicable. Certain tests are more robust that others; some do not assume that the sample follows a normal law. We used the SSURFER software (Iooss [7]) in the suite, which is limited to the use of the "common locations" (CL) test based on the Kruskal-Wallis test (Conover [2]).

The Kruskal-Wallis test can be considered as a generalisation of the Wilcoxon-Mann-Whitney test with more than two samples. It is a non-parametric test and therefore does not offer any hypothesis on the shape of the underlying distributions. Like many non-parametric tests, it does not focus on the observation values but on their ranks, once these observations have been pooled into the one mega-sample. The statistics of the Kruskal-Wallis test are built on the mean of the observation ranks in the different samples. This is why the Kruskal-Wallis test is sometimes called: univariate ANOVA on the ranks. As we have 300 data for each model, we chose a breakdown into 10 segments in relation to the values of an input parameter, which results in tests between 10 samples of 30 data each. A test was performed for each input parameter and each output. The result of a statistical test is a p-value. A p-value equal to 0.1 means that the postulated hypothesis cannot be rejected at confidence levels greater than or equal to 90%, i.e. that each sample has the same Kruskal-Wallis statistics. Our final interpretation will therefore be: if the p-value is greater than 0.1, the samples are statistically homogeneous and therefore the input parameter does not affect the output. Below the threshold of 0.1, it can be said that the different samples are no longer statistically homogeneous, and that the lower the p-value, the greater the impact of the input parameter on the output.

Table 2.4 provides the results of sensitivity analyses based on the CL test for each output and each model (with and without geostatistical simulation). For the sake of simplifying our interpretation, we have not given the p-values but only the classification (in order of decreasing influence) of the inputs whose p-value is below 0.1.

	géosta	kd	kd2	kd3	d3	I1	i2	i3	per	per2	per3	pz	pz2	pz3	pz4	po	(	(
p1-76	Withou	2	1			3					4							
	With		1							2								
p102K	Withou	2	1					3			4		6					
	With		1							2								
p103	Withou	1	4	5				3		2	2	6						
	With	2	1		4					3								
p104	Withou	1						2			3							
	With	1	3							2								
p106	Withou	1						3					2					
	With	1	3							2								
p107	Withou	1						3					2					
	With	2						4	1		3							
p109	Withou				6		3	1	2	5	7					4		
	With	2							1		4							
p110	Withou	2	3					1			4				5	6		
	With	1	3							2								
p2-76	Withou	2	1			4				5	3							
	With	4	1				3			2								
p23	Withou	3	1					2			4							
	With		1			4				2	3							
p27K	Withou		2					1			3							
	With	3	1				5	2		4								
p29K	Withou	2	1					3		6	5	4	7					
	With	2	1	5						3	4	6						
p31K	Withou		1					2			3							
	With		1															
p35K	Withou		1					2	5		4	3						
	Avec		1	3						2								
p36K	Withou	1		2	4						5	3						
	With	1		3						2	4							
p37K	Withou	5	3	6				1		2	4							
	With		1							2	3							
p38	Withou	1	2	4				3										
	With	2	1	5						3	4							
p4-76	Withou	3	1					2					5					
	With	2	1							3								
p4a	Withou						2	1						3				
	With	3	1	4				6		5	2							
p4b	Withou		2				4	1	7	3	6		8	5				
	With		1	3				5		4	2							

Table 2.4: Results of the sensitivity analysis between the inputs and the outputs using the CL test – Classification of the parameters whose p-values are below 0.1 (Blue: model without geostatistical simulation. Red: model with geostatistical simulation).

As a preliminary analysis, the results of the model without geostatistical simulation (blue) seem consistent with the results of Volkova et al. [14] which use indices based on the Sobol ranks and indices calculated using metamodels. For certain output variables (non monotonic and poorly modelled by a metamodel), slight differences can appear; the classification in Table 2.4 are to take priority. The CL test is robust and not based on any hypothesis (Helton et al. [6]). The most influential input parameters for this model are therefore the distribution coefficients of layers 1 and 2 (kd1 and kd2), and the intensity of infiltration in the leakage zones of pipes (i3). To a lesser extent, the permeability of layers 2 and 3 (per2 and per3) are also often influential. It can also be seen that the permeabilities in the different zones without coarse sand are influential for several piezometers.

For the model with geostatistical simulation, the three most influential parameters are present: kd1, kd2 and the permeability in layer 1 (per1). As previously mentioned, per2 and per3 are influential to a lesser extent. Last of all, the distribution coefficient of layer 3 (kd3) also has a rather significant impact. In terms of the sensitivity analysis, the only remarkable difference between the model without geostatistical simulation and that with geostatistical simulation is the influence of i3 and per1:

- The permeability of the first layer plays an important role in the model with geostatistical simulation, whereas it hardly has any influence in the first model. This is logical in terms of the numerical model: in the first model, there were 4 different parameters for the permeability of zones without coarse sand in layer 2. In the new model, the permeability of all these zones is combined with the permeability of layer 1 to shape parameter per1. It can be said that the influence of parameters perz1, perz2, perz3 and per1 can be explained by the influence of parameter per1. From a hydrogeological viewpoint, the transport of radionuclides is partially determined by the direction of flow in the ground water, which depends on the shapes of the different zones of permeability. The permeability of these zones in the second layer of the model (where the concentration of radionuclides is taken into account) is per1 and per2. For the model without geostatistical simulation, the permeabilities of these zones were perz1, perz2, perz3 and perz4.

- The intensity of infiltration i3 in the pipe leakage zones does not play a major role in the model with geostatistical simulation. This behaviour can be explained in the same way as beforehand. Without geostatistical simulation, the flow in the model domain was mainly influenced by the force of the leaks, with the forms of the less-permeable zones having been set. With geostatistical simulation, the direction of flow depends on the shapes of the zones (influenced by per1 and per2).

Through a finer analysis (output by output) of the influences of the inputs between the two models, notable differences can be seen for practically all outputs. Even though the most influential parameter is often the same, the following parameters differ most of the time. This confirms the potential impact of the geostatistical simulations on the dynamics of the MARTHE model.

2.5 METAMODELS

When a numerical model is costly and non-linear, it is worth considering replacing it by a simpler mathematical function, called a "metamodel" whose CPU time is negligible. Different types of metamodels are available (Fang et al. [5]). We decided to focus on the use of Gaussian processes, which is a very popular metamodel at the moment, as well as on the development of a joint model more suitable for our problem.

2.5.1 Gaussian processes

In this section, we recommend building a "Gaussian process" type metamodel for each output of each numerical model. We used the methodology developed by Marrel et al. [11]. We adjusted a metamodel for each output of each model. The predictive quality of the metamodel is given by the predictivity coefficient Q_2, calculated by a cross-validation procedure. The Q_2 coefficient represents the variance contribution explained by the metamodel in relation to the total variance of the output variable.

The construction of a metamodel is possible as a function of the scalar input parameters. As the random field results from geostatistical simulation (not being a scalar parameter), it is not possible to integrate it into the construction of the metamodel. For the model with geostatistical simulation, the metamodel can therefore not explain the variance contribution of the variable which is due to the effect of the geostatistical simulation. To indicate the effect of the geostatistical simulation, we can

therefore imagine using the Q_2 difference between the model without geostatistical simulation and that with geostatistical simulation

Table 2.5 provides the Q_2 results for the two models and their difference. The few negative values correspond to situations where the outputs of the model with geostatistical simulation were easier to adjust that those without geostatistical simulation. The heterogeneous shape of layer 2 probably tended to cancel out the non-linearities of the physical model. Generally speaking, a metamodel is considered predictive when Q_2 is greater than 80%. This is the case for 8 out of 19 situations for the model without geostatistical simulation, whereas this practically never occurs for the model with geostatistical simulation.

In view of Table 2.5, the MARTHE outputs can be classified into three categories:
- outputs where the prediction differences are low (< 15%): p2-76, p27K, p29K, p36K, p37K, p4a, p4b, which means that the shape of the second layer has little impact on the MARTHE model;
- outputs where the prediction differences are average (between 15% and 30%): p103, p104, p106, p109, p23, p35K, p38;
- outputs where the prediction differences are particularly high (> 30%): p1-76, p102K, p107, p31K, p4-76, which means that the shape of the second layer has a high impact on the MARTHE model.

Piezometer	p1.76	p102K	p103	p104	p106	p107	p109	p110	p2.76	p23
Without geostat.	84	78	50	96	45	86	50		86	94
With geostat.	47	0	33	71	63	22	69		63	77
Difference	37	78	17	25	-18	64	-19		13	17
Piezometer	p27K	p29K	p31K	p35K	p36K	p37K	p38	p4.76	p4a	p4b
Without geostat.	43	93	69	56	60	90	52	96	9	37
With geostat.	31	80	0	37	71	80	73	57	13	26
Difference	12	13	69	19	-11	10	-21	39	-4	11

Table 2.5: Predictivity coefficients Q_2 (data given as a percentage and calculated by cross-validation) of adjusted Gaussian process models.

As a first approach, these results appear rather different to the results mentioned in paragraphs 2.4.2.1 and 2.4.2.2. In view of these results and the difficulty in obtaining good metamodels by Gaussian processes for the MARTHE data, it was decided that this Q_2 difference criterion was not suitable for the given situation.

2.5.2 Joint modelling using Generalized Additive Model (GAM)

The joint model consists in adjusting a double metamodel to the data: one component for the mean and another component for dispersion. The input random field is in fact rejected as an uncontrollable (or noisy) parameter of the model. The mean and dispersion components are therefore expressed via other scalar input parameters of the model. Thus, the dispersion component includes everything that the scalar parameters only could not explain, i.e. the effect of the random field (including its interactions with the scalar parameters).

Iooss et al. [9] (see chapter 3) illustrated the use of the joint model with a MARTHE output. This result is therefore partial. Processing other outputs is problematic because MARTHE data with geostatistical simulation is particularly complex: the random field effect is often predominant, "outliers" threshold effects, highly-scattered values, etc. The joint model requires a manual, iterative adjustment procedure for each component, which is therefore not very suitable. Developing an automatic yet accurate adjustment procedure for this model therefore remains to be accomplished.

2.6 CONCLUSION

Developed at least twenty years ago, global sensitivity analysis methods for numerical models are limited to scalar input parameters. This research work consisted in investigating and in applying several simple tools to assess the sensitivity of a model output variable in relation to a stochastic input that is non-quantifiable by a small number of scalar parameters. Our application focused on a hydrogeological model dependent on the simulations of a random input field. This random field was built with the aim of correctly representing the heterogeneity of a hydrogeological parameter (permeability in a layer of coarse sand).

All of our analyses were based on the fact that we were no longer able to perform calculations with the numerical model. We only had the relatively limited calculation results obtained using both the model with geostatistical simulation and the model without geostatistical simulation, which correspond to the same sets of scalar input parameters. The different methods used to compare the results of these calculations (with and without geostatistical simulation) were tested:

- comparison of the output distributions of the two models. This analysis made it possible to graphically visualise the impact of the geostatistical simulation, without however quantifying it;

- analysis of the correlation coefficients between the outputs of the two models. These indicators were used to measure the change induced by the geostatistical simulations. They are sensitive to a few extreme values in a sample, and have to be considered qualitatively and with precaution;

- study of the correlation ratios between the output of both models and the "with/without geostatistical simulation" category. These indicators made it possible to quantitatively measure the effect of a qualitative variable (with/without geostatistical simulation) upon a quantitative variable (model output). However, the reliability of these results is relative seeing that the basic hypothesis of independence between data was not met in our study;

- comparison of sensitivity analyses for the two models in relation to scalar inputs. This is a qualitative method only, designed to check if both models have different influential input parameters. It is used to better understand the behaviour of models and the effect of geostatistical simulation upon other input parameters (via their interactions with the random field);

- comparison of the construction of metamodels (based on Gaussian processes) for both models. This is the same type of method as the previously one but this time based on the construction of a metamodel. This method produced very little information in our case;

- construction of a metamodel based on the joint modelling of the mean and of the dispersion. This method is the most accurate and made it possible to obtain a total sensitivity index for the "random field" input variable. However, this method requires the construction of a metamodel for the mean and a metamodel for dispersion. This method could not be implemented in our application owing to the extreme complexity of our data and an excessive number of input parameters. Iooss et al. [9] (see chapter 3) nevertheless managed to apply the method to an output of the model with geostatistical simulation.

In conclusion, our results showed the significant impact of geostatistical simulations on the dynamic of the MARTHE model. This demonstration supports the assumption supposing the limitation of our modelling in relation to the modelling of different layers with different hydrogeological behaviours. The piezometers that proved to be the most sensitive to the shape of the second layer are in fact those located in the background in relation to the direction in which contamination spreads over time. This corresponds to piezometers to low concentration values.

2.7 ACKNOWLEGMENTS

2.8 REFERENCES

[0] D. Busby, T. Romary, M. Feraille and S. Touzani, An integrated approach for uncertainty and sensitivity analysis in reservoir forecasting. *Journal of Computational Geoscience,* submitted, 2008.

[1] T. Hastie and R. Tibshirani. *Generalized additive models.* Chapman & Hall/CRC, 1990.

[2] W.J. Conover. *Practical non parametric statistics, Third edition,* Wiley, New-York, 1999.

[3] C.V. Deutsch and A.V. Journel. *GSLib - Geostatistical software library and user's guide.* Second edition, Oxford University Press, 1997.

[4] N. Devictor and R. Bolado Lavin. *Uncertainty and sensitivity methods in support of PSA level 2,* SARNET report, SARNET-PSA2-P06 Revision 0, European Commission, 2006.

[5] K.T. Fang, R. Li and A. Sudjianto. *Design and modelling of computer experiments.* Chapman & Hall/CRC, 2006.

[6] J.C. Helton, J.D. Johnson, C.J. Salaberry and C.B. Storlie, Survey of sampling-based methods for uncertainty and sensitivity analysis, *Reliability Engineering and System Safety,* 91:1175-1209, 2006.

[7] B. Iooss. *Manuel utilisateur du logiciel SSURFER V1.2: programmes en R d'analyse d'incertitudes, de sensibilités, et de construction de surfaces de réponse.* Note Technique CEA/DEN/CAD/DER/SESI/LCFR/NT DO 6 08/03/06, CEA Cadarache, 2006.

[8] B. Iooss and M. Ribatet. Global sensitivity analysis of computer models with functional inputs. *Reliability Engineering and System Safety,* submitted, 2008. Available at URL: http://fr.arxiv.org/abs/0802.1009v1.

[9] B. Iooss, M. Ribatet and A. Marrel. Global sensitivity analysis of stochastic computer models with generalized additive models. *Technometrics,* submitted, 2008. Available at URL: http://fr.arxiv.org/abs/0802.0443v1.

[10] A.M. Law and W.D. Kelton. *Simulation modelling and analysis,* third edition, New-York: McGraw-Hill, 2000.

[11] A. Marrel, B. Iooss, F. Van Dorpe and E. Volkova. An efficient methodology for modelling complex computer codes with Gaussian processes. *Computational Statistics and Data Analysis,* accepted, in revision, 2008. Available at URL: http://fr.arxiv.org/abs/0802.1099v1.

[12] R Development Core Team. *R: A language and environment for statistical computing,* 2006. ISBN 3-900051-07-0.

[13] W.N. Venables and B.B. Ripley. *Modern applied statistics with S.* Springer, 4th ed., 2002.

[14] E. Volkova, B. Iooss and F. Van Dorpe. Global sensitivity analysis for a numerical model of radionuclide migration from the "RRC Kurchatov Institute" waste disposal site. *Stochastic Environmental Research and Risk Assessment,* 22:17-31, 2008.

3   GLOBAL SENSITIVITY ANALYSIS OF STOCHASTIC COMPUTER MODELS WITH GENERALIZED ADDITIVE MODELS

3.1   ABSTRACT

The global sensitivity analysis, used to quantify the influence of uncertain input parameters on the response variability of a numerical model, is applicable to deterministic computer codes (for which the same set of input parameters gives always the same output value). This chapter proposes a global sensitivity analysis method for stochastic computer codes (having a variability induced by some uncontrollable parameters). The mean and the dispersion of the code outputs are modeled by two interlinked Generalized Additive Models (GAM). The "mean" model allows to obtain the controllable parameters sensitivity indices, while the "dispersion" model allows to obtain the uncontrollable parameters ones. The relevance of the proposed model is analyzed with two case studies. Results show that the joint modeling approach leads to more accurate sensitivity index estimations, especially for the joint GAM model.

3.2   INTRODUCTION

Many phenomena are modeled by mathematical equations which are implemented and solved by complex computer codes. These computer models often take as inputs a high number of numerical parameters and physical variables, and give several outputs (scalars or functions). For the development of such computer models, its analysis, or its use, the global Sensitivity Analysis (SA) method is an invaluable tool (Saltelli et al. [26], Kleijnen [12], Helton et al. [6]). It takes into account all the variation ranges of the inputs, and tries to apportion the output uncertainty to the uncertainty in the input factors. These techniques, often based on the probabilistic framework and Monte-Carlo methods, require a lot of simulations. The uncertain input parameters are modeled by random variables and characterized by their probabilistic density functions. The SA methods are used for model calibration, model validation, decision making process, i.e. all the processes where it is useful to know which variables mostly contribute to output variability.

The current SA methods are applicable to the deterministic computer codes, codes for which the same set of input parameters always gives the same output values. The randomness is limited to the model inputs, whereas the model itself is deterministic. Most computer codes belong to this kind of model. For example in the nuclear engineering domain, global sensitivity analysis tools have been applied to waste storage safety studies (Helton et al. [6]), environmental models of dose calculations (Iooss et al. [10]), pollutant transport models in the groundwater (Volkova et al. [31]). In such industrial studies, numerical models are often too time consuming for applying directly the global SA methods. To avoid this problem, one solution consists in replacing the time consuming computer code by an approximate mathematical model, called response surface or surrogate model or also metamodel (Sacks et al. [24], Fang et al. [3]). This function must be as representative as possible of the computer code, with good prediction capabilities and must require a negligible calculation time. Several metamodels are classically used : polynomials, splines, neural networks, Gaussian processes (Chen et al. [2], Fang et al. [3]).

In this chapter, we are not interested by deterministic computer models but by stochastic numerical models - i.e. when the same input parameters set leads to different output values. The model is therefore intrinsically stochastic because of some "uncontrollable" parameters. For the uncertainty analysis, Kleijnen [12] has raised this question, giving an example concerning a queueing model. In the nuclear engineering domain, examples are given by Monte-Carlo neutronic models used to calculate elementary particles trajectories, Lagrangian stochastic models for simulating a large number of particles inside turbulent media (in atmospheric or hydraulic environment). In our study, "uncontrollable" parameters correspond to parameters that are known to exist, but unobservable, inaccessible or non describable for some reasons. It includes the important case in which observable vectorial parameters are too complex to be described by a reasonable number of scalar parameters. This last

situation concerns the codes in which some simulations of random processes are used : the output values of the computer code depend on the realizations of these random functions. For example, one can quote some partial differential equation resolutions in heterogeneous random media simulated by geostatistical techniques (fluid flows in oil reservoirs, Zabalza-Mezghani et al. [36], acoustical wave propagation in turbulent fluids, Iooss et al. [8]), where the uncontrollable parameter is the simulated spatial field involving several thousand scalar values for each realization.

For an environmental assessment problem, Tarantola et al. [29] propose a first solution by introducing a binomial input parameter ξ governing the simulation of the random field. Therefore, the sensitivity index of ξ quantifies the influence of the random field on the model output variable. However, this method does not give any idea about the influence of the possible interactions between the uncontrollable parameter and the other uncertain input parameters. Moreover, to perform a sensitivity analysis, such approach requires a large number of computer model calculations (several hundreds per input parameter). For most applications, it is impossible due to intractable CPU times : computer codes have to be substituted for metamodels.

For stochastic computer models, classical metamodels (devoted to approximate deterministic computer models) are not pertinent. To overcome this problem, the commonly used Gaussian process (Gp) model is interesting. Kleijnen & van Beers [13] have demonstrated the usefulness of Gp for stochastic computer model. Moreover, Gp can include an additive error component (called the "nugget effect") by adding a constant term into its covariance function (Rasmussen & Williams [22]). However, it supposes that the error term is independent of the input parameters (homoscedasticity hypothesis), which means that the uncontrollable parameter does not interact with controllable parameters. This hypothesis limits the usefulness of the Gp model to particular cases. To construct heteroscedastic metamodels for stochastic computer codes, Zabalza-Mezghani et al. [35] model the mean and the dispersion of computer code outputs by two interlinked Generalized Linear Models (GLMs). This approach, called the joint model, has been previously studied in the context of experimental data modeling (McCullagh & Nelder [16]). Compared to the Gp model, this approach theoretically suits the study of heteroscedastic situations and allows the obtention of a model for the dispersion.

Following the work of Zabalza et al., Iooss & Ribatet [9] have recently introduced the joint model to perform a global sensitivity analysis of a stochastic model. Results show that a total sensitivity index of all the uncontrollable parameters can be computed using the dispersion component of the joint model. However, the parametric form of the GLM framework provides some limitations when modeling complex computer code outputs. To resolve this problem, this chapter suggests the use of non parametric models to allow more flexibility and complexity while fitting to the data. Due to its similarity with GLMs, Generalized Additive Models (GAM) are considered (Hastie & Tibshirani [4], Wood & Augustin [34]). GAMs allow variable and model selections *via* a quasi-likelihood function, classical statistical tests on coefficients, and graphical displays.

This chapter starts by describing the joint model construction, firstly with the GLM, secondly with the GAM. The fourth section describes the global sensitivity analysis for deterministic models, and its extension to stochastic models using joint models. Particular attention is devoted to the calculation of variance-based sensitivity indices (the so-called Sobol indices). Considering a simple analytic function, the performance of the proposed approach is compared to other commonly used models. Next, an application on an actual industrial case (groundwater radionucleide migration modeling) is given. Finally, some conclusions synthesize the contributions of this work.

3.3   JOINT MODELING OF MEAN AND DISPERSION

3.3.1   Using the Generalized Linear Models

The class of GLM allows to extend the class of the traditional linear models by the use of : (a) a distribution which belongs to the exponential family; (b) and a link function which connects the explanatory variables to the explained variable (Nelder & Wedderburn [19]). Let us describe the first

component of the model concerning the mean :

$$
\begin{cases}
\mathsf{E}(Y_i) & = \mu_i, \qquad \eta_i = g(\mu_i) = \sum_j x_{ij}\beta_j \,, \\
\mathsf{Var}(Y_i) & = \phi_i v(\mu_i) \,,
\end{cases}
\tag{1}
$$

where $(Y_i)_{i=1...n}$ are independent random variables with mean μ_i; x_{ij} are the observations of the parameter X_j; β_j are the regression parameters which have to be estimated; η_i is the mean linear predictor; $g(\cdot)$ is a differentiable monotonous function (called the link function); ϕ_i is the dispersion parameter and $v(\cdot)$ is the variance function. To estimate the mean component, the functions $g(\cdot)$ and $v(\cdot)$ have to be specified. Some examples of link functions are given by the identity (traditional linear model), root square, logarithm, and inverse functions. Some examples of variance functions are given by the constant (traditional linear model), identity and square functions.

Within the joint model framework, the dispersion parameter ϕ_i is not supposed to be constant as in a traditional GLM, but is supposed to vary according to the model :

$$
\begin{cases}
\mathbb{E}(d_i) & = \phi_i, \qquad \zeta_i = h(\phi_i) = \sum_j u_{ij}\gamma_j \,, \\
\mathsf{Var}(d_i) & = \tau v_d(\phi_i) \,,
\end{cases}
\tag{2}
$$

where d_i is a statistic representative of the dispersion, γ_j are the regression parameters which have to be estimated, $h(\cdot)$ is the dispersion link function, ζ_i is the dispersion linear predictor, τ is a constant and $v_d(\cdot)$ is the dispersion variance function. u_{ij} are the observations of the explanatory variable U_j. The variables (U_j) are generally taken among the explanatory variables of the mean (X_j), but can also be different. To ensure positivity, $h(\phi) = \log \phi$ is often chosen for the dispersion link function. For the statistic representing the dispersion d, the deviance contribution (which is close to the distribution of a χ^2) is considered. Therefore, as the χ^2 is a particular case of the Gamma distribution, $v_d(\phi) = \phi^2$ and $\tau \sim 2$. In particular, for the Gaussian case, these relations are exact : d is χ^2 distributed and $\tau = 2$.

The joint model is fitted using Extended Quasi-Loglikelihood (EQL) (Nelder & Pregibon [18]) maximization. The EQL behaves as a log-likelihood for both mean and dispersion parameters. This justifies an iterative procedure to fit the joint model. First, a GLM is fitted on the mean; then from the estimate of d, another GLM is fitted on the dispersion. From the estimate of ϕ, weights for the next estimate of the GLM on the mean are obtained. This process can be reiterated as many times it is necessary, and allows to entirely fit our joint model (McCullagh & Nelder [16]).

Statistical tools available in the GLM fitting are also available for each component of the joint model : deviance analysis, Student and Fisher tests, residuals graphical analysis. It allows to make some variable selection in order to simplify model expressions.

Remark : Let us note that it is possible to build polynomial models for the mean and the variance separately (Vining & Myers [30], Bursztyn & Steinberg [1]). This approach, called the dual modeling, consists in repeating calculations with the same sets of controllable parameters (which is not necessary in the joint modeling approach). The dual modeling approach has been successfully applied in many situations, especially for robust conception problems : optimizing a mean response function while minimizing the variance. However for our purpose (accurate fitting of the mean and dispersion components), it has been shown that this dual model is less competitive than the joint model (Zabalza et al. [35], Lee & Nelder [14]) : the dual modeling approach fits the dispersion model given the mean model and this approach does not always lead to optimal fits.

3.3.2   Extension to the Generalized Additive Models

Generalized Additive models (GAM) were introduced by Hastie & Tibshirani [4, 5] and allow a linear term in the linear predictor $\eta = \sum_j \beta_j X_j$ of equation (1) to be replaced by a sum of smooth functions $\eta = \sum_j s_j(X_j)$. The $s_j(.)$'s are unspecified functions that are obtained by fitting a smoother to the data, in an iterative procedure. GAMs provide a flexible method for identifying nonlinear covariate effects in exponential family models and other likelihood-based regression models. The fitting of

GAM introduces an extra level of iteration in which each spline is fitted in turn assuming the others known. GAM terms can be mixed quite generally with GLM terms in deriving a model.

One common choice for s_j is the smoothing spline (Wahba [32]) - i.e. splines with knots at each distinct value of the variables. In regression problems, smoothing splines have to be penalized in order to avoid data overfitting. Wood & Augustin [34] have described in details how GAMs can be constructed using penalized regression splines. This approach is particularly well-suited because it allows the integrated model selection via Generalized Cross Validation (GCV) and related criteria, the incorporation of multi-dimensional smooths and relatively well founded inference using the resulting models. Because numerical models often exhibit strong interactions between input parameters, the incorporation of multi-dimensional smooth (for example the bi-dimensional spline term $s_{ij}(X_i, X_j)$) is particularly important in our context.

GAMs are generally fitted using penalized likelihood maximization. For this purpose, the likelihood is modified by the addition of a penalty for each smooth function, penalizing its "wiggliness". Namely, the penalized loglikelihood is defined as :

$$PL = L + \sum_{j=1}^{p} \lambda_j \int \left(\frac{\partial^2 s_j}{\partial x_j^2} \right)^2 dx_j \qquad (3)$$

where L is the loglikelihood function, p is the total number of smooth terms and λ_j are "tuning" constants which compromise between goodness of fit and smoothness.

Estimation of these "tuning" constants is generally achieved using the GCV score minimization. The GCV score is defined as :

$$S_{GCV} = \frac{nd}{(n - DoF)^2} \qquad (4)$$

where n is the number of data, d is the deviance and DoF is the effective degrees of freedom, i.e. the trace of the so-called "hat" matrix. Extension to (E)QL models is straightforward by substituting the likelihood function L and the deviance d for their (extended) quasi counterparts.

We have seen that GAMs extend in a natural way GLMs. Therefore, it would be interesting to extend the joint GLM model to a joint GAM one. Such ideas have been proposed in Rigby & Stasinopoulos [23] where both the mean and variance were modeled using semi-parametric additive models (Hastie & Tibshirani [5]). This model is restricted to observations following a Gaussian distribution and is called Mean and Dispersion Additive Model (MADAM). As our model is based on GAMs and by analogy with the denomination "joint GLM", we call it "joint GAM" in the following. Rigby & Stasinopoulos [23] proposed an algorithm to fit the MADAM model. This fitting procedure is exactly the same than the one for the two interlinked GLMs, apart from the stopping rule. Indeed, the two interlinked GLMs (resp. GAMs) model is fitted when the EQL (resp. PEQL) remains stable within the iterative procedure.

3.4   GLOBAL SENSITIVITY ANALYSIS

3.4.1   Deterministic models

The global SA methods are applicable to deterministic computer codes, codes for which the same set of input parameters always leads to the same response value. This is considered by the following model :

$$f : \mathbb{R}^p \to \mathbb{R}$$
$$\mathbf{X} \mapsto Y = f(\mathbf{X}) \qquad (5)$$

where Y is the output, $\mathbf{X} = (X_1, \ldots, X_p)$ are p independent inputs, and f is the model function, which is analytically not known. In this section, let us recall some basic ideas on Sobol sensitivity indices applied on this model.

Among quantitative methods, variance-based methods are the most often used (Saltelli et al. [26]). The main idea of these methods is to evaluate how the variance of an input or a group of inputs contributes into the variance of output. We start from the following variance decomposition :

$$\text{Var}\,[Y] = \text{Var}\,[\mathbb{E}\,(Y|X_i)] + \mathbb{E}\,[\text{Var}\,(Y|X_i)] \,, \tag{6}$$

which is known as the total variance theorem. The first term of this equality, named variance of the conditional expectation, is a natural indicator of the importance of X_i into the variance of Y : the greater the importance of X_i, the greater is $\text{Var}[\mathbb{E}(Y|X_i)]$. Most often, this term is divided by $\text{Var}[Y]$ to obtain a sensitivity index in $[0, 1]$.

To express the sensitivity indices, we use the unique decomposition of any integrable function on $[0, 1]^p$ into a sum of elementary functions (see for example Sobol [28]) :

$$f(X_1, \cdots, X_p) = f_0 + \sum_i^p f_i(X_i) + \sum_{i<j}^p f_{ij}(X_i, X_j) + \ldots + f_{12..p}(X_1, \cdots, X_p) \,, \tag{7}$$

where f_0 is a constant and the other functions verify the following conditions :

$$\int_0^1 f_{i_1, \ldots, i_s}(x_{i_1}, \ldots, x_{i_s})\,dx_{i_k} = 0 \ \forall k = 1, \ldots, s \,, \ \forall \{i_1, \ldots, i_s\} \subseteq \{1, \ldots, p\} \,. \tag{8}$$

Therefore, if the X_is are mutually independent, the following decomposition of the model output variance is possible (Sobol [28]) :

$$\text{Var}\,[Y] = \sum_i^p V_i(Y) + \sum_{i<j}^p V_{ij}(Y) + \sum_{i<j<k}^p V_{ijk}(Y) + \ldots + V_{12..p}(Y) \,, \tag{9}$$

where $V_i(Y) = \text{Var}[\mathbb{E}(Y|X_i)]$, $V_{ij}(Y) = \text{Var}[\mathbb{E}(Y|X_iX_j)] - V_i(Y) - V_j(Y), \ldots$ One can thus defines the sensitivity indices by :

$$S_i = \frac{\text{Var}\,[\mathbb{E}\,(Y|X_i)]}{\text{Var}(Y)} = \frac{V_i(Y)}{\text{Var}(Y)}, \quad S_{ij} = \frac{V_{ij}(Y)}{\text{Var}(Y)}, \quad S_{ijk} = \frac{V_{ijk}(Y)}{\text{Var}(Y)}, \quad \ldots \tag{10}$$

These coefficients are called the Sobol indices, and can be used for any complex model functions f. The second order index S_{ij} expresses sensitivity of the model to the interaction between the variables X_i and X_j (without the first order effects of X_i and X_j), and so on for higher orders effects. The interpretation of these indices is natural as their sum is equal to one (thanks to equation (9)) : the larger and close to one an index value, the greater is the importance of the variable or the group of variables linked to this index.

For a model with p inputs, the number of Sobol indices is $2^p - 1$; leading to an intractable number of indices as p increases. Thus, to express the overall sensitivity of the output to an input X_i, Homma & Saltelli [7] introduce the total sensitivity index :

$$S_{T_i} = S_i + \sum_{j \neq i} S_{ij} + \sum_{j \neq i, k \neq i, j < k} S_{ijk} + \ldots = \sum_{l \in \#i} S_l \,, \tag{11}$$

where $\#i$ represents all the "non-ordered" subsets of indices containing index i. Thus, $\sum_{l \in \#i} S_l$ is the sum of all the sensitivity indices containing i in their index. For example, for a model with three input parameters, $S_{T_1} = S_1 + S_{12} + S_{13} + S_{123}$.

The estimation of these indices can be done by Monte-Carlo simulations (Sobol [28], Saltelli [25]) or by FAST method (Saltelli et al. [27]). Recent algorithms have also been introduced to reduce the number of required model evaluations significantly. As explained in the introduction, an alternative method consists in replacing complex computer models by metamodels which have negligible calculation time. Estimation of Sobol indices by Monte-Carlo techniques with their confidence intervals (requiring thousand of simulations) can then be done using these response surfaces. In practice, when the model has a great number of input parameters, only the first order and total Sobol indices are estimated.

3.4.2 Stochastic models

In this work, models containing some intrinsic alea, which is described as an uncontrollable random input parameter ε, are called "stochastic computer models". Similarly from equation (5), consider the following (stochastic) model :

$$g : \mathbb{R}^p \rightarrow \mathbb{R}$$
$$\mathbf{X} \mapsto Y = f(\mathbf{X}) + \nu(\varepsilon, \mathbf{X} : \varepsilon) \tag{12}$$

where $\mathbf{X}$ are the p controllable input parameters (independent random variables), Y is the output, f is the deterministic part of the model function and ν is the stochastic part of the model function. ν is considered to be centered : $\mathbb{E}(\nu) = 0$. The notation $\nu(\varepsilon, \mathbf{X} : \varepsilon)$ means that ν depends only on ε and on the interactions between ε and $\mathbf{X}$. The additive form of equation (12) is deduced directly from the decomposition of the function g into a sum of elementary functions depending on $(\mathbf{X}, \varepsilon)$ (like the decomposition in Eq. (7)).

For a stochastic model (12), the joint model introduced in section 3.3 enables us to recover two GLMs or two GAMs :

$$Y_m = \mathbb{E}(Y|\mathbf{X}) = \mu \tag{13}$$

by the mean component (Eq. (1)), and

$$Y_d = \text{Var}(Y|\mathbf{X}) = \phi v(\mu) \tag{14}$$

by the dispersion component (Eq. (2)). If there is no uncontrollable parameter ε, it leads to a deterministic model case with $Y_d = \text{Var}(Y|\mathbf{X}) = 0$. By using the total variance theorem (Eq. (6)), the variance of the output variable Y can be decomposed by :

$$\text{Var}[Y(\mathbf{X}, \varepsilon)] = \text{Var}[\mathbb{E}(Y|\mathbf{X})] + \mathbb{E}[\text{Var}(Y|\mathbf{X})] = \text{Var}(Y_m) + \mathbb{E}(Y_d) \ . \tag{15}$$

According to model (12), Y_m is the deterministic model part, and Y_d is the variance of the stochastic model part :

$$Y_m = f(\mathbf{X}) \ ,$$
$$Y_d = \text{Var}[\nu(\varepsilon, \mathbf{X} : \varepsilon)|\mathbf{X}] \tag{16}$$

The variances of Y and Y_m are now decomposed according to the contributions of their input parameters $\mathbf{X}$. For Y, the same decomposition than for deterministic models holds (Eq. (9)). However, it includes the additional term $\mathbb{E}(Y_d)$ (the mean of the dispersion component) deduced from equation (15). Consequently,

$$\text{Var}(Y) = \sum_i^p V_i(Y) + \sum_{i<j}^p V_{ij}(Y) + \sum_{i<j<k}^p V_{ijk}(Y) + \ldots + V_{12..p}(Y) + \mathbb{E}(Y_d) \ . \tag{17}$$

For the mean component Y_m, we have

$$\text{Var}(Y_m) = \sum_i^p V_i(Y_m) + \sum_{i<j}^p V_{ij}(Y_m) + \sum_{i<j<k}^p V_{ijk}(Y_m) + \ldots + V_{12..p}(Y_m) \ . \tag{18}$$

By noticing that

$$V_i(Y_m) = \text{Var}[\mathbb{E}(Y_m|X_i)] = \text{Var}\{\mathbb{E}[\mathbb{E}(Y|\mathbf{X})|X_i]\} = \text{Var}[\mathbb{E}(Y|X_i)] = V_i(Y) \ , \tag{19}$$

and from equation (10), the sensitivity indices for the variable $Y(\mathbf{X}, \varepsilon)$ according to the controllable parameters $\mathbf{X} = (X_i)_{i=1...p}$ can be computed using :

$$S_i = \frac{V_i(Y_m)}{\text{Var}(Y)}, \quad S_{ij} = \frac{V_{ij}(Y_m)}{\text{Var}(Y)}, \quad \ldots \tag{20}$$

These Sobol indices can be computed by classical Monte-Carlo techniques, the same ones used in the deterministic model case. These algorithms are applied on the metamodel defined by the mean component Y_m of the joint GLM or the joint GAM.

Thus, all terms contained in $\mathrm{Var}(Y_m)$ of the equation (15) have been considered. It remains to estimate $\mathbb{E}(Y_d)$ by a simple numerical integration of Y_d following the law of $\mathbf{X}$. Y_d is evaluated with a metamodel, for example the dispersion component of the joint GLM or joint GAM. $\mathbb{E}(Y_d)$ includes all the decomposition terms of $\mathrm{Var}(Y)$ (according to $\mathbf{X}$ and ε) not taken into account in $\mathrm{Var}(Y_m)$ i.e. all terms involving ε. Therefore, the total sensitivity index of ε is

$$S_{T_\varepsilon} = \frac{\mathbb{E}(Y_d)}{\mathrm{Var}(Y)} \ . \tag{21}$$

As Y_d is a positive random variable, positivity of S_{T_ε} is guaranteed. In practice, $\mathrm{Var}(Y)$ can be estimated from the data or from simulations of the fitted joint model :

$$\mathrm{Var}(Y) = \mathrm{Var}(Y_m) + \mathbb{E}(Y_d) \ . \tag{22}$$

If $\mathrm{Var}(Y)$ is computed from the data, it seems preferable to estimate $\mathbb{E}(Y_d)$ with $\mathrm{Var}(Y) - \mathrm{Var}(Y_m)$ to satisfy equation (15). In our applications, the total variance will be estimated using the fitted joint model (Eq. (22)).

Finally, let us note that it is not possible to quantitatively distinguish the various contributions in S_{T_ε} (S_ε, $S_{i\varepsilon}$, $S_{ij\varepsilon}$, ...). However, the analysis of the terms in the regression model Y_d and their t-values give qualitative contributions. For example, if an input parameter X_i is not present in Y_d, we can deduce the following correct information : $S_{i\varepsilon} = 0$. Moreover, if the t-values analysis and the deviance analysis show that an input parameter X_i has a smaller influence than another input parameter X_j , we can suppose that the interaction between X_i and ε is less influential than the interaction between X_j and ε. Therefore, giving this kind of information is an improvement compared to the Tarantola's method (Tarantola et al. [29], see introduction).

In conclusion, this new approach, based on joint models to compute Sobol sensitivity indices, is useful if the following conditions hold :
 − if the computer model contains some uncontrollable parameters (the model is no more deterministic but stochastic) ;
 − if a metamodel is needed due to large CPU times of the computer model ;
 − if some of the uncontrollable parameters interact with some controllable input ones ;
 − if some information about the influence of the interactions between the uncontrollable parameters and the other input parameters is of interest.

3.5   APPLICATIONS

3.5.1   An analytic test case : the Ishigami function

The proposed method is first illustrated on an artificial analytical model with 3 input variables, called the Ishigami function (Homma & Saltelli [7], Saltelli et al. [26]) :

$$Y = f(X_1, X_2, X_3) = \sin(X_1) + 7\sin(X_2)^2 + 0.1X_3^4 \sin(X_1) \ , \tag{23}$$

where $X_i \sim \mathcal{U}[-\pi; \pi]$ for $i = 1, 2, 3$. For this function, all the Sobol sensitivity indices (S_1, S_2, S_3, S_{12}, S_{13}, S_{23}, S_{123}, S_{T_1}, S_{T_2}, S_{T_3}) are known. This function is used in most intercomparison studies of global sensitivity analysis algorithms. In our study, the classical problem is altered by considering X_1 and X_2 as the controllable input random variables, and X_3 as an uncontrollable input random variable. It means that the X_3 random values are not used in the modeling procedure ; this parameter is considered to be inaccessible. However, sensitivity indices have the same theoretical values as in the standard case.

For the model fitting, 1000 samples of (X_1, X_2, X_3) were simulated leading to 1000 observations for Y. The GLM and GAM (with their relative joint extensions) are compared to the Gaussian process

(Gp) model including or not the additive error component (the nugget effect). The fitting methodology is the one proposed by Marrel et al. [15] (based on the Welch et al. [33] sequential algorithm) which contains a linear regression component and a Gp defined by a generalized exponential covariance. To compare the predictivity of different metamodels, we use the predictivity coefficient Q_2, which is the determination coefficient R^2 computed from a test sample (composed here by 10000 randomly chosen points). For the joint model, Q_2 is computed on the mean component.

Simple GLM

First, a fourth order polynomial for the GLM is considered. Only the explanatory terms are selected in our regression model using analysis of deviance and the Fisher statistics. The Student test on the regression coefficients and residuals graphical analysis make it possible to judge the model quality. For a simple GLM fitting, one obtains

$$Y = 1.92 + 2.69X_1 + 2.17X_2^2 - 0.29X_1^3 - 0.29X_2^4 . \tag{24}$$

The explained deviance of this model is $D_{\text{expl}} = 61.3\%$. The predictivity coefficient is of the same order : $Q_2 = 60.8\%$. We see that it remains 39% of non explained deviance due to the model inadequacy and/or to the uncontrollable parameter.

Joint GLM

One tries to model the data by a joint GLM. The mean component gives the same model (24) as the simple GLM. For the dispersion component, using analysis of deviance techniques, no significant explanatory variable was found. Thus, the dispersion component is supposed to be constant; and the joint GLM is equivalent to the simple GLM approach - but with a different fitting process. In addition, as one obtains the same explained deviance value as the simple GLM one, it corroborates the joint GLM approach relevance - even for a homoscedastic parameterization.

Simple GAM

We will be now studying the non parametric modeling. A simple GAM gives the following result :

$$Y = 3.76 - 2.67X_1 + s(X_1) + s(X_2) , \tag{25}$$

where $s(\cdot)$ is a spline term and where we have kept some parametric terms by applying a term selection procedure. The explained deviance of this model is $D_{\text{expl}} = 76.8\%$: the simple GAM approach clearly outperforms the simple GLM one. Even if this is obviously related to an increasing number of parameters, it is also explained by the fact that GAMs are more adjustable than GLMs : the number of parameters remains very small compared to the data size (1000). This is confirmed by the value of the predictivity coefficient $Q_2 = 75.1\%$ which is very close to the explained deviance (76.8%).

Gp model

Let's now compare this GAM with the popular Gp metamodel. Without introducing any nugget effect, the obtained Gp gives $Q_2 = 72.8\%$. By introducing of the nugget effect (additional error with constant variance), the obtained Gp gives $Q_2 = 74.3\%$. Consequently, the Gp model including a nugget effect is similar to the simple GAM one. The variance of the nugget effect is estimated to 10% of the total variance, when one expects to obtain the residual variance : $1 - Q_2 = 25.7\%$. We will be discussing in the following section the consequence of this wrong estimation.

Joint GAM

One models now the data by a joint GAM. The resulting model is described by the following features :

$$Y_m = 3.75 - 3.06X_1 + s(X_1) + s(X_2) ,$$
$$Y_d = 0.59 + s(X_1) . \tag{26}$$

The explained deviances are $D_{\text{expl}} = 92.8\%$ for the mean component and $D_{\text{expl}} = 36.7\%$ for the dispersion component. The predictivity coefficient of the mean component is $Q_2 = 75.5\%$, which is slightly better than the simple GAM and Gp results.

Discussion

The explained deviance given by the joint GAM mean component is clearly larger than the one given

by the simple GAM approach. This last point demonstrates the efficiency of the joint modeling of the mean and dispersion approach when heteroscedasticity is involved. Indeed, the joint procedure leads to suited prior weights for the mean component. The joint GAM improves both the joint GLM, simple GAM and Gp approaches :

(a) due to the GAMs flexibility, the explanatory variable X_1 is identified to model the dispersion component (the interaction between X_1 and the uncontrollable parameter X_3 is therefore retrieved) ;

(b) the joint GAM explained deviance (93%) for the mean component is clearly larger than the simple GAM and joint GLM ones (Joint GLM : 61%, simple GAM : 77%).

Figure 3.1 shows the observed response against the predicted values for the three models Joint GLM, Simple GAM and Joint GAM. In the following graphical analyses, we restrict our attention to these three models, and not to the Gp model. Indeed, comparisons are not possible with the Gp model because it interpolates the observed responses and the observed residuals are worth zero. Even if the nugget effect introduction allows to obtain non zero residuals, it is not appropriate to perform a statistical analysis of these residuals and a comparison with another model residuals.

On one hand, the advantage of the GAM approaches is visible in the Figure 3.1 as the dispersion around the $y = x$ line is clearly reduced. On the other hand, Figure 3.2 shows that the deviance residuals for the mean component of the joint GAM seem to be more homogeneously dispersed around the x-axis ; leading to a better prediction on the whole range of the observations. Thus, the joint GAM approach is the most competitive model.
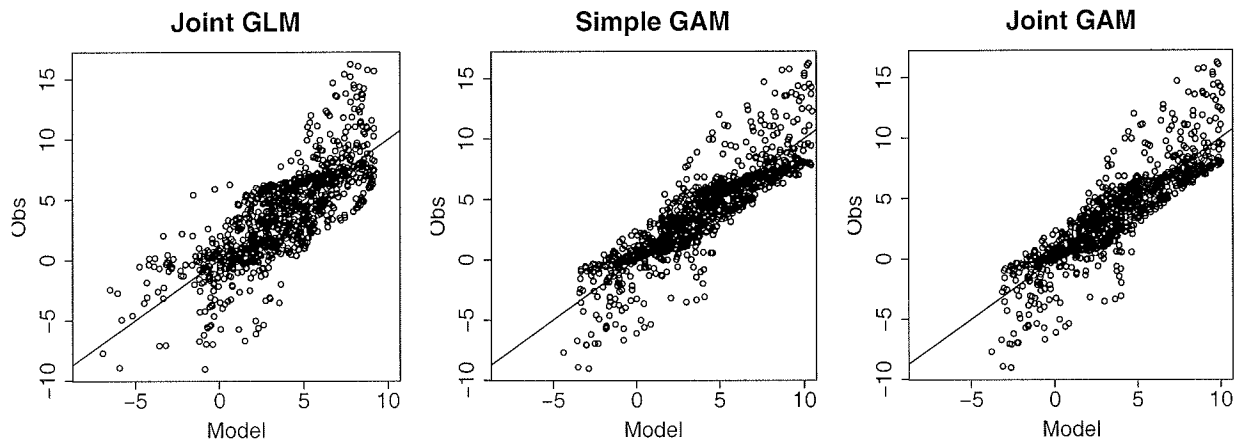
Fig. 3.1 – **Observed response variable versus the predicted values for the three models : Joint GLM, Simple GAM, Joint GAM (Ishigami application).**
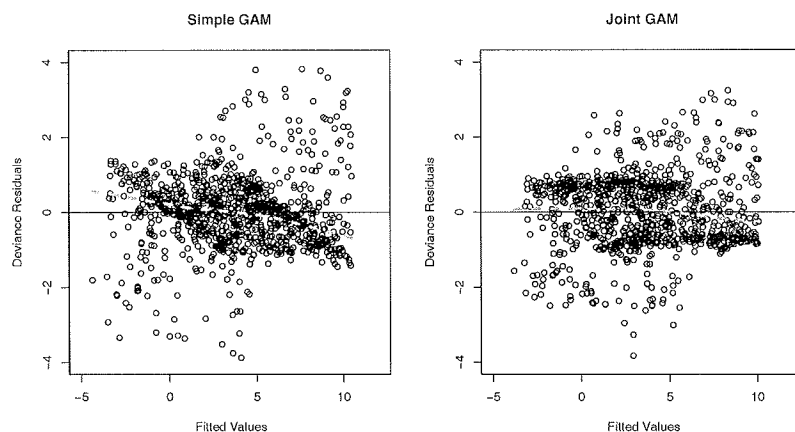

Fig. 3.2 – **Deviance residuals for the Simple and Joint GAMs versus the fitted values (Ishigami application). Dashed lines correspond to local polynomial smoothers.**

Figure 3.3 shows the proportion Δ of observations that lie within the $\alpha\%$ theoretical confidence

interval in function of the confidence level α. By definition, if a model is suited for both mean and dispersion modelings, the points should be located around the $y = x$ line. As a consequence, this plot is useful to quantify the goodness of fitting accuracy of the models. Figure 3.3 shows that joint GLM approach is the most accurate model. The joint GAM is less relevant but has a homogeneous dispersion around the $y = x$ line. The simple GAM approach systematically lead to overestimations. In particular, it means that the variance, supposed to be a constant, is overestimated and that the dispersion is poorly predicted.
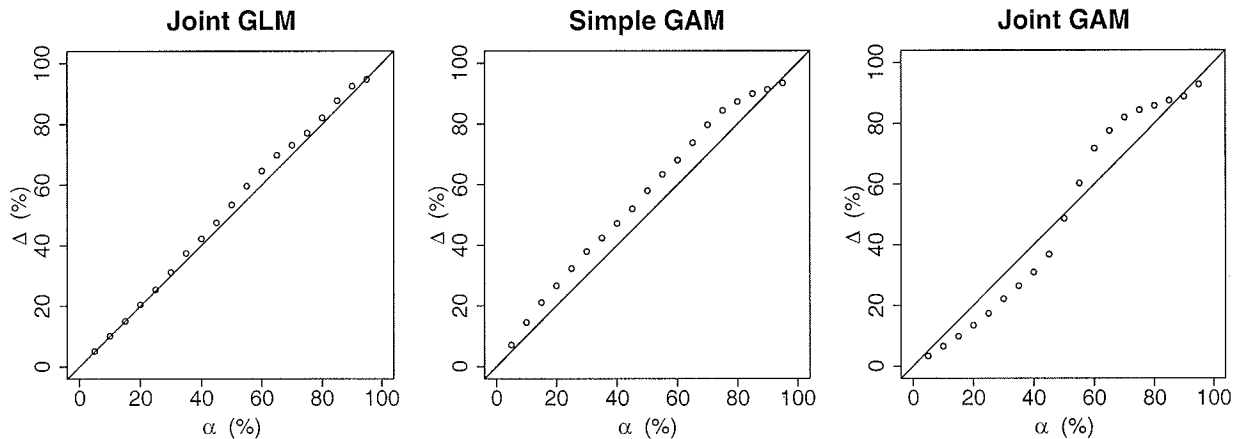

Fig. 3.3 – **Proportion Δ (in percent) of observations that lie within the α% theoretical confidence interval in function of the confidence level α (Ishigami application).**

Lastly, from Figures 3.1–3.3, the joint GAM seems to be the most competitive one. Indeed, the GAM flexibility allows to model accurately the mean component while the dispersion seems to be correctly modeled.

Sobol indices

Table 3.5.1 depicts the Sobol sensitivity indices for the joint GLM and the joint GAM using equations (20) and (21). The standard deviation estimates (sd) are obtained from 100 repetitions of the Monte-Carlo estimation procedure (which uses 10^4 model computations for one index estimation). When this Monte-Carlo procedure is used to estimate the Sobol index, we report "MC" in the "Method" column; while "Eq" indicates that the sensitivity indices have been deduced from the joint model regressive equations. Therefore, no estimation errors (sd) are associated to these indices (except for total indices S_{T_i} which can be deduced from S_i). When no quantitative deduction on the sensitivity index can be made with this process, the three column values are marked with the symbol "—".

The joint GLM gives only a good estimation of S_1, while S_2 and S_{T_3} are badly estimated (errors greater than 30%). S_{12} is correctly put to zero by looking directly at the joint GLM mean component formula (the same as the equation (24)). However, some conclusions drawn from the GLM dispersion component formula (which is a constant) are wrong. As no explanatory variable is involved in this formula, the deduced interaction indices are equal to zero : $S_{13} = S_{23} = S_{123} = 0$. Thus, $S_3 = S_{T_3} = 0.366$ while the correct values of S_3 and S_{T_3} are respectively zero and 0.243.

Contrary to the joint GLM, the joint GAM gives good approximations of all the Sobol indices (errors smaller than 7%), including S_{T_3}. Moreover, the deductions drawn from the model formulas (25) are correct ($S_{T_2} = S_2$, $S_{12} = S_{23} = S_{123} = 0$). The only drawback of this method is that some indices remain unknown due to the non separability of the dispersion component effects. However, it can be deduced that S_{13} is non null due to the explicative effect of X_1 in the dispersion component.

Table 3.5.1 gives also the Sobol indices computed by the same Monte-Carlo procedure using two classical metamodels as the simple GAM and the Gp models. To estimate the first order Sobol indices $S_i = V_i(Y_m)/\text{Var}(Y)$ (for $i = 1, 2$), the metamodel is used to compute $V_i(Y_m)$ and the fitted data (the 1000 observations of Y) to compute $\text{Var}(Y)$. To estimate the total sensitivity index S_{T_3} of the uncontrollable parameter, the metamodel predictivity coefficient $Q_2 = 0.751$ is used.

In fact, by supposing that the metamodels fit correctly the computer code, one deduces that all

Indices	Exact Values	Joint GLM			Joint GAM			Simple GAM			Gp		
		Values	sd	Method	Values	sd	Method	Values	sd	Method	Values	sd	Method
S_1	0.314	0.314	4e-3	MC	0.325	5e-3	MC	0.333	6e-3	MC	0.328	7e-3	MC
S_2	0.442	0.318	5e-3	MC	0.414	5e-3	MC	0.441	6e-3	MC	0.442	7e-3	MC
S_{T_3}	0.244	0.366	2e-3	MC	0.261	2e-3	MC	0.249	—	Q_2	0.257	—	Q_2
S_{12}	0	0	—	Eq	0	—	Eq	0	—	Eq	0.004	8e-3	MC
S_{13}	0.244	0	—	Eq	> 0	—	Eq	—	—	—	—	—	—
S_{23}	0	0	—	Eq	0	—	Eq	—	—	—	—	—	—
S_{123}	0	0	—	Eq	0	—	Eq	—	—	—	—	—	—
S_{T_1}	0.557	0.314	4e-3	Eq	—	—	—	—	—	—	—	—	—
S_{T_2}	0.443	0.318	5e-3	Eq	0.414	5e-3	Eq	—	—	—	—	—	—
S_3	0	0.366	2e-3	Eq	—	—	—	—	—	—	—	—	—

TAB. 3.1 – **Sobol sensitivity indices (with standard deviations) for the Ishigami function : exact and estimated values from joint GLM, joint GAM, simple GAM and Gp model. "Method" indicates the estimation method : MC for the Monte-Carlo procedure, Eq for a deduction from the model equations and Q_2 for the deduction of the predictivity coefficient Q_2. "—" indicates that the value is not available.**

the unexplained part of these metamodels is due to the uncontrollable parameter : $S_{T_3} = 1 - Q_2$. This is a strong hypothesis, which is verified here due to the simplicity of the analytical function. However, it will not be satisfied for all application cases. Moreover in practical and complex situations, the Q_2 estimation (usually done by a cross-validation method) can be difficult and subject to caution. For the Ishigami function, S_1, S_2, S_{T_3} are correctly estimated. S_{12} can be deduced from the formula (25) for the simple GAM and estimated by Monte-Carlo method for the Gp model. However, any other sensitivity indices can be proposed as no dispersion modeling is involved.

Remark : By using the Gp model including a nugget effect, one can think that estimating the nugget effect would give an estimation of the total sensitivity index. In this example, the variance of the nugget effect has been estimated to 10% of the total variance, which is far from the exact value (24%). Other tests (not presented here) have shown that it is difficult to have an optimization algorithm which gives an efficient and robust estimation of the nugget effect.

In conclusion, this example shows that the joint models, and specially the joint GAM, can adjust complex heteroscedastic situations for which classical metamodels are inadequate. Moreover, the joint models offer a theoretical basis to compute efficiently global sensitivity indices of stochastic models.

3.5.2   Application to an hydrogeologic transport code

This methodology is now applied to a complex industrial model of radioactive pollutants transport in saturated porous media using the MARTHE computer code (developed by BRGM, France). In the context of an environmental impact study, MARTHE has been applied to a model of strontium 90 (^{90}Sr) transport in saturated media for a radwaste temporary storage in Russia (Volkova et al. [31]). Only a partial characterization of the site has been made and, consequently, values of the model input parameters are not known precisely : 20 scalar input parameters have been considered as random variables, each of them associated to a specified probability density function. The model output variables of interest concern the ^{90}Sr concentration values in different spatial locations. One of the main goals of this study is to identify the most influential parameters of the computer code in order to improve the characterization of the site in a judicious way. Because of large computing times of the MARTHE code, the Sobol sensitivity indices are computed using metamodels (boosting regression trees model for Volkova et al. [31] and Gaussian process model for Marrel et al. [15]).

As a perspective of their work, Volkova et al. [31] propose to study more precisely the influence of the spatial form of an hydrogeologic layer. It consists in performing a geostatistical simulation of this layer (which is a two-dimensional spatial random field), before each calculation of the computer model. This geostatistical simulation is rather complex and the resulting spatial field cannot be summarized by a few scalar values. Therefore, as explained in our introduction, this hydrogeologic layer form has to be considered as an uncontrollable parameter of the computer model. Additionally to the uncontrollable parameter, 16 scalar input parameters remain uncertain and are treated as random variables. It concerns the permeability of different geological layers, the longitudinal and transversal dispersivity coefficients, the sorption coefficients, the porosity and meteoric water infiltration intensities.

The Latin Hypercube Sampling method is used to obtained a sample of 298 random vectors (each of dimension 16). In addition, 298 independent realizations of the spatial random field (noticed by ε) are obtained by a specific geostatistical simulation algorithm. This leads to obtain 298 observations (after 8 days of calculations) of the output variable of the MARTHE model (^{90}Sr concentration at the domain center). For the GLMs and GAMs construction phase, the large data dispersion suggests the use of logarithmic link functions for g and h (see Eqs (1) and (2)). Due to the large number of inputs, a manual term selection process has been applied. No interaction term has been found to be explicative in the GLMs. However, a bi-dimensional spline term has been added in the GAMs because of convincing deviance contribution and negligible p-value. One synthesizes the results by giving the explained deviance and the explanatory terms involved in the formulas :

- Simple GLM : $D_{\text{expl}} = 60\%$ with the terms $kd1$, $kd2$, $per1$, $per2$.
- Joint GLM : D_{expl}(mean) $= 66.4\%$, with the same terms than the simple GLM, D_{expl}(dispersion) $=$ 8.7% with the terms $kd1$ and $per3$.
- Simple GAM : $D_{\text{expl}} = 81.8\%$ with $s(kd1)$, $s(kd2)$, $s(per3)$, $s(per2, kd2)$.
- Joint GAM : D_{expl}(mean) $= 98.1\%$ with the same terms than the simple GAM, D_{expl}(dispersion) $=$ 29.7% with $kd1$, $kd2$.
- Gp model : the regression and covariance parts include the terms $kd1$, $kd2$, $per1$, $per2$, $per3$. The nugget effect is estimated to 21.1% of the total variance, which shows that the Gp model explains 79.9% of the total variance.

$kd1$, $kd2$ and $per1$, $per2$, $per3$ are respectively the sorption coefficients and the permeabilities of the different hydrogeologic layers. One observes that the GAM models outperform the GLM ones. The predictivity coefficient (computed by the leave-one-out method) of the simple GAM gives $Q_2 = 76.4\%$, while for the simple GLM $Q_2 = 58.8\%$. The Gp model is slightly more efficient than the simple GAM ($Q_2 = 80.4\%$). This small improvement may be due to a larger flexibility of Gps and to the specific fitting procedure (Marrel et al. [15]), which is suited to large dimensional problems (16 input parameters here).

Figure 3.4 shows the deviance residuals against the fitted values for the joint GLM, simple GAM and joint GAM models. As for the Ishigami application, Gp model residuals cannot be compared to these three models residuals. For the joint GLM approach, some outliers are not visible to keep the figure readable. As a consequence, the GAMs clearly lead to smaller residuals. Moreover, the joint GAM outperforms the simple GAM due to the right explanation of the dispersion component. It can be seen that the joint GAM allows to suppress the bias involved by the heteroscedasticity, while simple GAM residuals are affected by this bias. Figure 3.5 shows the observed values against the predicted ones. This figure confirms the conclusions drawn from the Figure 3.4. Indeed, the GAM's flexibility allows to suppress the bias for the smallest data values.

Figure 3.6 shows the proportion Δ of observations that lie within the $\alpha\%$ theoretical confidence interval against the confidence interval α. It can be seen that the joint GAM is clearly the most accurate model. Indeed, all its points are close to the theoretical $y = x$ line, while the joint GLM (resp. simple GAM) systematically leads to underestimations (resp. overestimations). Consequently, from the Figures 3.4–3.6, one deduces that the joint GAM model is the most competitive one. On one hand, the mean component is modeled accurately without any bias. On the other hand, the dispersion component is competitively modeled leading to reliable confidence intervals.

Joint GLM   **Simple GAM**   **Joint GAM**
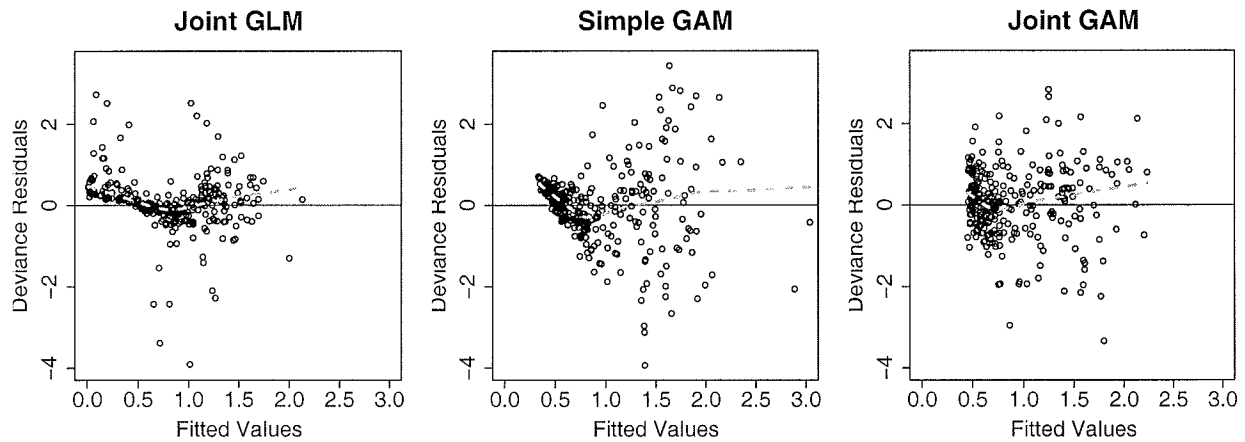
Fig. 3.4 – **Deviance residuals (mean component) for the Simple GAM, Joint GAM and Joint GLM versus the fitted values (MARTHE application). Dashed lines correspond to local polynomial smoothers.**

Joint GLM   **Simple GAM**   **Joint GAM**
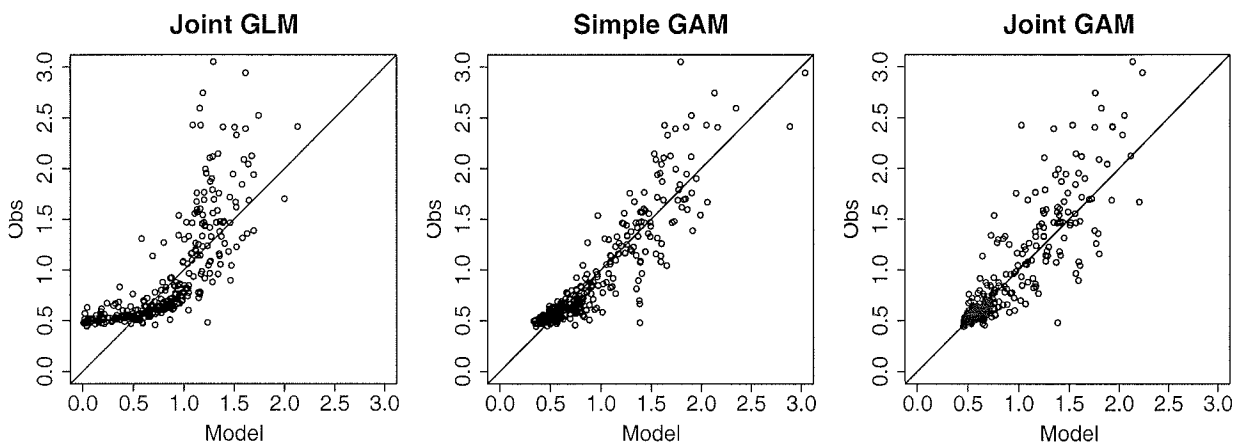
Fig. 3.5 – **Observed response variable versus the predicted values for the three models : Joint GLM, Simple GAM, Joint GAM (MARTHE application)**

Table 3.5.2 gives the main Sobol sensitivity indices for the joint GLM, joint GAM, simple GAM and Gp models (using 10^4 model computations for one index estimation). The Sobol indices of the interactions between controllable parameters are not given (except between $kd2$ and $per2$) because these interactions are not included in the formulas of the two joint models. Therefore, their Sobol indices are zero. The two joint models give similar results for all first order sensitivity indices. The sorption coefficient of the second layer $kd2$ explained more than 52% of the output variance, while the permeability of the second layer $per2$ explained more than 5%. Some large differences arise in the total influence of the uncontrollable parameter ε : 38.2% for the joint GLM and 27.7% for the joint GAM. Moreover, the joint GLM shows an influence of the interaction between $per3$ and ε, while the joint GAM shows an influence of the interaction between $kd2$ and ε. In this application, we consider the joint GAM results more reliable than the joint GLM ones because the joint GAM captures more efficiently the mean and dispersion components of the data than the joint GLM.

By comparing the joint GAM results with the simple GAM and Gp model results, some significant differences can be printed out :

- The $kd1$ first order sensitivity index is overestimated using the simple GAM and Gp model (14.0% and 12.6% instead of 3.7% for the joint GAM). Indeed, the deviance analysis of the joint GAM dispersion component shows a high contribution of $kd1$, which means that the interaction between $kd1$ and the uncontrollable parameter is probably large. For a standard metamodel, like the simple GAM and Gp models, this interaction is not found out and leads to a wrong

Joint GLM   **Simple GAM**   **Joint GAM**
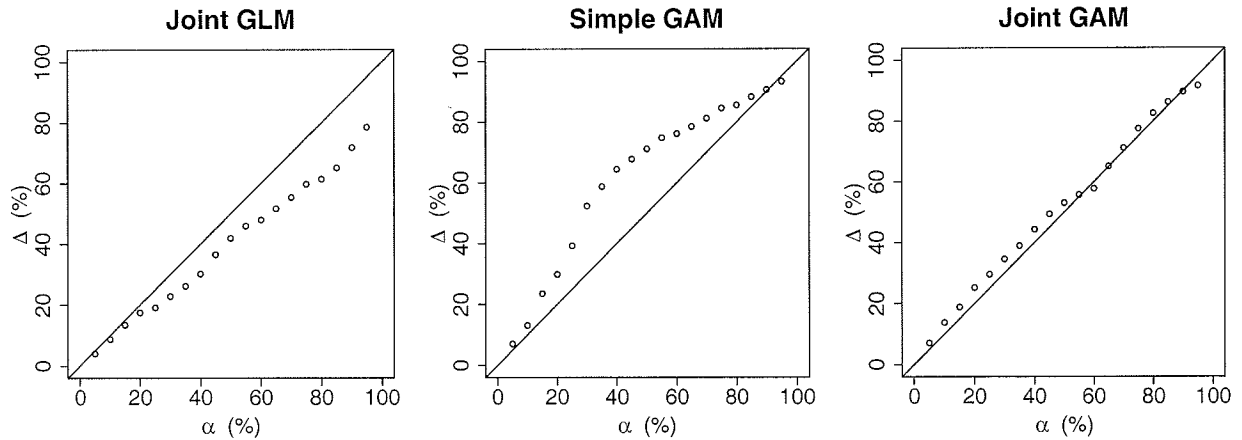
Fig. 3.6 – **Proportion Δ (in percent) of observation that lie within the α% theoretical confidence interval in function of the confidence level α. MARTHE application.**

estimation of the first order sensitivity index of $kd1$.

- For the simple metamodels, using the relation $S_T(\varepsilon) = 1 - Q_2$, the total sensitivity index of the uncontrollable parameter is underestimated : 23.5% (simple GAM) and 19.6% (Gp model) instead of 27.7% (joint GAM). The classical metamodels tend to explain some parts of the data which can be adequately included in the dispersion component of the joint GAM during the iterative fitting algorithm.
- Contrary to the other metamodels, the joint GAM allows to prove that only $kd1$ and $kd2$ interact with the uncontrollable parameter.

As a conclusion, these sensitivity analysis results will be very useful to the physicist or the modeling engineer during the model construction and calibration steps. In this specific application, the sensitivity analysis shows that the geometry of the second hydrogeological layer has a strong influence (up to 28%) on the predicted ^{90}Sr concentration. Therefore, an accurate modeling of this geometry, coupled with a better knowledge of the most influential parameter $kd2$, are the key steps to an important reduction of the model prediction uncertainties.

3.6   CONCLUSION

This chapter proposes a solution to resolve the problem of uncertainty and sensitivity analyses on stochastic computer models (Kleijnen [12]). A natural solution is to model the mean and the dispersion of the code outputs by two explanatory models. The classical way is to separately build these models. In this chapter, the use of the joint modeling is preferred. This theory, proposed by Pregibon [20] and extensively developed by Nelder [17], is a powerful tool to fit the mean and dispersion components simultaneously. Zabalza et al. [35] already applied this approach to model stochastic computer code. However, the behavior of some numerical models can be highly complex and non linear. In the present chapter, some examples show the limit of this parametric joint model. Being inspired by Rigby & Stasinopoulos [23] who use non parametric joint additive models (restricted to Gaussian cases), we propose to use more general models using GAMs. Like GLMs, GAMs are a suited framework because it allows variable and model selections via quasi-likelihood function, classical statistical tests on coefficients and graphical displays.

An analytic case on the Ishigami function shows that the joint GAM is adapted to complex heteroscedastic situations where classical response surfaces are inadequate. Moreover, it offers a theoretical basis to compute Sobol sensitivity indices in an efficient way. The performance of the Joint GAM approach was assessed on an industrial application. Compared to other methods, the modeling of the dispersion component allows to obtain a robust estimation of the total sensitivity index of the uncontrollable parameter, which leads to correct estimations of the first order indices of the controllable parameters. In addition, it reveals the influential interactions between the uncontrollable parameter

Indices	Joint GLM			Joint GAM			Simple GAM			Gp		
	Values	sd	Method	Values	sd	Method	Values	sd	Method	Values	sd	M
$S(\mathrm{kd1})$	0.002	0.6e-2	MC	0.037	1.0e-2	MC	0.140	1.0e-2	MC	0.126	1.3e-2	]
$S(\mathrm{kd2})$	0.522	0.6e-2	MC	0.524	1.0e-2	MC	0.550	1.1e-2	MC	0.603	0.9e-2	]
$S(\mathrm{per1})$	0.018	0.7e-2	MC	0	—	Eq	0	—	Eq	0.012	1.1e-2	]
$S(\mathrm{per2})$	0.052	0.6e-2	MC	0.078	1.0e-2	MC	0.044	1.0e-2	MC	0.048	1.2e-2	]
$S(\mathrm{per3})$	0	—	Eq	0.005	1.0e-2	MC	0.008	1.0e-2	MC	0.003	1.1e-2	]
$S(\mathrm{kd2,per2})$	0	—	Eq	0.063	1.0e-2	MC	0.026	1.0e-2	MC	0.021	1.4e-2	]
$S_T(\varepsilon)$	0.382	0.2e-2	MC	0.277	0.3e-2	MC	0.235	—	Q_2	0.196	—	
$S(\mathrm{kd1},\varepsilon)$	> 0	—	Eq	> 0	—	Eq	—	—	—	—	—	
$S(\mathrm{kd2},\varepsilon)$	0	—	Eq	> 0	—	Eq	—	—	—	—	—	
$S(\mathrm{per1},\varepsilon)$	0	—	Eq	0	—	Eq	—	—	—	—	—	
$S(\mathrm{per2},\varepsilon)$	0	—	Eq	0	—	Eq	—	—	—	—	—	
$S(\mathrm{per3},\varepsilon)$	> 0	—	Eq	0	—	Eq	—	—	—	—	—	

TAB. 3.2 – **Estimated Sobol sensitivity indices (with standard deviations obtained by** 100 **repetitions) for the MARTHE code. "Method" indicates the estimation method : MC for the Monte-Carlo procedure, Eq for a deduction from the model equations and** Q_2 **for the deduction of the predictivity coefficient** Q_2. **"—" indicates that the value is not available.**

and the other input parameters.

The joint GAM has proven its flexibility to fit complex data : we have obtained the same performance for its mean component as the powerful Gaussian process model. Moreover, the analytical formulas available with the joint GAM are very useful to complete the sensitivity analysis results and to improve our model understanding and knowledge. Finally, the joint GAM can also serve in propagation uncertainty and reliability studies of complex models, with unquantifiable random input variables, to obtain some mean predictions with their confidence intervals.

For some applications, joint GAM could be inadequate, and other models can be proposed. For example, for Gaussian observations, Juutilainen & Röning [11] have used a neural network model for mean and dispersion. It is shown to be more efficient than joint GLM and joint additive models in a context of numerous explanatory variables (25) and of a large amount of data (100000). Moreover, in the joint GAM as in the joint GLM, only diagnosis tools to analyze separately the two components of the joint model are available. It would be very convenient in the future to have accurate tools to analyse the two components simultaneously.

In the whole, all statistical analysis were performed using the R software environment [21]. In particular, the following functions and packages were useful : the "glm" function to fit a simple GLM, the "mgcv" (Multiple Smoothing Parameter Estimation by GCV) package to fit a simple GAM, and the "sensitivity" package to compute Sobol indices. We also developed the "JointModeling" package to fit joint models (including joint GLM and joint GAM).

3.7   ACKNOWLEGMENTS

3.8   REFERENCES

[1] D. Bursztyn and D.M. Steinberg. Screening experiments for dispersion effects. In A. Dean and S. Lewis, editors, *Screening - Methods for experimentation in industry, drug discovery and genetics*. Springer, 2006.

[2] V.C.P. Chen, K-L. Tsui, R.R. Barton, and M. Meckesheimer. A review on design, modeling and applications of computer experiments. *IIE Transactions*, 38 :273–291, 2006.

[3] K-T. Fang, R. Li, and A. Sudjianto. *Design and modeling for computer experiments*. Chapman & Hall/CRC, 2006.

[4] T. Hastie and R. Tibshirani. Generalized additive models. *Statistical Science*, 1 :297–318, 1986.

[5] T. Hastie and R. Tibshirani. *Generalized additive models*. Chapman and Hall, London, 1990.

[6] J.C. Helton, J.D. Johnson, C.J. Salaberry, and C.B. Storlie. Survey of sampling-based methods for uncertainty and sensitivity analysis. *Reliability Engineering and System Safety*, 91 :1175–1209, 2006.

[7] T. Homma and A. Saltelli. Importance measures in global sensitivity analysis of non linear models. *Reliability Engineering and System Safety*, 52 :1–17, 1996.

[8] B. Iooss, C. Lhuillier, and H. Jeanneau. Numerical simulation of transit-time ultrasonic flowmeters due to flow profile and fluid turbulence. *Ultrasonics*, 40 :1009–1015, 2002.

[9] B. Iooss and M. Ribatet. Analyse de sensibilité globale de modèles numériques à paramètres incontrôlables. In *Proceedings of 38èmes Journées de Statistique*, Clamart, France, May-June 2006.

[10] B. Iooss, F. Van Dorpe, and N. Devictor. Response surfaces and sensitivity analyses for an environmental model of dose calculations. *Reliability Engineering and System Safety*, 91 :1241–1251, 2006.

[11] I. Juutilainen and J. Röning. A comparaison of methods for joint modelling of mean and dispersion. In *Proceedings of the 11th Symposium on ASMDA*, Brest, France, May 2005.

[12] J. Kleijnen. Sensitivity analysis and related analyses : a review of some statistical techniques. *Journal of Statistical Computation and Simulation*, 57 :111–142, 1997.

[13] J. Kleijnen and W.C.M. van Beers. Robustness of kriging when interpolating in random simulation with heterogeneous variances : some experiments. *European Journal of Operational Research*, 165 :826–834, 2005.

[14] Y. Lee and J.A. Nelder. Robust design via generalized linear models. *Journal of Quality Technology*, 35(1) :2–12, 2003.

[15] A. Marrel, B. Iooss, F. Van Dorpe, and E. Volkova. An efficient methodology for modeling complex computer codes with Gaussian processes. *Computational Statistics and Data Analysis*, accepted, in revision, 2008. Available at URL : http ://fr.arxiv.org/abs/0802.1099v1.

[16] P. McCullagh and J.A. Nelder. *Generalized linear models*. Chapman & Hall, 1989.

[17] J.A. Nelder. A large class of models derived from generalized linear models. *Statistics in Medicine*, 17 :2747–2753, 1998.

[18] J.A. Nelder and D. Pregibon. An extended quasi-likelihood function. *Biometrika*, 74 :221–232, 1987.

[19] J.A. Nelder and R.W.M. Wedderburn. Generalized linear models. *Journal of the Royal Statistical Society A*, 135 :370–384, 1972.

[20] D. Pregibon. Review of "Generalized Linear Models" by McCullagh and Nelder. *Annals of Statistics*, 12 :1589–1596, 1984.

[21] R Development Core Team. R : A language and environment for statistical computing. 2006. ISBN 3-900051-07-0.

[22] C.E. Rasmussen and C.K.I. Williams. *Gaussian processes for machine learning.* MIT Press, 2006.

[23] R.A. Rigby and D.M. Stasinopoulos. A semi-parametric additive model for variance heterogeneity. *Statistics and Computing*, 6 :57–65, 1996.

[24] J. Sacks, W.J. Welch, T.J. Mitchell, and H.P. Wynn. Design and analysis of computer experiments. *Statistical Science*, 4 :409–435, 1989.

[25] A. Saltelli. Making best use of model evaluations to compute sensitivity indices. *Computer Physics Communication*, 145 :280–297, 2002.

[26] A. Saltelli, K. Chan, and E.M. Scott, editors. *Sensitivity analysis.* Wiley Series in Probability and Statistics. Wiley, 2000.

[27] A. Saltelli, S. Tarantola, and K. Chan. A quantitative, model-independent method for global sensitivity analysis of model output. *Technometrics*, 41 :39–56, 1999.

[28] I.M. Sobol. Sensitivity estimates for non linear mathematical models. *Mathematical Modelling and Computational Experiments*, 1 :407–414, 1993.

[29] S. Tarantola, N. Giglioli, N. Jesinghaus, and A. Saltelli. Can global sensitivity analysis steer the implementation of models for environmental assesments and decision-making ? *Stochastic Environmental Research and Risk Assesment*, 16 :63–76, 2002.

[30] G.G. Vining and R.H. Myers. Combining Taguchi and response-surface philosophies - a dual response approach. *Journal of Quality Technology*, 22 :38–45, 1990.

[31] E. Volkova, B. Iooss, and F. Van Dorpe. Global sensitivity analysis for a numerical model of radionuclide migration from the RRC "Kurchatov Institute" radwaste disposal site. *Stochastic Environmental Research and Risk Assesment*, 22 :17–31, 2008.

[32] G. Wahba. *Spline models for observational data.* SIAM, 1990.

[33] W.J. Welch, R.J. Buck, J. Sacks, H.P. Wynn, T.J. Mitchell, and M.D. Morris. Screening, predicting, and computer experiments. *Technometrics*, 34(1) :15–25, 1992.

[34] S.N. Wood and N.H. Augustin. GAMs with integrated model selection using penalized regression splines and applications to environmental modelling. *Ecological modelling*, 157 :157–177, 2002.

[35] I. Zabalza, J. Dejean, and D. Collombier. Prediction and density estimation of a horizontal well productivity index using generalized linear models. In *ECMOR VI, Peebles*, September 1998.

[36] I. Zabalza-Mezghani, E. Manceau, M. Feraille, and A. Jourdan. Uncertainty management : From geological scenarios to production scheme optimization. *Journal of Petroleum Science and Engineering*, 44 :11–25, 2004.

4   GLOBAL SENSITIVITY ANALYSIS OF COMPUTER MODELS WITH FUNCTIONAL INPUTS

4.1   ABSTRACT

Global sensitivity analysis is used to quantify the influence of uncertain input parameters on the response variability of a numerical model. The common quantitative methods are applicable to computer codes with scalar input variables. This chapter aims at illustrating different variance-based sensitivity analysis techniques, based on the so-called Sobol indices, when some input variables are functional, such as stochastic processes or random spatial fields. In this work, we focus on large cpu time computer codes which need a preliminary metamodeling step before performing the sensitivity analysis. We propose the use of the joint modeling approach, i.e., modeling simultaneously the mean and the dispersion of the code outputs using two interlinked Generalized Linear Models (GLM) or Generalized Additive Models (GAM). The "mean" model allows to estimate the sensitivity indices of each scalar input variables, while the "dispersion" model allows to derive the total sensitivity index of the functional input variables. The proposed approach is compared to some classical SA methodologies on an analytical function. Lastly, the proposed methodology is applied to an industrial computer code that simulates the nuclear fuel irradiation.

4.2   INTRODUCTION

Modern computer codes that simulate physical phenomenas often take as inputs a high number of numerical parameters and physical variables, and return several outputs - scalars or functions. For the development and the use of such computer models, Sensitivity Analysis (SA) is an invaluable tool. The original technique, based on the derivative computations of the model outputs with respect to the model inputs, suffers from strong limitations for most of computer models. More recent global SA techniques take into account all the variation ranges of the inputs and aim to apportion the whole output uncertainty to the input factor uncertainties (Saltelli et al. [18]). The global SA methods can also be used for model calibration, model validation, decision making process, i.e., any process where it is useful to know which variables that mostly contribute to the output variability.

The common quantitative methods are applicable to computer codes with scalar input variables. For example, in the nuclear engineering domain, global SA tools have been applied to numerous models where all the uncertain input parameters are modeled by random variables, possibly correlated - such as thermal-hydraulic system codes (Marquès et al. [12]), waste storage safety studies (Helton et al. [6]), environmental model of dose calculations (Iooss et al. [9]), reactor dosimetry processes (Jacques et al. [10]). Recent research papers have tried to consider more complex input variables in the global SA process, especially in petroleum and environmental studies :

- Tarantola et al. [23] work on an environmental assessment on soil models which use spatially distributed maps affected by random errors. For the SA, they propose to replace the spatial input by a "trigger" parameter that governs the random field simulation;
- Ruffo et al. [15] evaluate an oil reservoir production using a model that depends on different heterogeneous geological media scenarios. These scenarios, which are of limited number, are then substituted for a discrete factor (a scenario number) before performing the SA;
- Iooss et al. [8] (see chapter 3) study a groundwater radionuclide migration model which is based on geostatistical simulations of the hydrogeological layer heterogeneity. The authors propose to consider the spatial input parameter as an "uncontrollable" parameter.

In this chapter, we tackle the problem of the global SA for numerical models and when some input parameters ε are functional. $\varepsilon(u)$ is a one or multi-dimensional stochastic function where u can be spatial coordinates, time scale or any other physical parameters. Our work focuses in models that depend on scalar parameter vector X and need some stochastic processes simulations or random fields $\varepsilon(u)$ as input parameters. The computer code output value Y depends on the realizations of these random functions. These models are typically non linear with strong interactions between input

parameters. Therefore, we concentrate our methodology on the variance based sensitivity indices estimation; that is, the so-called Sobol indices (Sobol [22], Saltelli et al. [18]).

To deal with this situation, a first natural approach consists in the discretization of the input functional parameter $\varepsilon(u)$ or its decomposition into an appropriate basis of orthogonal functions. Then, for all the new scalar parameters which represent $\varepsilon(u)$, sensitivity indices are computed. However, in the case of complex functional parameters, this approach seems to be rapidly intractable as these parameters cannot be represented by a small number of scalar parameters (Tarantola et al. [23]). Moreover, when dealing with non physical parameters (for example coefficients of orthogonal functions used in the decomposition), sensitivity indices interpretation may be labored. Indeed, most often, physicists would prefer to obtain one global sensitivity index related to $\varepsilon(u)$.

The following section presents three different strategies to compute the Sobol indices with functional inputs : (a) the macroparameter method, (b) the trigger parameter method and (c) the proposed joint modeling approach. Section 4.4 compares the relevance of these three strategies an analytical function : the WN-Ishigami function. Then, the proposed approach is illustrated on an industrial computer code simulating fuel irradiation in a nuclear reactor.

4.3   COMPUTATIONAL METHODS OF SOBOL INDICES

First, let us recall some basic notions about Sobol indices. Let define the model

$$f : \mathbb{R}^p \to \mathbb{R}$$
$$X \mapsto Y = f(X) \tag{1}$$

where Y is the code output, $X = (X_1, \ldots, X_p)$ are p independent inputs, and f is the model function, which is analytically not known. The main idea of the variance-based SA methods is to evaluate how the variance of an input or a group of input parameters contributes to the output variance. These contributions are described using the following sensitivity indices :

$$S_i = \frac{\mathrm{Var}\left[\mathbb{E}\left(Y | X_i\right)\right]}{\mathrm{Var}(Y)}, \quad S_{ij} = \frac{\mathrm{Var}\left[\mathbb{E}\left(Y | X_i X_j\right)\right]}{\mathrm{Var}(Y)} - S_i - S_j, \quad S_{ijk} = \ldots \tag{2}$$

These coefficients, namely the Sobol indices, can be used for any complex model functions f. The second order index S_{ij} expresses the model sensitivity to the interaction between the variables X_i and X_j (without the first order effects of X_i and X_j), and so on for higher orders effects. The interpretation of these indices is natural as all indices lie in $[0, 1]$ and their sums are equal to one. The larger an index value is, the greater is the importance of the variable or the group of variables related to this index.

For a model with p inputs, the number of Sobol indices is $2^p - 1$; leading to an intractable number of indices as p increases. Thus, to express the overall output sensitivity to an input X_i, Homma & Saltelli [7] introduce the total sensitivity index :

$$S_{T_i} = S_i + \sum_{j \neq i} S_{ij} + \sum_{j \neq i, k \neq i, j < k} S_{ijk} + \ldots = \sum_{l \in \#i} S_l \tag{3}$$

where $\#i$ represents all the "non-ordered" subsets of indices containing index i. Thus, $\sum_{l \in \#i} S_l$ is the sum of all the sensitivity indices having i in their index. The estimation of these indices (Eqs. (2) and (3)) can be performed by Monte-Carlo simulations based on independent samples (Sobol [21], Saltelli [17]), or by refined sampling designs introduced to reduce the number of required model evaluations significantly, for instance FAST (Saltelli et al. [20]) and quasi-random designs (Saltelli et al. [19]).

Let us now consider a supplementary input parameter which is a functional input variable $\varepsilon(u) \in \mathbb{R}$ where $u \in \mathbb{R}^d$ is a d-dimensional location vector. $\varepsilon(u)$ is defined by all its marginal and joint probability distributions. In this work, it is supposed that random function realizations can be simulated. For

example, these realizations can be produced using geostatistical simulations (Lantuéjoul [11]) or stochastic processes simulations (Gentle [4]). Our model writes now

$$Y = f(\boldsymbol{X}, \varepsilon) \tag{4}$$

and in addition to the Sobol indices related to $\boldsymbol{X}$, our goal is to derive methods to compute the sensitivity indices relative to ε, i.e., S_ε (first order index), S_{T_ε} (total sensitivity index), $S_{i\varepsilon}$ (second order indices), $S_{ij\varepsilon}$, ...

4.3.1   The macroparameter method

To solve the problem of correlated input parameters in the Sobol indices calculations, Jacques et al. [10] propose the use of multi-dimensional sensitivity indices (Sobol [22]) : each group of correlated parameters is considered as a multi-dimensional parameter or macroparameter. The different Sobol indices (first order, second order, ..., total) are then computed using independent Monte-Carlo sampling techniques (Sobol [21], Saltelli [17]). These techniques allow correlations between input parameters; while it is prohibited with other methods - for example FAST.

In our context, this approach seems to be relevant as the input functional parameter $\varepsilon(u)$ can be considered as an unique input multi-dimensional parameter (i.e. a macroparameter). For instance, the first order Sobol index related to $\varepsilon(u)$ is defined as previously by

$$S_\varepsilon = \frac{\mathrm{Var}\left[\mathbb{E}\left(Y|\varepsilon\right)\right]}{\mathrm{Var}(Y)} \tag{5}$$

A simple way to estimate $S_\varepsilon = D_\varepsilon/D$ is based on the Sobol [21] algorithm :

$$\hat{f}_0 = \frac{1}{N} \sum_{k=1}^{N} f(\boldsymbol{X}_k^{(1)}, \varepsilon_k) \tag{6a}$$

$$\hat{D} = \frac{1}{N} \sum_{k=1}^{N} f^2(\boldsymbol{X}_k^{(1)}, \varepsilon_k) - \hat{f}_0^2 \tag{6b}$$

$$\hat{D}_\varepsilon = \frac{1}{N} \sum_{k=1}^{N} f(\boldsymbol{X}_k^{(1)}, \varepsilon_k) f(\boldsymbol{X}_k^{(2)}, \varepsilon_k) - \hat{f}_0^2 \tag{6c}$$

where $(\boldsymbol{X}_k^{(1)})_{k=1...N}$ and $(\boldsymbol{X}_k^{(2)})_{k=1...N}$ are two independent sets of N simulations of the input vector $\boldsymbol{X}$ and $(\varepsilon_k)_{k=1...N}$ is a sample of N realizations of the random function $\varepsilon(u)$. To compute the sensitivity indices S_i, the same algorithm is used with two independent samples of $(\varepsilon_k)_{k=1...N}$. In the same way, the total sensitivity index S_{T_ε} is derived from the algorithm of Saltelli [17].

The major drawback of this method is that it may be cpu time consuming. An accurate estimation of Sobol indices by this naive Monte-Carlo method requires more than thousand model evaluations for one input parameter. In complex industrial applications, it is intractable due to the cpu time cost of one model evaluation and the possible large number of input parameters.

4.3.2   The "trigger" parameter method

Dealing with spatially distributed input variables, Tarantola et al. [23] propose an alternative that uses an additional scalar input parameter ξ - called "trigger" parameter. $\xi \sim U[0,1]$ governs the random function simulation. For each simulation, if $\xi < 0.5$, the functional parameter $\varepsilon(u)$ is fixed to a nominal value $\varepsilon_0(u)$ (for example the mean $\mathbb{E}[\varepsilon(u)]$), while if $\xi > 0.5$, the functional parameter $\varepsilon(u)$ is simulated. Using this methodology, it is possible to estimate how sensitive the model output is to the presence of the random function. Tarantola et al. [23] use the Extended FAST method to compute the first order and total sensitivity indices of 6 scalar input factors and 2 additional "trigger" parameters.

For their study, the sensitivity indices according to the "trigger" parameters are small and the authors conclude that it is unnecessary to model these spatial errors more accurately.

Contrary to the previous method, there is no restriction about the sensitivity indices estimation procedure - i.e. Monte-Carlo, FAST, quasi Monte-Carlo. However, there are two major drawbacks for this approach :

- As the macroparameter method, it also requires the use of the computer model to perform the SA and it may be problematic for large cpu time computer models. This problem can be compensate by the use of an efficient quasi Monte-Carlo algorithm.
- As underlined by Tarantola et al. [23], ξ reflects only the presence or the absence of the stochastic errors on $\varepsilon_0(u)$. Therefore, the term $\mathrm{Var}[E(Y|\xi)]$ does not quantify the contribution of the random function variability to the output variability $\mathrm{Var}(Y)$. We will discuss about the significance of $\mathrm{Var}[E(Y|\xi)]$ later, during our analytical function application.

4.3.3   The joint modeling approach

To perform a variance-based SA for time consuming computer models, some authors propose to approximate the computer code by a mathematical function (Marseguerra et al. [13], Volkova et al. [24]), often called response surface or metamodel (Fang et al. [2]). For metamodels with sufficient prediction capabilities, the bias due to the use of the metamodel instead of the true model is negligible. Several choices of metamodel can be found in the literature : polynomials, splines, Gaussian processes, neural networks, ... Thus, for the functional input problem, one strategy may be to fit a metamodel with a multi-dimensional scalar parameters representing $\varepsilon(u)$ as an input parameter - i.e. its discretization or its decomposition into an appropriate basis. However, this approach seems to be impracticable due to the potential large number of scalar parameters.

A second option is to substitute each random function realization for a discrete number, which can correspond to the scenario parameter of Ruffo et al. [15] (where the number of geostatistical realizations is finite and fixed, and where each different value of the discrete parameter corresponds to a different realization). However, in the general context, this restriction of the possible realizations of the input random function to a few ones is not acceptable.

The last solution considers $\varepsilon(u)$ as an uncontrollable parameter and a metamodel is fitted in function of the other scalar parameters X :

$$Y_m = E(Y|X) \tag{7}$$

Therefore, using the relation

$$\mathrm{Var}(Y) = \mathrm{Var}[E(Y|X)] + E[\mathrm{Var}(Y|X)] \tag{8}$$

it can be easily shown that the sensitivity indices of Y according to the scalar parameters $X = (X_i)_{i=1...p}$ write (Iooss et al. [8])

$$S_i = \frac{\mathrm{Var}[E(Y_m|X_i)]}{\mathrm{Var}(Y)}, \quad S_{ij} = \frac{\mathrm{Var}[E(Y_m|X_iX_j)]}{\mathrm{Var}(Y)} - S_i - S_j, \quad \ldots \tag{9}$$

and can be computed by classical Monte-Carlo techniques applied on the metamodel Y_m. Therefore, using equation (8), the total sensitivity index of Y according to $\varepsilon(u)$ corresponds to the expectation of the unexplained part of $\mathrm{Var}(Y)$ by the metamodel Y_m :

$$S_{T_\varepsilon} = \frac{E[\mathrm{Var}(Y|X)]}{\mathrm{Var}(Y)} \tag{10}$$

Using this approach, our objective is altered because we cannot decompose the ε effects into elementary effect (S_ε) and interaction effects between ε and the scalar parameters $(X_i)_{i=1...p}$. However, we see below that our technique allows a qualitative appraisal of the interaction indices.

The sensitivity index estimations from equations (9) and (10) raise two difficulties :

1. It is well known that classical parametric metamodels (based on least squares fitting) are not adapted to estimate $\mathbb{E}(Y|X)$ accurately due to the presence of heteroscedasticity (induced by the effect of ε). Such cases are analyzed by Iooss et al. [8] (see chapter 3). The authors show that heteroscedasticity may lead to sensitivity indices misspecifications.

2. Classical non parametric methods, such as Generalized Additive Model (Hastie and Tibshirani [5]) and Gaussian process (Sacks et al. [16]) which can provide efficient estimation of $\mathbb{E}(Y|X)$ (examples are given in Iooss et al. [8]), even in high dimensional input cases ($p > 5$), are based on homoscedasticity hypothesis and do not propose the estimation of $\text{Var}(Y|X)$.

To solve the second problem, Zabalza-Mezghani et al. [26] propose the use of a theory developed for experimental data (McCullagh and Nelder [14]) : the simultaneous fitting of the mean and the dispersion by two interlinked Generalized Linear Models (GLM), which is called the joint modeling. Besides, to resolve the first problem, this approach has been extended by Iooss et al. [8] (see chapter 3) to non parametric models. This generalization allows more complexity and flexibility while fitting the data. The authors propose the use of Generalized Additive Models (GAMs) based on penalized smoothing splines (Wood [25]). GAMs allow model and variable selections using quasi-likelihood function, statistical tests on coefficients and graphical display. However, compared to other complex metamodels, GAMs impose an additive effects hypothesis. Therefore, two metamodels are obtained : one for the mean component $Y_m = \mathbb{E}(Y|X)$; and the other one for the dispersion component $Y_d = \text{Var}(Y|X)$. The sensitivity indices of X are computed using Y_m with the standard procedure (Eq. (9)), while the total sensitivity index of $\varepsilon(u)$ is computed from $\mathbb{E}(Y_d)$ (Eq. (10)). Using the explicit formula on Y_d and the associated regression diagnostics, qualitative sensitivity indices for the interactions between $\varepsilon(u)$ and the scalar parameters of X can also be deduced.

4.4   APPLICATION TO AN ANALYTICAL EXAMPLE

The three previously proposed methods are first illustrated on an artificial analytical model with two scalar input variables and one functional input :

$$Y = f(X_1, X_2, \varepsilon(t)) = \sin(X_1) + 7\sin(X_2)^2 + 0.1[\max_t(\varepsilon(t))]^4 \sin(X_1) \qquad (11)$$

where $X_i \sim \mathcal{U}[-\pi; \pi]$ for $i = 1, 2$ and $\varepsilon(t)$ is a white noise, i.e. an i.i.d. stochastic process $\varepsilon(t) \sim \mathcal{N}(0, 1)$. In our model simulations, $\varepsilon(t)$ is discretized in one hundred values : $t = 1 \dots 100$. The function (11) is similar to the well-known Ishigami function (Homma and Saltelli [7]) but substitute the third parameter for the maximum of a stochastic process. Consequently, we call our function the white-noise Ishigami function (WN-Ishigami). Although the WN-Ishigami function is an artificial model, the introduction of the maximum of a stochastic process inside a model is quite realistic. For example, some computer models simulating physical phenomena can use the maximum of time-dependent variable - river height, rainfall quantity, temperature. Such input variable can be modeled by a temporal stochastic process.

As for the Ishigami function, we can immediately deduce from the formula (11) the sensitivity indices which are worse zero :

$$S_\varepsilon = S_{12} = S_{2\varepsilon} = S_{12\varepsilon} = 0 \qquad (12)$$

Then, we have

$$S_{T_1} = S_1 + S_{1\varepsilon}, \quad S_{T_2} = S_2, \quad S_{T_\varepsilon} = S_{1\varepsilon} \qquad (13)$$

In the following, we focus our attention on the estimation of S_1, S_2 and S_{T_ε}.

Because of a particularly complex probability distribution of the maximum of a white noise, there is no analytical solution for the theoretical Sobol indices S_1, S_2 and $S_{1\varepsilon}$ for the WN-Ishigami function. Even with the asymptotic hypothesis (number of time steps tending to infinity), where the maximum of the white noise follows Generalized Extreme Value distribution, theoretical indices are unreachable. Therefore, our benchmark Sobol indices values are derived from the Monte-Carlo method. However, these benchmark values can be considered as relevant because of the negligible computation time required to evaluate equation (11).

| Indices | Macroparameter | | | | "Trigger" parameter | | | |
| | Sobol algo | | Saltelli algo | | Sobol algo | | Saltelli algo | |
	Values	sd	Values	sd	Values	sd	Values	sd
S_1	0.540	1.3e-2	0.551	1.6e-2	0.304	1.3e-2	0.330	1.8e-2
S_{T_1}	—	—	0.808	2.0e-2	—	—	0.656	1.4e-2
S_2	0.197	1.1e-2	0.207	0.8e-2	0.329	1.4e-2	0.348	1.5e-2
S_{T_2}	—	—	0.212	0.7e-3	—	—	0.532	1.3e-2
$S_{1\varepsilon}$	0.268	2.4e-2	—	—	0.177	2.2e-2	—	—
S_{T_ε}	—	—	0.248	1.3e-2	—	—	0.336	1.4e-2

TAB. 4.1 – **Sobol sensitivity indices (with standard deviations sd) obtained from two Monte-Carlo algorithms (Sobol [21] and Saltelli [17]) and two integration methods of the functional input ε (macroparameter and "trigger" parameter) on the WN-Ishigami function. "—" indicates that the value is not available.**

4.4.1   The macroparameter and "trigger" parameter methods

Table 4.1 contains the Sobol indices estimates using the macroparameter and "trigger" parameter methods. As explained before, we can only use the two algorithms based on independent Monte-Carlo samples : the algorithm of Sobol [21] which computes S_1, S_2, $S_{1\varepsilon}$, and the algorithm of Saltelli [17] which computes the first order indices S_1, S_2 and the total sensitivity indices S_{T_1}, S_{T_2}, S_{T_ε}. For the estimation, the size of the Monte-Carlo samples are limited to $N = 10000$ because of memory computer limit. Indeed, the functional input $\varepsilon(u)$ contains for each simulation set 100 values. Then, the input sample matrix has the dimension $N \times 102$ which becomes extremely large when N increases. To evaluate the effect of this limited Monte-Carlo sample size N, each Sobol index estimate is associated to a standard-deviation estimated by bootstrap - with 100 replicates of the input-output sample. The obtained standard-deviations are relatively small, of the order of 0.01, which is rather sufficient for our exercise.

For the macroparameter method, the theoretical relations between indices given in (13) are verified. We are therefore confident with the estimates obtained with this method (which is in addition theoretically well-founded) and we choose the Sobol indices obtained with Saltelli's algorithm as the indices references :

$$S_1 = 55.1\%, \quad S_2 = 20.7\%, \quad S_{T_\varepsilon} = 24.8\%$$

The S_ε, S_{12}, $S_{\varepsilon 2}$ and $S_{12\varepsilon}$ indices (Eq. (12)) are not reported in table 4.1 as estimates are negligible.

With the "trigger" parameter method, the obtained values in table 4.1 are not close to the reference values. The inadequacies are larger than 30% for all the indices, and can be larger than 60% for a few ones (S_2 and S_{T_2}). Moreover, the relations given in (13) are not satisfied at all. Actually, replacing the input parameter $\varepsilon(u)$ by ξ which governs the presence or the absence of the functional input parameter changes the model. When ε is not simulated, it is replaced by its mean (zero) and the WN-Ishigami function becomes $Y = \sin(X_1) + 7\sin(X_2)^2$. Therefore, the mix of the WN-Ishigami model and this new model perturbs the estimation of the sensitivity indices, even those unrelated to ε (like X_2).

This example confirms our expectation : the sensitivity indices derived from the "trigger" parameter method have not the same sense that the classical ones, i.e., the measure of the contribution of the

input parameter variability to the output variable variability. The sensitivity indices obtained with these two methods are unconnected because the "trigger" parameter method changes the structure of the model.

4.4.2   The joint modeling approach

We apply now the joint modeling approach which requires an initial input-output sample to fit the joint metamodel - the mean component Y_m and the dispersion component Y_d. For our application, a learning sample size of $n = 500$ was considered; i.e., n independent random samples of $(X_1, X_2, \varepsilon(u))$ were simulated leading to n observations for Y. Let first remark that this method is extremely less cpu time consuming than the previous ones which needed a 10000-size sample.

Joint GLM and joint GAM fitting procedures are fully described in Iooss et al. [8] (see chapter 3). Some graphical residual analyses are particularly well suited to check the relevance of the mean and dispersion components of the joint models. In the following, we give the results of the joint models fitting on a learning sample $(X_1, X_2, \varepsilon(u), Y)$. Let us recall that we fit a model to predict Y in function of (X_1, X_2).

Joint GLM fitting
For the joint GLM, fourth order polynomial for the parametric form of the model is considered. Moreover, only the explanatory terms are retained in our regression model using analysis of deviance and the Fisher statistics. The Student test on the regression coefficients and residuals graphical analysis make it possible to appreciate the model goodness-of-fit. The mean component gives :

```
Deviance Residuals:
      Min         1Q     Median        3Q        Max
 -5.79193   -0.59880    0.03988   0.64202    3.51148

Coefficients:
              Estimate Std. Error t value Pr(>|t|)
(Intercept)    1.92634    0.22128    8.706   <2e-16 ***
X1             4.74256    0.16198   29.278   <2e-16 ***
I(X2^2)        2.22879    0.14130   15.773   <2e-16 ***
I(X1^3)       -0.51398    0.02453  -20.951   <2e-16 ***
I(X2^4)       -0.28501    0.01588  -17.952   <2e-16 ***
---
Signif. codes:  0 '***' 0.001 '**' 0.01 '*' 0.05 '.' 0.1 ' ' 1

(Dispersion parameter for quasi family taken to be 1.010101)

    Null deviance: 1901.0  on 499  degrees of freedom
Residual deviance:  500.0  on 495  degrees of freedom
AIC: NA

Number of Fisher Scoring iterations: 2
```

The explained deviance of this model is $D_{expl} = 74\%$. It can be seen that it remains 26% of non explained deviance due to the model inadequacy and/or to the functional input parameter. The predictivity coefficient, i.e. coefficient of determination R^2 computed on a test sample, is $Q_2 = 71\%$. Q_2 is relatively coherent with the explained deviance.

For the dispersion component, using analysis of deviance techniques, none significant explanatory variable were found : the heteroscedastic character of the data has not been retrieved. Thus, the dispersion component is supposed to be constant; and the joint GLM model is equivalent to a simple GLM - but with a different fitting process.

Joint GAM fitting
At present, we try to model the data by joint GAM. The resulting model is described by the following features ($s(.)$ denotes a penalized spline smoothing term) :

```
Mean component:
```

```
Family: quasi
Link function: identity
Formula:
y ~ X1 + s(X1) + s(X2)


Parametric coefficients:
            Estimate Std. Error t value Pr(>|t|)
(Intercept) 4.19914    0.08727   48.12  <2e-16 ***
X1          -5.39131    0.34285  -15.72  <2e-16 ***
---
Signif. codes:  0 '***' 0.001 '**' 0.01 '*' 0.05 '.' 0.1 ' ' 1


Approximate significance of smooth terms:
        edf Est.rank      F p-value
s(X1) 5.503        8  144.1  <2e-16 ***
s(X2) 8.738        9  316.5  <2e-16 ***
---
Signif. codes:  0 '***' 0.001 '**' 0.01 '*' 0.05 '.' 0.1 ' ' 1


R-sq.(adj) =  0.979   Deviance explained = 90.5%
GCV score = 1.0683   Scale est. = 1.0336   n = 500

Dispersion component:

Family: Gamma
Link function: log
Formula:
d ~ s(X1)


Parametric coefficients:
            Estimate Std. Error t value Pr(>|t|)
(Intercept) 0.98812    0.07965   12.41  <2e-16 ***
---
Signif. codes:  0 '***' 0.001 '**' 0.01 '*' 0.05 '.' 0.1 ' ' 1


Approximate significance of smooth terms:
        edf Est.rank      F p-value
s(X1) 8.814        9  28.39  <2e-16 ***
---
Signif. codes:  0 '***' 0.001 '**' 0.01 '*' 0.05 '.' 0.1 ' ' 1


R-sq.(adj) =  0.0481   Deviance explained = 26.3%
GCV score = 3.2355   Scale est. = 3.172   n = 500
```

The explained deviance of the mean component is $D_{expl} = 90\%$ and the predictivity coefficient is $Q_2 = 77\%$. Therefore, the joint GAM approach outperforms the joint GLM one. Indeed, the proportion of explained deviance is clearly greater for the GAM model. Even if this is obviously related to an increasing number of parameters; this is also explained as GAMs are more adjustable than GLMs. This is confirmed by the increase of the predictivity coefficient - from 71% to 77%. Moreover, due to the GAMs flexibility, the explanatory variable X_1 is identified for the dispersion component. The interaction between X_1 and the functional input parameter $\varepsilon(u)$ which governs the heteroscedasticity of this model is therefore retrieved.

Sobol indices

From the joint GLM and the joint GAM, Sobol sensitivity indices can be computed using equations (9) and (10) - see Table 4.2. The reference values are extracted from the macroparameter method and Saltelli's algorithm in table 4.1. The standard deviation estimates (sd) are obtained from 100 repetitions of the Monte-Carlo estimation procedure - which uses $N = 10000$ model computations for one index estimation. The joint GLM and joint GAM gives good estimations of S_1 and S_2. Despite the joint GLM leads to an accurate estimation for S_{T_ε}, we will see later that it is a lucky break. A problem occurs with the estimation of S_{T_ε} with joint GAM. In fact, an efficient modeling of $\mathrm{Var}(Y|X)$ is difficult, which is a common statistical difficulty in heteroscedastic regression problems (Antoniadis & Lavergne [1]). Another way to estimate the total sensitivity index S_{T_ε} is to compute the unexplained variance of the mean component model given directly by $1 - Q_2$, with Q_2 the predictivity coefficient of the mean component model. In practical applications, Q_2 can be estimated via leave-one-out or

cross validation procedures. In our analytical case, the index estimated with this method and the joint GAM gives a correct estimation - 0.23 instead of 0.25.

Indices	Reference Values	Joint GLM			Joint GAM		
		Values	sd	Method	Values	sd	Method
S_1	0.551	0.572	4e-3	MC	0.569	5e-3	MC
S_2	0.207	0.179	8e-3	MC	0.233	7e-3	MC
S_{T_ε}	0.248	0.250	2e-3	MC	0.197	1e-3	MC
		0.29	—	Q_2	0.23	—	Q_2
S_{12}	0	0	—	Eq	0	—	Eq
$S_{1\varepsilon}$	0.248	0	—	Eq	> 0	—	Eq
$S_{2\varepsilon}$	0	0	—	Eq	0	—	Eq
$S_{12\varepsilon}$	0	0	—	Eq	0	—	Eq
S_{T_1}	0.808	0.832	4e-3	Eq	—	—	—
S_{T_2}	0.212	0.179	8e-3	Eq	0.233	7e-3	Eq
S_ε	0	0.250	2e-3	Eq	—	—	—

TAB. 4.2 – **Sobol sensitivity indices (with standard deviations) for the WN-Ishigami function : exact and estimated values from joint GLM and joint GAM (fitted with a 500-size sample). "Method" indicates the estimation method : MC for the Monte-Carlo procedure, Eq for a deduction from the model equations and** Q_2 **for the deduction of the predictivity coefficient** Q_2. **"—" indicates that the value is not available.**

For the other sensitivity indices, the conclusions draw from the GLM formula are completely erroneous : as the dispersion component is constant, the interaction indices are null. Thus, $S_\varepsilon = S_{T_\varepsilon} = 0.25$ while $S_\varepsilon = 0$ in reality. In contrary, the deductions draw from GAM formulas are correct : (X_1, ε) interaction sensitivity is positive, $S_{2\varepsilon} = S_{12\varepsilon} = 0$, $S_{T_2} = S_2$, $S_{12} = S_{23} = S_{123} = 0$. The drawback of this method is that some indices (S_{T_1} and S_ε) remain unknown due to the non separability of the dispersion component effects.

By estimating Sobol indices with those obtained from other learning samples, we observe that the estimates are rather dispersed : it seems that the estimates are not robust according to different learning samples for the joint models. To examine this effect, we propose to study two different sample sizes ($n = 200$ and $n = 500$). For each sample size, we repeat 25 times, the fitting process on different learning samples, and we compute Sobol indices as previously. In fact, for each sample size, we obtain 25 estimates of each sensitivity index. The variability of the indices is due at present to the learning sample variability. Figures 4.1 and 4.2 show the results of this investigation, which are particularly convincing. The boxplots are based on the 25 different estimates. From these figures, several conclusion can be drawn :

- for the joint GAM, the boxplot interquartile interval of each index contains its reference value. In contrary, the joint GLM fails to obtain correct estimates : except for S_1, the sensitivity reference values are outside the interquartile intervals of the obtained boxplots ;
- the superiority of the joint GAM with respect to the joint GLM is corroborated, especially for S_2 and S_{T_ε} ;
- the increase of the learning sample size has no effect on the joint GLM results (due to the parametric form of this model). However, for the joint GAM, boxplots widths are strongly reduced

from $n = 200$ to $n = 500$. In addition, the mean estimates seem to converge to the reference values;

– as explained before, the estimation of S_{T_ε} using the predictivity coefficient Q_2 is markedly better than through the dispersion component model. This is not the case for the joint GLM.

Learning size = 200
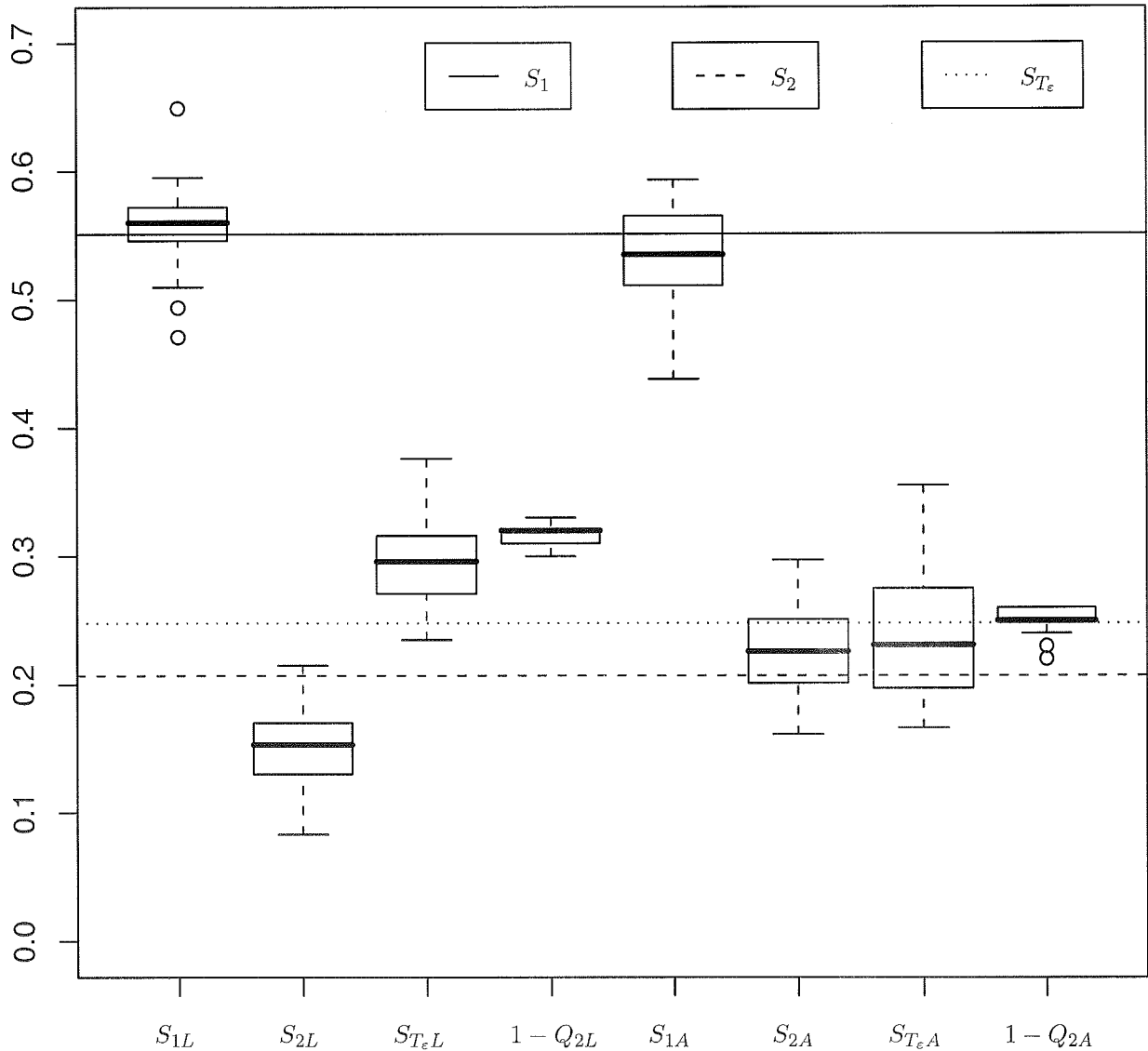
Fig. 4.1 – **WN-Ishigami application. Comparison of Sobol indices estimates. Reference values :** $S_1, S_2, S_{T_\varepsilon}$. **Joint GLM :** $S_{1L}, S_{2L}, S_{T_\varepsilon L}, 1 - Q_{2L}$. **Joint GAM :** $S_{1A}, S_{2A}, S_{T_\varepsilon A}, 1 - Q_{2A}$. $1 - Q_{2L}$ **(resp.** $1 - Q_{2A}$**) is the estimation of** S_{T_ε} **via the joint GLM (resp. joint GAM)** Q_2 **coefficient. Learning sample size :** $n = 200$.

In conclusion, this example shows that the joint models, and specially the joint GAM, can adjust complex heteroscedastic situations. Moreover, the joint models offer a theoretical basis to compute efficiently global sensitivity indices for models with functional input parameter.

Learning size = 500
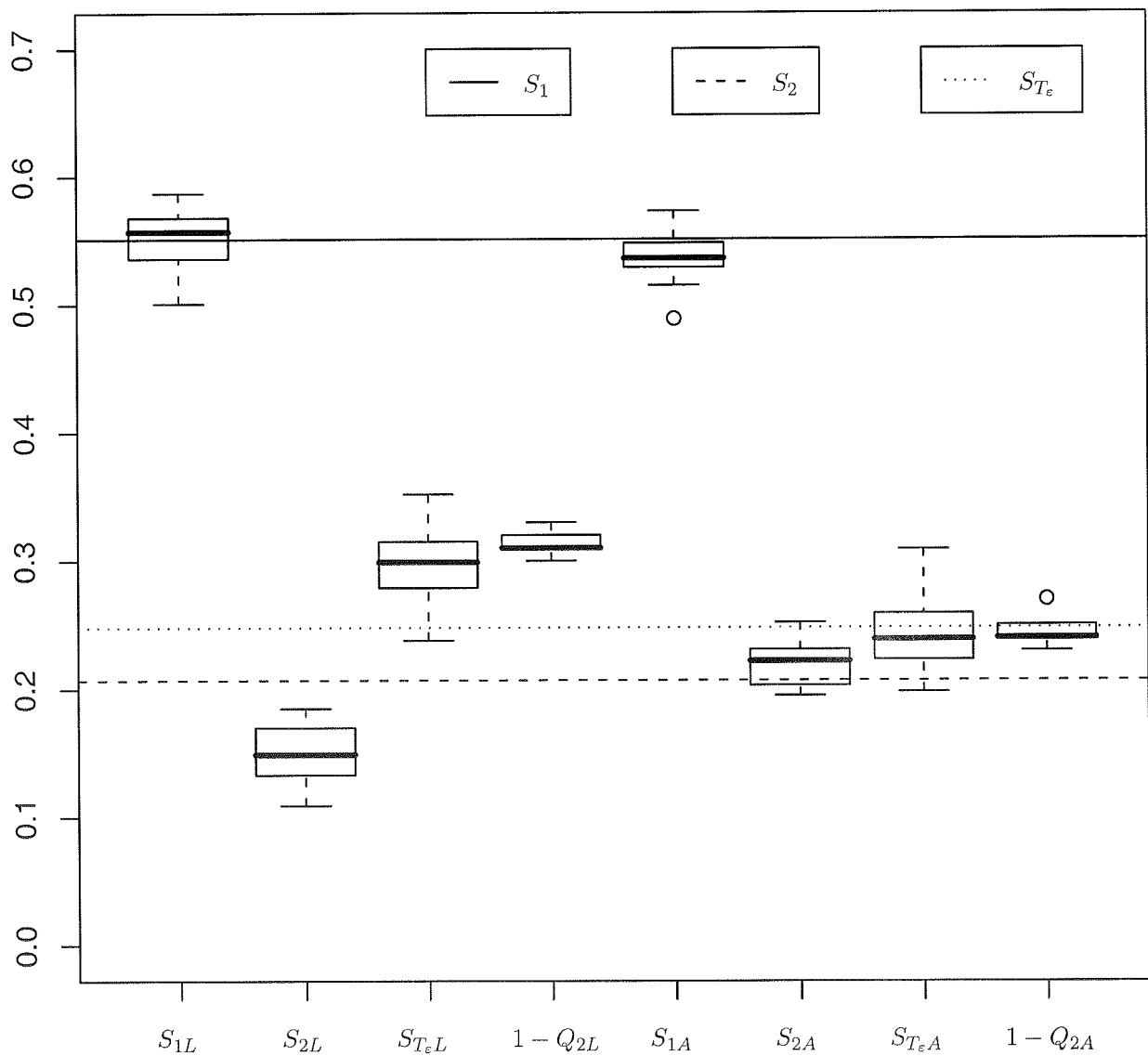
Fig. 4.2 – **WN-Ishigami application. Comparison of Sobol indices estimates. Reference values :** S_1, S_2, S_{T_ϵ}. **Joint GLM :** $S_{1L}, S_{2L}, S_{T_\epsilon L}, 1 - Q_{2L}$. **Joint GAM :** $S_{1A}, S_{2A}, S_{T_\epsilon A}, 1 - Q_{2A}$. $1 - Q_{2L}$ **(resp.** $1 - Q_{2A}$**) is the estimation of** S_{T_ϵ} **via the joint GLM (resp. joint GAM)** Q_2 **coefficient. Learning sample size :** $n = 500$.

4.5   APPLICATION TO A NUCLEAR FUEL IRRADIATION SIMULATION

The METEOR computer code, developed within the Fuel Studies Department in CEA Cadarache, studies the thermo-mechanical behavior of the fuel rods under irradiation in a nuclear reactor core. In particular, it computes the fission gas swelling and the cladding creep (Garcia et al. [3]). These two output variables are considered in our analysis. These variables are of fundamental importance for the physical understanding of the fuel behavior and for the monitoring of the nuclear reactor core.

Input parameters of such mechanical models can be evaluated either by database analyses, arguments invoking simplifying hypotheses, expert judgment. All these considerations lead to assign to each input parameter a nominal value associated with an uncertainty. In this study, six uncertain input parameters are considered : the initial internal pressure X_1, the pellet and cladding radius X_2, X_3, the microstructural fuel grain diameter X_4, the fuel porosity X_5 and the time-dependent irradiation power $P(t)$. X_1, ..., X_5 are all modeled by Gaussian independent random variables with the following coefficient of variations : $cv(X_1) = 0.019$, $cv(X_2) = 1.22 \times 10^{-3}$, $cv(X_3) = 1.05 \times 10^{-3}$, $cv(X_4) = 0.044$, $cv(X_5) = 0.25$. The last variable $P(t)$ is a temporal function (discretized in 3558 values) and its uncertainty $\varepsilon(t)$ is modelled like a stochastic process. For simplicity, a temporal white noise (of uniform law ranging between -5% and $+5\%$) was introduced.

As in the previous application, additionally to its scalar random variables, the model includes an input functional variable $P(t)$. To compute Sobol indices of this model, we have first tried to use the macroparameter method. We have succedeed to perform the calculations with $N = 1000$ (for the Monte-Carlo sample sizes of Eqs. (6a), (6b) and (6c)). The sensitivity indices estimates have been obtained after 10 computation days and were extremely imprecise, with strong variations between 0 and 1. Because of the required cpu time, an increase of the sample size N to obtain acceptable sensitivity estimates was unconceivable. Therefore, the goal of this section is to show how the use of the joint modeling approach allows to estimate the sensitivity indices of the METEOR model and, in particular, to quantify the functional input variable influence.

500 METEOR calculations were carried out using 500 Monte-Carlo sampling of the input parameters. As expected, the white noise on $P(t)$ generates an increase in the standard deviation of the output variables (compared to simulations without a white noise) : 6% increase for the variable *fission gas swelling* and 60% for the variable *cladding creep*.

4.5.1   Gas swelling

We start by studying the gas swelling model output. With a joint GLM, the following result for Y_m and Y_d were obtained :

$$\begin{cases} Y_m & = -76 - 0.4X_1 + 20X_2 + 8X_4 + 134X_5 + 0.02X_4^2 - 2X_2X_4 - 6X_4X_5 \\ \log(Y_d) & = -2.4X_1 \end{cases} \qquad (14)$$

The explained deviance of the mean component is $D_{expl} = 86\%$. As the residual analyses of mean and dispersion components do not show any biases, the resulting model seems satisfactory. The joint GAM was also fitted on these data and led to similar results. Thus, it seems that spline terms are useless and that a joint GLM model is suited.

Table 4.3 shows the results for the Sobol indices estimation using Monte-Carlo methods applied on the metamodel (14). The standard deviation (sd) estimates are obtained from 100 repetitions of the Monte-Carlo estimation procedure -which uses 10^5 model computations for one index estimation. It is useless to perform the Monte-Carlo estimation for some indices because they can be deduced from the joint model equations. For example, $S_3 = 0$ (resp. $S_{\varepsilon 2} = 0$) because X_3 (res. X_2) is not involved in the mean (resp. dispersion) component in equation (14). Moreover, we know that $S_{\varepsilon 1} > 0$ because X_1 is an explanatory variable inside the dispersion component Y_d. However, this formulation does not allow to have any idea about S_ε which reflects the first order effect of ε. Therefore, some indices are not accessible, such as S_ε and $S_{\varepsilon 1}$ non distinguishable inside the total sensitivity index S_{T_ε}. Finally,

we can check that $\sum_{i=1}^{5} S_i + \sum_{i,j=1,i<j}^{5} S_{ij} + S_{T_\varepsilon} = 1$ holds - up to numerical approximations.

It can be seen that X_4 (grain diameter) and X_5 (fuel porosity) are the most influent factors (each one having 40% of influence), and do not interact with the irradiation power $P(t)$ (representing by its uncertainty ε). In addition, the effect of $P(t)$ is not negligible (14%) and parameter X_1 (internal pressure) acts only with its interaction with $P(t)$. A sensitivity analysis by fixing X_1 could allow us to obtain some information about the first order effect of ε in the model.

4.5.2   Cladding creep

We study now the cladding creep model output. With a joint GLM, the model for Y_m and Y_d is :

$$
\begin{cases}
Y_m & = -2.75 + 1.05X_2 - 0.15X_3 - 0.58X_5 \\
\log(Y_d) & = 156052 - 76184X_2 + 9298X_2^2
\end{cases}
\tag{15}
$$

The explained deviance of the mean component is $D_{expl} = 26\%$. As the residual analyses of mean and dispersion components show some biases, the resulting model is not satisfactory.

For the joint GAM, the spline terms $\{s(X_2), s(X_3), s(X_5)\}$ and $s(X_2)$ are added within the mean component and the dispersion component respectively. The explained deviance of the mean component is $D_{expl} = 29\%$ which is not significantly greater than 26%. However, as the mean component residual biases of the joint GAM are smaller than those observed for the joint GLM, the joint GAM seems to be more relevant than the joint GLM.

Table 4.3 shows the Sobol indices estimates using Monte-Carlo methods and deductions from the joint model equations. For the joint GLM and joint GAM of the cladding creep, $\sum_{i=1}^{5} S_i + \sum_{i,j=1,i<j}^{5} S_{ij} + S_{T_\varepsilon} = 1$ holds − up to numerical imprecisions. Due to the proximity of the two joint models, results are similar. This analysis shows that the parameter X_2 (pellet radius) explains 28% of the uncertainty of the cladding creep phenomenon, while the other scalar parameters have negligible influence. The greater part of the cladding creep variance (70%) is explained by the irradiation power uncertainty. Physicists may be interested in quantifying the interaction influence between the pellet radius and the irradiation power. Unfortunately, this interaction is not available for the moment in our analysis.

Indices	Gas swelling Joint GLM			Cladding creep Joint GLM			Joint GAM		
	Values	sd	Method	Values	sd	Method	Values	sd	Method
S_1	0.029	6e-3	MC	0.000	1e-3	MC	0.000	1e-3	MC
S_2	0.024	5e-3	MC	0.294	1e-4	MC	0.282	2e-4	MC
S_3	0	—	Eq	0.006	1e-3	MC	0.007	1e-3	MC
S_4	0.394	5e-3	MC	0.000	1e-3	MC	0.000	1e-3	MC
S_5	0.409	6e-3	MC	0.006	1e-3	MC	0.006	1e-3	MC
S_{24}	0.002	5e-3	MC	0	—	Eq	0	—	Eq
S_{45}	0.000	9e-3	MC	0	—	Eq	0	—	Eq
other S_{ij}	0	—	Eq	0	—	Eq	0	—	Eq
S_{T_ε}	0.143	1e-4	MC	0.694	1e-4	MC	0.704	3e-4	MC
S_ε	—	—	—	—	—	—	—	—	—
$S_{\varepsilon 1}$	—	—	—	0	—	Eq	0	—	Eq
$S_{\varepsilon 2}$	0	—	Eq	—	—	—	—	—	—
other $S_{\varepsilon i}$	0	—	Eq	0	—	Eq	0	—	Eq
S_{T_1}	—	—	—	0.000	1e-3	Eq	0.000	4e-3	Eq
S_{T_2}	0.026	7e-3	Eq	—	—	—	—	—	—
S_{T_3}	0	—	Eq	0.006	1e-3	Eq	0.007	4e-3	Eq
S_{T_4}	0.396	7e-3	Eq	0.000	1e-3	Eq	0.000	4e-3	Eq
S_{T_5}	0.409	0.011	Eq	0.006	1e-3	Eq	0.006	4e-3	Eq

TAB. 4.3 – **Sobol sensitivity indices (with standard deviations sd) from joint models fitted on the outputs of the METEOR code. "Method" indicates the estimation method : MC for the Monte-Carlo procedure and Eq for a deduction from the joint model equation. "—" indicates that the value is not available.**

4.6   CONCLUSION

This chapter has proposed a solution to perform global sensitivity analysis for time consuming computer models which depend on functional input parameters, such as a stochastic process or a random field. Our purpose concerned the computation of variance-based importance measures of the model output according the the uncertain input parameters. We have discussed a first natural solution which consists in integrating the functional input parameter inside a macroparameter, and using standard Monte-Carlo algorithms to compute sensitivity indices. This solution is not applicable for time consuming computer code. We have discussed another solution, used in previous studies, based on the replacement of the functional input parameter by a "trigger" parameter that governs the integration or not of the functional input uncertainties. However, the estimated sensitivity indices are strongly biased due to changes in the model structure carrying out by the method itself. Finally, we have proposed an innovative solution, the joint modeling method, based on a preliminary step of double (and joint) metamodel fitting, which resolves the large cpu time problem of Monte-Carlo methods. It consists in rejecting the functional input parameters in noisy input variables. Then, two metamodels depending only on the scalar random input variables are simultaneously fitted : one for the mean function and one for the dispersion (variance) function.

Tests on an analytical function have shown the relevance of the joint modeling method, which provides all the sensitivity indices of the scalar input parameters and the total sensitivity index of the functional input parameter. In addition, it reveals in a qualitative way the influential interactions between the functional parameter and the scalar input parameters. A research way for the future would be to distinguish the contributions of several functional input parameters, who are at the moment totally mixed in one sensitivity index. This is the main drawback of the proposed method.

In an industrial application, the feasibility and usefulness of our methodology was established. Indeed, other methods are not applicable in this application because of large cpu time of the computer code. To a better understanding of the model behavior, the information brought by the global sensitivity analysis can be very useful to the physicist or the modeling engineer. The joint model can also serve in propagation uncertainty and reliability studies of complex models, containing input random functions, to obtain some mean predictions with their confidence intervals.

4.7   ACKNOWLEDGMENTS

4.8   REFERENCES

[1] A. Antoniadis and C. Lavergne. Variance function estimation in regression by wavelet methods. In A. Antoniadis and G. Oppenheim, editors, *Wavelets and statistics*. Springer, 1995.

[2] K-T. Fang, R. Li, and A. Sudjianto. *Design and modeling for computer experiments*. Chapman & Hall/CRC, 2006.

[3] P. Garcia, C. Struzik, M. Agard, and V. Louche. Mono-dimensional mechanical modelling of fuel rods under normal and off-normal operating conditions. *Nuclear Science and Design*, 216 :183–201, 2002.

[4] J.E. Gentle. *Random number generation and Monte Carlo methods*. Springer, second edition, 2003.

[5] T. Hastie and R. Tibshirani. *Generalized additive models*. Chapman and Hall, London, 1990.

[6] J.C. Helton, J.D. Johnson, C.J. Salaberry, and C.B. Storlie. Survey of sampling-based methods for uncertainty and sensitivity analysis. *Reliability Engineering and System Safety*, 91 :1175–1209, 2006.

[7] T. Homma and A. Saltelli. Importance measures in global sensitivity analysis of non linear models. *Reliability Engineering and System Safety*, 52 :1–17, 1996.

[8] B. Iooss, M. Ribatet, and A. Marrel. Global sensitivity analysis of stochastic computer models with generalized additive models. *Technometrics*, submitted, 2008. Available at URL : http ://fr.arxiv.org/abs/0802.0443v1.

[9] B. Iooss, F. Van Dorpe, and N. Devictor. Response surfaces and sensitivity analyses for an environmental model of dose calculations. *Reliability Engineering and System Safety*, 91 :1241–1251, 2006.

[10] J. Jacques, C. Lavergne, and N. Devictor. Sensitivity analysis in presence of model uncertainty and correlated inputs. *Reliability Engineering and System Safety*, 91 :1126–1134, 2006.

[11] C. Lantuéjoul. *Geostatistical simulations - Models and algorithms*. Springer, 2002.

[12] M. Marquès, J.F. Pignatel, P. Saignes, F. D'Auria, L. Burgazzi, C. Müller, R. Bolado-Lavin, C. Kirchsteiger, V. La Lumia, and I. Ivanov. Methodology for the reliability evaluation of a passive system and its integration into a probabilistic safety assesment. *Nuclear Engineering and Design*, 235 :2612–2631, 2005.

[13] M. Marseguerra, R. Masini, E. Zio, and G. Cojazzi. Variance decomposition-based sensitivity analysis via neural networks. *Reliability Engineering and System Safety*, 79 :229–238, 2003.

[14] P. McCullagh and J.A. Nelder. *Generalized linear models*. Chapman & Hall, 1989.

[15] P. Ruffo, L. Bazzana, A. Consonni, A. Corradi, A. Saltelli, and S. Tarantola. Hydrocarbon exploration risk evaluation through uncertainty and sensitivity analysis techniques. *Reliability Engineering and System Safety*, 91 :1155–1162, 2006.

[16] J. Sacks, W.J. Welch, T.J. Mitchell, and H.P. Wynn. Design and analysis of computer experiments. *Statistical Science*, 4 :409–435, 1989.

[17] A. Saltelli. Making best use of model evaluations to compute sensitivity indices. *Computer Physics Communication*, 145 :280–297, 2002.

[18] A. Saltelli, K. Chan, and E.M. Scott, editors. *Sensitivity analysis*. Wiley Series in Probability and Statistics. Wiley, 2000.

[19] A. Saltelli, M. Ratto, T. Andres, F. Campolongo, J. Cariboni, D. Gatelli, M. Salsana, and S. Tarantola. *Global sensitivity analysis - The primer*. Wiley, 2008.

[20] A. Saltelli, S. Tarantola, and K. Chan. A quantitative, model-independent method for global sensitivity analysis of model output. *Technometrics*, 41 :39–56, 1999.

[21] I.M. Sobol. Sensitivity estimates for non linear mathematical models. *Mathematical Modelling and Computational Experiments*, 1 :407–414, 1993.

[22] I.M. Sobol. Global sensitivity indices for non linear mathematical models and their Monte Carlo estimates. *Mathematics and Computers in Simulation*, 55 :271–280, 2001.

[23] S. Tarantola, N. Giglioli, N. Jesinghaus, and A. Saltelli. Can global sensitivity analysis steer the implementation of models for environmental assesments and decision-making ? *Stochastic Environmental Research and Risk Assesment*, 16 :63–76, 2002.

[24] E. Volkova, B. Iooss, and F. Van Dorpe. Global sensitivity analysis for a numerical model of radionuclide migration from the RRC "Kurchatov Institute" radwaste disposal site. *Stochastic Environmental Research and Risk Assesment*, 22 :17–31, 2008.

[25] S. Wood. *Generalized Additive Models : An Introduction with R*. CRC Chapman & Hall, 2006.

[26] I. Zabalza-Mezghani, E. Manceau, M. Feraille, and A. Jourdan. Uncertainty management : From geological scenarios to production scheme optimization. *Journal of Petroleum Science and Engineering*, 44 :11–25, 2004.

3. Review of spatial variability in Performance Assessments

Review of Spatial Variability in Performance Assessments

In contrast to engineered systems, the geosphere shows a strong spatial variability of facies, materials and material properties. Although this phenomenon can be interpreted as a specific type of (statistical) variability, it also results in (often considerable) uncertainties when describing and modelling a site and its hydrogeological setting. While the presence / absence of facies and their properties is often known at specific locations (outcrops, exploration drillings), the remaining larger part of the domain of interest remains unknown. Moreover, reducing uncertainties by means of drilling might result in adverse impacts on the safety functions to be performed by the geosphere and should therefore be planned with caution. Model assumptions can be made on the basis of borehole and outcrop interpretation, of geophysical measurements, but also on other (often called "soft") information, e.g., about site genesis. Such assumptions are either made "manually" based on expertise or by using mathematical models describing the evolution of a site. In both cases, however, the remaining uncertainties are not quantifiable.

Geostatistical methods provide means for uncertainty quantification but are rather weak with regard to the incorporation of "soft knowledge". Although it is recognised that the utilisation of geostatistical methods in hydrogeology might contribute to a consistent treatment of uncertainties in probabilistic safety assessments, most existing PAs are still based on manually-derived hydrogeological models. Some attempts to utilise geostatistical methods have been undertaken (e.g., (LaVenue, et al., 1992); (Zimmerman, et al., 1998); (Jaquet, et al., 1998), (Jaquet, et al., 2006); (Röhlig, et al., 2005); (Srivastava, 2007)), and these and other examples are compiled and compared.

1 General Remarks

In the frame of post-closure safety analyses for radioactive waste repositories several types of uncertainties have to be taken into account due to the complexity of the phenomena of concern and the large timeframes under consideration. During the last two decades, remarkable progress has been made in the development of deterministic and probabilistic methodologies for the treatment especially of parameter uncertainties, but also for the handling of scenario and model uncertainties. Provided that the uncertainties in question can be expressed using random variables in an adequate manner, probabilistic techniques generate estimates for the resulting uncertainties of performance indicators and give insight into the relevant processes by identifying key ("sensitive") entities. One of the advantages of such probabilistic techniques is their ability to fully explore the space of uncertain parameters and to widely cover possible parameter combinations.

It seems however conceptually difficult to address spatial variability of the geosphere and resulting uncertainties consistently in probabilistic safety assessments. Problems arise due to the wide variety of qualitatively different information sources (exploration drillings, outcrops, geophysics, knowledge of site genesis, pumping and tracer tests, etc.). Traditionally, models are derived "manually" from the available geological and hydrogeological information. This allows accounting for the variety of "soft" information and knowledge which is typical of geosciences but also causes a certain degree of subjectivity. In any case, the traditional approach usually results in one "best estimate" image of reality (or, at the most, in a very limited number of "variant" images). With the rapidly growing capacities and capabilities of electronic computing, it became manageable to derive geological and hydrogeological models of great complexity based on geomathematical algorithms. It became also feasible to generate a multitude of realisations for a model domain of concern which is an essential prerequisite for accounting for the associated uncertainties in probabilistic assessments.

In their review of methods Koltermann & Gorelick (Koltermann, et al., 1995) distinguish between

- structure-imitating methods,
- process-imitating methods, and
- descriptive methods,

the "traditional" approach belonging to the latter. Although the review is restricted to sedimentary basins, the categorisation seems to be applicable to crystalline formations as well.

According to (Koltermann, et al., 1995), structure-imitating methods comprise spatial statistical methods and sedimentation pattern methods. The former interpret reality as a realisation of a random function (of position), while the latter model the temporal evolution of sedimentation patterns, but without accounting for flow processes or transport of sediments. Statistical methods are able to produce best-estimates as well as series of realisations, both for so-called categorical (discrete) variables (indicating the presence or absence of stratigraphic, petrographic, hydrogeological, or other units) and continuous variables (for entities such as permeability or porosity). They can account for "hard" information coming, e.g., from

borehole logs. In contrast, sedimentation pattern methods generate single realisations (best estimates) for categorical variables based on "soft" information.

Process-imitating methods imitate either groundwater flow processes or geologic processes. Under the former category, summarise "aquifer model calibration methods", i.e., inverse approaches. There exists a variety of geologic process models, accounting for phenomena such as flow processes, transport of sediments, tectonics, climate changes, changes of sea level, etc. These models generate single realisations (best estimates) for continuous variables based on "soft" information.

In the opinion of the authors of this paper, the categorisation by (Koltermann, et al., 1995) is comprehensive although one might argue about details. E.g., it seems that sedimentation pattern methods are more closely related to geologic process models than to aquifer model calibration methods since both methods, sedimentation pattern methods as well as geologic process models, attempt to model site generation while aquifer model calibration models are concerned with a different kind of process (groundwater flow). Moreover, aquifer model calibration models in most cases do not work from scratch but require the existence of an initial model which has to be generated by means of one of the other methods as, e.g., in (Zimmerman, et al., 1998).

Given the specific context of our work (performance and safety assessment), we suggest a categorisation somewhat deviating from (Koltermann, et al., 1995) with regard to statistical methods. There, a distinction between Kriging, Gaussian, and non-Gaussian methods (the latter comprising indicator methods, simulated annealing, Boolean methods, and Markov chains). We propose to distinguish either

- by the type of result to be produced ([best] estimate vs. multiple realisations), or
- by the underlying models for the random functions in use.

In the latter case, models such as

- spatial co-variance / variogram ("classical" geostatistics),
- objective functions (simulated annealing),
- marked point processes (Boolean models, e.g. fracture networks), and
- transition probabilities (Markov chains)

can be identified.

In this study we have compiled a list of articles and reports dealing with geostatistical methods in the light of performance assessment. We focused on methods with the potential to account for variability and resulting uncertainty in probabilistic analyses, i.e., on the statistical methods in Koltermann & Gorelick's categorisation. Nevertheless, not all of the reports and articles reviewed explicitly strive for feeding probabilistic analyses.

Both estimate (kriging) and multiple realisation methods (simulation) are considered. The underlying models are either of the variogram type with the objective of estimating and/or simulating spatial distributions of facies and/or parameters or Boolean with the objective of

simulating fracture networks. Upscaling methods have been comprehensively dealt with else-where in PAMINA's work package 2.2.D (Milestone 2.2.D.2).

We connect the considered reports with the safety functions related to the layout of the repository under consideration. All papers discuss the modelling of the groundwater flow, so that the safety function under consideration is the delay or attenuation of radionuclide migration in the host rock or the overburden. We also study if the articles deal with a normal evolution scenario or with alternative scenarios (glaciation, leakage, human intrusion by drilling through the repository). A third item of attention is whether validation / calibration techniques have been applied to strengthen the confidence in the used model.

In the reviewed papers, the following three approaches can be identified to model the spatial variability and heterogeneity:

- Direct simulation of hydraulic conductivity, sorption, etc.
- Distribution of strata (binary approach): clay / silt, sand / salt, etc.
- Simulation of fracture networks

These approaches may be mixed to form realistic models. For example, first a material type is determined per grid element, and then the material properties are varied within certain boundaries prescribed by the material type. Or, lower-dimensional fracture networks are included in an otherwise continuous porous media model.

2 Compilation of examples

With the rapid development of computing power in the last decades the usage of geostatistically generated distributions of permeabilites or transmissivities in hydrogeological models became more and more practicable (Delhomme, 1979), (Ahmed, et al., 1987), (Gelhar, 1993), (Gutjahr, et al., 1993). Although the potential of these methods for the assessment of the log-term safety of repositories was known (Bonano, et al., 1993), steps into the development of such an approach were only taken reluctantly. As a notable exception, the studies conducted within the WIPP project take up this development. Remarkably, the performance assessments conducted within the licensing process were based on probabilistic calculations of geostatistical models, see Section 2.1.

Geostatistical methods were also used in studies for locations in Sweden (Section 2.3), Switzerland and France (Section 2.4). Studies conducted in Germany at the Gorleben site are considered in Section 2.2. For literature on the simulation of fracture networks carried out for locations in Sweden, Belgium, and Canada see Section 2.5.

An overview of the studied literature can be found in the table below.

Reference	Location	Target	Remarks
(Porter, et al., 1997), (Röhlig, 1999)- (Röhlig, et al., 2005)	Gorleben (Salt): – sedimentary overburden	Modelling of heterogeneities Handling of incomplete geospatial knowledge	Geostatistics 3D, modelling 2D vertically, scale 10^4 x 10^2 m^2, stepwise integration of different information types, probabilistic for fresh water calculations, iterative approach to density flow
(LaVenue, et al., 1992), (LaVenue, et al., 1995), (Capilla, et al., 1998), (Beauheim, et al., 2007)	WIPP (Salt): overlying beds	Modelling of heterogeneities Handling of incomplete geospatial knowledge Derivation of local sensitivities regarding ground water travel times $\rightarrow$ location of new wells	2D horizontally, scale 10^4 x 10^4 m^2, probabilistic in licensing procedure (US DOE, 1996), (US DOE, 2004), later works not for compliance, but for supporting geological understanding in the safety case, calibration with ground water heads
(Jaquet, et al., 1998)	Wellenberg: claystone	Handling of incomplete geospatial knowledge	3D, scale 10^3 x 10^3 x 10^3 m^3, "probabilistic" (12 realisations)
(Deraisme, et al., 2004), (Jaquet, et al., 2003), (Jaquet, et al., 2006)	Äspö: crystalline	Modelling of heterogeneities	3D, scale 10^5 x 10^4 x 10^3 m^3, density dependent flow, used for licensing in (Auqué, et al., 2006), (SKB, 2006)

Reference	Location	Target	Remarks
(Jaquet, et al., 1999)	Site du Gard: clay and over-lying cretaceous deposits	Modelling of heterogene-ities	3D, scale 10^4 x 10^4 x 10^3 m^3
(Xu, et al., 2000), (Wörmann, et al., 2003)	Äspö: crystal-line	Modelling of heterogene-ities	1D calculation of migra-tion, scale $10^{-3}...10^{-2}$ m
(Huysmans, et al., 2005)	Mol: Boom Clay (ductile)	Modelling of heterogene-ities in the host rock in-cluding fracturing of the EDZ	Simplified 3D-model (symmetry assumption) for calculation of migration, scale 10^1 x 10^1 x 10^2 m^3
(Srivastava, 2007)	Hypothetical Canadian crys-talline site	Modelling of large scale fractures (based on statistics of the Canadian Shield, un-certainty considerations planned for several realisa-tions)	3D, scale 84 km^2 x 1,5 km
(Park, et al., 2004), (Park, et al., 2005)	Whiteshell / Lac du Bonnet: crystalline	Derivation of spatially varying effective properties for fractured material Prediction of tracer test results	Scale 50 m x 50 m x 50 m, calibration of conductivities, porosity, dilution by categorical Markov-realisations
(McKenna, 2001)	MIU, Japan: crystalline	Modelling of heterogeneities	3D, scale 10^3 x 10^3 x 10^3 m^3
(Iooss, 2008)	Moscow: sands and clays	Modelling of heterogene-ities Sensitivity analysis	Scale 250 m × 350 m, 3 vertical layers

2.1   WIPP (overburden of a repository in bedded salt)

A series of articles spanning more than a decade deals with the Waste Isolation Pilot Plant (WIPP). The earlier works (LaVenue, et al., 1992), (Jackson, 1995), (Larsson, et al., 1997), (Capilla, et al., 1998), (LaVenue, et al., 1995) model the porosity of the Culebra dolomite layer with the help of several geostatistical methods which are derived in the associated theo-retical parts (Gómez-Hernández, et al., 1997), (Capilla, et al., 1997), (RamaRao, et al., 1995). The dolomite layer is the assumed main pathway for contaminated brines in a human intru-sion scenario. This scenario postulates drilling through the repository that is located below the dolomite layer in a halite layer of the Salado formation. Hence all reports of this section are concerned with a human intrusion scenario in which contaminated brine enters a highly frac-tured dolomite layer.

The Sandia report (LaVenue, et al., 1992) studies conditionally simulated (CS) transmissivity fields. The grid consists of 50×57×1 (x/y/z) grid blocks and has a finer grid in the central portion of the model. Grid-block dimensions range from 50m near the center of the site to approximately 2800m at the model boundary spanning an overall region of 25km×30km. Particle tracking for 70 different realisations of the transmissivity field was used to determine the most likely travel path out of the WIPP repository.

In (LaVenue, et al., 1995), this approach is extended by using the Pilot Point method of (RamaRao, et al., 1995). Conditionally simulated (CS) transmissivity fields are simulated for the previously described grid. The CS fields are calibrated with measured heads data. For each of these 70 CS fields the groundwater travel path and travel time were calculated for a point located within the WIPP boundary. To reduce the uncertainty of the model suggestions for the location of further boreholes are made.

The article (Capilla, et al., 1998) uses the self-calibrated method developed in (Gómez-Hernández, et al., 1997), (Capilla, et al., 1997) to create equally likely realisations of transmissivity fields conditional to transmissivity measurements and to steady-state head data. The simulation grid corresponds to the same area considered in the above-mentioned study. Confined groundwater flow has been simulated using finite-differences over a 61×43 mesh of square blocks of 500m×500m. Particle-tracking was used to determine travel times of 300 realisations for different scenarios.

The available data from the WIPP was also used in (Jackson, 1995) where studies of five different teams from the INTRAVAL project are considered. These results are also presented in section 4.5 of (Larsson, et al., 1997). In different stochastic approaches the transmissivity of the Culebra layer was modelled. The measured heads were in most cases not included in the model, but compared with the computed values. The AEA project team considered four different stochastic models, the model with an exponential covariance structure was studied in detail. Bi-quadratic finite elements were used on a 40×60 grid. The UPV project team generated realisations using sequential simulation, a predecessor of the self-calibrated method of (Gómez-Hernández, et al., 1997). Both transmissivity data and heads data are used for modelling. Pathlines for 300 realisations are tracked for particles starting near the center of the WIPP site. The AECB project team chose a model in which the transmissivity distribution was calibrated against the transient head data as a base model. They considered model variants with increased salinity or with freshwater everywhere. The finite-difference code works on a 2D grid with 1344 blocks. The BGR project team considered a vertical cross-section through the model area. The SNL project team explored the use of a 3D model to study the importance of vertical flow between the Culebra Dolomite and the overlying units. This model has 15 layers to model 10 stratigraphic units.

Another collection of different methods is presented in the article (Zimmerman, et al., 1998) which discusses many of the used geostatistical algorithms presented in earlier WIPP articles. These algorithms have been tested on synthetic data (producing a "WIPP-like" scenario). The results have been compared with each other. This article comes to the conclusion that good results depend to a lesser extent on the type of used geostatistical method and much more on a good model (i.e., choice of variogram).

The article (Beauheim, et al., 2007) deals with the absence/presence of a halite layer above the dolomite layer, which indicates if the dolomite is washed-out and therefore fractured or if the layer is intact and therefore has a low permeability. Without this halite indicator, some of the data obtained from the wells would contradict a stationary variance assumption which has already been reported in (Capilla, et al., 1998) and in the UVP study of (Jackson, 1995).

The WIPP Compliance Certification Application and the Compliance Recertification Application (US DOE, 1996), (US DOE, 2004) both use geostatistical methods to predict the ground water flow and radionuclide migration through the repository via particle tracking.

2.2 Sedimentary overburden of the Gorleben site (salt dome)

The INTRAVAL report (Porter, et al., 1997), the Federal Ministry of Environment's (BMU) reports (Röhlig, 1999), (Röhlig, et al., 2000), (Röhlig, et al., 2001), and the article (Röhlig, et al., 2005) consider the overburden of the Gorleben salt dome which is a proposed site for a repository of heat-generating high level waste in Germany.

The considered domain in (Porter, et al., 1997) is a 2D model of a vertical cut along the so-called Gorleben erosion channel. A nonlinear transformation takes the stratigraphic data into account that is available in form of borehole logs. The clay distribution in the sedimentary overburden is modelled via indicator kriging. The cross-section is 4km long and 200m deep. A 20×50 grid is used. Note that the vertical resolution into 50 intervals is relatively dense in order to respect the stratigraphy derived from the borehole data.

In the subsequent GRS articles instationary indicator simulation is used to generate realisations for facies distributions and superimposed parameter distributions. Three dimensional studies involving the spatial variability of the thickness of clay-layers accompany the 2D model of the erosion channel overburden. Density-driven flow and radionuclide migration is calculated for the realisations and the results of the former are compared to salinity profiles measured on-site.

These approaches are not relevant for a normal evolution scenario, they are only of interest if geological and geotechnical barriers in the salinary host rock fail and particles are released into the overburden.

2.3 SKB glaciation studies (crystalline)

The reports (Svensson, 1999), (Jaquet, et al., 2003), (Jaquet, et al., 2006) consider the influence of an ice sheet located over the proposed repository on the groundwater flow and on the salinity of the water. Major fracture zones are included in the computer models. In (Svensson, 1999), the computational domain of the area around the Äspö Hardrock Laboratory has a size of 250km×10km×4km (length/width/depth) which gives 250×50×47 cells with non-uniform spacing. The hydraulic conductivity is generated on a per-cell-basis with no correlation between the cells. Cell wall conductivities are calculated as geometric means of adjacent cells and then modified to take the effects of fracture zones into account. Particles released directly below the ice sheet are tracked for at most 600 years.

The report (Jaquet, et al., 2003) extends the results of (Svensson, 1999). Some parameters and boundary conditions differ from the previous study as newly available information has been integrated, but the domain geometry (location of the ice channels and the glacier) and processes remain identical. A different software package using finite element methods replaces the finite volume code. Hydraulic properties are estimated using variograms which are based on regional experiments. The maximum time scale for tracked particles is lowered to 122 years. The porosity has proven most influential in reducing the time scale by factor 10 at which salt transfer occurs when compared with the previous study.

In the third report (Jaquet, et al., 2006) the set of governing equations modelling the physical processes are slightly modified, the salt transport now includes the effects of rock-matrix diffusion. The model domain contains now the Simpevarp region for which a detailed map of deformation zones is available. This regional model has a width of 21.6km and height of 13km. This height is extended for the glaciation model about 300km upstream and 100km downstream. The depth of the glaciation model is 2.3km. The 3D mesh has a horizontal resolution of 100m/300m (inside/outside the Simpevarp model area) and the vertical resolution corresponds to a global discretisation of 100m giving 3.3 million cuboid finite elements. The hydraulic conductivity and porosity outside the Simpevarp model area were estimated using a turning-bands method based on the parameters from the model area. Moreover, fractures and moulins through the glacier are modelled so that the sub-glacial groundwater flow is fed not only by basal melt water but also by glacial surface melt water. This contrasts to earlier studies where the ice channels are prescribed. Furthermore, the built-up and melt-down of the ice-sheet have been simulated. A tracking of particles starting in a depth of 500m results in average travel times of 2200 years until the surface is reached. This travel time is drastically reduced during phases of glacial build-up and retreat.

A glaciation period is considered part of the normal evolution and hence results derived from these computational experiments have direct impact on the performance assessment for this scenario.

2.4   Studies in argillaceous rock formations

The report (Jaquet, et al., 1998) studies the groundwater flow through the (in the meantime rejected) repository in Wellenberg marlstone. The questions under consideration are in which way the groundwater flow is modified by setting up a deep-underground repository and in which time-scales the undisturbed flow is re-established. To answer these questions a 3D model of the Wellenberg Mountain is considered in which hydraulic conductivity is split into a linear drift term and a kriged residual. As a result of the simulations the resaturation of the repository structure after closure takes between 400 and 29000 years. The model covers a 40km^2 area and uses volume elements of 100m side length which results in a model of 425000 nodes. Representative tectonic faults are modelled by 2D elements. Six deep boreholes were used for hydraulic tests. These results are used for calibrating a linear drift model.

A study of the Gard site in France which had been investigated in the course of the French disposal program was conducted in (Jaquet, et al., 1999). The used model follows the above mentioned design of linear drift plus a random perturbation. Data from three boreholes were available for the study. The Gard site was given up by the French government in late 1998.

In Mol, the Belgian nuclear repository program is characterizing the host rock capacities of the Boom Clay. Some of the results are reported in (Huysmans, et al., 2005). The models under consideration include simulations of hydraulic conductivity via kriging and of fractures using Monte-Carlo methods. The local hydrogeological model has a size of 20m×15m×102m (x/y/z) with a grid spacing of 1m×0.17m×(0.2m to 1m). The results of the simulation differ only slightly from the results obtained by a simple homogeneous model.

The German Federal Office for Radiation Protection Agency (Bundesamt für Strahlenschutz) is conducting a study on the effectivity of barrier systems. In this context, the report (Colenco, 2007) applies geomathematical methods to examples in claystone (Callovo-Oxfordian and Opalinus). 2D permeability on a 1m×1m scale is simulated using a variogram model based on experimental data. In 3D, three mineral fractions are estimated for volumes of 1m×1m×1m and of 100m×200m×100m to study model upscaling. Different mineral fraction have been overlaid which different permeabilities.

2.5   Fracture Networks

In the glaciation reports considered above, the fracture topology of the region under consideration has been included in the model. There are other studies which are devoted to the study of simulating fracture networks. Examples which also consider the Äspö area are found in the article (Xu, et al., 2000) and the SKI report (Wörmann, et al., 2003). In the article (Xu, et al., 2000), a 1D solute transport model is derived based upon exponentially determined auto-covariance functions for fracture aperture and advective velocity along a trajectory. A 2D model is presented and trajectory paths for this model are simulated on a 1m×1m domain. The report (Wörmann, et al., 2003) analyses the radionuclide transport in rock fractures. It considers a 3D discrete fracture model in which a Monte-Carlo technique accounts for the randomness of the fracture network. The solute transport is computed by a 1D-code which allows for uncertainties in the parameters of the underlying partial differential equations. Moreover, the spatial variability of the host rock is honored by semi-variograms taken from data collected on-site. A demonstration case for the 3D model is based on a 5km×5km area with depth of 1km. Results for the 3D model are compared with results from the 1D model for which suitable parameters were extracted from the 3D model.

The following three studies consider the Whiteshell research area located in crystalline rock formations in the Canadian Shield. In (Park, et al., 2004) and (Park, et al., 2005) a porous media approximation model was calibrated with data from experiments conducted in AECL's Underground Research Laboratory. Transition probabilities between different material types (sparsely/moderately/highly fractured rocks) have been used for Monte-Carlo simulation. Realisations from this model were used to predict results from other experiments. The experimental area has a size of 58m×58m×50m (x/y/z). In (Srivastava, 2007), Sequential Gaussian Simulation (SGS) is applied to geometric attributes on an irregular grid to create a fractured zone. First, strike directions and length (using information from observed fractures) are determined via SGS on a 2D grid to create the surface traces of the network. After this simulation has completed, the propagation to depth into a 3D model is performed, again using SGS. With this procedure, fracture networks for regions with ground cover and lakes have been simulated on the basis of data from the Surface Lineament Database for the AECL's Whiteshell Research. An area of 50km×40km was studied with a depth of over 850m. The

probability of intersecting a fracture at different depths has been computed with a set of 100 fracture network models.

2.6 Other studies

The SANDIA report (McKenna, 2001) considers the host rock of the Mizunami Underground Research Laboratory (MIU) (crystalline rock) in Japan. A volume of 464m×664m×962m (x/y/z) is discretised into blocks of 8m×8m×6.5m. This size matches the interval length of the conducted packer tests to measure the hydraulic conductivity. 14 borehole data were used in the study. Five additional datasets were used to perform model validation. The hydraulic conductivity is estimated via variograms.

The report (Iooss, 2008) studies the contamination and spread of Strontium-90 on the disposal site of the Russian Research Center "Kurchatov Institute" where waste packages have been flooded by leaking sewage waters. The study uses geostatistical simulations for the distribution of a coarse sand layer which influences the radionuclide transport. The model domain is 250m×350m, with a discretisation of 5m×m. Three vertical layers have been chosen in accordance with filtration and migration characteristics of the sands in the upper aquifer. A sensitivity analysis is carried out for the results of the simulation. To ease the computational burden of this analysis, meta-models are used instead of full model runs.

3   Discussion

Geospatial methods are used to increase the levels of confidence in the used modelling process, either by showing that a model can cope with variations in the geospatial layout or by verifying that already a simpler model (i.e. a model based on the "conventional/manual" descriptive approach) reflects all the important factors from a complex model. See Section 3.1 for more details.

Many of the cited articles are only indirectly connected to performance assessments; they support the local geological understanding for use in a safety case. Reports with direct impact on a safety case are mentioned in Section 3.2.

In recent years, more emphasis is put on the role of safety functions in the performance assessments. Safety functions are used to classify FEPs and to derive alternative scenarios. The connection of safety functions to geospatial variability is investigated in Section 3.3.

The role of the methods investigated in relation to probabilistic safety assessments and their potential of contributing to a safety case is briefly discussed in Section 3.4.

3.1   Reliability of models

In any scientific discussion, results including unresolved issues and newly occurring questions are fed back into the scientific community. The same holds for the stepwise evolution of a repository programme and the associated safety case. The use of methods which involve geospatial variability has the benefit of verifying or questioning possible spatial parameter distributions, proving or disproving assumptions made upon nominal models, etc., especially when combined with experimental data. For the WIPP, the locations of new boreholes were suggested via geostatistical studies so that the largest local uncertainty would be reduced. In the SKB glaciation studies questionable results are replaced by new model approaches in later reports.

An integration of these results into a research and development cycle is important for the scientific and public acceptance of the used modelling process. The usage of all available measurement data also improves the quality of computational models.

As another field of application, geospatial methods are used to test whether the output from a complex model is more meaningful than the output from a simple model. In the Boom Clay study (Huysmans, et al., 2005), it was shown that a simple transport model faithfully reproduces the output from the more complex model which also includes fracture network simulations. In the study (Wörmann, et al., 2003), parameters for a 1D transport model were derived from a complex 3D model.

3.2   Connection to recent safety cases

In the WIPP Compliance Recertification Application (US DOE, 2004), the article (LaVenue, et al., 1990) is referred to as source for the Culebra flow and transport model. This article is also the basis for the subsequent reports (LaVenue, et al., 1992), (LaVenue, et al., 1995).

The study (Jaquet, et al., 2006) is cited in the SR-Can climate reports (Auqué, et al., 2006) and (SKB, 2006). Here the glaciation scenario is part of the standard scenario.

The Belgian SAFIR-2 report (ONDRAF/NIRAS, 2001) predates the article (Huysmans, et al., 2005), however the investigation of fracture networks is formulated in SAFIR-2 as an active area of research. In the same way, the study of fracture network models as in (Srivastava, 2007) is part of Ontario Power's nuclear waste management research and development program, see the Annual Report 2006 (Ontaria Power Generation, 2007).

The Swiss Entsorgungsnachweis (nagra, 2002) mentions no geostatistical methods, only probabilistic parameter studies. The international review team states in (NEA, 2004) that other national projects place more emphasis on probabilistic analysis. For the Swiss legislator, see (BFE, 2008), one criteria group for the site evaluation regarding safety and technical feasibility is the reliability of geological statements, which might be backed up by geostatistical studies in a forthcoming safety report.

3.3   The role of safety functions

With respect to performance assessment, the articles considered in this report only deal with issues related to the safety function of "delay or attenuation of radionuclide migration in the host rock or the overburden" while other safety functions like "containment" or "(mechanical/ chemical / thermodynamical /hydraulical / geological) stability" are not connected to issues of spatial variability. Maybe the study of glacial built-up and retreat can be subsumed under the study of the safety function "hydraulical stability".

The use of spatially varying parameters may, however, also be of interest when addressing the safety function "mechanical stability" by conducting geomechanical computations. This approach is not used in the reviewed literature. Presently, stress-strain calculations are usually based on the assumption of a limited number of homogeneous domains (e.g. vault, excavation disturbed zone EDZ, undisturbed host rock). The introduction of heterogeneities in these domains might have a significant impact on the mechanical performance and should therefore be investigated.

3.4   Probabilistic safety assessments: Addressing spatial variability in a safety case

Simulation (both variogram-based and Boolean) has the potential of representing uncertainties caused by spatial variability in an integrated probabilistic safety assessment model which might be either requested by regulation and/or be used to explore the space of conceivable parameter configurations as comprehensively as possible in order to gain better system understanding. Although it is recognised that the utilisation of geostatistical methods in hydrogeology might contribute to a consistent treatment of uncertainties in probabilistic safety assessments (Bonano, et al., 1993), most existing safety assessments are still based on the "manual" approach even though some attempts to utilise geostatistical methods have been undertaken. The only case of directly using such methods in the integrated modelling for probabilistic

safety assessments the authors are aware of is the WIPP project where the regulation was a strong driver for doing so.

Over the last years, safety assessments and safety cases became increasingly focussed on safety functions. Hydrogeological modelling as a means for consequence calculations got decreasing weight in those concepts where host rock performance (containment or migration delay and attenuation) was paramount. The authors are nevertheless of the opinion that safety cases

- should discuss spatial variability with regard to its potential of influencing or jeopardizing the safety functions claimed,
- investigate, where necessary, its impact as discussed in Section 3.1, and
- either justify its omission in assessments or explicitly account for it.

The review presented here demonstrates that the means of doing so are available. These remarks are not restricted to the traditional application area of hydrogeological and migration modelling, but might, dependent on the safety concept, well be valid for other areas.

4   Bibliography

Ababou, R., Sagar, B. and Wittmeyer, G. 1992. Testing procedures for spatially distributed flow models. *Advances in Water Resources.* 1992, Vol. 15.

Ahmed, S. and de Marsily, G. 1987. Comparison of geostatistical methods for estimating transmissivity using data on transmissivity and specific capacity. *Water Resour. Res.* 1987, Vol. 23(9), p. 1717-1737.

Auqué, L. F., et al. 2006. *Groundwater chemistry around a repository for spent nuclear fuel over a glacial cycle - Evaluation for SR-Can .* Stockholm : Svensk Kärnbränslehantering (SKB), 2006. TR-06-31.

Beauheim, R. L., et al. 2007. *Geoscientific data collection and integration for the waste isolation pilot plant.* Toronto : OECD NEA, 2007.

BFE. 2008. *Sachplan geologische Tiefenlager.* Bern : Bundesamt für Energie, 2008.

Bonano, E. J. and Thompson, B. G. J. 1993. Guest Editorial. *Reliability Engineering & System Safety.* 1993, Vol. 42(2-3), p. 103-109.

Capilla, J. E., Gómez-Hernández, J. J. and Sahuquillo, A. 1997. Stochastic simulation of transmissitivity fields conditional to both transmissivity and piezometric data - 2. Demonstation on a synthetic aquifer. *Journal of Hydrology.* 1997, Vol. 203.

—. 1998. Stochastic simulation of transmissitivity fields conditional to both transmissivity and piezometric data - 3. Application to the Culebra Formation at the Waste Isolation Pilot Plant (WIPP), New Mexico, USA. *Journal of Hydrology.* 1998, Vol. 207.

Colenco. 2007. *TA5: Ableitung von Anforderungen zur Reduzierung von Modell- & Datenunsicherheiten bei Anwendung geomathematischer Methoden.* Bundesamt für Strahlenschutz, 2007. FKZ SR 2470A.

Delhomme, J. P. 1979. Spatial Variability and Uncertainty in Groundwater Flow Parameters: A Geostatistical Approach. *Water Resources Research.* 1979, Vol. 15(2).

Deraisme, J., Jaquet, O. and Jeannée, N. 2004. Uncertainty management for environmental risk assessment using geostatistical simulations. [Buchverf.] X. Sanchez-Vila, J. Carrera and J. J. Gómez-Hernández. *geoENV IV - Geostatistics for Environmental Applications.* Dordrecht : Kluwer Academic, 2004.

Gelhar, L. W. 1993. *Stochastic Subsurface Hydrology.* Englewood Cliffs, New Jersey : Prentice Hall, 1993.

Gómez-Hernández, J. J., Sahuquillo, A. and Capilla, J. E. 1997. Stochastic simulation of transmissitivity fields conditional to both transmissivity and piezometric data - 1. Theory. *Journal of Hydrology.* 1997, Vol. 203.

Gutjahr, L. and Bras, R. L. 1993. Spatial variability in subsurface flow and transport: a review. *Reliability Engineering & System Safety.* 1993, Vol. 42(2-3).

Huysmans, M., Berckmans, A. and Dassargues, A. 2005. Simulation of radionuclide mass fluxes in a heterogeneous clay formation locally disturbed by excavation. In: **P. Renard, H. Demougeot-Renard and R. Froidevaux.** *Geostatistics for Environmental Applications.* Berlin : Springer, 2005.

Iooss, B. 2008. *Treatment of spatially dependent input variables in sensitivity analysis of model output methods.* PAMINA - European Commission, 2008.

Jackson, C. P. 1995. *The WIPP-2 Test Case.* Harwell : AEA Technology, 1995.

Jaquet, O. and Siegel, P. 2003. *Groundwater flow and transport modelling during a glaciation period.* Stockholm : Svensk Kärnbränslehantering AB, 2003.

—. 2006. *Regional groundwater flow model for a glaciation scenario.* Stockholm : Svensk Kärnbränslehantering (SKB), 2006. SKB R-06-100.

Jaquet, O., et al. 1998. *Modelling of Groundwater Flow at Wellenberg Using Monte Carlo Simulations.* Materials Research Society, 1998.

Jaquet, O., et al. 1999. *Site du Gard: Hétérogénéités, simulations géostatistiques et modélisation hydrodynamique.* Foutainebleau : Centre de Géostatistique, 1999.

Koltermann, C. E. and Gorelick, S. M. 1995. Heterogeneity in sedimentary deposits: A review of structure-imitating, process-imitating and descriptive approaches. *Water Resource Research.* 1995, Vol. 32(9).

Larsson, A., Pers, K., Skagius, K. and Dvenstorp, B. 1997. *The international INTRAVAL Project. Phase 2: Summary report.* Paris : OECD-NEA, 1997.

LaVenue, A. M. and RamaRao, B. S. 1992. *A Modelling Approach to Address Spatial Variability within the Culebra Dolomite Transmissivity Field.* Albuquerque : Sandia National Laboratories, 1992. SAND92-7306.

LaVenue, A. M., et al. 1995. Pilot Point Methodology for Automated Calibration of an Ensemble of Conditionally Simulated Transmissivity Fields 2. Application. *Water Resources Research.* 1995, Vol. 31(3).

LaVenue, A.M., Cauffman, T.L. and Pickens, J.F. 1990. *Ground-Water Flow Modeling of the Culebra Dolomite: Volume 1 - Model Calibration.* Albuquerque : Sandia National Laboratories, 1990. SAND89-7068/1.

McKenna, S. A. 2001. *Probabilistic Approach to Site Characterization: MIU Site, Tono Region, Japan.* Albuquerque : Sandia National Laboratories, 2001.

nagra. 2002. *Project Opalinus Clay - Safety Report.* Wettingen : nagra, 2002. Technical Report NTB 02-05.

NEA. 2004. *Die Sicherheit der geologischen Tiefenlagerung von BE, HAA und LMA in der Schweiz - Eine internationale Expertenprüfung der radiologischen Langzeitsicherheitsanalyse der Tiefenlagerung im Opalinuston des Zürcher Weinlands.* Paris : OECD, 2004. NEA No. 5569.

ONDRAF/NIRAS. 2001. *Technical overview of the SAFIR 2 report - Safety Assessment and Feasibility Interim Report 2.* s.l. : ONDRAF/NIRAS, 2001. NIROND 2001–05 E.

Ontaria Power Generation. 2007. *Technical Research and Development Program for Long-Term Management of Canada's Used Nuclear Fuel - Annual Report 2006.* Toronto : Ontario Power Generation, 2007. No. 06819-REP-01200-10163-R00.

Park, Y.-J., et al. 2004. Analysis of Hydraulic and Tracer Response Tests within Moderately Fractured Rock Based on a Transition Probability Geostatistical Approach. *Water Resource Research.* 2004, Vol. 40.

—. 2005. *Moderately Fractured rock experiment: Modelling flow and transport using a transition probability based geostatistical approach.* Toronto : University of Waterloo, 2005. No. 06819-REP-01300-10077-R00.

Porter, J. D. and Hartley, L. J. 1997. *The treatment of uncertainty in groundwater flow and solute transport modelling.* Luxembourg : European Commision, 1997. Report EUR17829EN.

RamaRao, B .S., et al. 1995. Pilot point methodology for automated calibration of an ensemble of conditionally simulated transmissivity fields. 1. Theory and computational experiments. *Water Resources Research.* 1995, Vol. 31(3).

Röhlig, K.-J. and Pöltl, B. 2001. Uncertainty and Sensitivity Analyses for Contaminant Transport Models Based on Conditional Indicator Simulations. *geoENV 2000 "3rd European Conference on Geostatistics for Environmental Applications, Avignon.* Dordrecht : Kluwer Academics, 2001.

—. **2001.** *Unsicherheits- und Sensitivitätsanalysen für Grundwasser- und Schadstofftransportmodelle mit räumlich variierenden Parametern.* BMU-Schriftenreihe Reaktorsicherheit und Strahlenschutz, 2001. BMU-2001-589.

—. **2000.** *Unsicherheits- und Sensitivitätsanalysen für Grundwasser- und Transportmodelle auf der Basis geostatischer Untersuchungen.* BMU-Schriftenreihe Reaktorsicherheit und Strahlenschutz, 2000. BMU-2000-551.

Röhlig, K.-J. 1999. *Zur räumlichen Variabilität an Standorten für Endlager radioaktiver Abfälle.* BMU-Schriftenreihe Reaktorsicherheit und Strahlenschutz, 1999. BMU-1999-529.

Röhlig, K.-J., Fischer, H. and Pöltl, B. 2005. Modeling density-dependent flow using hydraulic conductivity distributions obtained by means of non-stationary indicator simulation. In: **P. Renard, H. Demougeot-Renard and R. Froidevaux.** *Geostatistics for Environmental Applications.* Berlin : Springer, 2005.

SKB. 2006. *Climate and climate-related issues for the safety assessment SR-Can.* Stockholm : Svensk Kärnbränslehantering (SKB), 2006. TR-06-23.

Smith, L. and Schwartz, F. W. 1981. *The role of hydraulic conductivity data in reducing uncertainty in radionuclide transport modeling.* 1981.

Srivastava, R. M. 1995. An Overview of Stochastic Methods for Reservoir Characterization. In: **J. M. Yarus and R. L. Chambers.** *Stochastic Modeling and Geostatistics.* American Association of Petroleum Geologists, 1995.

—. **2007.** *Fracture network modelling: An integrated approach for realisation of complex fracture network geometries.* Toronto : OECD NEA, 2007.

Svensson, U. 1999. *Subglacial groundwater flow at Äspö as governed by basal melting and ice tunnels.* Stockholm : Svensk Kärnbränslehantering (SKB), 1999. SKB R-99-38.

The Probabilistic Assessment Group. 1997. *History and Achivement 1985-1994.* Paris : OECD NEA, 1997.

US DOE. 1996. *1996 WIPP Compliance Certification Application.* US Department of Energy, 1996. http://www.wipp.energy.gov/library/CRA/BaselineTool/Index.htm.

—. **2004.** *2004 WIPP Compliance Recertification Application.* US Department of Energy, 2004. http://www.wipp.energy.gov/library/CRA/BaselineTool/Index.htm.

Wörmann, A., Geier, J. and Xu, S. 2003. *Modelling of Radionuclide Transport by Groundwater Motion in Fractured Bedrock for Performance Assessment Purposes.* Swedish Nuclear Power Inspectorate (SKI), 2003.

Xu, S., Wörmann, A. and Dverstrop, B. 2000. Heterogeneous matrix diffusion in crystalline rock - implications for geosphere retardation of migrating radionucides. *Contaminant Hydrology.* 2000, Vol. 1007.

Zimmerman, D. A., et al. 1998. A comparison of seven geostatistically based inverse approaches to estimate transmissitivities for modeling advective transport by groundwater flow. *Water Resources Research.* 1998, Vol. 34(6).

4. Plan for PA exercises to test techniques for upscaling

Introduction

Upscaling is the process by which information at the measurement scale (e.g. core samples) is transferred to a coarser scale given by the numerical model grid-blocks used in PA models. At present, upscaling techniques commonly used in current PA models and tools only consider the transfer of small-scale information to obtain grid-block parameter values. Then, the grid-block values are used to evaluate the uncertainty in the model predictions. In doing so, this approach considers that the uncertainty in the predictions estimated with the coarse model is the same as the one associated with the small-scale information. This suppresses the heterogeneity or spatial variability within grid-blocks, and may have a significant impact on the uncertainty in model predictions.

In other documents reported on the PAMINA project, the issue of upscaling, and its impact on the uncertainties of radionuclide transport in the geosphere, has been studied. Their objective was to make a review of experience and tools available to treat the upscaling of flow and transport parameters and to definite a set of exercises to evaluate the impact of upscaling on the uncertainty in PA for repositories in granite and clay host rocks.

The main objective of this work has been to assess the impact of upscaling on the uncertainty of the safety assessments of radioactive waste repositories in both granite and clay host rocks. The advantages and disadvantages of commonly used analyses in the treatment of uncertainties due to upscaling will be elucidated, and will lead to a set of guidelines for the treatment of this source of uncertainty.

In this document, a Plan to evaluate upscaling on PA exercises is presented. This Plan has been designed to be developed under those considerations included on the rest of the documents of PAMINA RTDC 2, WP 2.2.D, "State of the Art on Upscaling Techniques" and "Review of Spatial Variability in Performance Assesmment".

Available techniques for flow and transport parameters upscaling

Hydraulic conductivity upscaling is a process that transforms a grid of hydraulic conductivity defined at the scale of the measurements, into a coarser grid of block conductivity tensors amenable for input to a numerical flow simulator. The need for upscaling stems from the disparity between the scales at which measurements are taken and the scale at which aquifers are discretized for the numerical solution of flow and transport.

The techniques for upscaling range from the simple averaging of the heterogeneous values within the block to sophisticated inversions, after the flow equation at the measurement scale within an area embedding the block being upscaled.

All techniques have their own advantages and limitations. The definition of the geometry of the grid has been intimately linked to the upscaling problem; promising results have been obtained using elastic gridding. The need to perform Monte-Carlo analyses, involving many realizations of hydraulic conductivity, has steered the development of methods that generate directly the block conductivities in accordance with the rules of upscaling, yet conditional to the measurement data.

The alternatives taken into consideration for the upscaling of flow parameters are the following:

- Local techniques
- Non-local techniques
- Block Geometry
- Direct block-conductivity generation

There exist mainly two alternatives to perform transport parameters upscaling considering or not a Fickian approach. Under the fickian approach three different alternatives can be used:

- The stochastic approach
- Fractal models of heterogeneity
- Inclusion models

On the other hand, under the non-Fickian approach three alternatives are available:

- Continuous Time Random Walk Framework
- Advection-Dispersion Equation and Upscaling
- Alternative Effective Transport Formulations

On the following Plan to Evaluate Upscaling on PA Exercises a comprehensive list af alternatives is developed, so the use of the alternative used on the upcaling procedure could be justify. The Plan has been prepared on a fact-sheet form under a question-answer scheme so it can be easily completed after finishing the PA exercise. The main objective of this Plan is to provide a realistic view of how upscaling has been considered on the PA Exercise.

Plan to evaluate Upscaling on PA Exercises

PART 1.- General treatment of upscaling on the PA Exercise

1.- ¿Has been upscaling taken into account when first designing the modeling procedure?

☐ Yes

☐ No

2.- Specify the reasons why it was necessary/unnecessary to perform upscaling in the PA Exercise.

3.- ¿Have flow and transport parameters been upscaled?

☐ None of them

☐ Only flow parameters

☐ Only transport parameters

☐ Both of them

4.- Specify which of the flow parameters have been upscaled

5.- Specify which of the transport parameters have been upscaled

PART 2.- Upscaling of flow parameters

6.- If flow parameters upscaling has been developed, specify which one of the available techniques has been used:

- ☐ Local techniques
- ☐ Non-local techniques
- ☐ Block Geometry Methods
- ☐ Direct block-conductivity generation

7.- If local techniques have been used, specify which one of those available has been developed:

- ☐ Simple average
- ☐ Power average
- ☐ Renormalization
- ☐ Stream tube
- ☐ Flow anisotropy
- ☐ Other method (specify)

8.- If non-local techniques have been used, specify which one of those available has been developed:

- ☐ Simple laplacian
- ☐ Simple laplacian extended
- ☐ Laplacian using flow solution at the measurement scale over the entire aquifer
- ☐ Laplacian with skin
- ☐ Laplacian with periodic boundary conditions
- ☐ Non-parallel flow
- ☐ Analytical approaches
- ☐ Method of moments
- ☐ Energy dissipation
- ☐ Other method (specify)

9.- If Block Geometry Methods have been used, specify which one of those available has been developed:

- ☐ Elastic Grid
- ☐ Elastic Grid with flow variables
- ☐ Simplified elastic grid with flow variables
- ☐ Potential-streamfunction space discretization
- ☐ Other method (specify)

10.- If a Direct block-conductivity generation method has been used, specify which one of those available has been developed:

- ☐ Scalar block conductivities
- ☐ Training images
- ☐ Regularization
- ☐ Energy dissipation
- ☐ Other method (specify)

11.- Explain the reasons why a particular method for flow parameters upscaling has been used on the PA Exercise.

12.- Explain the reasons why the other methods for flow parameters upscaling available have not been considered in the PA Exercise.

PART 3.- Upscaling of transport parameters

13.- If transport parameters upscaling has been developed, specify which one of the available techniques has been used:

☐ Fickian approach

☐ Non-fickian approach

14.- If a Fickian approach has been developed, specify which one of the available techniques has been used:

☐ Stochastic approach

☐ Fractal models

☐ Inclusion models

☐ Other method (specify)

15.- If a non-Fickian approach has been developed, specify which one of the available techniques has been used:

☐ Continuous Time Random Walk

☐ Upscaling of the Advection-Dispertion equation

☐ Alternative effective Transport formulations

☐ Other method (specify)

16.- Explain the reasons why a particular method for transport parameters upscaling has been used on the PA Exercise.

17.- Explain the reasons why the other methods for transport parameters upscaling available have not been considered in the PA Exercise.

References

PAMINA Document M2.2.D.1. "Review of spatial variability in PA"

PAMINA Document M2.2.D.2. "State of the Art on Upscaling Techniques"

PAMINA Document M2.2.D.4. "Spatial variability – CEA Contribution"

Ababou, R. and Wood, E.F., 1990. Comment on "Effective roundwater model parameter values: Influence of spatial variability of hydraulic conductivity, leakage and recharge" by J.J. Gómez-Hernández and S.M. Gorelick, Water Resour. Res. 26(8): 1843-1846.

Aris, R., 1956. On the dispersion of a solute in a fluid flowing through a tube. Proc. R. Soc. London. Ser. A, 235: 67-77.

Bachu, S. and cuthiell, D., 1990. Effects of core-scale heterogeneity on steady state and transient fluid flow in porous media: Numerical analysis. Water Resour. Res., 26(5): 683-874.

Begg, S.H. and King, P.R., 1985. Modelling the effects of shales on reservoir performance: Calculation of effective vertical permeability. Paper SPE 13529.

Begg, S.H., Chang, D.M. and Haldorsen, H.H., 1985. A simple statistical method for calculating the effective vertical permeability of a reservoir containing discontinous shales. Paper SPE 14271.

Begg, S.H. and Carter, R.R., 1987. Assigning effective values to simulator grid-block parameter for heterogeneous reservoir. Paper SPE 16754.

Begg, S.H., Carter, R.R. and Dranfield, P., 1989. Assigning effective values to simulator gridblock parameters for heterogeneous reservoirs. SPE Reservoir Engineering, November: 455-463.

B∅e, ∅., 1994. Analysis of an upscaling method based on conservation of dissipation. Transport in Porous Media, 17(1): 77-86.

Bouwer, H., 1969. Planing and interpreting soil permeability measurements. J. of the Irrigation and Drainage Division of the A.S.C.E., IE(3): 391-402.

Brenner, H., 1980. Dispersion resulting from flow through spatially periodic porous media. Philos. Trans. R. Soc. London, Ser. A, 297 (1498): 81-133.

Cardwell, W.T. and Parsons, R.L., 1945. Averaging permeability of heterogeneous oil sands. Trans. Am. Inst. Min. Metall. Pet. Eng., 160: 34-42.

Clifton, M.P. and Neuman, S.P., 1982. Effect of kriging and inverse modelling on conditional simulation of the Avra Valley aquifer in Southern Arizona. W.R.R., 18(4): 1215-1234

Dagan, G., 1979. Models of groundwater flow in statistically homogeneous porous formations. W.R.R., 15(1); 47-63.

Dagan, G., 1982a. Stochastic modelling of groundwater flow by unconditional and conditional probabilities, 1: Conditional simulation and the direct problem. W.R.R., 18(4): 813-833.

Dagan, G., 1982b. Analysis of flow through heterogeneous random aquifers, 2: Unsteady flow in confined formations. W.R.R., 18: 1571-1585.

Dagan, G., 1985. Stochastic modelling of groundwater flow by unconditional and conditional probabilities, 2: The inverse problem. W.R.R., 21(1): 65-72.

Dagan, G., 1989. Flow and Transport in Porous Formations. Springer-Verlag, New York.

Desbarats, A.J., 1987. Numerical estimation of effective permeability in sand-shale formation. W.R.R., 23(2): 273-286.

Desbarats, A.J., 1989. Support effect and the spatial average of transport properties. Math. Geology, 21(3): 383-389.

Desbarats, A.J., 1992a. Spatial averaging of transmissivity in heterogeneous fields with flow toward a well. W.R.R., 28(3):757-767.

Desbarats, A.J., 1992b. Spatial averaging of hydraulic conductivity in three-dimensional heterogeneous porous media. Math. Geology, 24(3): 249-267.

Desbarats, A.J., 1993. Geostatistical analysis of interwell transmissivity in heterogeneous aquifers. W.R.R., 29(4): 1239-1246.

Desbarats, A.J. and Dimitrakopoulos, R., 1990. Geostatistical modelling of transmissivity for two-dimensional reservoir studies. SPE formation Evaluation, Dic.: 437-443.

Deutsch, C., 1989. Calculating effective absolute permeability in sandstone/shale sequences. SPE Formation Evaluation, September: 343-348.

Deutsch, C. and Journel, A.G., 1992. GSLIB: Geostatistical Software Library and User's Guide. Oxford University Press, New York, 340 pp.

Durlofsky, L.J. and Chung, E.Y., 1990. Effective permeability of heterogeneous reservoir regions. 2nd European Conference on the Mathematics of Oil Recovery, Paris, 1990, pp-57-64.

Durlofsky, L.J., 1991. Numerical calculation of equivalent grid block permeability tensors for heterogeneous porous media. W.R.R., 27(5): 699-708.

Durlofsky, L.J:, 1992. Representation of grid block permeability in coarse scale models of randomly heterogeneous porous media. W.R.R., 28(7): 1791-1800.

Durlofsky, L.J., Jones, R.C. and Milliken, W.J., 1994a. A new method for the scale up of displacement processes in heterogeneous reservoirs. 4th European Conference on the Mathematics of Oil Recovery, Roros, Norway, June, 1994.

Durlofsky, L.J., Milliken, W.J., Dehghani, K. and Jones, R.C., 1994b. Application of a new scale up methodology to the simulation of displacement process in heterogeneous reservoirs. SPE International Petroleum Conference & Exhibition of Mexico, Veracruz, October 1994.

Dykaar, B.B. and Kitanidis, P.K., 1992a. Determination of the effective hydraulic conductivity for heterogeneous porous media using a numerical spectral approach, 1: Method. W.R.R., 28(4): 1155-1166.

Dykaar, B.B. and Kitanidis, P.K., 1992b. Determination of the effective hydraulic conductivity for heterogeneous porous media using a numerical spectral approach, 2: Application. W.R.R., 28(4): 1167-1178.

Farmer, C.L., Heath, D.E. and Moody, R.O., 1991. A global optimization approach to grid generation. 11th SPE Symposium on Reservoir Simulation, Anaheim, CA, February 1991, pp. 341-350.

Fayers, F.J. and Hewett, T.A., 1992. A review of current trends in petroleum reservoir description and assessment of the impacts on oil recovery. Adv. In Water Resources, 15(4): 341-365.

Garcia, M.H., Journel, A.G. and Aziz, K., 1990. An automatic grid generation and adjustment method for modelling reservoir heterogeneities. Report 3, Stanford Center for Reservoir Forecasting, Stanford, CA.

Garcia, M.H., Journel, A.G. and Aziz, K., 1992. Automatic grid generation for modelling reservoir heterogeneities. SPE Reservoir Engineering: 278-284.

Gelhar, L.W. and Axnexx, C.L., 1983. Three-dimensional stochastic analysis of macrodispersion in aquifers. W.R.R., 19(1): 161-180.

Gómez-Hernández, J.J. and Gorelick, S.M., 1989. Effective groundwater model parameter values: Inference of spatial variability of hydraulic conductivity, leakance and recharge. W.R.R., 25(3): 405-419.

Gómez-Hernández, J.J., 1990. Simulation of block permeability conditioned upon data measured at a different scale. In: ModelCARE 90: Calibration and Reliability in Groundwater Modelling. IAHS Publ. no. 195, pp. 407-416.

Gómez-Hernández, J.J., 1991. A stochastic approach to the simulation of block conductivity fields conditioned upon data measured at a smaller scale. Ph. D. thesis, Stanford University, CA.

Gómez-Hernández, J.J. and Wen, X.H., 1994. Probabilistic assessment of travel times in groundwater modelling. J. Stochastic Hydrology and Hydraulics, 8(1): 19-55.

Grindheim, A.O., 1990. An evaluation of homogeneization techniques for estimating effective absolute block permeability by use of a stochastic reservoir description simulator. Master thesis, Norwegian Institute of Technology (NTH).

Gutjahr, A.L., Gelhar, L.W., Bakr, A.A. and MacMillan, J.R., 1978. Stochastic analysis of spatial variability in subsurface flows, 2: Evaluation and application. W.R.R., 14(5): 953-959.

Haldorsen, H.H. and Lake, L.W., 1984. A new approach of shale's management in field scale simulation models. Soc. Of Petrol. Eng. Jour., 24 (August): 447-457.

Haldorsen, H.H., 1986. Simulation parameters assignment and the problem of scale in reservoir engineering. In: Lake, L.W. and Carroll, H.B. (eds.), Reservoir Characterization. Academic Press, pp. 445-485.

Haldorsen, H.H. and Chang, D.M., 1986. Notes on stochastic shale's; from outcrop to simulation model. In: Lake, L.W. and Carroll, H.B. (eds.), reservoir Characterization. Academic Press, pp-445-485.

Hoeksema, R.J. and Kitanidis, P.K., 1984. An application of the geostatistical approach to the inverse problem in two-dimensional groundwater modelling. W.R.R., 20(7): 1003-1020.

Hoekssema, R.J. and Kitanidis, P.K., 1985. Comparison of Gaussian conditional mean and kriging estimation in the geostatistical solution of the inverse problem. W.R.R., 21(6): 825-836.

Holden, L., Hoiberg, J. and Lia, O., 1989. Homogeneization of absolute permeability. Norwegian Computer Centre (NCC) Report.

Holden, L. and Lia, O., 1992. A tensor estimator for the homogeneization of absolute permeability. Transport in Porous Media, 8: 37-46.

Indelman, P. and Dagan, G., 1993a. Upscaling of permeability of anisotropic heterogeneous formations, 1: The general framework. W.R.R., 29(4): 917-923.

Indelman, P. and Dagan, G., 1993b. Upscaling of permeability of anisotropic heterogeneous formations, 2: General structure and small perturbation analysis. W.R.R., 29(4): 925-933.

Journel, A.G., Deutsch, C. and Desbarats, A.J., 1986. Power averaging for block effective permeability. SPE 15128.

Journel, A.G. and Huijbregts, C.J., 1978. Mining Geostatistics. Academic Press, London.

Kasap, E. and Lake, L.W., 1989. An analytical method to calculate the effective permeability tensor of a grid block and its application in an outcrop study. SPE 18434.

King, P.R., 1989. The use of renormalization for calculating effective permeability. Transport in porous Media, 4(1): 37-58.

Kirkpatrick, S., 1973. Percolation and conduction. Rev. Mod. Phys., 45(4): 574-588.

Kitanidis, P.K., 1990. Effective hydraulic conductivity for gradually varying flow. W.R.R., 26(6): 1197-1208.

Lake, L.W., 1988. The origins of anisotropy. J. of Petroleum Tech.: 395-396.

Malick, K.M., 1995. Boundary effects in the successive upscaling of absolute permeability. Master thesis, Stanford University, CA.

Mantoglou, A. and Gelhar, L.W., 1987. Effective hydraulic conductivity of transient unsaturated flow in stratified soils. W.R.R., 23(1): 57-67.

Matheron, G., 1967. Éléments pour une théorie des milieux. Mason et Cie.

Mohanty, S. and Sharma, M.M., 1990. A recursive method for estimating single and multiphase permeabilities. SPE paper 20477 presented at the 65th Annual Technical conference and Exhibition in New Orleans, LA, September 23-26, 1990.

Muggeridge, A.H., 1991. Generation of effective relative permeabilities from detailed simulation of flow in heterogeneous porous media. In: Lake, L.W., carroll, H.B. and Wesson, T.C. (eds.), Reservoir Characterisation II. Academic Press, San Diego, pp. 197-225.

Naff, R.L., 1991. Radial flow in heterogeneous porous media: An analysis of specific discharge. W.R.R., 27(3): 307-316.

Neumann, S.P. and Orr, S., 1993. Prediction of steady flow in nonuniform geologic media by conditional moments: Exact nonlocal formalism, effective conductivities, and weak approximation. W.R.R., 29(2): 341-364.

Pickup, G.E., Jensen, J.L., Ringrose, P.S. and Sorbie, K.S., 1992. A method for calculating permeability tensors using perturbed boundary conditions. In 3rd European Conf. on the Mathematics of Oil Recovery, Delft, The Netherlands, June 1992.

Pickup, G.E., Ringrose, P.S., Jensen, J.L. and Sorbie, K.S., 1994. Permeability tensors for sedimentary structures. Math. Geology, 26(2): 227-250.

Poley, A.D., 1988. Effective permeability and dispersion in locally heterogeneous aquifers. W.R.R., 24(11): 1921-1926.

Robey, T.H., 1995. An adaptive grid technique for minimizing heterogeneity of cells or elements. Math. Geology, 27(6): 706-729.

Rubin, Y. and Gómez-Hernández, J.J., 1990. A stochastic approach to the problem of upscaling of conductivity in disordered media: Theory and unconditional numerical simulations. W.R.R., 26(4): 691-701.

Russo, D., 1992. Upscaling of hydraulic conductivity in partially saturated heterogeneous porous formation. W.R.R., 28(2): 397-409.

Sáez, A., Otero, C.J. and Rusinek, I., 1989. The effective homogeneous behavior of heterogeneous porous media. Transport in Porous Media, 4: 213-238.

Sánchez-Vila, X., 1995. On the geostatistical formulations of the groundwater flow and solute transport equations. Ph. D. thesis, Universitat Politécnica de Catalunya, Barcelona, Spain.

Sánchez-Vila, X., Girardi, J.P. and Carrera, J., 1995. A synthesis of approaches to upscaling of hydraulic conductivity. W.R.R., 31(4): 867-882.

Shah, N. and Ottino, J.M., 1986. Effective transport properties of disordered, multiphase composites: Application of real-space renormalization group theory. Chem. Eng. Sci., 41(2): 283-296.

Tran, T.T., 1995. Stochastic simulation of permeability field and their scale-up for flow modelling. Ph. D. thesis. Stanford University, CA.

Tran, T.T. and Journel, A.G., 1995. Automatic generation of corner-point-geometry flow simulation grids from detailed geostatistical descriptions. Adv. of Water Resour.

Warren, J.E. and Price, H.H., 1961. Flow in heterogenous porous media. Society of Petroleum Engineering Journal, 1: 153-169.

Wen, X.H., 1996. Stochastic simulation of groundwater flow and mass transport in heterogenpus formations: Conditioning and problem of scales. Ph. D. thesis, Universidad Politécnica de Valencia, Spain.

White, C.D., 1987. Representation of heterogeneity for numerical reservoir simulation. Ph. D. thesis, Stanford University, CA.

White, C.D. and Horne, R.N., 1987. Computing absolute transmissivity in the presence of fine-scale heterogeneity. Paper SPE 16011, pp. 209-221.

Williams, J.K., 1989. Simple renormalization schemes for calculating effective properties of heterogeneous reservoirs. In: 1st European Conf. on the Mathematics of Oil recovery, Cambridge, UK, July 1989, pp. 281-298.

Wilson, K.G., 1979. Problems in physics with many scales length. Sci. am. 241 (August): 158-179.

Yamada, T., 1995. A dissipation-based coarse grid system and its application to the scale-up of two phase problems. Ph. D. thesis, Stanford University, CA.

Yeh, T.C., Gelhar, L.W. and Gutjahr, A.L., 1985. Stochastic analysis of unsaturated flow in heterogenous soils, 1: Statistically isotropic media. W.R.R., 21(4): 447-456.